MID-AMERICA TRANSPORTATION CENTER

Report # MATC-UNL: 004-48

Final Report

WBS: 25-1121-0005-004-48

Crashworthy Foundations for Soil-Embedded Roadside Safety Hardware

Joshua S. Steelman, PhD, PE
Associate Professor
Department of Civil and Environmental Engineering
Midwest Roadside Safety Facility
The University of Nebraska-Lincoln

Mojdeh Asadollahi Pajouh, PhD
Research Assistant Professor

Cody S. Stolle, PhD
Research Associate Professor

Chen S. Fang, PhD
Post-Doctoral Research Associate

Tewodros Yosef, PhD
Research Assistant Professor

Chung R. Song, PhD
Associate Professor

Seunghee Kim, PhD, PE
Associate Professor

Basil Abualshar, MSCE
Graduate Research Assistant

2024

A Cooperative Research Project sponsored by
U.S. Department of Transportation- Office of the Assistant Secretary for Research and Technology

Crashworthy Foundations for Soil-Embedded Roadside Safety Hardware

Joshua S. Steelman, Ph.D., P.E.
Associate Professor

Mojdeh Asadollahi Pajouh, Ph.D.
Research Assistant Professor

Cody S. Stolle, Ph.D.
Research Associate Professor

Chen S. Fang, Ph.D.
Post-Doctoral Research Associate

Tewodros Yosef, Ph.D.
Research Assistant Professor

Chung R. Song, Ph.D.
Associate Professor

Seunghee Kim, Ph.D., P.E.
Associate Professor

Basil Abualshar, M.S.C.E
Graduate Research Assistant

Midwest Roadside Safety Facility

A Report on Research Sponsored by

Mid-America Transportation Center

University of Nebraska–Lincoln

July 2, 2024

TECHNICAL REPORT DOCUMENTATION PAGE

<table>
<tr><td>1. Report No.
MATC report no. 25-1121-0005-004-48
MwRSF report no. TRP-03-483-24</td><td>2. Government Accession No.</td><td colspan="2">3. Recipient's Catalog No.</td></tr>
<tr><td colspan="2" rowspan="2">4. Title and Subtitle
Evaluation of Light Pole Foundation Embedment for Alaska DOT&PF</td><td colspan="2">5. Report Date
July 2, 2024</td></tr>
<tr><td colspan="2">6. Performing Organization Code</td></tr>
<tr><td colspan="2">7. Author(s)
Steelman, J.S., Asadollahi Pajouh, M., Stolle, C.S., Fang, C., Yosef, T., Song, C., Kim, S., and Abualshar, B.</td><td colspan="2">8. Performing Organization Report No.
25-1121-0005-004-48</td></tr>
<tr><td colspan="2" rowspan="2">9. Performing Organization Name and Address
Midwest Roadside Safety Facility (MwRSF)
Nebraska Transportation Center
University of Nebraska-Lincoln
Main Office:
Prem S. Paul Research Center at
Whittier School
Room 130, 2200 Vine Street
Lincoln, Nebraska 68583-0853
Outdoor Test Site:
4630 N.W. 36th Street
Lincoln, Nebraska 68524</td><td colspan="2">10. Work Unit No.</td></tr>
<tr><td colspan="2">11. Contract
69A3551747107</td></tr>
<tr><td colspan="2" rowspan="2">12. Sponsoring Agency Name and Address
Office of the Assistant Secretary for Research and Technology
1200 New Jersey Ave., SE
Washington, D.C. 20590</td><td colspan="2">13. Type of Report and Period Covered
Final Report: 2020-2024</td></tr>
<tr><td colspan="2">14. Sponsoring Agency Code
TRB RiP# 91994-74</td></tr>
<tr><td colspan="4">15. Supplementary Notes
Prepared in cooperation with U.S. Department of Transportation, Federal Highway Administration</td></tr>
<tr><td colspan="4">16. Abstract
Foundations commonly used by the Alaska Department of Transportation and Public Facilities (AK DOT&PF), supporting steel light poles with single mast arms, mounted using frangible couplings, were evaluated to assess their suitability to provide crashworthy performance during vehicle impacts when foundations are located in weak soils. Preliminary LS-DYNA models suggested that 2.5-ft diameter, 6-ft deep foundations could perform adequately. Four bogie tests were performed on foundations with embedded steel posts and with various soil compaction and moisture conditions. Additionally, two bogie tests were performed on steel light poles with single mast arms and attached to foundations with Transpo frangible couplings, with foundations surrounded by loose sand fill in both dry and saturated conditions. Breakaway activation was achieved regardless of soil compaction and moisture content, relying primarily on foundation inertia rather than soil resistance. Furthermore, foundation permanent set was less than 1 in. for both tests with Transpo couplings, suggesting that foundations could likely be reused after vehicle impacts by replacing the impacted pole and fractured couplings. Refined soil modeling demonstrated that a hybrid Finite Element Method + Arbitrary Lagrangian-Eulerian (FEM+ALE) approach could provide improved predictions of soil response when subjected to extreme dynamic load effects. Lastly, preliminary LS-DYNA models simulated full-scale vehicle crash tests according to the Test Level 3 (TL-3) criteria of the Manual for Assessing Safety Hardware, Second Edition. The results suggest that the light poles would not be likely to pass MASH criteria for test designation no. 3-60 regardless of acceptable frangible coupling activation due to excessive occupant compartment deformation.</td></tr>
<tr><td colspan="2">17. Key Words
Crashworthiness, Foundation, Weak Soil, Light Pole, Coupling, Breakaway, Bogie Test, LS-DYNA</td><td colspan="2">18. Distribution Statement
No restrictions. This document is available through the National Technical Information Service.
5285 Port Royal Road
Springfield, VA 22161</td></tr>
<tr><td>19. Security Classification (of this report)
Unclassified</td><td>20. Security Classification (of this page)
Unclassified</td><td>21. No. of Pages
356</td><td>22. Price</td></tr>
</table>

Form DOT F 1700.7 (8-72) Reproduction of completed page authorized

Disclaimer Statement

This material is based upon work supported by the Federal Highway Administration, U.S. Department of Transportation and the Alaska Dept. of Transportation and Public Facilities under IRIS# HFHWY00139, Fedaid# 4000(186). The contents of this report reflect the views and opinions of the authors who are responsible for the facts and the accuracy of the data presented herein. The contents do not necessarily reflect the official views or policies of the University of Nebraska-Lincoln, the Alaska Dept. of Transportation and Public Facilities, nor the Federal Highway Administration, U.S. Department of Transportation. This report does not constitute a standard, specification, or regulation. Trade or manufacturers' names, which may appear in this report, are cited only because they are considered essential to the objectives of the report. The United States (U.S.) government and the State of Nebraska do not endorse products or manufacturers.

Uncertainty of Measurement Statement

The Midwest Roadside Safety Facility (MwRSF) has determined the uncertainty of measurements for several parameters involved in standard full-scale crash testing and non-standard testing of roadside safety features. Information regarding the uncertainty of measurements for critical parameters is available upon request by the sponsor and the Federal Highway Administration. Test nos. AKLP-1 – AKLP-6 were non-certified component tests conducted for research and development purposes only and are outside the scope of the MwRSF's A2LA Accreditation.

Acknowledgements

The authors wish to acknowledge several sources that made a contribution to this project: Alaska Dept. of Transportation and Public Facilities for sponsoring this project; (2) MwRSF personnel for constructing the test articles and conducting the crash tests, and (3) the Holland

Computing Center at the University of Nebraska, which receives support from the Nebraska Research Initiative, for providing computational resources.

Acknowledgement is also given to the following individuals who contributed to the completion of this research project.

Midwest Roadside Safety Facility
R.K. Faller, Ph.D., P.E., Research Professor & MwRSF Director
J.C. Holloway, M.S.C.E., Research Engineer & Assistant Director –Physical Testing Division
K.A. Lechtenberg, M.S.M.E., Research Engineer
R.W. Bielenberg, M.S.M.E., Research Engineer
S.K. Rosenbaugh, M.S.C.E., Research Engineer
B.J. Perry, M.E.M.E., Research Engineer
A.T. Russell, B.S.B.A., Testing and Maintenance Technician II
E.W. Krier, B.S., Engineering Testing Technician II
D.S. Charroin, Engineering Testing Technician II
R.M. Novak, Engineering Testing Technician II
T.C. Donahoo, Engineering Testing Technician I
J.T. Jones, Engineering Testing Technician I
E.L. Urbank, B.A., Research Communication Specialist
Z.Z. Jabr, Engineering Technician
Undergraduate and Graduate Research Assistants

Alaska Department of Transportation
A. Bosin
N. Geary
I. A. Grant
E. Marx
D. A. Hemstreet
C. M. Wagner
P. Forsling (FHWA)

SI* (MODERN METRIC) CONVERSION FACTORS

APPROXIMATE CONVERSIONS TO SI UNITS

Symbol	When You Know	Multiply By	To Find	Symbol
		LENGTH		
in.	inches	25.4	millimeters	mm
ft	feet	0.305	meters	m
yd	yards	0.914	meters	m
mi	miles	1.61	kilometers	km
		AREA		
in^2	square inches	645.2	square millimeters	mm^2
ft^2	square feet	0.093	square meters	m^2
yd^2	square yard	0.836	square meters	m^2
ac	acres	0.405	hectares	ha
mi^2	square miles	2.59	square kilometers	km^2
		VOLUME		
fl oz	fluid ounces	29.57	milliliters	mL
gal	gallons	3.785	liters	L
ft^3	cubic feet	0.028	cubic meters	m^3
yd^3	cubic yards	0.765	cubic meters	m^3
		NOTE: volumes greater than 1,000 L shall be shown in m^3		
		MASS		
oz	ounces	28.35	grams	g
lb	pounds	0.454	kilograms	kg
T	short ton (2,000 lb)	0.907	megagrams (or "metric ton")	Mg (or "t")
		TEMPERATURE (exact degrees)		
°F	Fahrenheit	5(F-32)/9 or (F-32)/1.8	Celsius	°C
		ILLUMINATION		
fc	foot-candles	10.76	lux	lx
fl	foot-Lamberts	3.426	candela per square meter	cd/m^2
		FORCE & PRESSURE or STRESS		
lbf	pound-force	4.45	newtons	N
lbf/in^2	pound-force per square inch	6.89	kilopascals	kPa

APPROXIMATE CONVERSIONS FROM SI UNITS

Symbol	When You Know	Multiply By	To Find	Symbol
		LENGTH		
mm	millimeters	0.039	inches	in.
m	meters	3.28	feet	ft
m	meters	1.09	yards	yd
km	kilometers	0.621	miles	mi
		AREA		
mm^2	square millimeters	0.0016	square inches	in^2
m^2	square meters	10.764	square feet	ft^2
m^2	square meters	1.195	square yard	yd^2
ha	hectares	2.47	acres	ac
km^2	square kilometers	0.386	square miles	mi^2
		VOLUME		
mL	milliliter	0.034	fluid ounces	fl oz
L	liters	0.264	gallons	gal
m^3	cubic meters	35.314	cubic feet	ft^3
m^3	cubic meters	1.307	cubic yards	yd^3
		MASS		
g	grams	0.035	ounces	oz
kg	kilograms	2.202	pounds	lb
Mg (or "t")	megagrams (or "metric ton")	1.103	short ton (2,000 lb)	T
		TEMPERATURE (exact degrees)		
°C	Celsius	1.8C+32	Fahrenheit	°F
		ILLUMINATION		
lx	lux	0.0929	foot-candles	fc
cd/m^2	candela per square meter	0.2919	foot-Lamberts	fl
		FORCE & PRESSURE or STRESS		
N	newtons	0.225	pound-force	lbf
kPa	kilopascals	0.145	pound-force per square inch	lbf/in^2

*SI is the symbol for the International System of Units. Appropriate rounding should be made to comply with Section 4 of ASTM E380.

Table of Contents

List of Figures

List of Tables

Executive Summary

The research presented herein aimed to evaluate the suitability of systems composed of steel light poles, frangible couplings, and soil-embedded reinforced concrete foundations commonly used by the Alaska Department of Transportation and Public Facilities (AK DOT&PF) to facilitate crashworthy performance during vehicle impacts when foundations are located in weak soils. Note that the analysis and testing focused exclusively on vehicle impacts, and did not consider other applicable considerations for light pole foundation designs, such as ice, wind, or earthquake loading.

An initial review of light pole foundations used by other states in the US found that the foundation sizes used by AK DOT&PF are consistent with the typical range of sizes used by other agencies. Furthermore, little information was generally available to guide foundation designs in weak and/or saturated soils. Agencies tended to defer designs in such conditions to Geotechnical specialists.

Physical tests included two general configurations: foundations with steel posts embedded in and extending above the top of the concrete foundation; foundations supporting steel light poles connected to concrete foundations using Transpo frangible couplings. Embedded steel posts did not include a breakaway mechanism, and thus produced high demands on the foundations and surrounding soil limited by the plastic hinging strength of the post. The steel post was selected to reach a peak force similar to the Transpo couplings, but the impulse and momentum transfer were greater for the embedded steel post due to the ductile hinging mechanism compared to the brittle frangible mechanism of the couplings.

Simulations for this research were performed using LS-DYNA. Preliminary modeling of the embedded steel post suggested that 6-ft deep foundations, a typical depth used historically, but a reduction from the minimum 7-ft depth currently specified in the applicable AK DOT&PF

Standard Plan, may be adequate to achieve frangible coupling activation. Similarly, preliminary modeling of the steel light pole with frangible couplings concurred that a 6-ft foundation depth should be adequate to reliably achieve frangible coupling breakaway activation by relying only on the inertial resistance of the foundation. Permanent foundation displacements were predicted to be adequately small when momentum transfer was limited by frangible couplings in the preliminary models so that foundations should be able to be reused following an impact without requiring excavation, re-setting, and backfilling.

Four tests were performed with surrogate vehicles (bogies) approximately simulating small cars impacting steel posts embedded in concrete foundations. Although the intent was to simulate lower-bound weak soil conditions consistent with soil boring logs provided by AK DOT&PF, targeting a Standard Penetration Test (SPT) blow count of approximately 7 throughout the depth, achieving this soil condition was found to be challenging. For the first test, the SPT value was 7 for the first 18 in. of soil, but increased to 15 and 20 for the next successive 18-in. depth increments. Soil was placed loose around the foundation for the second test, resulting in SPT values of 0 at the top layer of soil and values of only 2 to 9 around 48 in. of depth. The third and fourth tests used a modified protocol that resulted in intermediate SPT values between the first and second tests. The third test was also performed with an increased moisture content. Impact response was similar for all tests, except that the foundation experienced a large rotation for the test with loose soil fill. The post experienced plastic hinging in all four tests, confirming that foundation inertia was sufficient to achieve frangible coupling activation load levels, regardless of soil stiffness.

Two tests were performed with bogies impacting steel posts mounted to foundations with Transpo frangible couplings, consistent with AK DOT&PF Standard Plans. Soil was placed loose around foundations in both tests. One test was performed with dry soil conditions, and the other was performed after placing a liner to retain moisture and adding water until the soil was fully saturated with standing water. Results for both tests confirmed that breakaway was achieved despite loose soil conditions with SPT values of less than 2 throughout 6-ft soil depths, and regardless of dry or saturated conditions. Thus, foundations consistent with the current AK DOT&PF Standard Plan L-30.11, with depths of at least 6 ft, provide compliance with previously accepted crashworthiness standards predating the *Manual for Assessing Safety Hardware, Second Edition (MASH 2016)*, regardless of surrounding soil stiffness and moisture content.

Furthermore, foundation permanent set was less than 1 in. for both cases, suggesting that foundations would likely be reuseable by replacing the steel pole and frangible couplings after a vehicle impact in service. However, the results were obtained with a simulated vehicle with a rigid impacting head. Commuter vehicles have crushable features, such as bumpers, which will lengthen the impulse and may result in increased foundation displacements.

Additional simulations were performed to investigate the capability for alternative modeling techniques to produce more accurate foundation response predictions than those obtained from preliminary models. A hybrid Finite Element Method + Arbitrary Lagrangian-Eulerian (FEM+ALE) approach was employed and validated against bogie test data for the embedded steel post and steel pole-on-couplings test articles. The hybrid FEM+ALE method produced superior predictions compared to preliminary modeling methods, although the benefits were most evident for predictions with very large foundation movement in soil, which is not anticipated to occur nor desirable for light pole foundations subjected to impact. Nonetheless, the modeling methodology may offer benefits in other situations beyond the scope of the present project where large soil displacements are anticipated, such as soil-embedded posts intended to experience large displacements through soil, or deep foundations undergoing seismic excitation.

Simulations were also performed to provide preliminary predictions for full-scale vehicle crash tests according to a critical test designations required according to the Test Level 3 (TL-3) criteria of *MASH 2016*. The simulations used soil models identical to those selected for preliminary modeling, not the hybrid FEM+ALE refined models, and thus tended to overestimate soil deformations. As soil deformation does not influence crashworthiness, provided that breakaway activation is achieved reliably, use of the preliminary soil models was justified to optimize computational costs. Pole breakaway and foundation responses were similar to bogie tests, suggesting that foundation response would be acceptable in a physical test. However, the poles and foundations were not predicted to pass MASH safety criteria due to secondary impacts of the pole with the vehicle, which were unrelated to the foundation and breakaway components.

Future research is recommended to (1) evaluate and develop crashworthy roadside light poles, (2) improve breakaway steel couplings modeling, and (3) improve soil dynamics modeling. Crash safety for light poles is a challenging issue for agencies throughout the US due to excessive occupant compartment intrusion – roof and windshield crush – during low-speed impacts, as confirmed in recent analytical studies and crash tests. AK DOT&PF is recommended to review results from other studies addressing crash safety for light poles as they become available, such as NCHRP Projects 03-119, 22-43, and 17-105, as well as other studies outside NCHRP, such as research in-progress at laboratories such as the Midwest Roadside Safety Facility and the Texas Transportation Institute. While research efforts through these other studies may address this research need for AK DOT&PF, it should be noted that frangible couplings represent a smaller portion of the breakaway light pole inventory throughout the United States in comparison to transformer bases and slip bases according to a survey performed under NCHRP 03-119, and therefore may be a lower priority for pooled fund and nationally funded studies.

Chapter 1 Introduction

1.1 Introduction

This research project was motivated by a case study initiated by a member of the Alaska Department of Transportation and Public Facilities (DOT&PF) team. The objective of the case study was to design a light pole foundation that would be suitable for the environmental conditions in Alaska, using sample AK DOT&PF light pole sizing dimensions such as a 22-ft long mast arm mounted at a height of 37.5 ft, and a 16-ft^2 sign. A 3-ft diameter by 8-ft deep concrete foundation was found to be sufficient for most soil conditions when considering *American Association of State Highway and Transportation Officials* (AASHTO) recommended design criteria [1, 2] and limiting design considerations to gravity and environmental loads. However, the study also found that the foundation would be deemed insufficient if evaluated under vehicle impact loading using available design criteria and methods (e.g., Broms' method [3, 4] for soil response, vehicle loading estimated from frangible coupling capacity).

Run-off-road crashes with light poles generate dynamic loads which are not well-accounted for in traditional civil structural design or geotechnical design. The state of Alaska currently represents dynamic vehicle impact loads on light poles with a nominally equivalent static load corresponding to the ultimate capacity of frangible couplings. This approach neglects potentially beneficial aspects of dynamic behavior, such as structure and foundation inertia, short duration impulse loading, soil-structure interaction, nonlinear dynamic soil behavior and energy dissipation. Light pole foundation designs governed by vehicle impact loads are therefore likely to be unnecessarily overdesigned, leading to high material and labor costs, and increased worker exposure to traffic.

Additionally, Alaska DOT&PF does not currently possess an approved standard light pole foundation design appropriate to the relatively high water table found in Southeast Alaska.

Standard designs have previously been available, but were either non-optimal, such as requiring drilled shafts socketed into bedrock, or restricted to medium to dense or stiff soils and where the installation would not encounter the water table. Conditions in Southeast Alaska may not conform to these requirements, so an alternative design or design methodology would be beneficial.

The project was focused on vehicle impact performance. Ideally, designs developed for considerations other than vehicle impacts will envelope the design requirements for vehicle impacts. Typical design procedures addressing only gravity and environmental loads may therefore potentially be justified to be adequate without modifications to address vehicle impacts.

1.2 Objective

The objective of this research effort was to develop foundation design recommendations to provide crashworthy performance for light poles located in critical weak soil conditions found in southeast Alaska. Soils may be dry or saturated. Acceptable performance required activation of frangible couplings commonly used by AK DOT&PF. Furthermore, a limited post-activation foundation set was desirable.

1.3 Scope

This project focused exclusively on vehicle impacts and did not consider other environmental design influences that do not directly influence crash performance, such as ice or wind loads on light pole structures. Only steel poles with frangible base connections were considered, which were indicated by Alaska DOT&PF to be the primary light pole and foundation connection types used in the state. Analytical modeling included detailed, nonlinear finite element analyses using LS-DYNA. However, material properties for steel light poles, concrete foundations, soils surrounding foundations, and connecting hardware were based only on information available from supplier certifications, or by estimating from property correlations found in literature. The project focused on soil properties and characteristics appropriate to conditions found in southeast Alaska, according to documentation supplied by AK DOT&PF. Physical testing was limited to bogie impact tests. Full-scale crash tests were not within the project scope.

Chapter 2 Literature Review

2.1 Overview

Alaska DOT&PF standards and available soil data were first reviewed. Past impact tests on poles and on foundations embedded in soil were then examined to establish context and expectations for tests to be conducted under this project. A review was then performed to identify standards and guidelines for light pole foundation design and installation used by other DOTs within the United States. Finally, resources from state DOTs and other sources were compiled to facilitate soil property characterization from data sources readily available from Alaska DOT&PF for use in analytical modeling.

2.2 Review of Alaska Standards and Soil Data

Alaska DOT&PF light pole foundation details were available in Standard Plan L-30.11, shown in Figure 2.1, and a datasheet for the typical coupling used with the foundation is provided in Figure 2.2. Standard foundations were 30-in. average diameter formed by a corrugated metal pipe per Note 3 in Standard Plan L-30.11. Standard foundation depth ranged from 8 ft to 10 ft, depending on surface grade at the installation location. However, according to Note 9, the foundation depth could be reduced by 1 ft if the mast arm length did not exceed 12 ft or if no mast arm were used, resulting in a minimum depth of 7 ft.

The design standard is noted as the AASHTO 2013 Standard Specifications for Structural Supports for Highway Signs, Luminaires and Traffic Signals with 2019 Interims, and design loads are noted as 1,000 lb axial, 2,000 lb shear, and 50,000 ft-lb moment. Simultaneously, the frangible coupling loads are noted in the Material Requirements section as 5.5 kips for ultimate shear, corresponding to a peak shear load of 22 kips acting from four couplings onto the foundation, more than 10 times the noted design shear load.

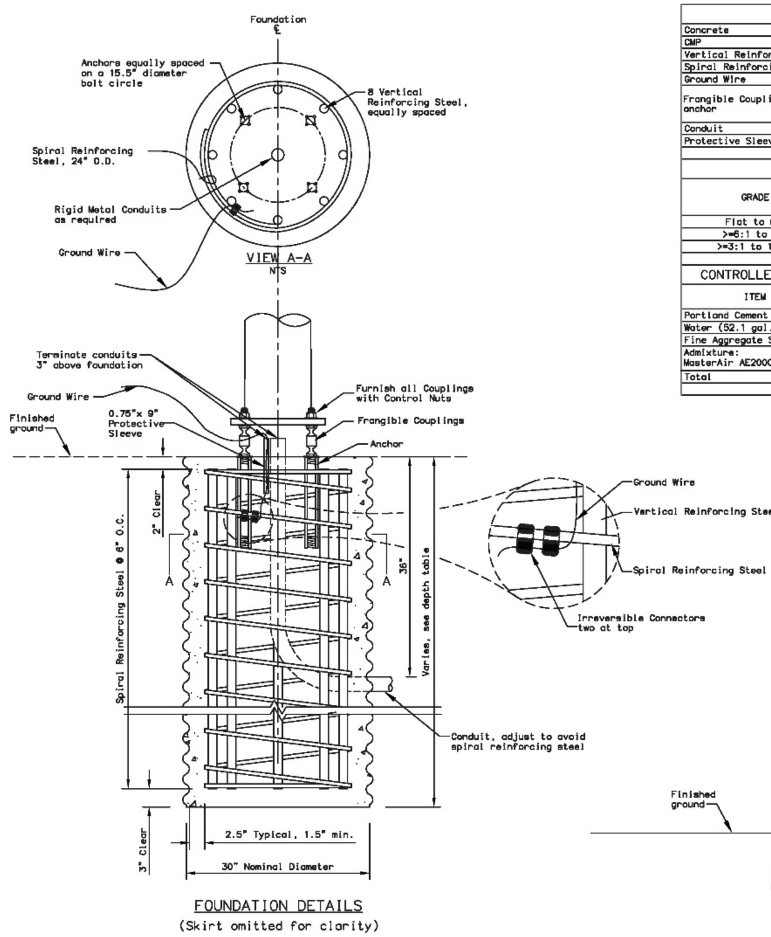

MATERIAL REQUIREMENTS		
Concrete	Class A	f'c = 4000 psi
CMP	AASHTO M218	14 ga.
Vertical Reinforcing Steel	AASHTO M31 #11	GR 60
Spiral Reinforcing Steel	AASHTO M31 #5	GR 60
Ground Wire		#4 AWG
Frangible Coupling and anchor	NCHRP 350 TL3 (See note 11)	Vu = 5.5 kips Tu = 43.2 kips
Conduit	Sch 40	RMC
Protective Sleeve	Sch 40	PVC

DEPTH TABLE		
GRADE	FOUNDATION DEPTH BY APPLICATION (ft.)	
	ELECTROLIER * SEE NOTE 9	BREAKAWAY TRAFFIC SIGNAL
Flat to 6:1	8	6.5
>=6:1 to 3:1	9	7
>=3:1 to 1.5:1	10	8

CONTROLLED LOW STRENGTH MATERIAL MIX DESIGN		
ITEM	BATCHING QUANTITIES PER CYD BATCH (lbs.)	APPLICABLE SPECS.
Portland Cement Concrete	188	701-2.01
Water (52.1 gal.)	435	712-2.01
Fine Aggregate SSD	3041	703-2.01
Admixture: MasterAir AE2000	2.0 oz.	711-2.02
Total	3664	

L-30.11

SHEET 1 of 1

DESIGN NOTES:

Design Standard: 2013 Standard Specifications for Structural Supports for Highway Signs, Luminaires and Traffic Signals with 2019 interim.

Design Load: 1,000 lbs axial, 2,000 lbs shear, 50,000 ft-lbs moment.

NOTES:

1. This foundation is approved for electrolier and breakaway traffic signal applications in cohesionless soils with an N1-60 value of 10 or greater per AASHTO T-206, "Standard Penetration Test" (SPT). This foundation shall not be used if any of the following are encountered; water table above the bottom of foundation, very loose soils, organic soils, cohesive soils (clay), or soils susceptible to frost jacking. If any of these conditions are encountered, stop foundation work and contact the Engineer.
2. Place foundation in drilled or excavated hole with centerline of foundation located at the station, offset, and elevation specified in plans. Set foundation to satisfy the conditions depicted in clearance detail.
3. Form the foundation in corrugated metal pipe conforming to Subsection 707-2.01 of the Specifications.
4. Provide 1.5 extra turns at each end of the spiral reinforcing steel. Reinforcing steel shall not be spliced. Tie vertical reinforcing steel to each intersection of the spiral reinforcing steel.
5. Connect ground wire near the top of spiral reinforcing steel with two irreversible connectors as shown. Fasten connectors according to the manufacturers' recommendations including the use of manufacturer specified tools. The ground wire may be bare solid, stranded, or braided copper. Protect ground wire with protective sleeve as shown and fill with silicon sealant.
6. Complete all concrete work in conformance with Sections 501, 503, and 660 of the Specifications. Use a tube or tremie with a hopper head or other approved device when dropping concrete more than 5 feet per Subsection 501-3.05. Vibrate concrete during placement by mechanical vibration per Subsection 501-3.06. Ensure anchor threads are protected from contact with concrete during pour.
7. Backfill and compact according to Section 205, and Subsections 203-3.04 and 660-3.01 of the Specifications. Use select material, Type A or controlled low strength material as backfill material. Ensure area below foundation meets compaction requirements and is free of loose material and debris prior to concrete work.
8. Install all anchors according to the manufacturer's written installation instructions. Anchors shall be installed plumb. Anchors greater than 1:40 out-of-plumb will result in foundation rejection.
9. When used for electrolier reduce the foundation depth 1 foot when there is no luminaire arm or the luminaire arm is less than or equal to 12 feet.
10. Grade in depth table refers to fill slopes. If foundation is in a cut slope assume flat grade in table. To determine grade in fill slopes, use the most severe grade found within an 8 foot radius of the center of the foundation.
11. The frangible coupling referenced in this ASP is NCHRP 350 compliant. There is no MASH compliant device available at this time. See SPDR report for more info.
12. Special grading detail and/or shielding may be required to maintain 4" maximum clear distance.

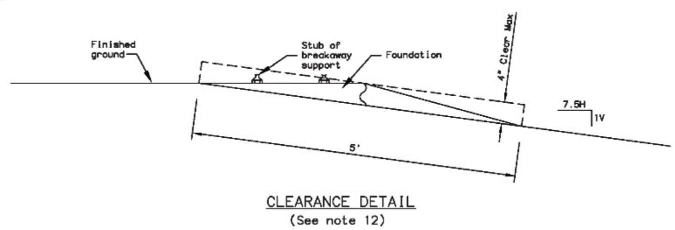

State of Alaska DOT&PF
ALASKA STANDARD PLAN

CONCRETE STREET LIGHT POLE FOUNDATION

Adopted as an Alaska Standard Plan by: Carolyn Morehouse

Carolyn Morehouse, P.E.
Chief Engineer

Adoption Date: 7/17/2020

Last Code and Stds. Review By: KLK,MJM Date: 7/8/2020

Next Code and Standards Review Date: 7/8/2030

L-30.11

Figure 2.1 AK DOT&PF Light Pole Foundation Standard

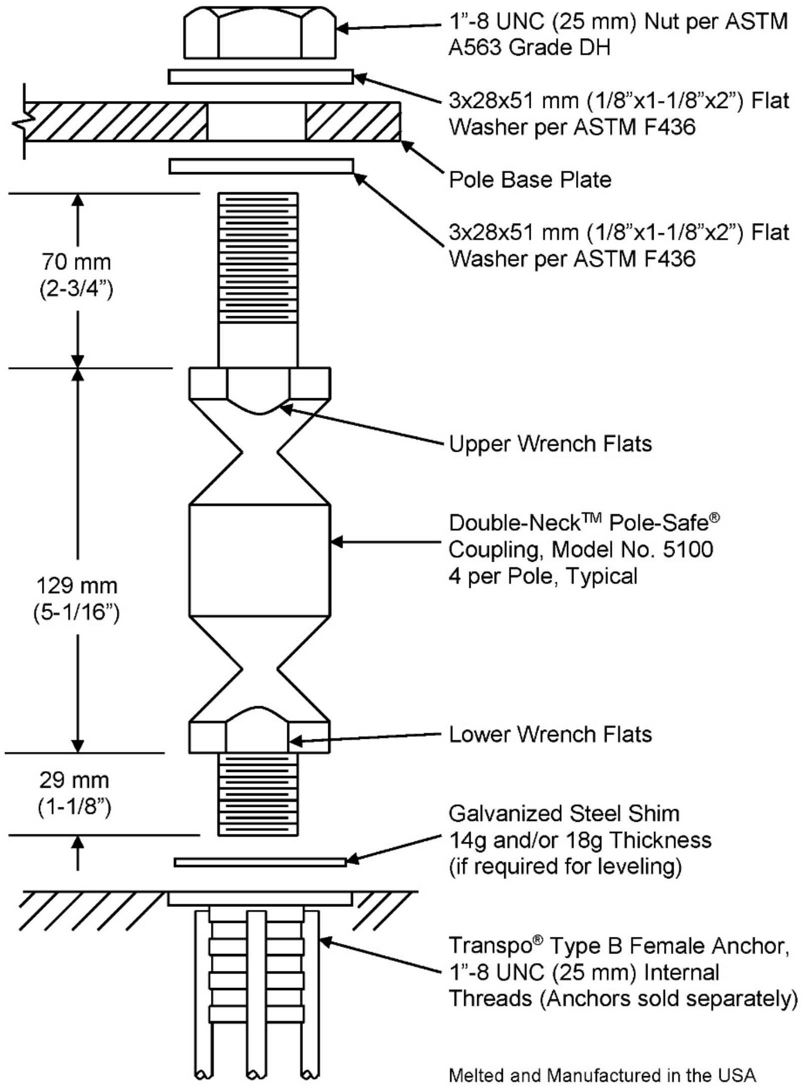

SPECIFICATIONS

Performance Criteria:

1. Double-Neck™ Pole-Safe® conforms to AASHTO “Standard Specifications for Structural Supports for Highway Signs, Luminaires and Traffic Signals.”
2. Double-Neck™ Pole-Safe® has been crash-tested and FHWA approved in accordance with the requirements of NCHRP Report 350, “Recommended Procedures for the Safety Performance Evaluation of Highway Features.”
3. Maximum Allowable Pole Mass = 423 kg (930 lb) (total, including fixtures).

Physical Properties per Coupling:

1. Ultimate Tensile Strength = 221.5 kN (49.8 kips), minimum.
2. Tensile Yield Strength = 192.0 kN (43.2 kips), minimum.
3. Ultimate Restrained Shear Strength = 16.9 kN (3.8 kips), minimum.
4. Ultimate Restrained Shear Strength = 24.4 kN (5.5 kips), maximum.

Corrosion Protection:

1. All Double-Neck™ Pole-Safe® couplings, nuts, bolts, and washers are galvanized after fabrication in accordance with ASTM A153. All leveling shims are galvanized after fabrication in accordance with ASTM A653.

Pole-Safe® Model No. 5100
Breakaway Support System for Light Poles

TRANSPO® INDUSTRIES, INC.
Safer Transportation Through Innovation

20 Jones Street
New Rochelle, NY 10801
914-636-1000
www.transpo.com

Figure 2.2 Typical Transpo Coupling Used with AK DOT&PF Light Pole Foundations

Geotechnical soil characterization may include the use of in-situ and/or laboratory techniques. In-situ techniques are commonly used as they allow for testing soils in their natural, undisturbed condition. On the other hand, laboratory techniques are utilized to test soils under well-controlled conditions and thus provide standardized, objective, and replicable data for detailed characterization of soils. In this research, data was available in the form of boring logs provided by AK DOT&PF, thus focusing on in-situ soil characterization. These logs provide information along subsurface depths for general soil type categorizations, moisture contents, and Standard Penetration Test (SPT) blow counts. According to Note 1, the foundation standard was approved for installation in cohesionless soils with an SPT $(N_1)_{60}$ value of at least 10. Installation sites with the water table above the bottom of the foundation or with very loose soils, among other conditions, required consultation with an Engineer.

This study focused on addressing soil conditions in the region near Juneau, AK. The region includes problematic soil conditions at a relatively high frequency, with loose, potentially saturated soil due to the high water table near the Pacific ocean. A summary of data from boring logs provided by AK DOT&PF is shown in Figures 2.3 and 2.4. Boring log locations included Angoon Airport (ANG), a Rink Creek Road Bridge Replacement (GST), Haines Airport Access Road (HNS), Glacier Highway Improvements in Juneau (JNU_G), Mendenhall Loop Road Capacity Improvements in Juneau (JNU_M), Riverside and Stephen Richards Congestion Mitigation in Juneau (JNU_S), Kake Keku Road Upgrade (KAE), North Tongass Highway Resurfacing (KTN_N), South Tongass Highway Road Improvement Project (KTN_S), South Mitkof Highway Upgrade-Ohmer Creek Bridge (PSG), Klondike Highway MP 4-5 Repairs (SGY), Sawmill Creek Resurfacing & Pedestrian Improvements (SIT) at hole locations SIT18-TH004, SIT18-TH005, and SIT18-TH006, and Wrangell and Bennett St / Airport Rd at hole locations WGR17-TH001 (WRG_A1) and WGR17-TH006 (WRG_A2).

Boring log locations with shaded cells in Figure 2.4 indicate MPT values, obtained using a 340-lb hammer and a 2-ft long by 3-in. outside diameter split spoon sampler, rather than a 140-lb hammer and a 1.5-ft long by 2-in. outside diameter split spoon sampler for SPT. Blow counts were extracted for the upper 10 ft from each provided boring log, consistent with the maximum depth noted for light pole foundations in Figure 2.1, anticipating that a foundation would not need to be deeper for purposes of crashworthiness. The blow counts were then correlated to a soil characterization schema used by the Washington State DOT (WSDOT) [5] , as shown in Figure 2.5 (see also Figure B.39), treating the MPT results as functionally equivalent to SPT for purposes of this general characterization. According to this schema, soil conditions varied from Very Soft to Very Hard soil.

Documented subsurface conditions could be highly variable, both from location to location, and along the depth at particular locations. JUN_S, for example, appeared to exhibit refusal with 50 blows to advance 4 in. around 2.5 ft below the ground surface, corresponding to Very Hard soil. However, the soil underlying that Very Hard layer was classified as Poor. Bedrock was generally encountered at depths greater than typical light pole foundations would extend according to AK DOT&PF Standard L-30.11. Bedrock only occurred within the upper 10 ft below grade for KAE, for which bedrock was encountered at 9 ft.

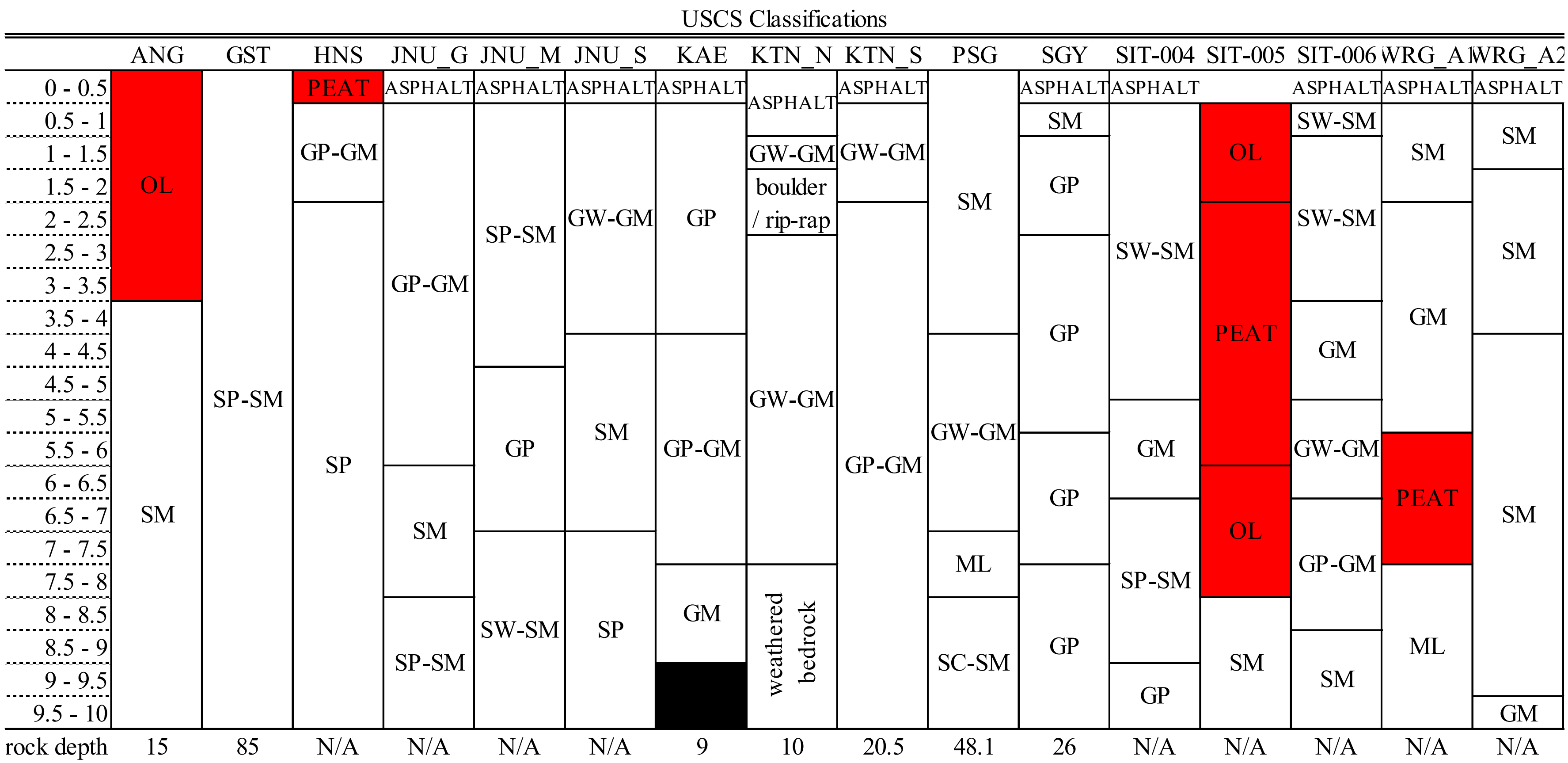

Figure 2.3 AK DOT&PF Boring Log USCS Classifications

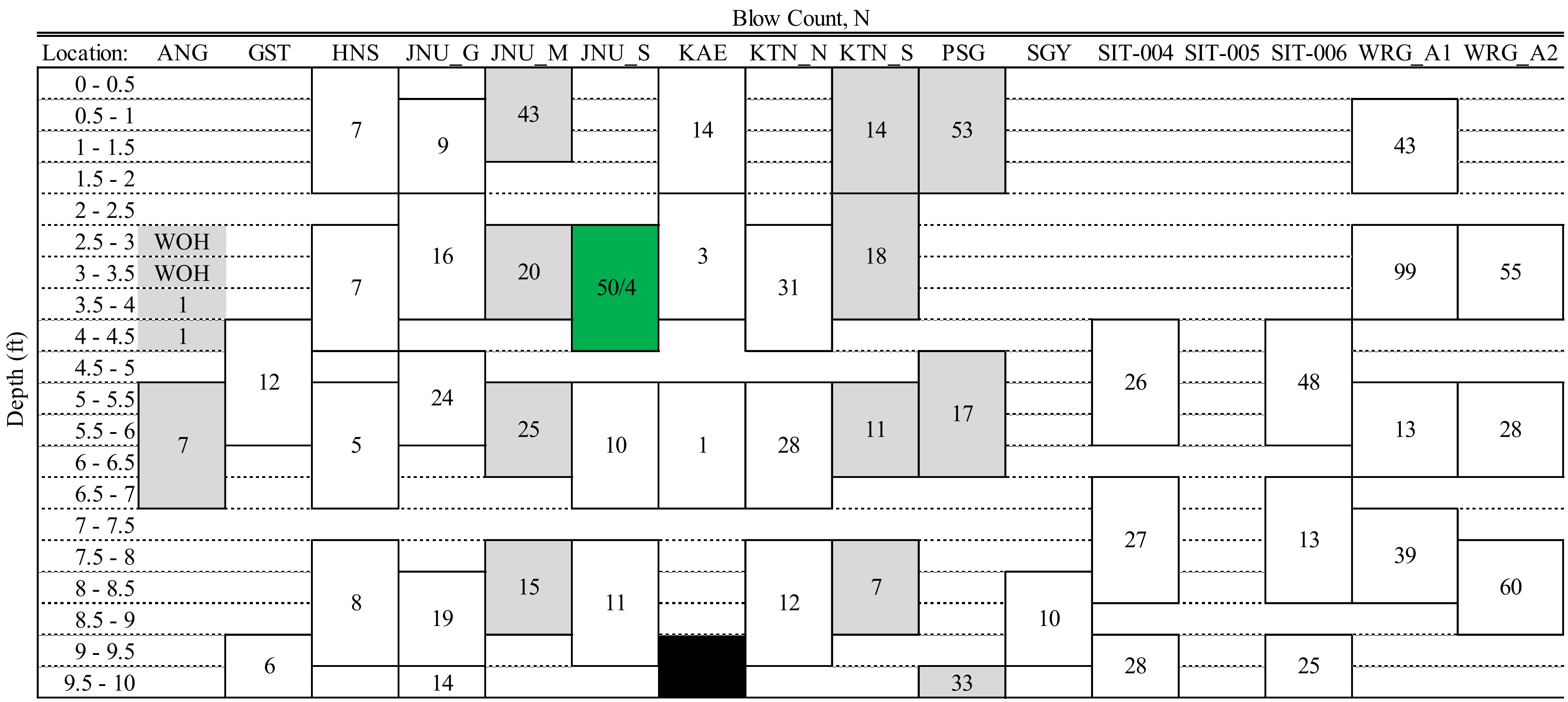

Figure 2.4 AK DOT&PF Boring Log SPT or MPT Blow Counts

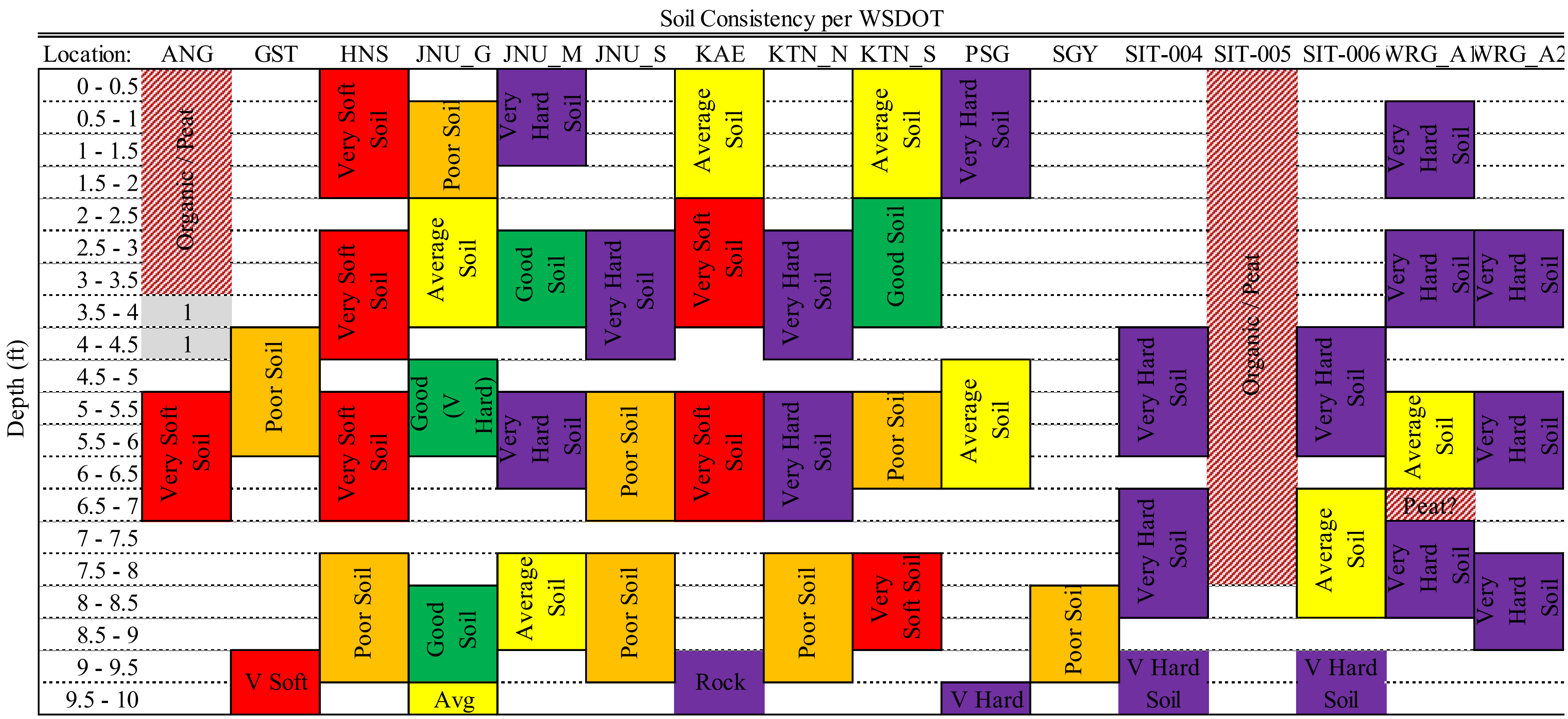

Figure 2.5 AK DOT&PF WSDOT Soil Characterization [5]

Locations such as ANG and SIT-005 were regarded as out of scope due to the presence of organic material (peat) with negligible geotechnical strength or stiffness. Such materials were expected to be removed and replaced with more competent material during foundation installation. Location HNS was selected as a representative, lower-bound critical case, with predominantly "Very Soft Soil" within the anticipated depth of the foundation corresponding to SPT blow counts ranging from 5 to 8. An SPT blow count of 7 was selected as the target for crash testing soil conditions, extending the applicability of the study findings beyond the existing lower bound of 10 (assuming that corrected blow counts will be approximately equal to uncorrected blow counts).

2.3 Previous Pole Impact Testing Research

Research studies including full-scale crash tests and component-level (bogie) tests on light and utility poles have been conducted under NCHRP Report 230 [6], NCHRP Report 350 [7], and MASH criteria [8, 9]. This section summarizes completed research and available reports relevant to this project.

A study published in 2009 investigated pedestrian street crossing signal poles used by the New York State Department of Transportation (NYSDOT) [10] using a pendulum system to impart a simulated impact load. The poles typically used frangible bases, but NYSDOT believed the aluminum pole itself could break away near its base if the frangible connection was eliminated. Compliance testing and evaluation were performed to satisfy NCHRP Report 350 (test designation nos. 3-60 and 3-61 for low speed and high speed, respectively). Low-speed impact was simulated using Valmont Industries' pendulum and impact head with a crushable nose (Figures 2.6 and 2.7) at Valley, NE. Occupant impact criteria satisfied NCHRP Report 350, but a base connection remnant was 4.5 in., too tall to satisfy the AASHTO permissible limit of 4 in. [11]. Occupant impact criteria were determined satisfactory for high-speed impact by analysis using an extrapolation method recommended by FHWA [12, 13], and the study concluded with recommendations offered for modifications to satisfy the remnant height limit.

MwRSF has also used pendulum testing to evaluate alternative, non-proprietary brass breakaway couplings for Illinois light poles in a study published in 2011 [14]. While the focus of the study was to evaluate non-proprietary couplings, the testing program included one test to evaluate Transpo double-neck couplings, similar to those shown in Alaska DOT&PF standard details. Compliance testing and evaluation were performed to satisfy NCHRP Report 350 (test designation nos. 3-60 and 3-61 for low speed and high speed, respectively). Seven tests were performed at Valmont using a pendulum and impact head with a crushable nose (Figure 2.6) to simulate low-speed impact. Tall, heavy steel light poles were tested to evaluate maximum occupant impact velocities, and medium height, lighter aluminum luminaire poles were tested to evaluate structural adequacy and verify activation of frangible couplings. The study found that steel structures should be limited to 45 ft to maintain acceptable occupant impact velocity (OIV), but aluminum structures were acceptable from 30 to 55 ft tall.

Both the non-proprietary brass couplings and the Transpo couplings activated reliably, as shown in Figures 2.8 through 2.11. Three out of four Transpo couplings fractured at the upper neck, leaving remnants projecting approximately 6 in. above ground, violating the 4-in. limit in AASHTO [11], but were deemed acceptable based on an existing FHWA eligibility letter. It should be noted that only a subset of luminaire configurations was tested, and configurations different than those tested require case-by-case evaluations.

Figure 2.6 NYSDOT Aluminum Sign Testing – Pendulum and Crushable Nose [10]

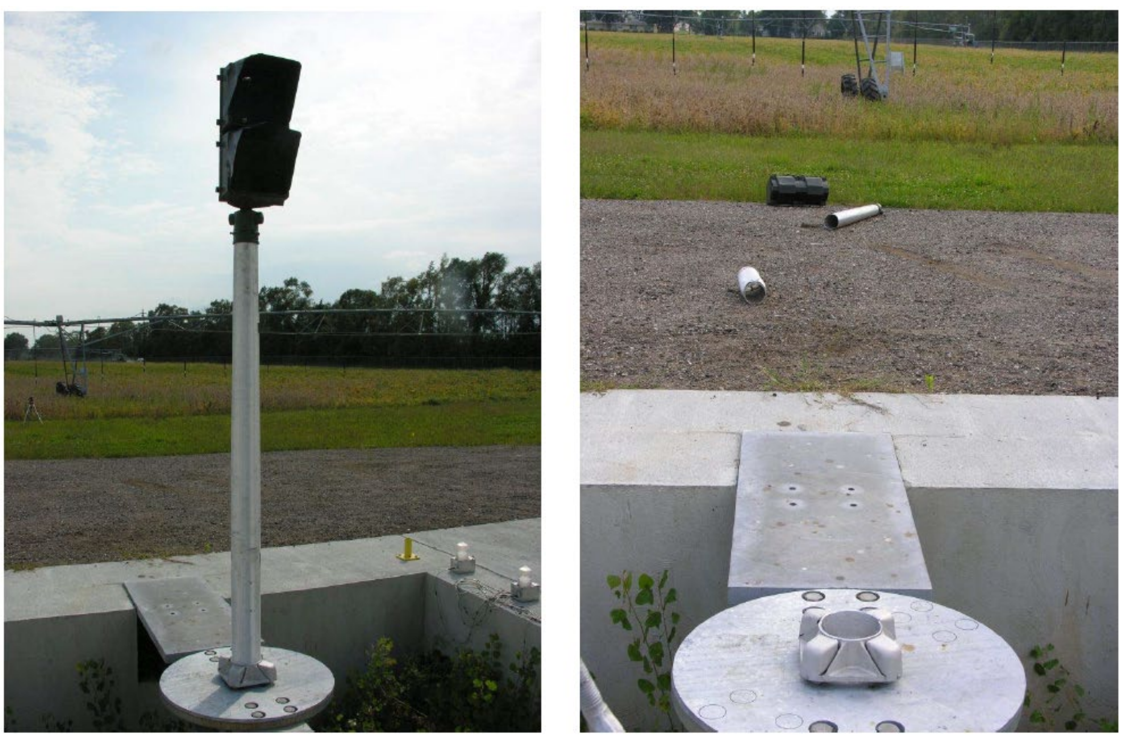

Figure 2.7 NYSDOT Aluminum Sign Testing – Pre-test and Post-test Specimen Photos [10]

Figure 2.8 IL DOT Non-proprietary Brass Breakaway Coupling Study – Non-proprietary Couplings Pre-test Photos [14]

Luminaire Pole　　　　Foundation

Figure 2.9 IL DOT Non-proprietary Brass Breakaway Coupling Study – Non-proprietary Couplings Post-test Photos [14]

Figure 2.10 IL DOT Non-proprietary Brass Breakaway Coupling Study – Transpo Double-neck Couplings Pre-test Photos [14]

Light pole Foundation

Figure 2.11 IL DOT Non-proprietary Brass Breakaway Coupling Study – Transpo Double-neck Couplings Post-test Photos [14]

The test with Transpo couplings was designated test no. BBC-4 in the testing program. The pendulum weighed 1,849 lb for the test and was instrumented with 3 accelerometer units for redundancy. When the pendulum impacted the test article, its momentum was transferred as an impulsive force acting simultaneously and in opposing equilibrium between the pendulum head and the pole shaft. Force magnitudes over time can be determined from the multiplication of recorded accelerations and the known pendulum mass. A deceleration log recorded during the impact is shown in Figure 2.12. The data is similar to that shown in the appendices of the report [14], except that the data in Figure 2.12 was processed using a CFC 60 filter, as recommended to determine impact forces, rather than using a CFC 180 filter, which is recommend to determine velocities and displacements by integration.

The peak deceleration in the plot is -12.9 g, which corresponds to an impulsive force of 23.9 kips acting between the pendulum and pole. The couplings used in the test were Pole-Safe Model No. 4100, which are functionally identical to the Model No. 5100 used by AK DOT&PF (see Figure 2.2). The difference between the models is due to the base connection. Model No. 4100 incorporates an internally threaded base for attachment to threaded extensions. Model No. 5100 has an externally threaded base for insertion into female anchors cast into concrete. Both models are fabricated with 1-in. diameters and machined to provide strategically weakened sections and a maximum ultimate restrained shear strength of 5.5 kips. The peak value compares well with the maximum shear capacity of the connectors, considering that deformation of the pole would be required to transmit load from the impact location to the couplings. Pole deformation requires inertial activation and slightly increases the peak force developed against the pendulum.

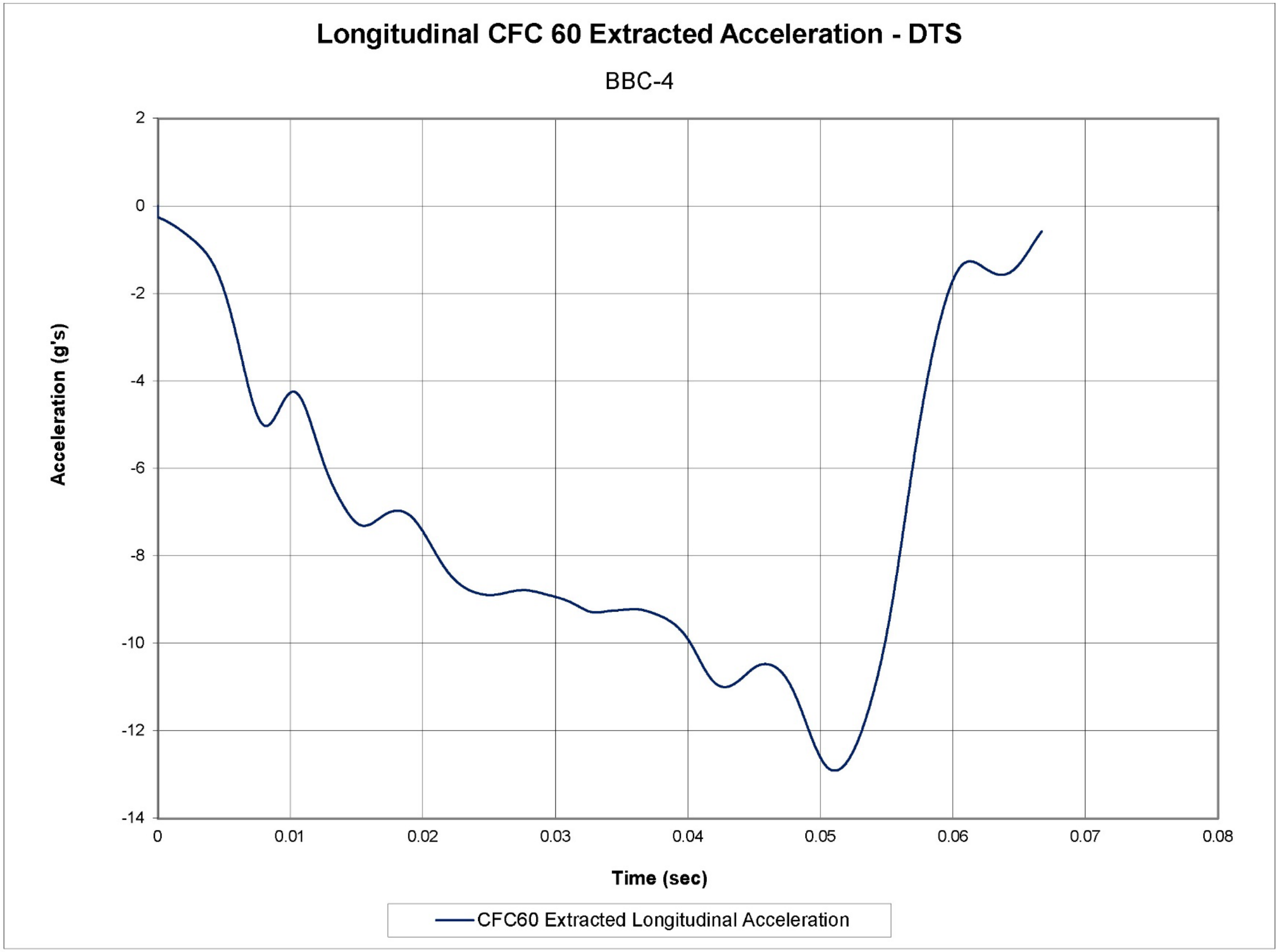

Figure 2.12 Longitudinal Deceleration (DTS-BF57H), Test No. BBC-4

2.4 Previous Soil-Embedded Foundation Impact Testing Research

Researchers at MwRSF have conducted foundation and anchorage studies including full-scale crash tests and component-level (bogie) tests for sponsors including state Departments of Transportation and the U.S. Department of Defense. DOT-sponsored research is publicly accessible, and the research most relevant to the present project evaluated foundations using bogie tests for weak (sandy) soil, strong soil, and with asphalt paving in a study published in 2015 [15]. “Weak” and “strong” (or “standard”) soils are defined in MASH [9], which refers to earlier definitions provided in NCHRP Report 350 [7]. All foundations were HSS sockets encased in reinforced concrete cylinders. Concrete cylinders were 12- and 15-in. diameter in strong soil. Only 12-in. diameter cylinders were tested in weak soil, although depths were increased relative to strong soil test articles.

Images are provided in Figures 2.13 and 2.14 for test nos. HTCB-17 and HTCB-18, respectively, in strong soil. Previous foundation specimens with a 12-in. diameter in strong soil in test nos. HTCB-10 and HTCB-11 experienced concrete breakout. In test no. HTCB-17, the foundation diameter was increased to 15 in., and the foundation was installed with a depth of 30 in. The specimen experienced a peak force of approximately 17.7 kips, a maximum dynamic deflection of approximately 1.2 in., and a permanent displacement of approximately 0.6 in. (see Figure 2.13). Damage to the specimen was negligible. In test no. HTCB-18, the 15-in. specimen depth was reduced to 24 in. The peak force was similar and slightly higher than the 30-in. depth specimen, at 18.7 kips. Plastic hinging in the weak post socketed into the foundation occurred in all strong soil tests but was less pronounced in test no. HTCB-18 due to significantly larger foundation displacement within the soil (see Figure 2.14). The foundation experienced a permanent lateral displacement of approximately 6 in. at the ground line, highlighting the potential sensitivity of foundation response to small changes in embedment depth. Summary tabulated results and bogie force-displacement plots are provided in Table 2.1 and Figure 2.15 for all strong-soil tests.

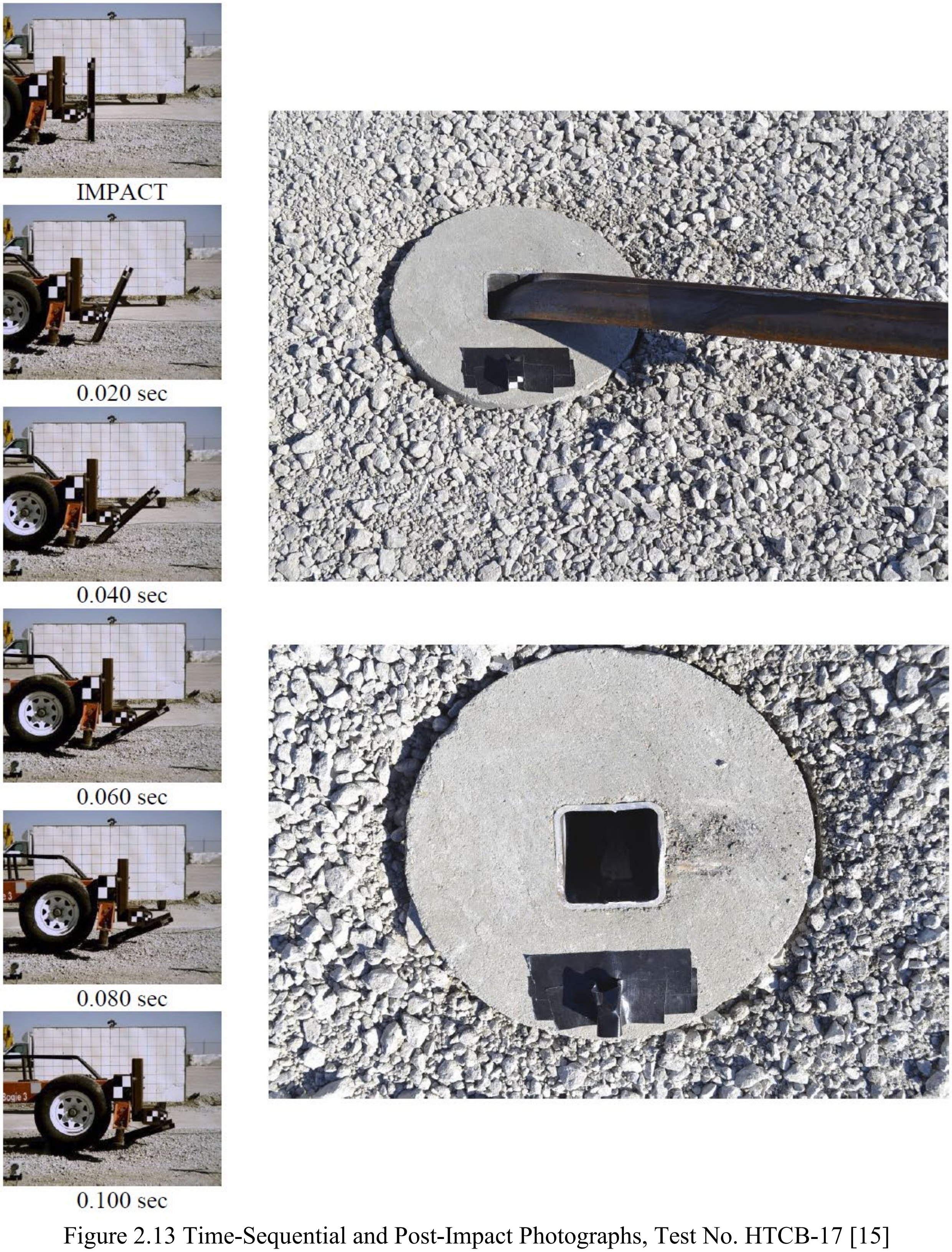

Figure 2.13 Time-Sequential and Post-Impact Photographs, Test No. HTCB-17 [15]

IMPACT

0.020 sec

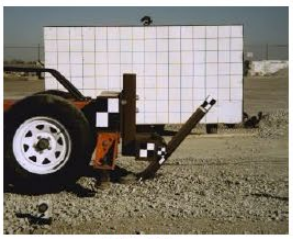

0.040 sec

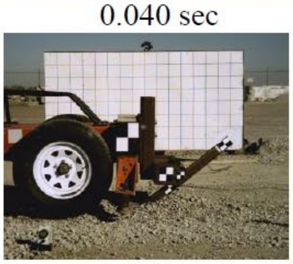

0.060 sec

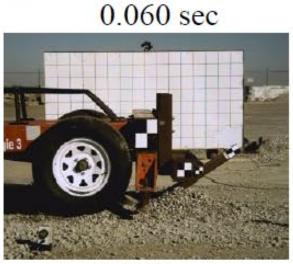

0.080 sec

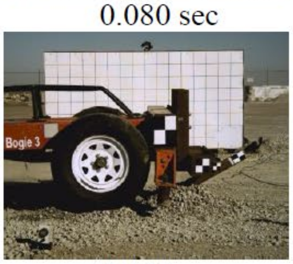

0.100 sec

Figure 2.14 Time-Sequential and Post-Impact Photographs, Test No. HTCB-18 [15]

Table 2.1 Dynamic Testing Summary, Foundations Installed in Strong Soil [15]

Test No.	Design	Diameter in.	Embed. Depth in.	Impact Velocity mph	Average Force kips			Peak Force kips	Total Energy kip-in.	Permanent Foundation Deflection in.	Foundation Damage
					@ 10"	@ 15"	@ 20"				
HTCB-10	J	12	30	20.6	10.8	8.3	6.8	20.7	149.6	2.2	Concrete cracking and fracture
HTCB-11	K	12	36	20.0	9.3	7.1	5.5	17.9	120.0	0.8	Concrete shear cracking
HTCB-17	M	15	30	20.8	8.6	6.8	5.8	17.7	141.6	0.6	None
HTCB-18	L	15	24	20.3	11.5	9.5	8.1	18.7	172.4	6.0	None

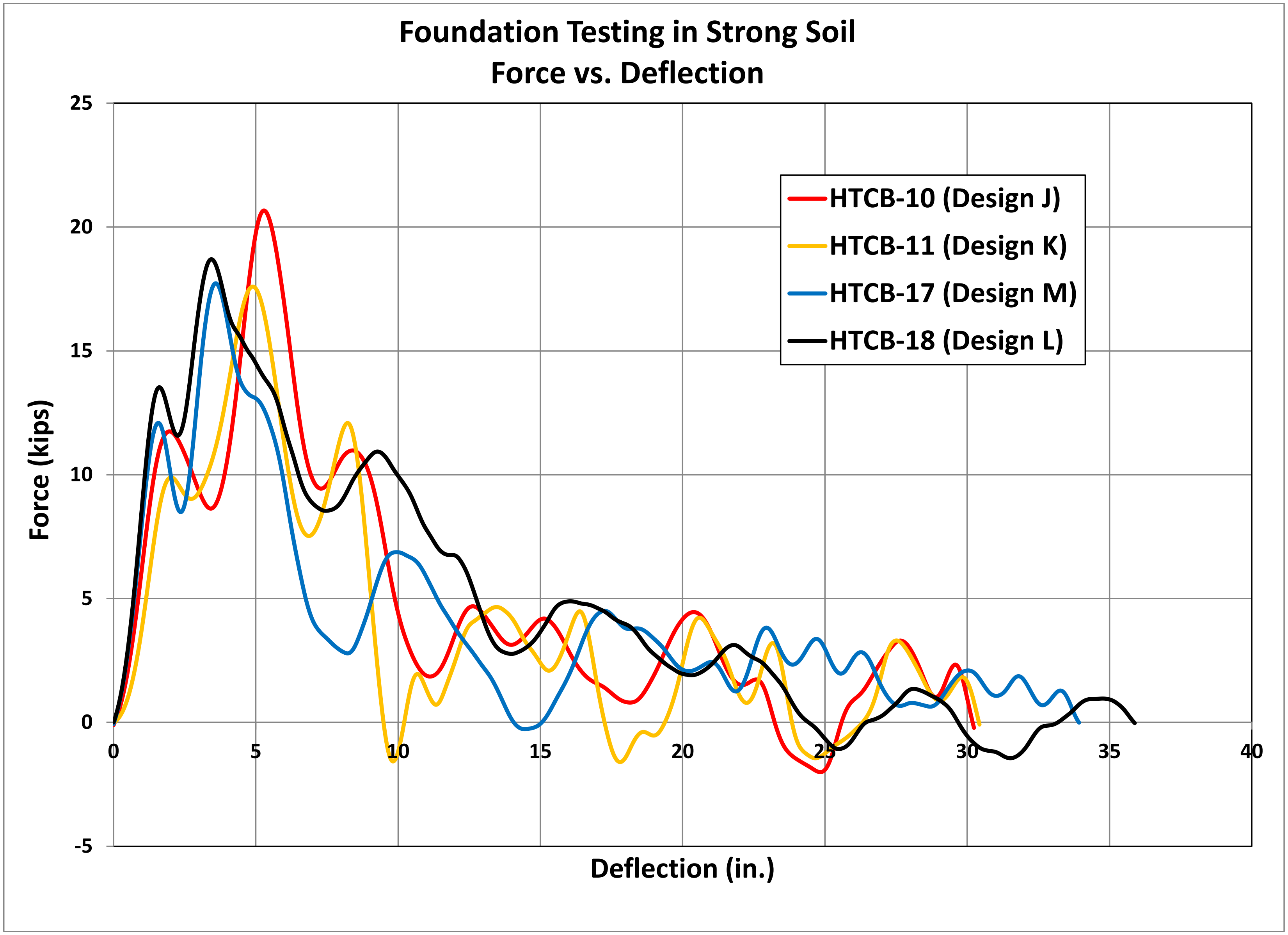

Figure 2.15 Force vs. Deflection, Foundations Installed in Strong Soil [15]

A total of five weak soil test articles, including four designs designated D through G, were subjected to bogie testing in test nos. HTCB-5 through HTCB-9. Foundation designs were similar, varying principally with reinforcing details intended to reduce or eliminate concrete breakout near the ground surface. All weak-soil foundation designs were 12-in. in diameter and embedded 60 in. deep. Images for test no. HTCB-9 are provided as a representative sample in Figure 2.16. The specimen experienced a peak force of approximately 13.7 kips, a maximum dynamic deflection of approximately 1.2 in., and a permanent displacement of approximately 1.1 in. (see Figure 2.13).

Summary tabulated results and bogie force-displacement plots are provided in Table 2.2 and Figure 2.17 for all strong weak tests. Peak forces were approximately 13 to 14 kips for weak soil, versus approximately 18 to 20 kips for strong soil, with the difference primarily attributed to the greater flexibility of the foundation due to surrounding soil deformations during impact events. These results suggest that a foundation will need to be proportioned with either a diameter greater than 12 in., a depth greater than 60 in., or both, in order to provide a resistance of at least 22 kips and activate frangible couplings typically used by AK DOT&PF.

Figure 2.16 Time-Sequential and Post-Impact Photographs, Test No. HTCB-9 [15]

Table 2.2 Dynamic Testing Summary, Foundations Installed in Weak Soil [15]

Test No.	Design	Impact Height in.	Impact Velocity mph	Average Force kips			Peak Force kips	Total Energy kip-in.	Permanent Foundation Deflection in.	Foundation Damage
				@ 10"	@ 15"	@ 20"				
HTCB-5	D	15	20.8	8.9	7.7	6.4	13.3	140.3	0.3	Shear cracking/fracture
HTCB-6	D	11	20.0	11.3	9.4	7.6	15.8	156.2	NA	Foundation fracture & socket bending
HTCB-7	E	11	20.7	10.0	8.4	6.8	13.6	144.6	0.8	Shear cracking/fracture
HTCB-8	F	11	20.9	9.8	8.0	6.4	13.3	143.9	0.8	Shear cracking/fracture
HTCB-9	G	11	20.8	9.8	7.7	6.1	13.9	130.2	1.1	Shear cracking/fracture

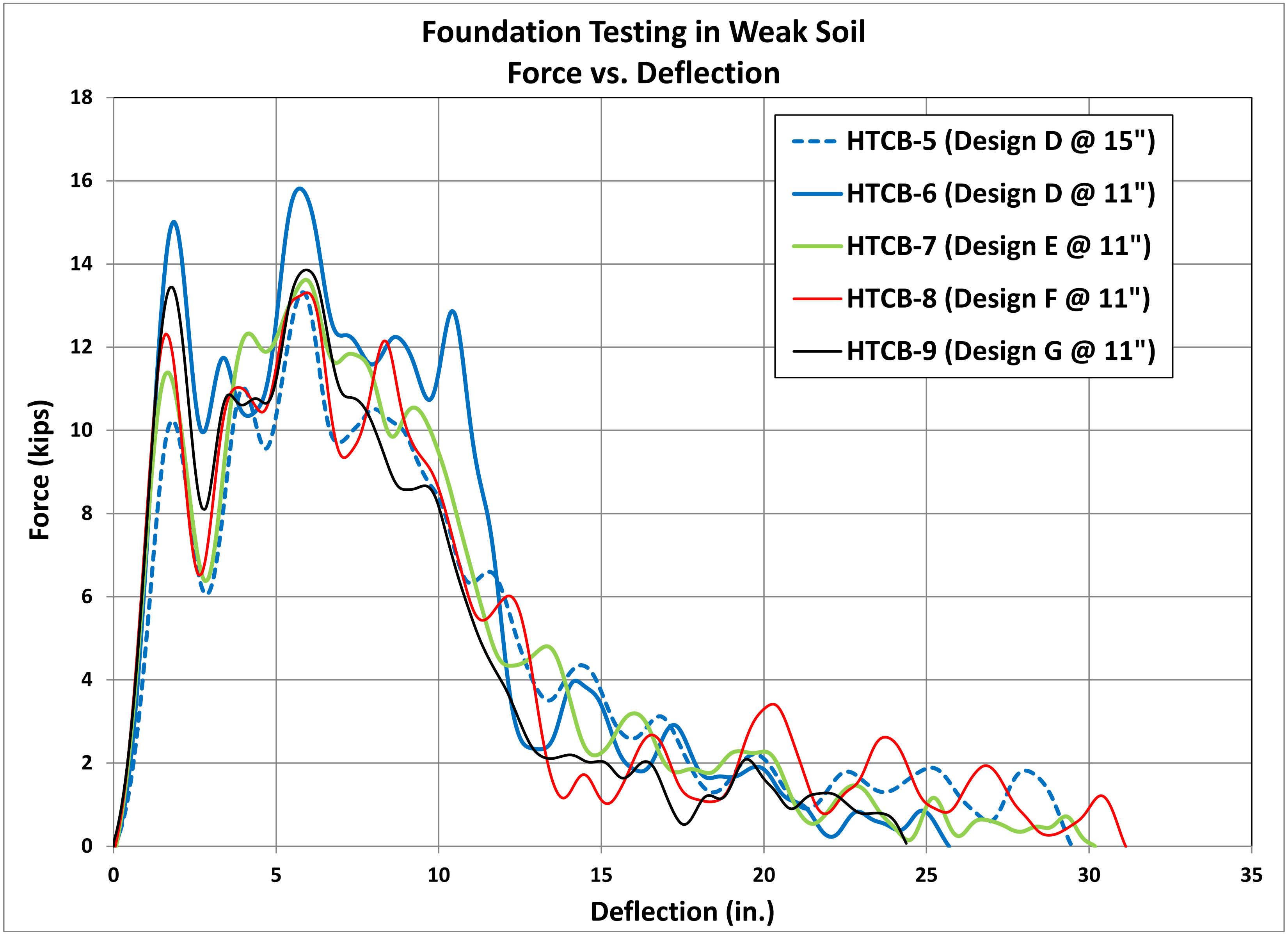

Figure 2.17 Force vs. Deflection, Foundations Installed in Weak Soil [15]

2.5 Review of State DOT Guidelines for Light Pole Foundations

2.5.1 Overview

A review of relevant literature and state DOT plans was conducted to gather and compile available information concerning soil conditions, SPT values, and state DOT practices in the design of light pole foundations. The goal was to gain insight into the current knowledge and practices regarding soil characteristics and testing methods, as well as to examine the design guidelines and standards followed by state DOTs in light pole foundation design. This information was sought to correlate available SPT data from AK DOT&PF to preliminary analytical models to guide foundation designs for testing and to assist in setting practical design configuration bounds.

Much of the data collection was performed by an undergraduate research assistant, Mr. Taylor Drahota, supported by the University of Nebraska-Lincoln Undergraduate Creative Activities and Research Experiences (UCARE) program. Key points are summarized in this chapter, but additional data collected as part of the UCARE project are provided in Appendix A through Appendix D. The review particularly sought to collect information regarding general design guidelines, characterization of soil types, foundation dimensions, and weak or saturated soil condition foundation design criteria.

Information was reviewed from 33 state DOTs, identified in Figure 2.18, with an effort to represent each of the four AASHTO Regions, and to prioritize states where weak and/or saturated soils were likely to be encountered. The scope of the light poles considered in this review involved pole heights of 40 ft or less and mast arm lengths of 15 ft or less. States were categorized according to the availability of guidance, as shown in Table 2.3, according to review focus topics shown in Table 2.4. A check mark in Table 2.4 indicates that detailed guidance and discussion was provided, while a bullet point indicates areas with some information available, but not as substantial as those receiving a check mark. Considerations for weak soil conditions were mentioned by 13 out of 33 reviewed states. Most states emphasized the need for personnel with expertise in foundations when encountering weak and/or saturated conditions.

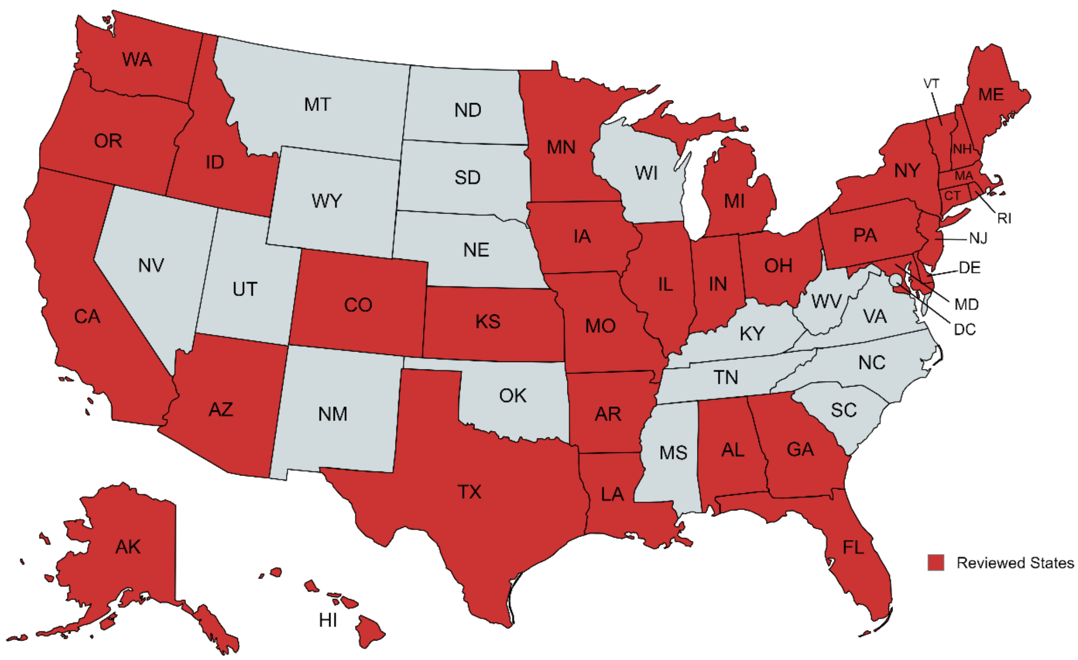

Figure 2.18 States Included in Light Pole Foundation in Weak Soil Review

States categorized as having “extensive guidance” in Table 2.3 had all four search criteria documented or at least three out of four with a substantial amount of information. Rhode Island serves as an example of a state with extensive guidance. States categorized as having “some guidance” provided between one and three sources of relevant information. Minnesota, with two out of the four search criteria, is an example of a state in this category. States categorized as having “no found guidance” are those for which an attempt to identify pertinent information was performed, but returned no results. The review was limited, and a result indicating no found guidance does not necessarily indicate that guidance is lacking for a particular state, but rather that the UCARE student was not able to locate it subject to his time constraints.

Table 2.3 State DOT Data Availability Summary Characterization

States with Extensive Guidance	States with Some Guidance	States with No Found Guidance	States Not Reviewed
CA	AL	GA	KY
CT	AK	ID	MS
OR	AZ	AR	MT
RI	DE	VT	NE
TX	FL		NV
MA	HI		NM
	IL		NC
	IN		ND
	IA		OK
	KS		SC
	MD		SD
	MI		TN
	MN		UT
	MO		VA
	NH		WV
	NJ		WI
	NY		WY
	OH		
	WA		
	LA		
	CO		
	ME		
	PA		
6	23	4	17

Table 2.4 State DOT Data Availability by Focus Topic

State	General Design Guidelines	Characterization of Soil Strength	Foundation Size with Soil Type	Weak or Saturated Soil Design
AL	•	•		
AK	✓	✓	✓	
AZ	✓	•	✓	•
AR				
CA	✓	✓	✓	
CO	✓	•	✓	•
CT	✓	✓	✓	•
DE	✓		✓	•
FL	✓	✓		✓
GA				
HI		✓		•
ID				
IL	✓	✓	✓	
IN			✓	
IA		✓	✓	
KS	✓			✓
LA	✓			
ME		✓	✓	
MD		✓	✓	
MA	✓	✓	✓	✓
MI		✓	✓	
MN	✓		✓	
MO			✓	
NH	✓		✓	
NJ	✓	•		✓
NY	•			✓
OH		✓	✓	
OR	✓	✓		✓
PA	✓	✓	✓	
RI	✓	✓	✓	•
TX		✓	✓	✓
VT				
WA		✓		

2.5.2 General Design Guidelines

A general design guideline is defined as a note or recommendation that was available to aid the understanding of criteria considered when designing or constructing a light pole and its foundation. Breadth and depth of detailed information varied significantly among state DOT guidelines. Some states, such as the Oregon DOT, provided an abundance of information. For example, Good, Average, and Poor soils were defined as having angles of friction at least 35 deg., between 35 and 25 deg., and less than 25 degrees, respectively. Poor soil was additionally defined to provide a design strength of 1500 psf.

For a significant proportion of states (14 out of 33), no specific recommendations or notes regarding weak soil conditions were identified. These states most likely design and construct light poles on a case-by-case basis with reliance on consulting services from Geotechnical specialists in each case. Alternatively, these agencies may restrict guidance for these conditions to internal use only and not provide standards readily accessible to public internet searches.

2.5.3 Characterization of Soil Parameters

Among the 33 reviewed states, 21 states offered soil condition categorization guidance, encompassing soil density or consistency, ranges for uncorrected or corrected SPT blow counts (N), shear strengths (tons per square foot, tsf, or kips per square foot, ksf, or lb per square foot, psf), angles of friction (deg.), or unit weights (lb per cubic foot, pcf). Example guidance from Oregon DOT to categorize cohesive and cohesionless soils is provided in Figures 2.19 and 2.20. Additionally, some states provided information on the friction coefficient between the soil and foundation interface. Recommended coefficients varied from 0.25 for silt/clay to 0.7 for bedrock.

Description	SPT N'60* value (blows/ft.)	Approximate Angle of Internal Friction (Φ)**	Moist Unit Weight (pcf)	Field Approximation
Very Loose	0 – 4	< 30	70 – 100	Easily penetrated many inches (>12) with ½ inch rebar pushed by hand.
Loose	4 – 10	30 – 35	90 – 115	Easily penetrated several inches (>12) with ½ inch rebar pushed by hand.
Medium	10 – 30	35 – 40	110 – 130	Easily to moderately penetrate with ½ inch rebar driven by 5 lb. hammer.
Dense	30 – 50	40 – 45	120 – 140	Penetrated one foot with difficulty using ½ inch rebar driven by 5 lb. hammer.
Very Dense	> 50	> 45	130 – 150	Penetrated only a few inches with ½-inch rebar driven by 5 lb. hammer.

* N'_{60} is corrected for overburden pressure and energy

** Use the higher phi angles for granular material with 5% or less fine sand and silt.

Figure 2.19 Oregon DOT Characterization Guidance for Cohesionless Soil

Consistency	SPT N60 value (blows/ft.)	Approximate Undrained Shear Strength (psf)	Moist Unit Weight (pcf)	Field Approximation
Very Soft	< 2	< 250	100 – 120	Squeezes between fingers when fist is closed; easily penetrated several inches by fist.
Soft	2 – 4	250 – 500		Easily molded by fingers; easily penetrated several inches by thumb.
Medium Stiff	5 – 8	500 – 1000	110 – 130	Molded by strong pressure of fingers; can be penetrated several inches by thumb with moderate effort.
Stiff	9 – 15	1000 – 2000	120 – 140	Dented by strong pressure by fingers; readily indented by thumb but can be penetrated only with great effort.
Very Stiff	16 – 30	2000 – 4000	125 – 140	Readily indented by thumbnail.
Hard	31 – 60	4000 - 8000	130 – 140	Indented with difficulty by thumb nail
Very Hard	> 60	> 8000		

Figure 2.20 Oregon DOT Characterization Guidance for Cohesive Soil

2.5.3.1 Consistency/Relative Density and SPT Ranges

Multiple states provided a density chart for cohesive soils, generally conforming to the categories and corresponding SPT ranges shown in Table 2.5. Minor differences were observed towards the upper end of SPT values, where all states, except for Oregon and Washington, lacked a “Very Hard” SPT range. However, in the interest of comprehensiveness, the table encompasses all ranges covered in the state DOT review. AK DOT&PF is therefore consistent with other state DOTs by having historically adopted the categorization as presented in Table 2.5, up to a consistency level of “Hard” for cohesive soils.

Table 2.5 Common SPT Ranges and Consistency Classifications for Cohesive Soils

SPT (Blows/ft)	Consistency
< 2	Very Soft
2-4	Soft
5-8	Medium Stiff
9-15	Stiff
16-30	Very Stiff
31-60	Hard
> 60	Very Hard

Provisions for cohesionless soils were generally in a similar form, correlating descriptive terms for “consistency” with a range of SPT values, similar to Table 2.6. Except for the Washington DOT, which included “Medium Dense” and “Dense” ranges defined by 11-24 and 25-50 blows respectively, the ranges and corresponding descriptions were uniform across all reviewed states. The uniformity observed across reviewed states for both cohesive and cohesionless soil consistency characterization suggests that a majority of DOTs follow a common standard when categorizing soil for geotechnical design based on common in-situ data.

Table 2.6 Common SPT Ranges and Density Classifications for Cohesionless Soils

SPT (Blows/Foot)	Consistency
0-4	Very Loose
5-10	Loose
11-30	Medium Dense
31-50	Dense
> 50	Very Dense

2.5.3.2 Friction Angle and SPT Ranges

The reviewed state DOTs adopted various methods and references to relate soil friction angles to SPT blow counts. The California DOT, Caltrans, provided plots intended to capture property correlations to SPT results for various types of soils, as shown in Figure 2.21. Friction angle correlations to SPT blow count values collected across the reviewed DOTs ranged from 25-35 degrees for an SPT value of 0-10, 30-40 degrees for an SPT value of 10-30, 33-45 degrees for an SPT value of 30-50, and 37-50 degrees for SPT values exceeding 50.

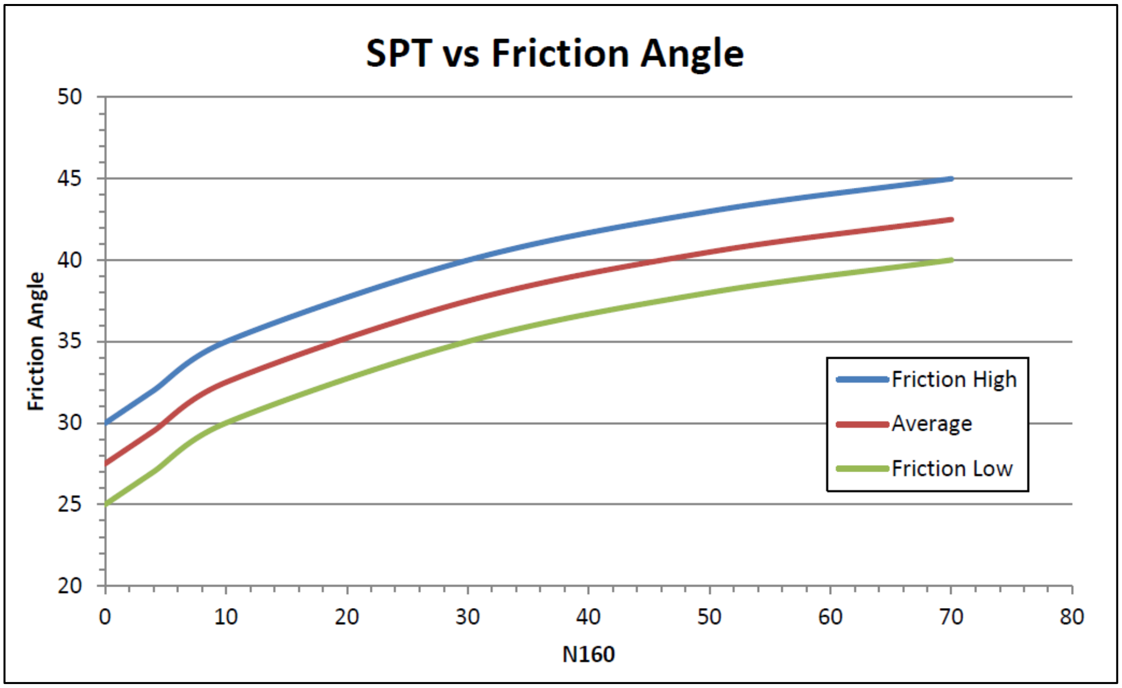

Figure 2.21 Correlation of SPT Values to Drained Friction Angle of Granular Soil, Caltrans Geotechnical Manual Guidelines - Soil Correlations

2.5.3.3 Undrained Shear Strength vs. SPT Ranges

The approximate relationship between undrained shear strength and SPT values can be extrapolated by utilizing data values and tables from various states. One example is shown in Figure 2.22 from Caltrans. It is believed that undrained shear strength is more linearly related to SPT than friction angle. Other agencies adopted alternate correlations, so that undrained shear strength for cohesive soils can be estimated to be approximately 0-0.45 tsf for SPT values of 0-4, 0.25-0.65 tsf for SPT values of 4-8, 0.5-1.0 tsf for SPT values of 8-15, 1-2.25 tsf for SPT values of 15-30, and 2-4 tsf for SPT values exceeding 30.

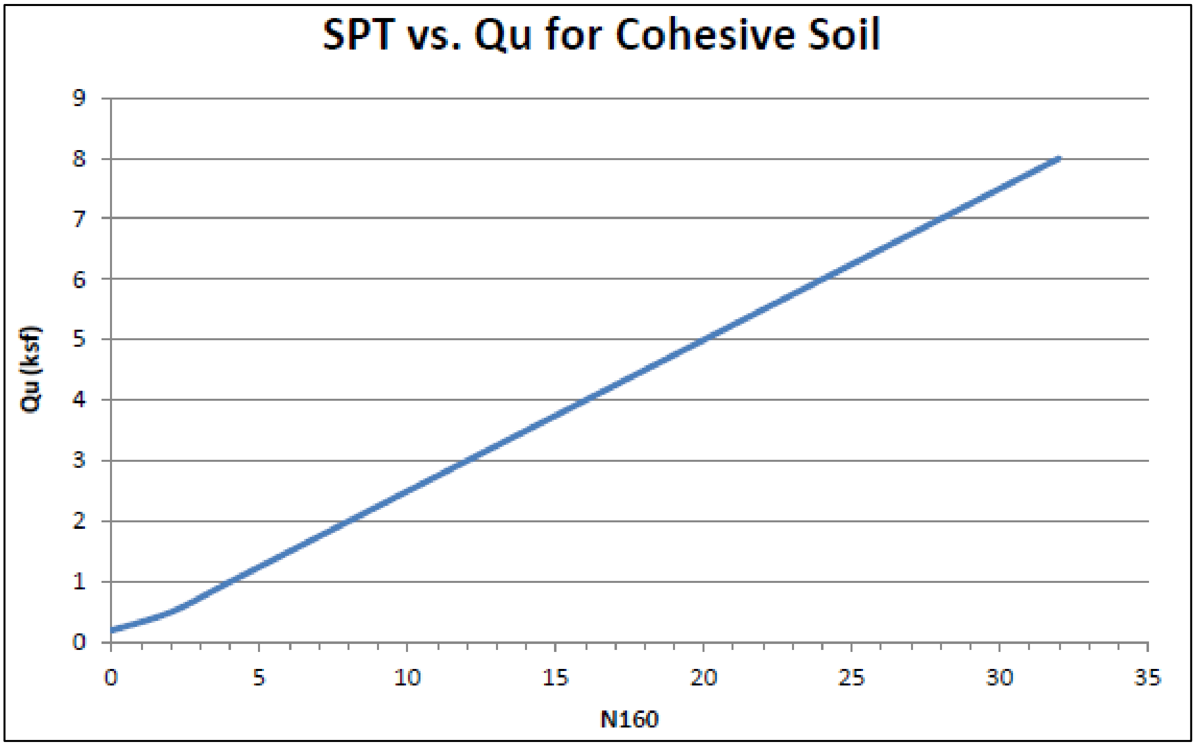

Figure 2.22 Correlation of SPT Values to Unconfined Compressive Strength, Caltrans Geotechnical Manual Guidelines - Soil Correlations

2.5.3.4 Density and SPT Ranges

States were more sparse and less uniform in their relations of soil unit weight and SPT ranges. A few states, such as Maine and Oregon, provided relatively detailed information regarding moist unit weight values based on SPT and soil type. For cohesive soils, unit weights ranged from 100 to 140 pcf corresponding to blow counts of 0 to 60. In the case of cohesionless soils, unit weights varied from 70 to 150 pcf based on blow counts ranging from 0 to 50. Caltrans also provided charts for moist unit weight values based on SPT in cases of granular and cohesive soil, as shown in Figure 2.23. Unit weight values based on SPT for cohesive soil are shown in Figure 2.24.

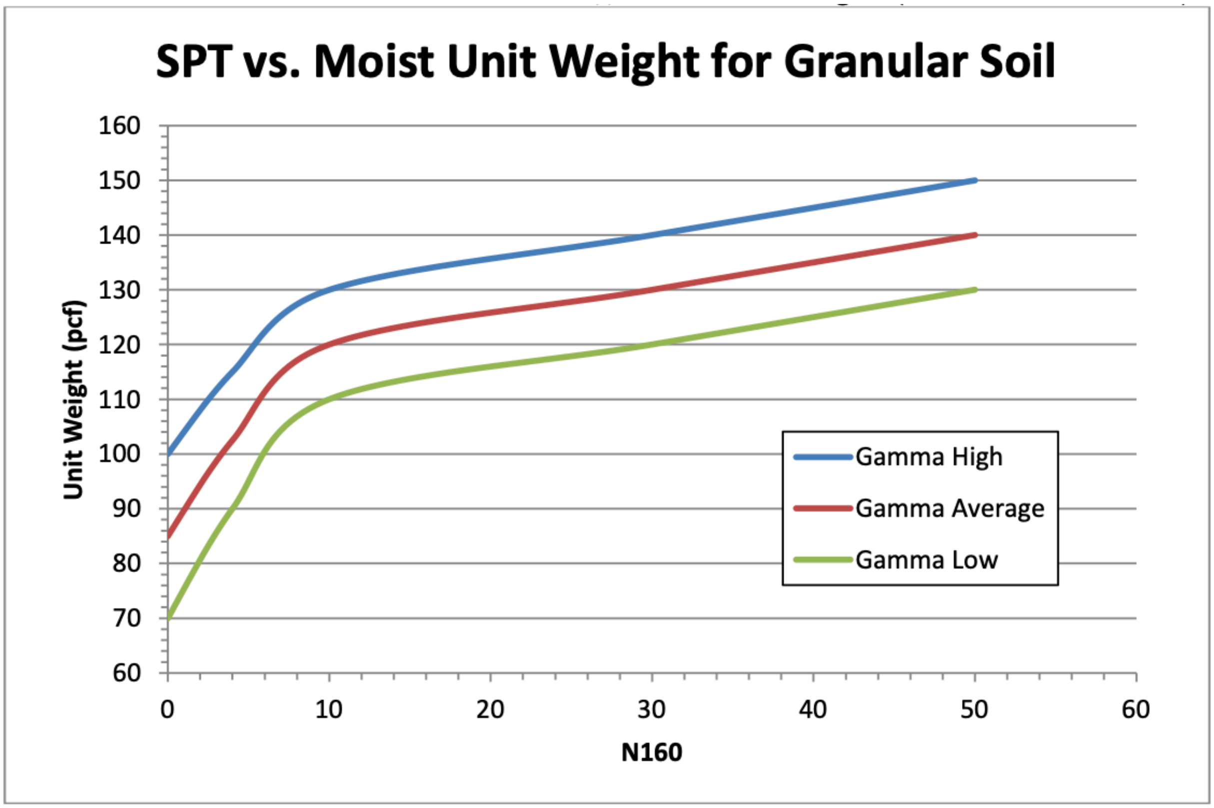

Figure 2.23 California DOT SPT vs. Moist Unit Weight for Granular Soil, Caltrans Geotechnical Manual Guidelines - Soil Correlations

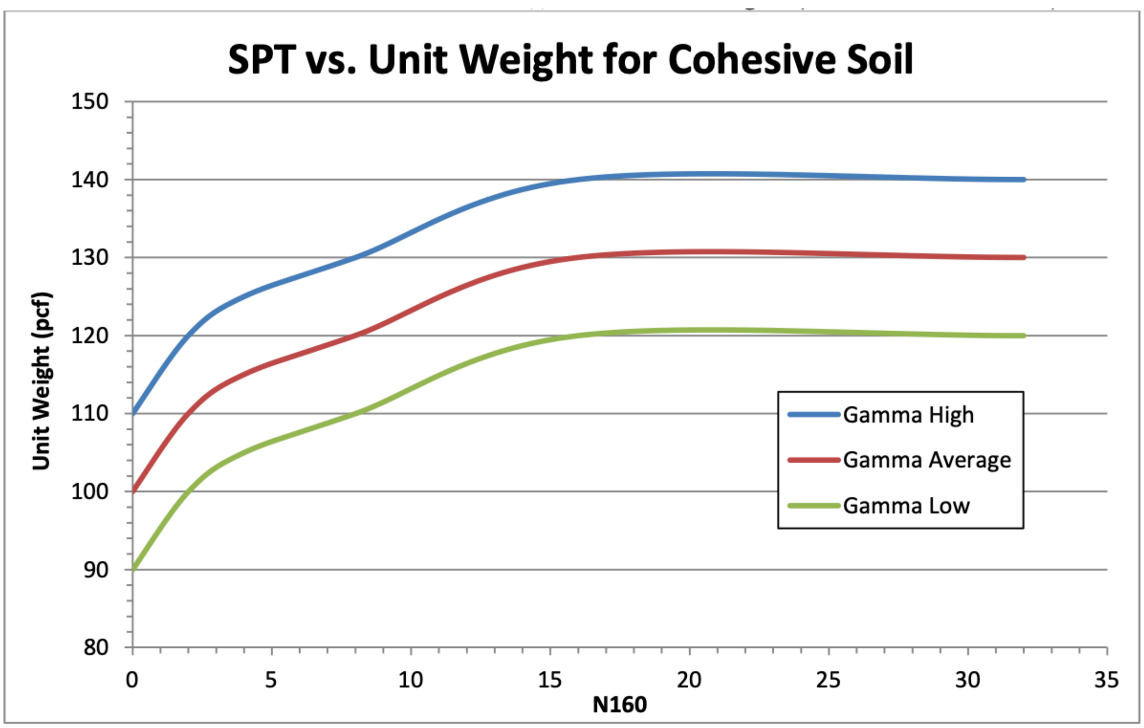

Figure 2.24 California DOT SPT vs. Unit Weight for Cohesive Soil, Caltrans Geotechnical Manual Guidelines - Soil Correlations

2.5.4 Foundation Dimensions

Typical foundation plans published by state DOTs showed varying ranges between the recommended minimum and maximum depths (refer to Appendix C for additional details). Some states, such as Delaware and New Hampshire, specified only a single depth, likely selected to cover a "worst-case" scenario. However, other states, such as Maryland and Texas, specified standard designs with minimum and maximum depths ranging 4 ft or more. These variations were primarily attributed to specific design considerations and field conditions, such as pole heights and/or mast arm lengths, environmental loading, and on-site soil characteristics.

The most common minimum and maximum depths were 6 ft and 8 ft, respectively. Extreme values noted from the review were 4 ft for the smallest minimum depth and nearly 12 ft for the largest maximum depth. The most common minimum and maximum diameters were 24 in. and 36 in., respectively. The extreme value for minimum diameter was 18 in., but no states in the review specified a maximum diameter greater than the common value of 36 in.

2.5.5 Weak and Saturated Soil Considerations

Saturated soil can be particularly detrimental to geotechnical designs as it lowers the soil's mechanical resistance to applied load by reducing its effective shear strength. However, information was sparse in state DOT guidance to address weak and/or saturated soil conditions. Data collected from state DOTs is provided in Appendix D. Additionally, a survey of selected state DOTs by the AASHTO Subcommittee on Traffic Engineering in 2015 was discovered during the review and is provided in Appendix E. Based on the reviewed data, states tend to design foundations for worst acceptable field conditions, avoid placing foundations on or in poor soil conditions, or engage the services of geotechnical specialists when other solutions are not viable.

2.6 Recommended Correlations of SPT to Other Soil Properties

As the primary source of information available to characterize soils was boring logs with SPT data, the review of property correlations in literature focused on characterizing soils primarily based on only this readily available information. The following key parameters related to soil properties are of particular interest in assessing the response of a pole foundation under vehicle impact load:

- Unit weight: The unit weight or bulk density of soil is used to determine its mass and its ability to provide inertial resistance against impact loads.
- Elastic modulus: The elastic modulus of the soil represents its stiffness or ability to deform elastically under stress. It affects the resulting deformations in the soil and foundation system.
- Poisson's ratio: Poisson's ratio describes the ratio of unconfined lateral strain to imposed axial strain in soil.
- Friction angle: The friction angle is a measure of the shear strength and internal frictional resistance of the soil. It affects the soil's ability to withstand lateral loads and resist sliding or failure.
- Dilation angle: The dilation angle represents the tendency of the soil to expand or contract under shear stress. It is relevant in assessing the soil's response to dynamic loading, such as vehicle impacts.
- Cohesion: Cohesion is the internal strength or bonding between soil particles in cohesive soils. It contributes to the soil's shear strength and resistance against deformations.

The following subsections explore recommended correlations between various granular soil properties and SPT results. By examining existing literature and guidelines, the aim was to identify established relationships between SPT values and important soil properties such as density, shear strength, angle of friction, and cohesion, and thereby facilitate numerical simulation, design, and evaluation of light pole foundations.

2.6.1 SPT Correction

During an SPT test, a 140-lb hammer is dropped from a height of 30 in. to strike a split-spoon sampler. The SPT sampler has an outer diameter of 2 in. and an inner diameter of 1.5 in. The test measures the number of blows required to drive the SPT shoe 12 in. into the ground.

It is important to note that the SPT does not incorporate any stress or strain measurement mechanism, and therefore, it does not provide direct measurements of soil strength or deformation modulus. However, it is observed that stronger or harder soils typically exhibit greater penetration resistance, indicated by higher SPT blow counts. Thus, engineers have utilized empirical correlations based on SPT data to estimate engineering properties of soils.

Correction factors for SPT values are commonly used to adjust the measured blow counts to account for various factors that can affect the test results. These correction factors help ensure consistency and accuracy in interpreting SPT data. An N_{60} value can be determined from a field-measured, uncorrected N value using the following equation:

- Energy efficiency correction factor (η_H): accounts for differences in energy efficiency between different SPT hammers and equipment.
- Borehole diameter correction factor (η_B): accounts for the influence of borehole size on the energy transferred to the soil during the test.
- Sampler factor (η_S): adjusts measured SPT blow counts based on the specific type of SPT sampler used during the test.

- Rod length correction factor (η_R): accounts for additional energy losses due to longer rod lengths.

These factors can be determined obtained from various sources, such as Figure 2.25.

Table 17.3 Variations of η_H, η_B, η_S, and η_R [Eq. (17.5)]

1. Variation of η_H

Country	Hammer type	Hammer release	η_H (%)
Japan	Donut	Free fall	78
	Donut	Rope and pulley	67
United States	Safety	Rope and pulley	60
	Donut	Rope and pulley	45
Argentina	Donut	Rope and pulley	45
China	Donut	Free fall	60
	Donut	Rope and pulley	50

2. Variation of η_B

Diameter		
mm	in.	η_B
60–120	2.4–4.7	1
150	6	1.05
200	8	1.15

3. Variation of η_S

Variable	η_S
Standard sampler	1.0
With liner for dense sand and clay	0.8
With liner for loose sand	0.9

4. Variation of η_R

Rod length (m)	η_R
>10	1.0
6–10	0.95
4–6	0.85
0–4	0.75

Figure 2.25 SPT Correction Factors η_H, η_B, η_S, and η_R [16]

An overburden correction factor (C_N) is then applied to adjust blow counts based on the effective stress conditions at the depth of the test. In the case of sand, the corrected N_{60} value, $(N_1)_{60}$, can be determined using the following equation:

$$(N_1)_{60} = C_N(N_{60}) \tag{2}$$

C_N denotes the overburden correction factor obtained from one of several equations derived from empirical observations. Das [16] presents a summary of available equations, including one equation from Liao and Whitman (1986) [17], three equations from Skempton (1986) [18], one equation from Seed et al. (1975) [19], one equation from Peck et al. (1974) [20], and two equations from Bazaraa (1967) [21]. Ultimately, the research team estimated that the combination of all correction factors resulted in a net aggregate correction factor of approximately 1.0.

2.6.2 Elastic Modulus and SPT

Several studies have explored the relationship between SPT blow counts and the elastic modulus to establish empirical correlations (e.g., [22-26]). In the current study, the elastic modulus of silty sand was estimated using Table C10.4.6.3-1 from the AASHTO LRFD Bridge Design Specifications [1]. This table provides guidance on estimating the elastic modulus based on soil type and SPT blow count.

Soil Type	Typical Range of Young's Modulus Values, E_s (ksi)	Poisson's Ratio, ν (dim)
Clay:		0.4–0.5 (undrained)
Soft sensitive	0.347–2.08	
Medium stiff to stiff	2.08–6.94	
Very stiff	6.94–13.89	
Loess	2.08–8.33	0.1–0.3
Silt	0.278–2.78	0.3–0.35
Fine Sand:		0.25
Loose	1.11–1.67	
Medium dense	1.67–2.78	
Dense	2.78–4.17	
Sand:		
Loose	1.39–4.17	0.20–0.36
Medium dense	4.17–6.94	
Dense	6.94–11.11	0.30–0.40
Gravel:		
Loose	4.17–11.11	0.20–0.35
Medium dense	11.11–13.89	
Dense	13.89–27.78	0.30–0.40

Estimating E_s from $SPT\ N$ Value	
Soil Type	E_s (ksi)
Silts, sandy silts, slightly cohesive mixtures	0.056 $N1_{60}$
Clean fine to medium sands and slightly silty sands	0.097 $N1_{60}$
Coarse sands and sands with little gravel	0.139 $N1_{60}$
Sandy gravel and gravels	0.167 $N1_{60}$

Figure 2.26 Correlation of Elastic Constants and SPT Values, Table C10.4.6.3-1 from AASHTO LRFD Bridge Design Specifications [1]

2.6.3 Friction Angle and SPT

Researchers have proposed various empirical correlations in the literature to estimate the friction angle based on the SPT blow count. These formulations produce estimates that varied significantly, an outcome mirrored in guidance adopted among DOTs. Figure 2.27 shows the correlations of friction angle and SPT blow count from various research studies, including Wolff (1989) [27], Peck et al. (1974) [20], Hatanaka and Uchida (1996) [28], Mayne et al. (2001) [29], and JRA (1996) [30].

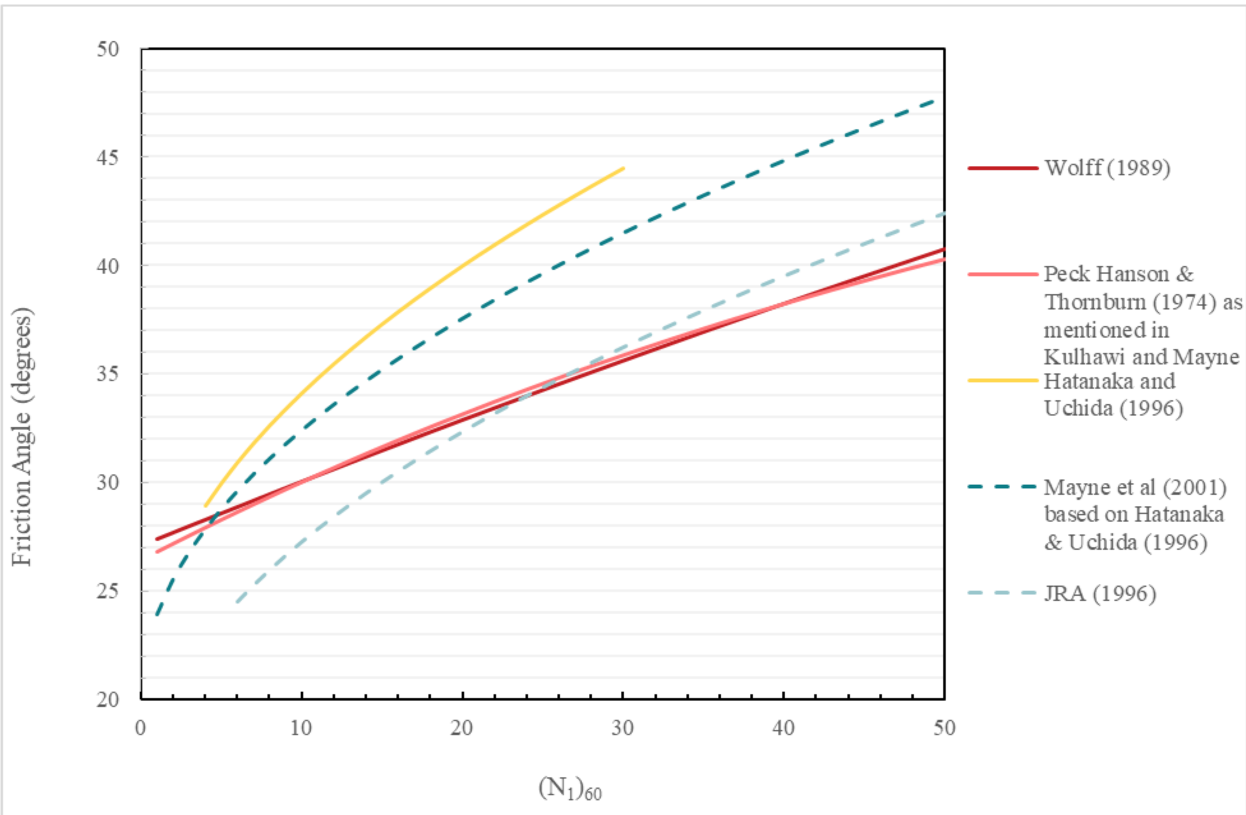

Figure 2.27 Recommended Correlations of Friction Angle and SPT Values

Peck et al. (1974) conducted a study on the behavior of foundation soils under static and dynamic loads. As part of this study, they investigated the correlation between SPT blow count and friction angle. The findings indicated a general trend of increasing friction angle with higher SPT blow counts. However, the correlation varied depending on the soil type and conditions.

Wolff (1989) conducted a comprehensive study to develop correlations between SPT blow count and friction angle for different soil types. The study involved field investigations and laboratory testing of various soils. The proposed correlations considered soil properties such as density, grain size, and soil classification.

Hatanaka and Uchida (1996) conducted field and laboratory tests to develop a correlation between SPT blow count and friction angle for sandy soils. The study focused on evaluating the influence of relative density and grain size on the correlation.

Mayne et al. (2001) performed an extensive research study to investigate the correlation between SPT blow count and friction angle for different soil types. The study incorporated a large database of SPT and friction angle data from various geotechnical projects.

Japan Road Association (JRA) (1996) conducted research to establish design guidelines for road structures in Japan. As part of their study, they developed correlations between SPT blow count and friction angle specifically for Japanese soil conditions.

Lastly, the AASHTO LRFD Bridge Design Specifications recommend ranges of friction angles corresponding to corrected SPT values, as shown in Figure 2.28. The ranges approximately bracket the results from the various methods mentioned above, except for the JRA values at low SPT values.

$N1_{60}$	ϕ_f
<4	25–30
4	27–32
10	30–35
30	35–40
50	38–43

Figure 2.28 Correlation of SPT $(N_1)_{60}$ Values to Drained Friction Angle of Granular Soil, Table 10.4.6.2.4-1 from AASHTO LRFD Bridge Design Specifications [1]

2.6.4 Unit Weight and SPT

The unit weight or density of soil is generally expected to correlate positively with SPT values – i.e., denser soils with higher unit weights generally exhibit higher SPT values, indicating stiffer, more resistant material. The correlation between unit weight and SPT results is not directly proportional and is influenced by other factors such as grain size distribution, the presence of fines, soil structure, stress history, and moisture content. An example of recommended correlations for cohesionless soil that are considered fairly reliable is presented in Figure 2.29. This guidance was used in combination with guidance collected from the review of state DOTs (recall Section 2.5.3.4) to establish values for preliminary analytical modeling.

SPT N-value		**0 to 4**	**4 to 10**	**10 to 30**	**30 to 50**	**>50**
Compactness		**very loose**	**loose**	**medium**	**dense**	**very dense**
Relative Density, D_r (%)		0 to 15	15 to 35	35 to 65	65 to 85	85 to 100
Angle of Internal Friction,φ(°)		<28	28 to 30	30 to 36	36 to 41	>41
Unit Weight (moist)	**pcf**	<100	95 to 125	110 to 130	110 to 140	>130
	kN/m^3	<15.7	14.9 to 19.6	17.3 to 20.4	17.3 to 22.0	>20.4
Submerged unit weight	**pcf**	<60	55 to 65	60 to 70	65 to 85	>75
	kN/m^3	<9.4	8.6-10.2	9.4 to 11.0	10.5 to 13.4	>11.8

Figure 2.29 Recommended Correlations of Unit Weight and SPT Values [20, 26]

Chapter 3 Preliminary LS-DYNA Modeling

3.1 Overview

The evaluation and design of roadside hardware, such as breakaway light poles, often requires full-scale crash tests to assess their performance in impact events. However, the cost and complexity associated with conducting such tests imposes limitations on the extent of evaluation that can be performed for a system. Alternative methods of evaluation, such as finite element analysis, can supplement evaluation efforts and reduce the needed testing scope by identifying critical configurations. Although computer simulation has become more prominent over time, numerical modeling alone has not been deemed sufficiently robust to entirely replace testing. A critical challenge in modeling soil-dependent systems, including pole foundations, relates to accurately representing the mechanical and inertial behavior of the soil and its interaction with the foundation when subjected to vehicle impacts.

In this study, a preliminary evaluation of the response of a soil-embedded foundation under impact was conducted using an LS-DYNA finite element analysis model. The model was developed using LS-DYNA Version 10.1 [31, 32] and had various components, which are described below. Preliminary models were developed for both a steel post embedded in a concrete foundation, as well as a pole and couplings connecting to the foundation. Both configurations modeled a soil medium surrounding the foundation.

3.2 Model Components

3.2.1 Post

The post was initially modeled as an ASTM A36 steel W6x16 section. This selection was based on previous research by Coon and Reid (1999) [33] and Pajouh et al. (2018) [34]. These studies showed that this type of post does not yield when displaced through a strong soil. However, it was acknowledged that when embedded in a rigid concrete foundation, post yielding may occur. The main objective of choosing this post was to preliminarily observe rotational movement during an impact event, intending to isolate the soil resistance from the resistance provided by the post and foundation.

The steel post was modeled with fully integrated shell elements, with a maximum element size of 10 mm (0.39 in.), and assigned a *MAT_PIECEWISE_LINEAR_PLASTICITY material formulation with parameters as shown in Table 3.1. In these initial simulations, the yield strength of the steel post was set to 47 ksi, which was derived from prior research [34]. As the portion of the post cast into the concrete was not expected to significantly influence the simulation results, the post was only modeled for the length extending above the top of the foundation. The base of the modeled post was rigidly constrained to the top surface of the foundation.

Table 3.1 Piecewise Linear Plasticity Material Model Input Parameters for Steel Post

Material parameter	**Value**							
Density (lb/in^3)	0.284							
Young's modulus (ksi)	29007							
Poisson's ratio	0.28							
Effective plastic strain	ep1	ep2	ep3	ep4	ep5	ep6	ep7	ep8
	0.000	0.0152	0.0226	0.0407	0.069	0.0983	0.1345	0.7093
Effective stress (ksi)	es1	es2	es3	es4	es5	es6	es7	es8
	47.00	47.60	54.94	64.02	72.08	76.87	80.60	110.28

3.2.2 Foundation

The foundation in the model was represented using solid elements with a fine mesh, with a maximum size of 25 mm (1 in.). The cylindrical foundation diameter was 30 in., matching the average diameter of the typical AK DOT&PF shown in Figure 2.1. Although the minimum depth specified in the AK DOT&PF foundation standard was 7 ft, AK DOT&PF personnel indicated that a depth of 6 ft had been used successfully in the past. Considering this indicated historic reliability, and that this depth was also common among reviewed DOTs elsewhere in the US, a depth of 6 ft was selected for preliminary modeling. Since no concrete breakout was anticipated in the test, the foundation was modeled as rigid, and no reinforcement was included in the model.

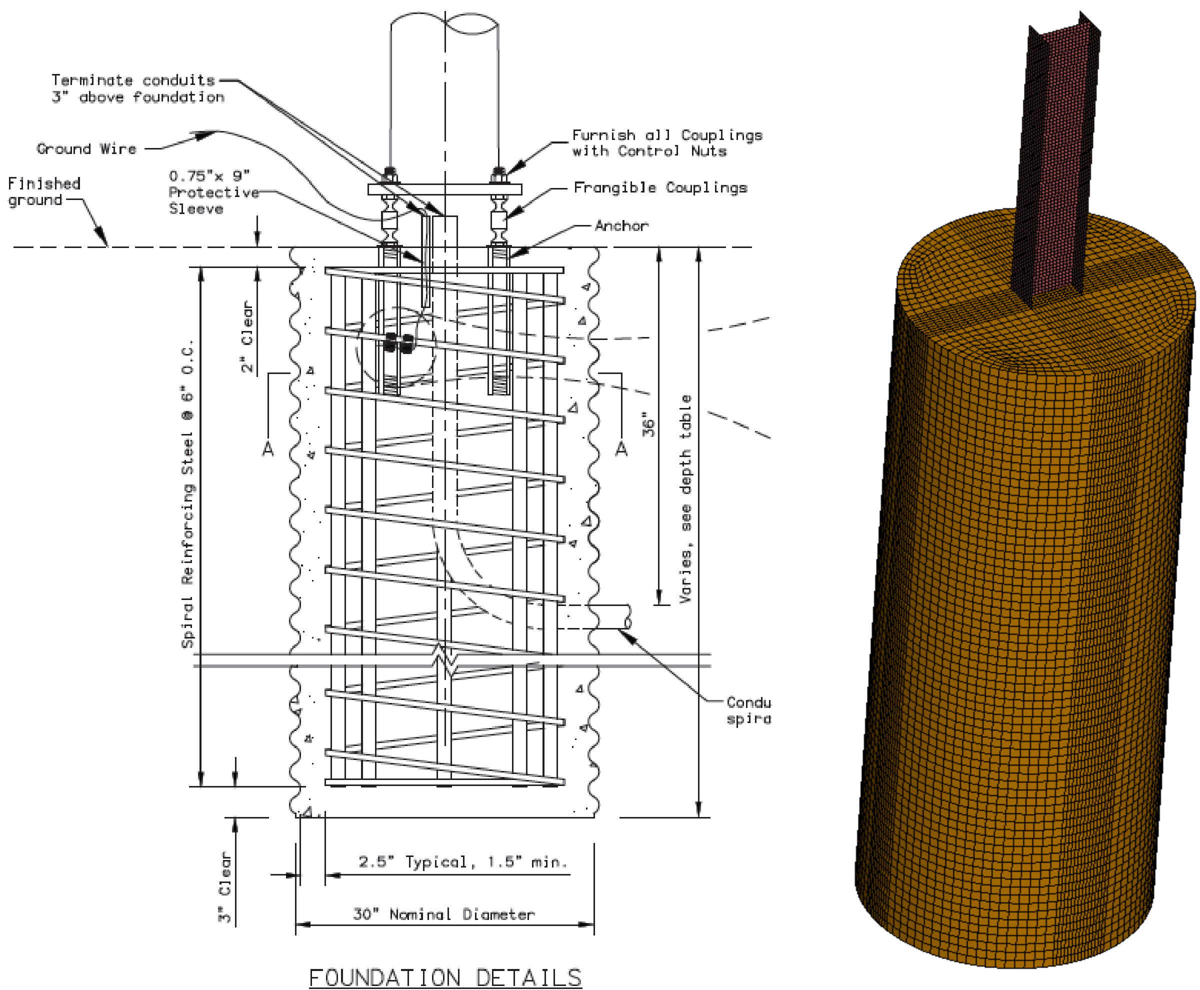

Figure 3.1 AK DOT&PF Foundation from L-30.11 (left), and Post and Foundation LS-DYNA Model (right)

3.2.3 Soil

A rigorous modeling method was adopted to represent soil for this study, modeling a discrete block of soil using solid elements, with an element size of 1.0 in. in the vicinity of the foundation and increasing to 2 in. in the surrounding region. Previous studies utilizing this approach include those conducted by Wu and Thomson (2007), Bligh et al. (2004), and Pajouh et al. (2017) [35-37]. While this approach is highly dependent on input parameters and may introduce non-physical hourglass energies due to large deformations, it was nonetheless deemed the preferred method for the present study in consideration of the lack of calibrated and validated simplified soil models in literature to represent weak soils.

The foundation was surrounded by solid soil elements assigned the Jointed Rock Model (MAT-198). The MAT-198 model was selected as it was found to be more stable compared to the MAT-193 model (Drucker Prager). A sensitivity analysis was conducted on the post-foundation-soil models with 10 ft x 10 ft, 12 ft x 12 ft, and 20 ft x 20 ft soil block plan dimensions to determine the appropriate size of the soil block, and it was found that there were no significant differences in the results of models with 12-ft and 20-ft soil blocks. Therefore, the soil block used in the analysis had dimensions of 12 ft x 12 ft x 12 ft. The boundaries at the bottom and sides of the soil block were restricted to simulate the actual conditions. Automatic Single Surface-to-Surface contact was defined between the concrete foundation and the soil.

The following soil parameters were considered essential for the analysis: density, elastic modulus, friction angle, cohesion, and Poisson's ratio. Conservative (lower bound) and common values for these parameters were selected to approximate the behavior of loose silty sand in the study's location of interest, based on available guidance in literature and state DOT resources, as discussed in Chapter 2. The soil density and elastic modulus were assumed to be 115 lb/ft^3 and 4.35 ksi, respectively, and the Poisson's ratio was set at 0.35. The friction angle was assumed to be 30 degrees, and a cohesion of 0.005 ksi was assigned (maintained as a non-zero value for numerical stability).

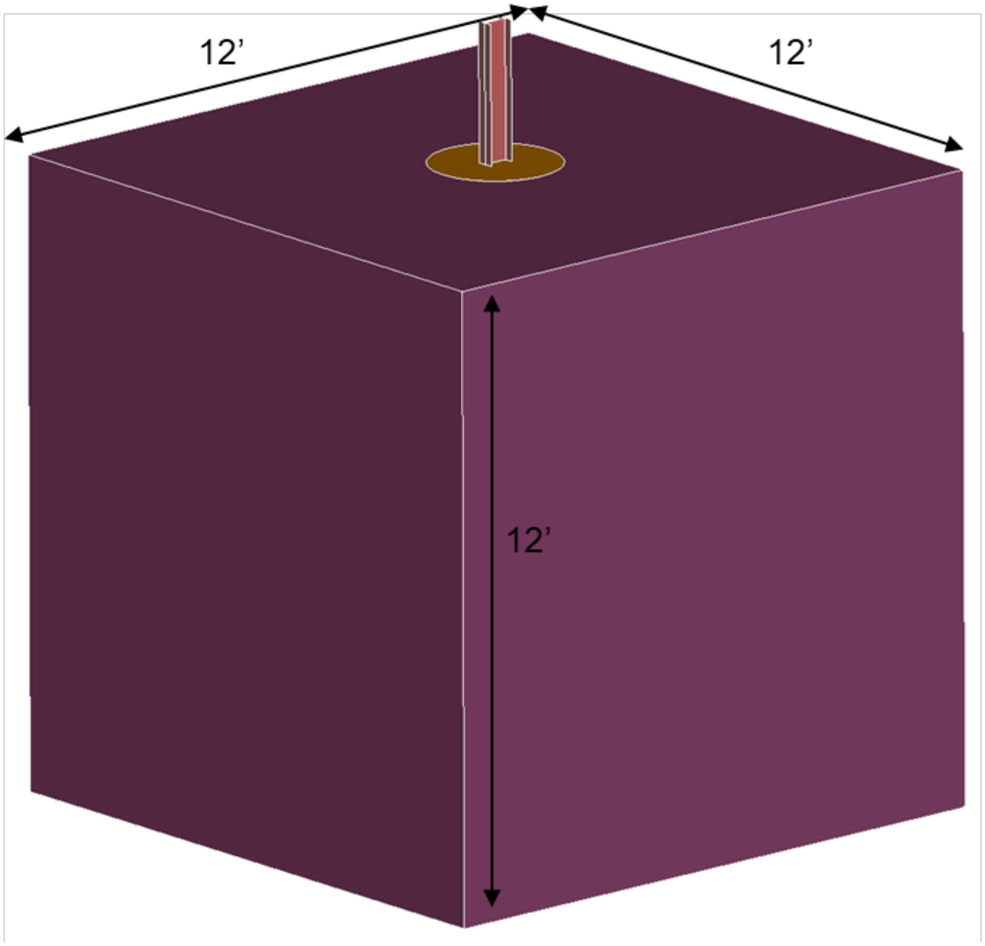

Figure 3.2 Soil, Post, and Foundation Model

3.2.4 Bogie (Surrogate Vehicle)

In bogie tests, a rigid-frame surrogate bogie vehicle, with a weight similar to that of a small passenger car, was used to impact the system head-on, as shown in Figure 3.3. The weight of the modeled bogie was 1,730 lb in initial models to match past testing but was later increased to better reflect anticipated testing conditions. In the bogie test, a pickup truck with a reverse cable tow system was used to propel the bogie to a target impact speed.

An impact speed of 20 mph and an impact height of 22 in. were initially considered in the analysis. The chosen impact speed is a common reference for evaluating the performance of roadside hardware, including light poles, similar to MASH test designation no. 3-60 impact conditions (which has an impact speed of 19 mph). The impact height of 22 in. was selected to be comparable to the average height of small passenger car bumpers, which typically range from 16 in. to 27 in. above the ground.

(a)

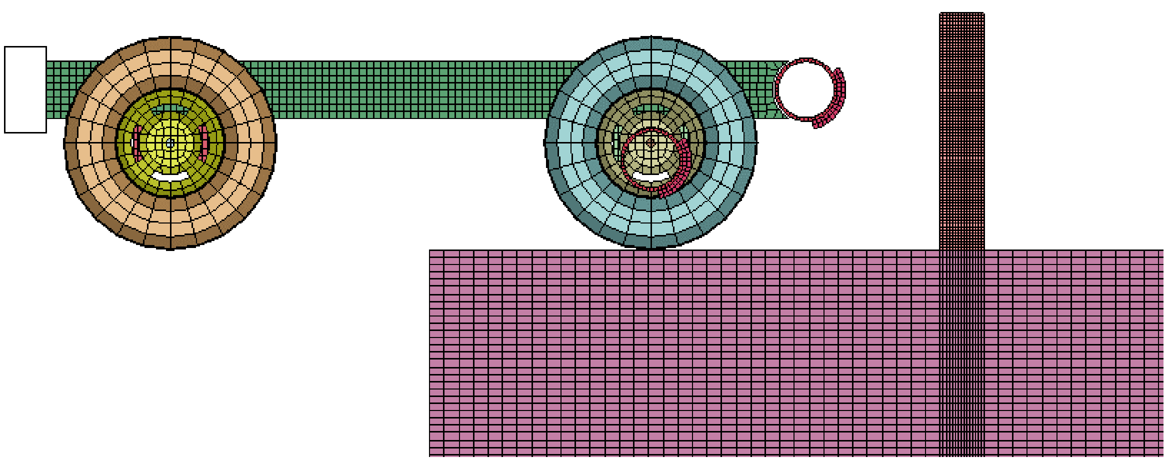

(b)

Figure 3.3 Bogie Impacting Post: (a) Physical Testing, and (b) LS-DYNA Modeling

3.2.5 Pole and Couplings

The modeled light pole system selected for modeling and testing was based on inventory recently procured by AK DOT&PF. A sample order of light poles was provided by AK DOT&PF, as shown in Figure 3.4. An LS-DYNA model was developed for the pole identified from recent AK DOT&PF procurement as a critical configuration (Pole No. 141 in Figure 3.4), consisting of a vertical pole, a single mast arm, a coupling base, a 6-ft deep reinforced concrete foundation, and soil domain. The light pole had a 10-gauge wall thickness and extended 35.5 ft above the ground surface. The tapered pole had top and bottom diameters of 5.53 in and 10.5 in., respectively. The mast arm had an 11-gauge wall thickness and a 20-ft length, rising 5.5 ft above the center of the connection attachment, establishing a luminaire mounting height of 40 ft. The light pole base was welded to a 15.5-in. square, 1⅜-in. thick steel plate. A visual representation of the system and connections in LS-DYNA is provided in Figure 3.5.

The materials employed included ASTM A595 Grade A steel for both the light pole and the mast arm. Support was provided by a breakaway coupling base from Transpo Industries, incorporating four 1-in. diameter, double-neck couplings, as illustrated in Figure 3.5(b).

The mast arm was connected to the light pole through a multi-component attachment featuring three ¾-in. diameter, ASTM A325 galvanized hex bolts. This attachment comprised an 8.75-in. tall × 8-in. wide × 1-in. thick, ASTM A709 mounting plate on the light pole side and an 8.75-in. tall × ¾-in. thick, ASTM A709 mounting plate on the mast arm side, with a width varying from 8-in. at the top to 6-in. at the bottom, as detailed in Figure 3.4 and shown for the computational model in Figure 3.5(c).

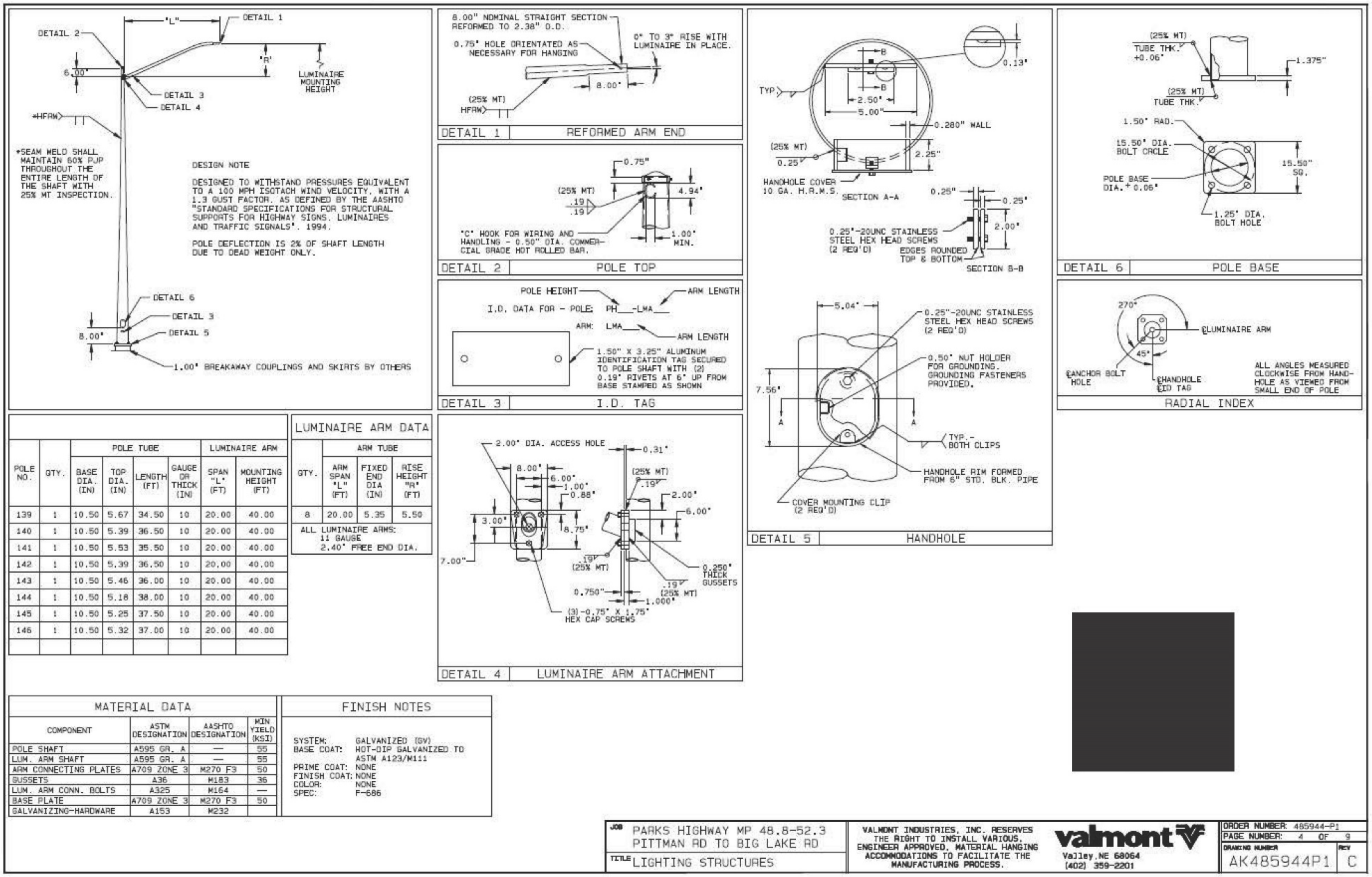

POLE NO.	QTY.	POLE TUBE: BASE DIA. (IN)	POLE TUBE: TOP DIA. (IN)	POLE TUBE: LENGTH (FT)	POLE TUBE: GAUGE OR THICK (IN)	LUMINAIRE ARM: SPAN "L" (FT)	LUMINAIRE ARM: MOUNTING HEIGHT (FT)
139	1	10.50	5.67	34.50	10	20.00	40.00
140	1	10.50	5.39	36.50	10	20.00	40.00
141	1	10.50	5.53	35.50	10	20.00	40.00
142	1	10.50	5.39	36.50	10	20.00	40.00
143	1	10.50	5.46	36.00	10	20.00	40.00
144	1	10.50	5.18	38.00	10	20.00	40.00
145	1	10.50	5.25	37.50	10	20.00	40.00
146	1	10.50	5.32	37.00	10	20.00	40.00

LUMINAIRE ARM DATA

QTY.	ARM TUBE: ARM SPAN "L" (FT)	ARM TUBE: FIXED END DIA (IN)	ARM TUBE: RISE HEIGHT "R" (FT)
8	20.00	5.35	5.50

ALL LUMINAIRE ARMS:
11 GAUGE
2.40" FREE END DIA.

MATERIAL DATA

COMPONENT	ASTM DESIGNATION	AASHTO DESIGNATION	MIN YIELD (KSI)
POLE SHAFT	A595 GR. A	—	55
LUM. ARM SHAFT	A595 GR. A	—	55
ARM CONNECTING PLATES	A709 ZONE 3	M270 F3	50
GUSSETS	A36	M183	36
LUM. ARM CONN. BOLTS	A325	M164	—
BASE PLATE	A709 ZONE 3	M270 F3	50
GALVANIZING-HARDWARE	A153	M232	

FINISH NOTES

SYSTEM: GALVANIZED (GV)
BASE COAT: HOT-DIP GALVANIZED TO ASTM A123/M111
PRIME COAT: NONE
FINISH COAT: NONE
COLOR: NONE
SPEC: F-686

Figure 3.4 AK DOT&PF Sample Light Pole Order

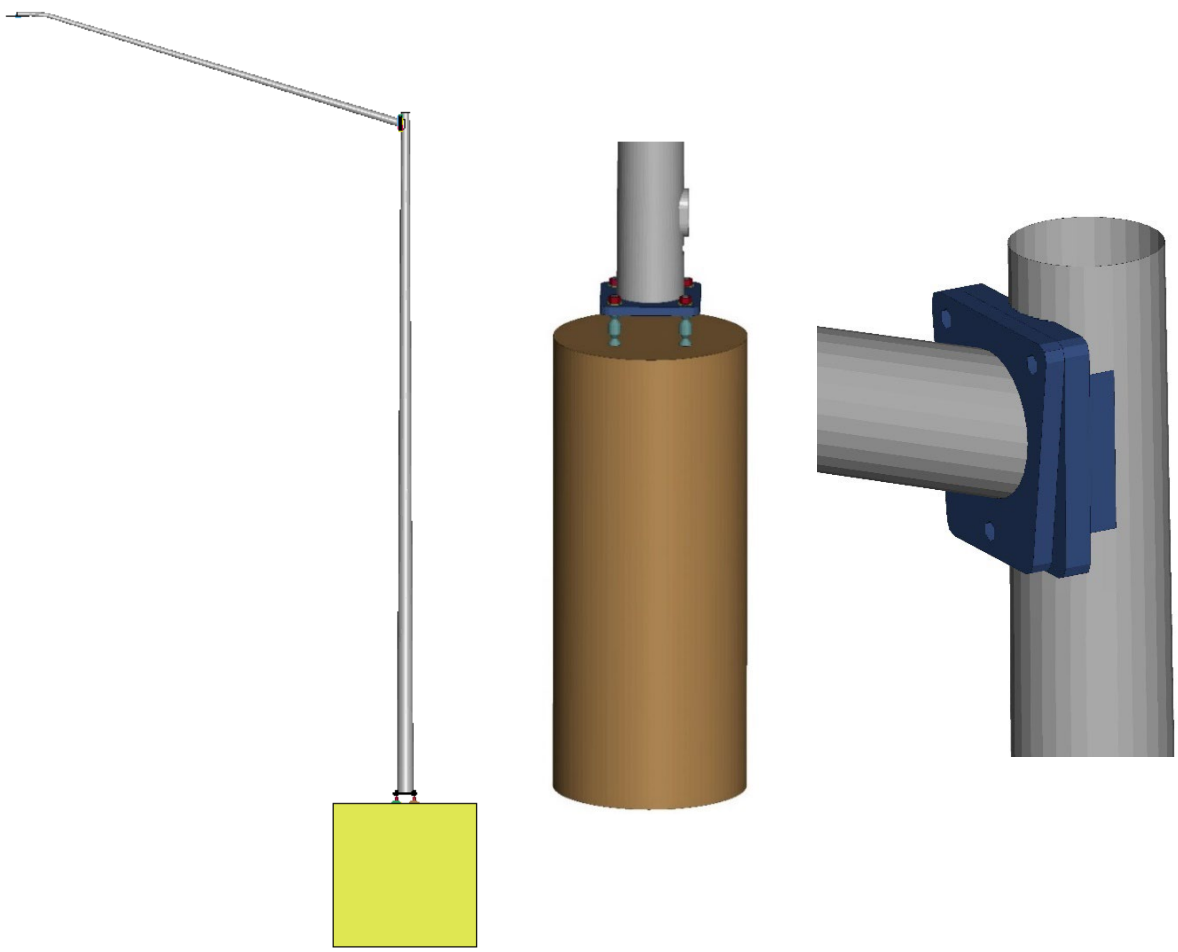

(a) (b) (c)

Figure 3.5 LS-DYNA Models for Light Pole Systems: (a) Light Pole System; (b) 6-ft Foundation; (c) Mast Arm-to-Pole Connection

The light pole and mast arm were modeled utilizing four-node, fully integrated, shell elements. The coupling, nut, light pole base plate, and mounting plates were represented by eight-node solid elements. The model incorporated hourglass control with the Flanagan-Belytschko viscous formulation for solid elements, and a specified hourglass coefficient of 0.05 to reduce hourglass effects. The light pole system was mounted to a 2.5-ft diameter reinforced concrete (RC) foundation, embedded in sand, with a depth of 6 ft. Although the physical concrete foundation specimen was planned to be reinforced with eight #8 longitudinal steel bars and #5 circular hoops for transverse reinforcing, no reinforcing was included in the preliminary model as foundation damage was anticipated to be minor, so the concrete material was assigned only elastic material properties. The foundation concrete was modeled using eight-node solid elements.

The light pole system's material response, which includes components such as the light pole, mast arm, mounting plates, base plate, couplings, nuts, and washers, was simulated using the Mat Piecewise Linear Plasticity model. The steel's elastic modulus was set at 2.9×10^4 ksi, with a Poisson's ratio of 0.3. The yield strength for ASTM A595 and ASTM A449 steel was specified as 55 ksi and 43.5 ksi, respectively, aligning with materials used in component tests. A plastic failure strain was set in the material model for couplings, to facilitate the breakaway mechanism during impact loading. The concrete for the foundation was simulated using Mat Elastic with concrete properties. The concrete elastic modulus and Poisson’s ratio were assumed to be 4.64 ksi and 0.2, respectively. Connections between the couplings and the foundation were simplified and modeled as rigid constraints.

Soil domain dimensions, element formulation, and constitutive properties were adopted from the post model, as described in Section 3.2.3. In order to bound potential soil behavior, simulations were performed using couplings attached to a rigid base, representing very stiff soil, as well as with weak (SPT = 7) and very weak (SPT = 3) soil. LS-DYNA parts, element types, element formulations, material types, and material formulations are summarized in Table 3.2.

.

Table 3.2 List of Simulation Model Parts and LS-DYNA Parameters

Part Name	Element Type	Element Formulation	Material Type	Material Formulation
Light pole	Shell	Belytschko-Tsay	ASTM A595 Grade A	Piecewise Linear Plasticity
Mast arm	Shell	Belytschko-Tsay	ASTM A595 Grade A	Piecewise Linear Plasticity
Light pole base plate	Solid	Constant stress	ASTM A709	Piecewise Linear Plasticity
Hex nut	Solid	Constant stress	ASTM A563 Grade DH	Rigid
Flat washer	Solid	Constant stress	ASTM A153	Rigid
Double-neck light pole-safe coupling	Solid	Constant stress	ASTM A449 (assumed)	Piecewise Linear Plasticity
Mounting plate	Solid	Constant stress	ASTM A709	Piecewise Linear Plasticity
Luminaire mass	Shell	Belytschko-Tsay	ASTM A595 Grade A	Rigid
Concrete	Solid	Constant stress	4,000 psi Concrete	Elastic
Soil	Solid	Constant Stress	AASHTO Type A-3 Sand	Jointed Rock

3.3 Simulation Results

3.3.1 Dynamic Bogie Impacting an Embedded Post System

In the initial round of simulation, the impact scenario involved a 1,730-lb bogie impacting the post embedded in a concrete foundation at a speed of 20 mph. The post was assumed to have a yield strength of 47 ksi, based on past testing performed by the testing facility using A36 steel W-shapes.

Foundation depth was varied from 2 to 8 ft in increments of 2 ft, as shown in Figure 3.6. Soil was initially modeled with parameters typically selected to represent MASH strong soil, as described previously. The post developed a plastic hinge in each case, and the foundation had maximum displacements of 7 in., 3.4 in., 2 in., and 1.2 in. for 2-ft, 4-ft, 6-ft, and 8-ft depths, respectively, recorded at a node at the top surface of the foundation. AK DOT&PF did not have a firm limitation on foundation displacement due to vehicle impact. However, a desire was noted to be able to remove and replace a damaged light pole without requiring the foundation to be excavated and reinstalled. Note 8 in Figure 2.1 specifies that "anchors greater than 1:40 out-of-plumb will result in foundation rejection." Adopting this Note as a proxy limit, and assuming that the foundation tips from its base, the maximum acceptable displacements for the considered foundation depths were 0.6 in., 1.2 in., 1.8 in., and 2.4 in.

The assumption of tipping from the base rather than rotating about a point along the foundation height, as well as use of MASH strong soil, were not conservative. Conversely, the use of a non-breakaway post was conservative due to the extended impulse imparted to the foundation rather than that expected with frangible couplings. Additionally, the contact force recorded at the impact location reached 35 kips for the post, whereas Transpo frangible couplings used by AK DOT&PF will limit the peak force to 22 kips. On balance, the 6-ft depth was deemed to have a reasonable likelihood of adequate performance, although its peak displacement of 2 in. exceeded the notional limit of 1.8 in. in the initial model. As this foundation depth had previously been noted as a desirable outcome from the project in discussions with the sponsor, it was selected as the focus for subsequent modeling.

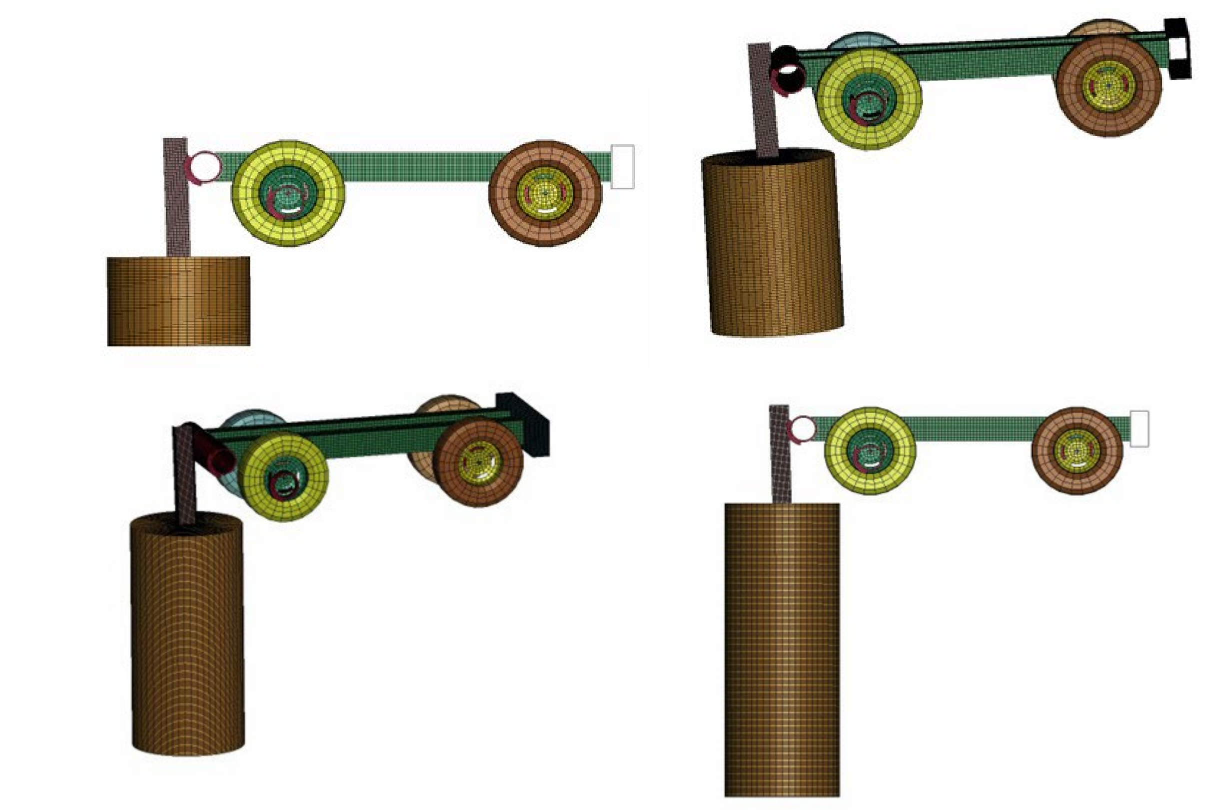

Figure 3.6 Foundations with Depths of 2, 4, 6, and 8 ft in MASH Strong Soil

In the second round of simulations, soil properties were modified to represent soils with SPT values of 7 (loose sand) and 3 (very loose sand). Properties for these two cases were determined using the AASHTO and Caltrans SPT relations noted previously. Specifically, the density was obtained from the Caltrans graph shown in Figure 2.23, elastic modulus and Poisson's ratio from Figure 2.26, and friction angle from Figure 2.28. In the case of loose sand, the density was selected as 103 pcf, with an elastic modulus of 1.5 ksi, a friction angle of 30 degrees, and a Poisson's ratio of 0.3. For very loose sand, the density was set at 85 pcf, with an elastic modulus of 0.3 ksi, a friction angle of 26 degrees, and a Poisson's ratio of 0.25. These selected soil conditions were intended to determine the influence of weak soil in comparison to the strong soil conditions simulated in the 1st round, as well as the sensitivity of foundation response to soil placement in physical testing. The impact force, determined from the recorded contact force at the impact location, and displacement of the foundation in the direction of impact, determined from a node at the top surface of the foundation, were compared and presented in Figures 3.7(a) and 3.7(b), respectively.

Figure 3.7(a) illustrates the variation in impact force for the SPT 3 and SPT 7 soil conditions. This shows how the soil properties affect the magnitude of the impact force experienced by the post-soil-foundation system. The peak recorded contact force for the simulation with soil having an SPT of 3 was found to be 36 kips, and for the simulation with soil having an SPT of 7, the value was found to be 37.2 kips. Thus, there was not a significant difference in the peak impact force for loose versus very loose sandy soil conditions.

Figure 3.7(b) shows the displacement of the foundation in the direction of impact for the SPT 3 and SPT 7 soil conditions. The foundation in soil with an SPT of 3 showed significantly greater deflection compared to the foundation in soil with an SPT of 7.

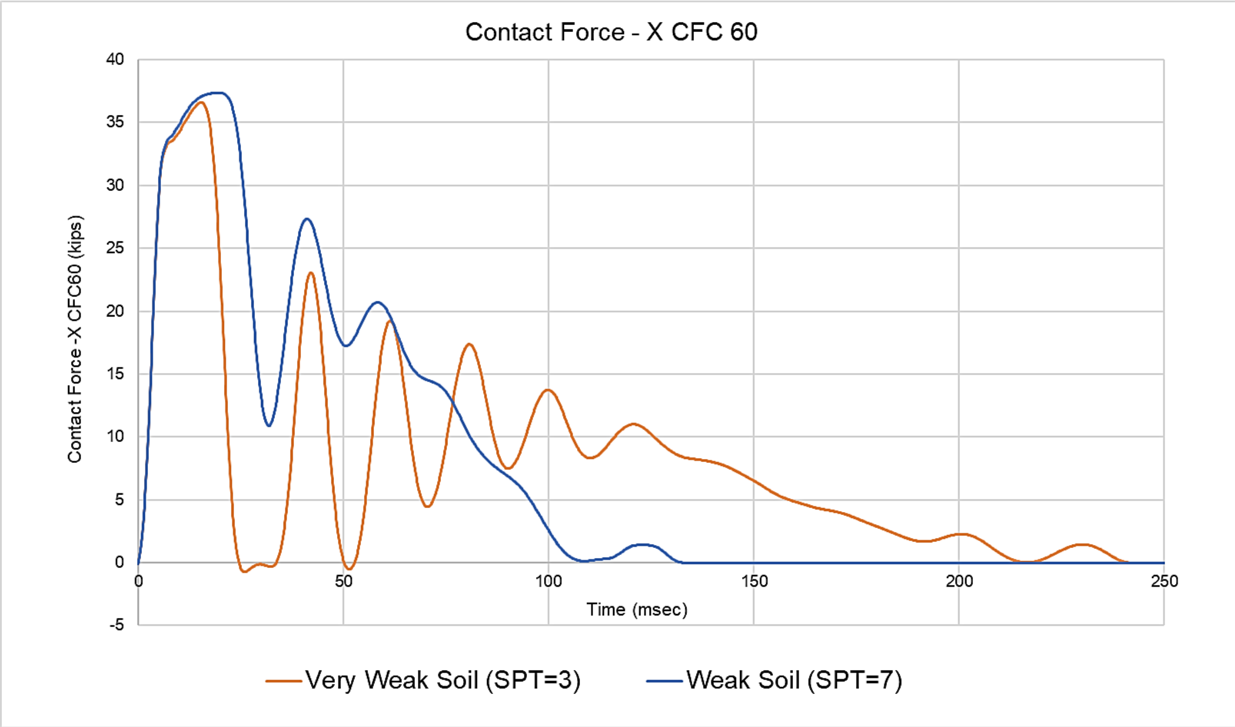

(a)

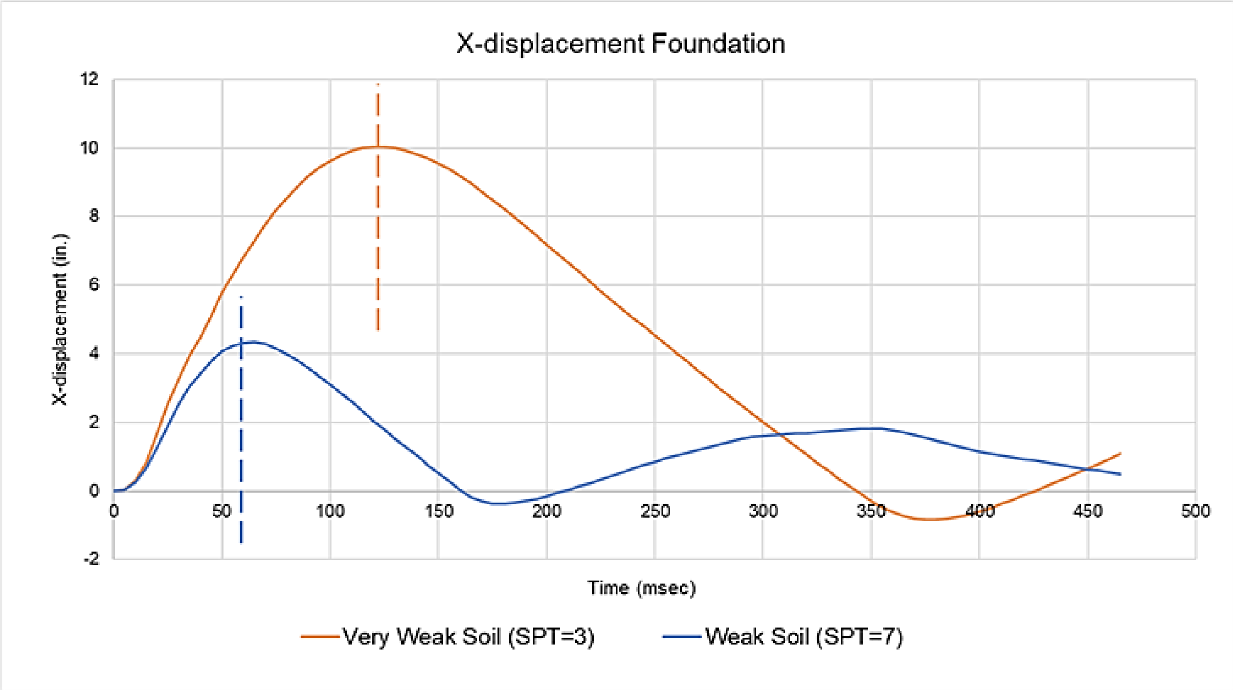

(b)

Figure 3.7 Second Round of Simulation Results: (a) Impact Force, and (b) Foundation Displacement in Direction of Impact

Residual displacement, or permanent set, is another important consideration in evaluating the performance of a foundation. Limiting foundation permanent set may allow a foundation to be reused without requiring earthwork, whereas unacceptably large displacements will require the foundation to be excavated, re-set, and backfilled. In the simulation of a 6-ft deep foundation, the secondary peak for the case of involving soil with an SPT of 7 was 1.8 in., which provides a reasonable upper bound for the simulation permanent set.

In the third round of simulation, only the soil with SPT of 7 was considered, and adjustments were made to match the actual bogie test conditions. The mass of the bogie was adjusted to 1,850 lb, the impact speed was set to 19 mph, and the impact height was adjusted to 25 in. Additionally, the yield strength of the post was modified to reflect the nominal material properties anticipated for the bogie test, which was 50 ksi for ASTM A992 steel. These adjustments aimed to align the simulation more closely with the real-world test conditions, allowing for a more accurate evaluation of the post-foundation performance and response to the impact. The contact force and foundation displacement are shown in Figures 3.8(a) and Figures 3.8(b), respectively.

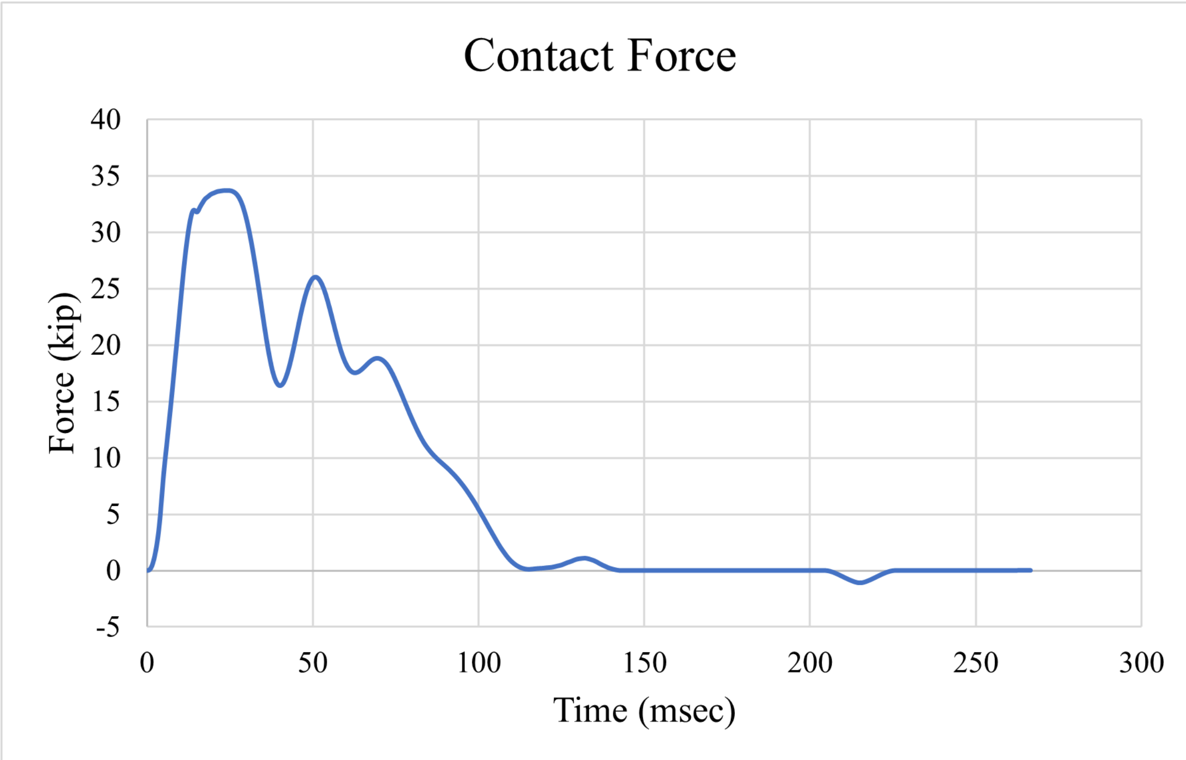

(a)

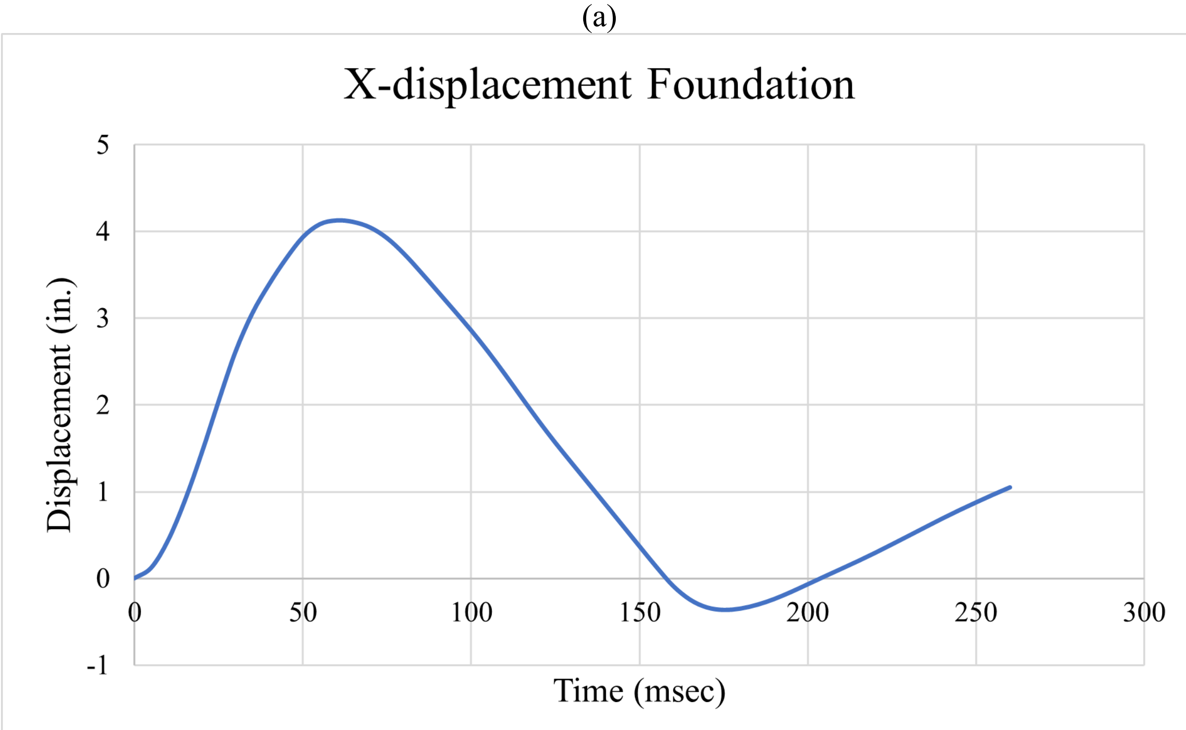

(b)

Figure 3.8 Third Round of Simulation Results: (a) Impact Force, and (b) Foundation Displacement in Direction of Impact

3.3.2 Dynamic Bogie Impacting a Light pole System

In the simulations, the bogie vehicle model with a mass of 1,850 lb impacted the light pole system at an angle of 0 degrees, as shown in Figure 3.9, and at a velocity of 19 mph, similar to MASH test designation no. 3-60. The height of the impact was 25 in. from the ground level to the center of the impact head. Soil properties and related parameters were applied to the models replicating the analyses of lateral impacts into the post foundation assembly-soil system, for weak (SPT = 7) and very weak soil (SPT = 3). An additional simulation involved the bogie vehicle model impacting the light pole model supported by a rigid base at a velocity of 19 mph to compare the analysis results and evaluate the breakaway mechanism of the coupling base. In all simulations, the single mast arm was set perpendicular to the direction of impact.

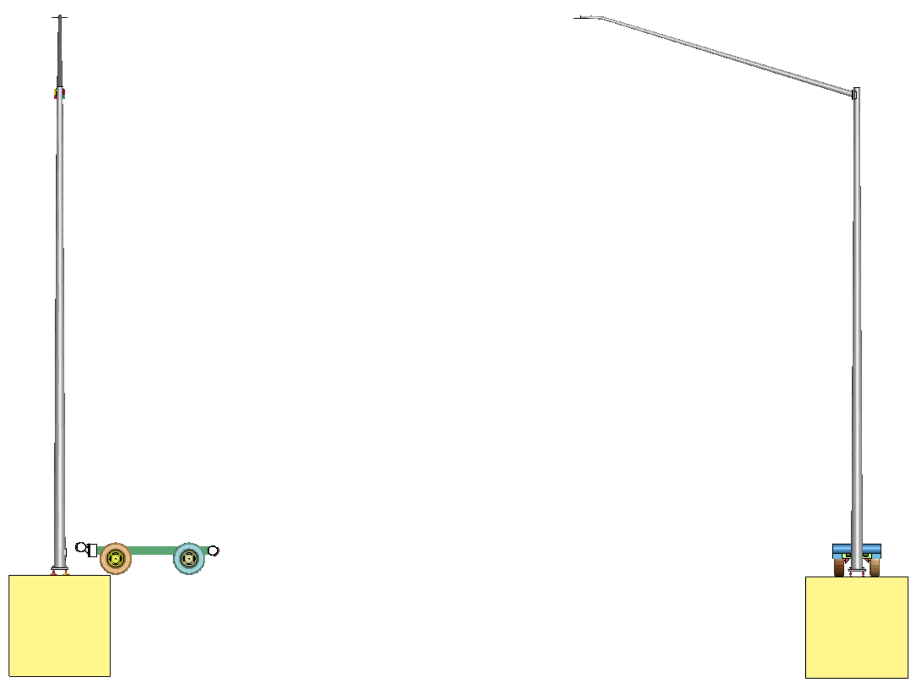

(a) Side view (b) Front view

Figure 3.9 Bogie Impacting Light Pole System

Figures 3.10 and 3.11show sequential views of the bogie vehicle impacting the light pole system. Within 10 ms, the light pole was dented at the impact location. As the event progressed to 20 ms, all four couplings fractured at both upper and lower neck locations. By 30 ms, the bogie head relinquished contact with the light pole. In all three simulations, the breakaway mechanism was activated through the failure of all four couplings at both neck locations.

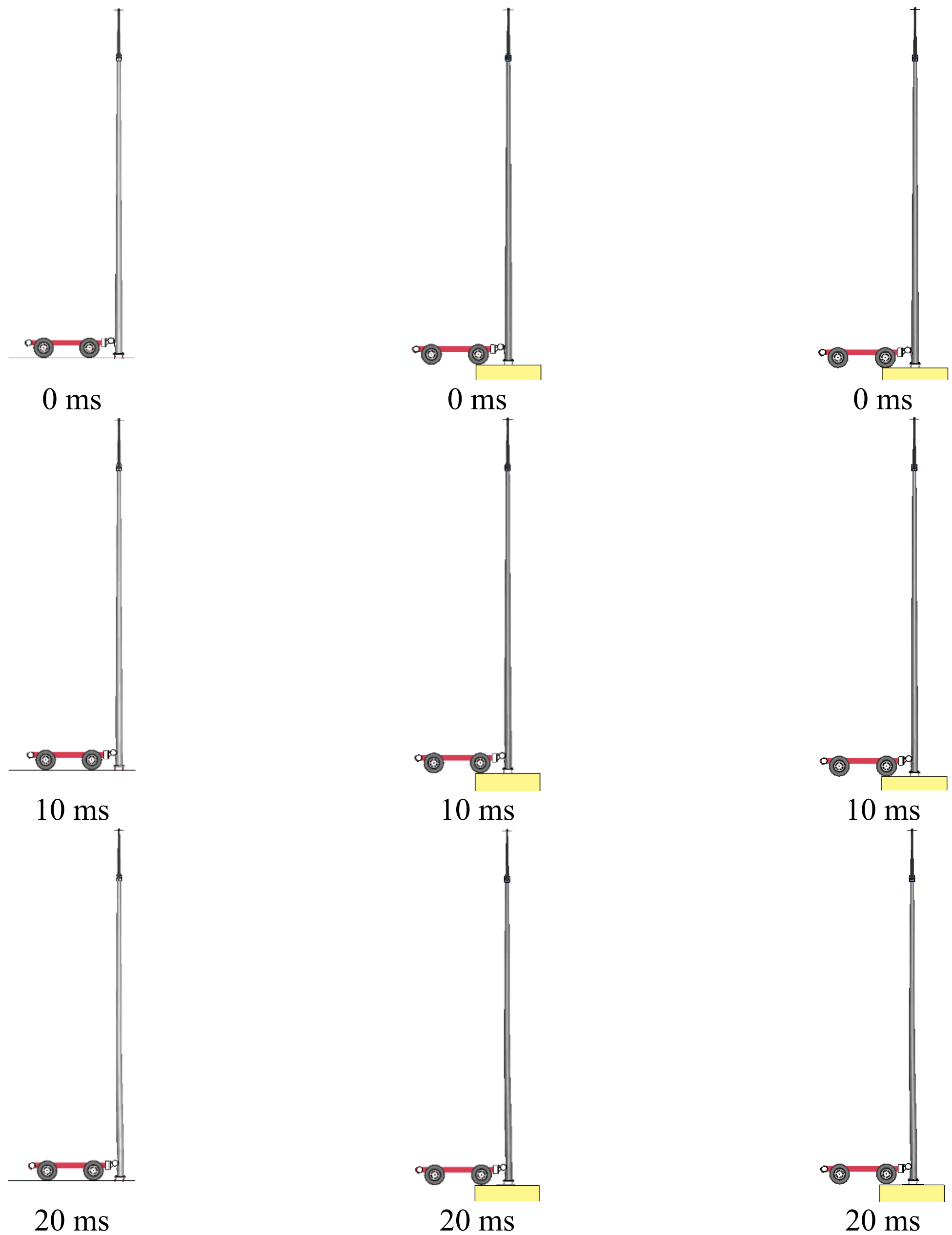

Figure 3.10 Sequential Views: (a) Rigid Base; (b) Weak Soil; and (c) Very Weak Soil

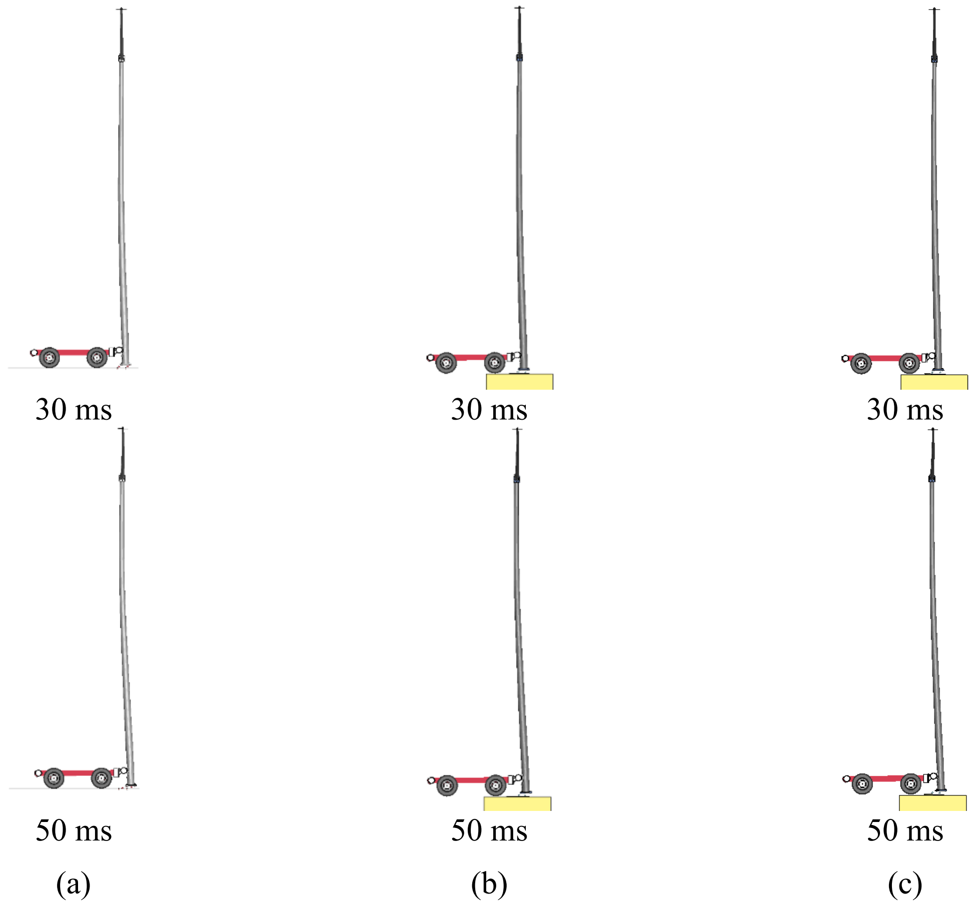

Figure 3.11 Sequential Views: (a) Rigid Base; (b) Weak Soil; and (c) Very Weak Soil, Cont.

Forces in the couplings at the lower neck location were obtained using *Database Cross Section Plane* in LS-DYNA to examine coupling response during the bogie impact, as shown in Figure 3.12(a). Peak horizontal forces of 31.4 kips and 32.5 kips were recorded at 0.012 s and 0.014 s after bogie impact for weak (SPT =7) and very weak (SPT = 3) soil, respectively, as illustrated in Figure 3.12(b). According to Transpo Industries, Inc., product specifications shown in Figure 2.2, the maximum restrained shear strength of an individual steel breakaway coupling is 5.5 kips, resulting in a total of 22 kips shear strength of the coupling base for the light pole system. Although bogie or pendulum decelerations may exceed the rated strength of the couplings due to inertial effects from mass activation of the pole, the simulations results should ideally not demonstrate such a discrepancy. The couplings may not have been adequately modeled with respect to material properties, geometric properties, or both. As the objective of the research was not to develop a robust model of proprietary Transpo products, the results were considered acceptable for the purposes of the project, acknowledging that the results may be slightly conservative due to greater than realistic impulse and momentum transfer into the foundation prior to frangible coupling activation.

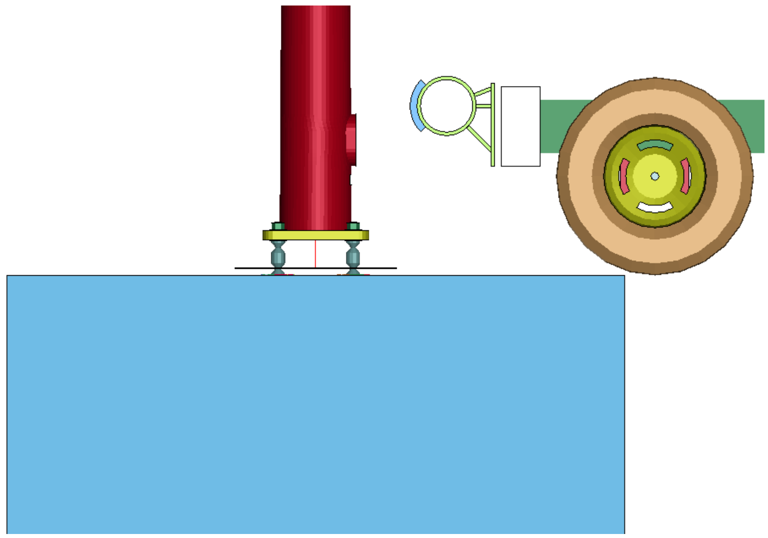

(a)

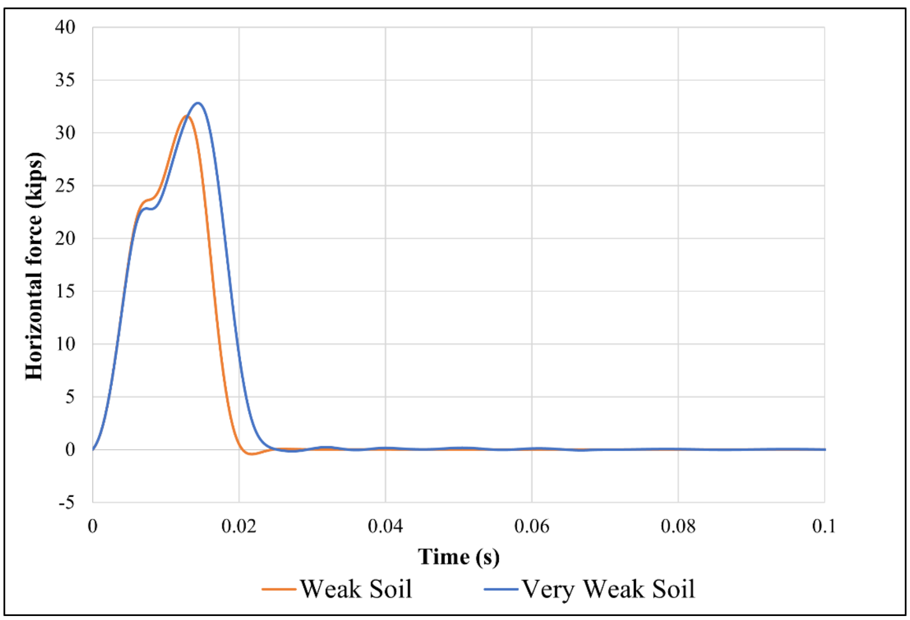

(b)

Figure 3.12 Horizontal Force at Lower Neck Location of Couplings: (a) Cross-sectional Force Location; (b) Horizontal Forces

Figure 3.13 shows the foundation displacement in the direction of bogie impact from the simulations with the weak soil (SPT =7) and the very weak soil (SPT = 3). In the weak soil condition, the top of the foundation attained a peak dynamic displacement of 1.0 in. When the light pole system was embedded in very weak soil, the dynamic peak displacement of the foundation was 3.03 in. Residual displacements were not obtained as the simulation was computationally expensive and was not run for a duration adequate to observe predicted stable final conditions. As expected, the foundation in very weak soil with an SPT of 3 was predicted to experience greater deflection compared to the foundation in the weak soil with an SPT of 7.

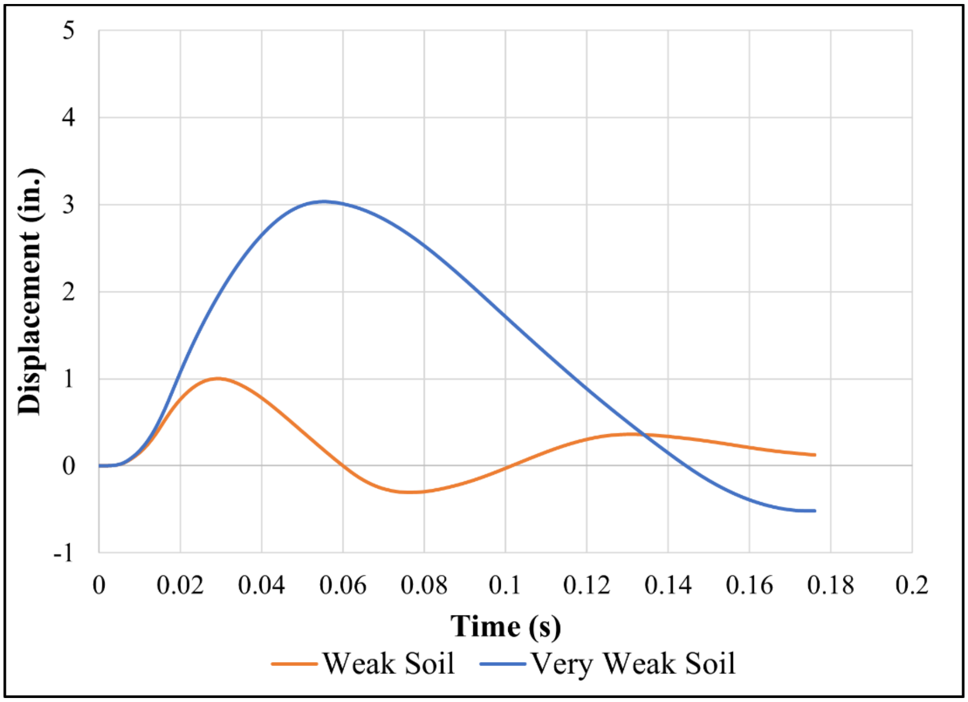

Figure 3.13 Foundation Displacement in Direction of Impact

3.4 Summary

Initial LS-DYNA models were configured to investigate the sensitivity of foundation depth when supporting an embedded steel post and surrounded by MASH strong soil. A depth of 6 ft resulted in a peak displacement of 2.0 in., slightly higher than a nominal approximate threshold residual displacement of 1.8 in. The peak displacement should be a conservative indicator of residual displacement due to elastic soil rebound and foundation rock-back. Additionally, the load was imparted through a steel post embedded in the foundation. Plastic hinging of the post results in a longer duration impulse than anticipated from frangible couplings present in a vehicle impact scenario. Lastly, the 6-ft depth had been used previously for installations by AK DOT&PF and had performed adequately in service. The 6-ft depth was therefore selected for further investigation.

When the 6-ft foundation model was revised to represent weak and very weak soil conditions, intended to correspond approximately to SPT values of 7 and 3, respectively, foundation displacements increased significantly. Peak foundations displacements were approximately 4.2 in. and 10.0 in. for SPT of 7 and 3, respectively. Although these displacements were unacceptable according to the target 1.8 in. threshold, the weak (SPT = 7) soil exhibited a secondary peak displacement slightly less than 2.0 in., suggesting that the residual displacement may satisfy the target threshold as the foundation would come to rest in subsequent oscillations. Additionally, the force-time responses for both weak and very weak soil conditions were identical up to approximately 33 kips, indicating that foundation inertia was adequate to reach embedded post plastification, and should also be adequate to activate Transpo couplings having a group maximum shear strength of 22 kips. The impulsive forces exceeding Transpo coupling breakaway strengths also suggest that peak displacement demands were overestimated with an embedded steel post compared to the values that would be expected with frangible couplings.

Finally, simulations were performed with 35.5-ft tapered steel poles with single 20-ft mast arms and mounted to breakaway couplings, similar to hardware used in-service by AK DOT&PF. Bogie impacts were simulated for 19 mph impact speeds at 0 deg impact angles, similar to MASH test designation no. 3-60. Simulation cases included couplings attached to a rigid base, to a concrete foundation surrounded by weak (SPT = 7) soil, and to a concrete foundation surrounded by very weak (SPT = 3) soil.

Coupling activation was observed in each model. Transpo couplings are a proprietary product, so modeling for these components in the preliminary models was based on assumed properties. Peak forces recorded in LS-DYNA for a plane passing through the couplings indicated that the peak shear force reached approximately 31 to 32 kips, regardless of modeled soil properties. This observation confirmed the expectation that foundation inertia alone was sufficient to activate the frangible couplings, even though they exhibited a greater strength in the model than would be expected for real-world installations. Additionally, the shorter duration of the impulse for the frangible couplings compared to the plastically hinging embedded steel post resulted in peak foundation displacements reducing from 4.2 in. to 1.0 in. for weak (SPT=7) soil, and from 10.0 in. to 3.0 in. for very weak (SPT = 3) soil.

Although these results are based on unvalidated, estimated material parameters, they provided confidence to proceed with initial physical testing of 6-ft deep, 2.5-ft diameter concrete foundations embedded in sandy soil with SPT values of approximately 7.

Chapter 4 Component Testing Conditions

4.1 Purpose

This study employed dynamic bogie testing to evaluate peak and residual displacements for concrete foundations embedded in weak soils and subjected to dynamic impact loading.

4.2 Scope

A total of six bogie tests were conducted on foundations embedded in sandy soils to simulate weak soil conditions. The impact tests simulated a vehicular impact from a small car at 19 mph with an impact angle of 0 degrees, creating a classical “head-on” or full-frontal collision. Impacts on test articles occurred at a height of 25 in. above the ground line to represent contact from a small car bumper.

As noted in Section 3.4, a foundation depth of 6 ft was selected as the priority configuration for testing, with a target peak displacement of 1.8 in. Tests were conducted in two rounds. The first round of tests used a steel post embedded in the foundation. A second round of tests mounted steel light poles to foundations using Transpo breakaway couplings. All tests were conducted with foundations surrounded by Type A-3 sand material per AASHTO specifications [38]. Further details on individual tests are included at the beginning of each respective testing chapter.

4.3 Test Facility

Physical testing of the post and foundation assembly in sand was conducted at the Midwest Roadside Safety Facility (MwRSF) outdoor proving grounds, which is located at the Lincoln Air Park on the northwest side of the Lincoln Municipal Airport. The facility is approximately 5 miles (8 km) northwest of the University of Nebraska-Lincoln’s city campus.

4.4 Equipment and Instrumentation

Equipment and instrumentation utilized to collect and record data during the dynamic bogie tests included a bogie vehicle, accelerometers, a retroreflective speed trap, high-speed and standard-speed digital video, still cameras, and a linear displacement transducer to record foundation displacement at the ground surface.

4.4.1 Bogie Vehicle

A rigid-frame bogie was used to impact the posts. A variable height, detachable impact head was used in the testing. The bogie head was constructed of 8-in. diameter, ½-in. thick standard steel pipe, with ¾-in. neoprene belting wrapped around the pipe to prevent local damage to the post from the impact. The impact head was bolted to the bogie vehicle, creating a rigid frame with an impact height of 25 in. The bogie with the impact head is shown in Figures 4.1 and 4.2 in preparation for tests impacting an embedded steel post and a steel light pole, respectively. The weight of the bogie with the addition of the mountable impact head and accelerometers was 1,860 lb and 1,860 lb for test nos. AKLP-1 through AKLP-4 and AKLP-5 and AKLP-6, respectively.

Figure 4.1 Rigid-Frame Bogie on Guidance Track Preparing to Impact Embedded Steel Post

Figure 4.2 Rigid-Frame Bogie on Guidance Track Preparing to Impact Light Pole

The tests were conducted using a steel corrugated beam guardrail to guide the tire of the bogie vehicle. A pickup truck with a reverse cable tow system was used to propel the bogie to the target impact velocity. When the bogie approached the end of the guidance system, it was released from the tow cable, allowing it to be free rolling when it impacted the post. A radiocontrolled brake system was installed on the bogie, allowing it to be brought safely to rest after the test.

4.4.2 Accelerometers

An accelerometer system was mounted on the bogie vehicle near its center of gravity (c.g.) to measure the acceleration in the longitudinal, lateral, and vertical directions. However, only the longitudinal acceleration was processed and reported.

The SLICE-1 and SLICE-2 units were modular data acquisition systems manufactured by Diversified Technical Systems, Inc. (DTS) of Seal Beach, California. The SLICE-1 unit was designated as the primary system for test nos. AKLP-1 through AKLP-4, and the SLICE-2 unit was designated as the primary system for AKLP-5 and AKLP-6. The acceleration sensors were mounted inside the bodies of custom-built, SLICE 6DX event data recorders and recorded data at 10,000 Hz to the onboard microprocessor. Each SLICE 6DX was configured with 7 GB of non-volatile flash memory, a range of ±500 g's, a sample rate of 10,000 Hz, and a 1,650 Hz (CFC 1000) anti-aliasing filter. The SLICEWare computer software program and a customized Microsoft Excel worksheet were used to analyze and plot the accelerometer data

4.4.3 Retroreflective Optic Speed Trap

A retroreflective optic speed trap was used to determine the speed of the bogie vehicle before impact. Three retroreflective targets, spaced at approximately 18-in. intervals, were applied to the side of the bogie vehicle. When the emitted beam of light was reflected by the targets and returned to the Emitter/Receiver, a signal was sent to the data acquisition computer, recording at 10,000 Hz, as well as the external LED box activating the LED flashes. The speed was then calculated using the spacing between the retroreflective targets and the time between the signals. LED lights and high-speed digital video analysis are used as a backup if vehicle speeds cannot be determined from the electronic data.

4.4.4 Digital Photography

Two AOS high-speed digital video cameras and two Panasonic digital cameras were used to document each of test nos. AKLP-1 through AKLP-4. Three AOS high-speed digital video cameras, two GoPro digital video cameras, and three Panasonic digital cameras were used to document each of test nos. AKLP-5 and AKLP-6. The AOS high-speed cameras had a frame rate of 500 frames per second, the GoPro video camera had a frame rate of 120 frames per second, and the Panasonic digital video cameras had a frame rate of 120 frames per second. The cameras were placed laterally from the test articles, with a view perpendicular to the bogie's direction of travel. A digital still camera was also used to document pre- and post-test conditions for all tests.

4.4.5 String Potentiometer

A linear displacement cable extension transducer, or string potentiometer or string pot, was installed at the edge of the sand pit to determine the displacement of the post foundation for each bogie test. The string pot was installed at the edge of the pit opposite the impact face of the test article for test nos. AKLP-1 and AKLP-2, as shown in Figure 4.3, where the impact side was on the left side of the test article from the camera's perspective. The string pot was installed at the edge on the same side as the impact face for AKLP-3 through AKLP-6, as shown in Figure 4.4, viewing the impact side of the test article. The string potentiometer was a UniMeasure PZ-50 with a range of 50 in. A Micro-Measurements Group Vishay Model signal conditioning amplifier was used to condition and amplify the low-level signals to high-level outputs for multichannel, simultaneous dynamic recording in LAbVIEW software. The sampling rate of the string potentiometers was 1,000 Hz.

<u>4.5 End of Test Determination</u>

When the impact head initially contacts the test article, the force exerted by the bogie vehicle is directly perpendicular to the test article. However, for tests impacting an embedded post, the post rotates and the bogie's orientation and become oblique to the post longitudinal (initially vertical) axis. This introduces two sources of error: (1) the contact force between the impact head and the post has a vertical component and (2) the impact head slides upward along the test article. Therefore, only the initial portion of the accelerometer trace should be used since variations in the data become significant as the system rotates. Additionally, guidelines were established to define the end of test time using the high-speed video of the impact. The first occurrence of either of the following events was used to determine the end of the test: (1) the test article fractured or (2) the bogie overrode or lost contact with the test article.

Figure 4.3 Typical String Potentiometer Setup, Test Nos. AKLP-1 and AKLP-2


Figure 4.4 Typical String Potentiometer Setup, Test Nos. AKLP-5 and AKLP-6

4.6 Data Processing

The electronic accelerometer data obtained in dynamic testing was filtered using the SAE Class 60 Butterworth filter, conforming to the SAE J211/1 specification [39]. The pertinent acceleration signal was extracted from the bulk of the data signals. The processed acceleration data was then multiplied by the mass of the bogie to obtain the impact force using Newton's Second Law. Next, the acceleration trace was integrated to find the change in velocity versus time. The initial velocity of the bogie, calculated from the retroreflective optic speed trap data, was then used to determine the bogie's velocity, and the calculated velocity trace was integrated to find the bogie's displacement. This displacement is also the displacement of the post at the impact height. Combining the previous results, a force vs. deflection curve was plotted for each test. These curves only illustrated the lateral resistive applied at displacements equal to the movement of the bogie vehicle and impact head, not the displacement of the foundation. Finally, integration of the force versus displacement produced the energy versus displacement curve for each test.

Similar to the accelerometer data, the pertinent data from the string potentiometer was extracted from the bulk signal. The extracted data signal was converted to a displacement using the transducer's calibration factor. Displacement versus time plots were created to describe the motion of the foundation at the ground line. The exact moment of impact could not be determined from the string potentiometer data as the impact may have occurred a few milliseconds prior to foundation movement. Thus, the extracted time shown in the displacement versus time plots should not be taken as a precise time after impact, but rather an approximate time in relation to the impact event.

Chapter 5 Design Details – Foundations with Embedded Steel Posts

Four bogie tests were performed to evaluate the behavior of foundations subjected to impact loading when surrounded by soft soil with varying conditions of compaction and moisture content. The test article for each test was an ASTM A992 W6x16 steel post embedded into a 30-in. diameter, 6-ft deep reinforced concrete foundation with a specified compressive strength of 4,000 psi. The post was oriented to resist impact in strong-axis flexure. Design details for test nos. AKLP-1 through AKLP-4 are provided in Figures 5.1 through 5.5, and sample representative photographs documenting the construction and installation of the foundations are shown in Figures 5.6 through 5.10. Material specifications, mill certifications, and certificates of conformity for the reinforced concrete, socketed foundations are shown in Appendix F.

The post size was selected to provide a shear approximately equal to the Transpo coupling breakaway force of 22 kips. Assuming an actual yield stress equal to the nominal stress, 50 ksi, a plastic section modulus of 11.7 in.^{3} for strong axis flexure resulting from impact against the flange face, and a moment arm equal to the impact height of 25 in., the theoretical peak expected shear was 23.4 kips, 6 percent higher than the target value of 22 kips. The post was embedded 3 ft into the 6 ft foundation.

Each foundation was constructed with a diameter matching the average diameter in AK DOT&PF L-30.11 (recall Figure 2.1), but a Sonotube form was substituted for the corrugated steel form, as shown in Figure 5.6. Substitution of the smooth Sototube form was considered a conservative modification by reducing tangential engagement between the foundation and soil, resulting in increased foundation displacement during the impact event. Longitudinal reinforcing was not expected to significantly influence test results, and so was reduced from #11 to #8 bars to approximately the minimum allowable reinforcing ratio for a column-type concrete element. Similarly, spiral reinforcing would provide improved performance if the foundation was required to develop its full capacity in combined axial and flexure effects, particularly if ductility was required such as for seismic demands. These considerations likely dictated the standard reinforcing used by AK DOT&PF for foundations. However, the transverse reinforcing only needed to resist breakout by shear from the embedded post, so the spiral reinforcing was changed to discrete circular hoop ties typically spaced at 12 in. but with three additional ties near the top of the foundation (spacing reduced to 6 in.) to ensure shear breakout at the post would not occur.

Boring logs provided by AKDOT&PF indicated that near-surface soils were generally sandy soils (recall Figure 2.3). Accordingly, a test pit was excavated and fill that met the criteria of Type A-3 sand material as specified by the American Association of State Highway and Transportation Officials (AASHTO) was placed around the foundation for each test. An initial effort was made to experiment with various compaction protocols using small test pits to achieve the target unit weight and corresponding target SPT blow count of 7. The small test pits were 3-ft diameter, 4-ft deep excavations in the native soil at the test site. Based on that initial effort, a compaction protocol was initially adopted to place soil in 8-in. lifts, with three passes using a pneumatic piston tamper after placing each lift. Figure 5.7 shows the compaction procedure in-progress for test no. AKLP-1. This procedure was similar to the protocol typically used when placing MASH strong soil, but the initial small test pits had indicated that SPT values remained low for sand fill regardless of this protocol.

SPT blow counts were obtained by Drs. Chung Rak Song and Seunghee Kim for each of test nos. AKLP-1 to AKLP-4 using a GeoProbe 7822DT drill rig fitted with a DH103 Automatic Drop Hammer. Sample photos taken during SPT testing for test no. AKLP-1 are provided in Figure 5.8 and 5.9. SPT blow counts are shown for each of test nos. AKLP-1 to AKLP-4 in Figures 57. For test no. AKLP-1, SPT blow counts were 7, 15, and 20 for the successive 18-in. tests progressing from the ground surface. This result was not in agreement with the objective to test weak soil conditions with low SPT values, likely due to overburden and repeated successive compaction passes with the piston tamper in the 10-ft x 10-ft x 8-ft deep foundation testing pit, resulting in higher SPT blow counts than had been observed previously for the 3-ft diameter x 4-ft deep small test pits.

After testing with a higher than desired soil stiffness for test no. AKLP-1, the foundation was excavated and most of the soil to the depth of the foundation was removed from the pit. A new test article was placed in the pit for test no. AKLP-2, sitting on a 2-ft thick base layer of previously compacted soil, and sand fill was placed loose around the foundation to bracket extreme lower bound soil stiffness conditions. The sand for test no. AKLP-2 was not subject to any compaction other than overburden from self-weight. SPT tests were performed at locations approximately midway between the test article and three of the soil pit corners for test no. AKLP-2. The sampler initially sank into the soil under the static weight of the 140 lb hammer at each location, represented by values of 0 for varying depths at different hole locations. Blow counts were generally less than 5 for the upper 4 ft of the soil, but increased noticeably as the sample depths neared previously compacted conditions from test no. AKLP-1 around 6 ft.

In an attempt to replicate a more uniform weak soil condition similar to the HNS boring log from AK DOT&PF, the soil compaction protocol was modified from that used for test no. AKLP-1 to reduce the compaction applied at moderate depths. Instead of three passes with the piston tamper, a single pass was performed after each 8-in. lift, except for the top 2 ft of soil. The top 2 ft received three passes, as the SPT for the first sample near the ground surface for test no. AKLP-1 exhibited the target SPT value of 7 after being placed with three passes. This modified protocol was followed for both test nos. AKLP-3 and AKLP-4, and resulted in SPT blow counts generally closer to the target value of 7 approximately uniformly along the depth, although the values were now too low at the uppermost layer and remained higher than desired at deeper locations.

Blow counts at approximately 2 ft and deeper were greater for test no. AKLP-4 in comparison to test no. AKLP-3. The two tests differed with respect to soil moisture content. Some boring logs provided by AK DOT&PF reported high water table elevations and moisture contents around 15% to 23%. In particular, the HNS log selected as a target reference for SPT blow counts reported a sampled moisture content of 18.4% around 4 ft below the ground surface. A target of 18% moisture content was selected to represent a high moisture content condition for the testing program (referred to as "Saturated" on the test plans). Test no. AKLP-3 was performed with increased moisture content, and test no. AKLP-4 was performed with nominally dry soils similar to test nos. AKLP-1 and AKLP-2. "Dry" referred to in-situ conditions, typically with moisture contents around 1% to 3%. 1500 gallons of water were added to the soil for test no. AKLP-3 during the day prior to testing. Additional water was added prior to performing the test, reaching a total of approximately 1800 gallons, which should have produced a moisture content close to 18%. Laboratory testing of samples obtained from the SPT testing shortly before executing the impact test indicated moisture contents ranging approximately 5% to 8%, reflecting that a significant portion of the water had flowed out of the sand fill into the soil underlying the test site concrete tarmac. This observation influenced test preparation procedures for a subsequent specimen with a light pole mounted to the concrete foundation, discussed later in this report.

Test Number	Impact Speed (mph)	Impact Orientation	Target Soil Condition	Post Length (in.)	Post Embedment Depth (in.)	Foundation Depth (in.)	Post Specifications	Impact height (in.)
1	19	Strong Axis	Dry, See Note 1	72	36	72	W6x16	25
2	19	Strong Axis	Dry, See Note 2	72	36	72	W6x16	25
3	19	Strong Axis	Saturated, See Note 3	72	36	72	W6x16	25
4	19	Strong Axis	Dry, See Note 4	72	36	72	W6x16	25

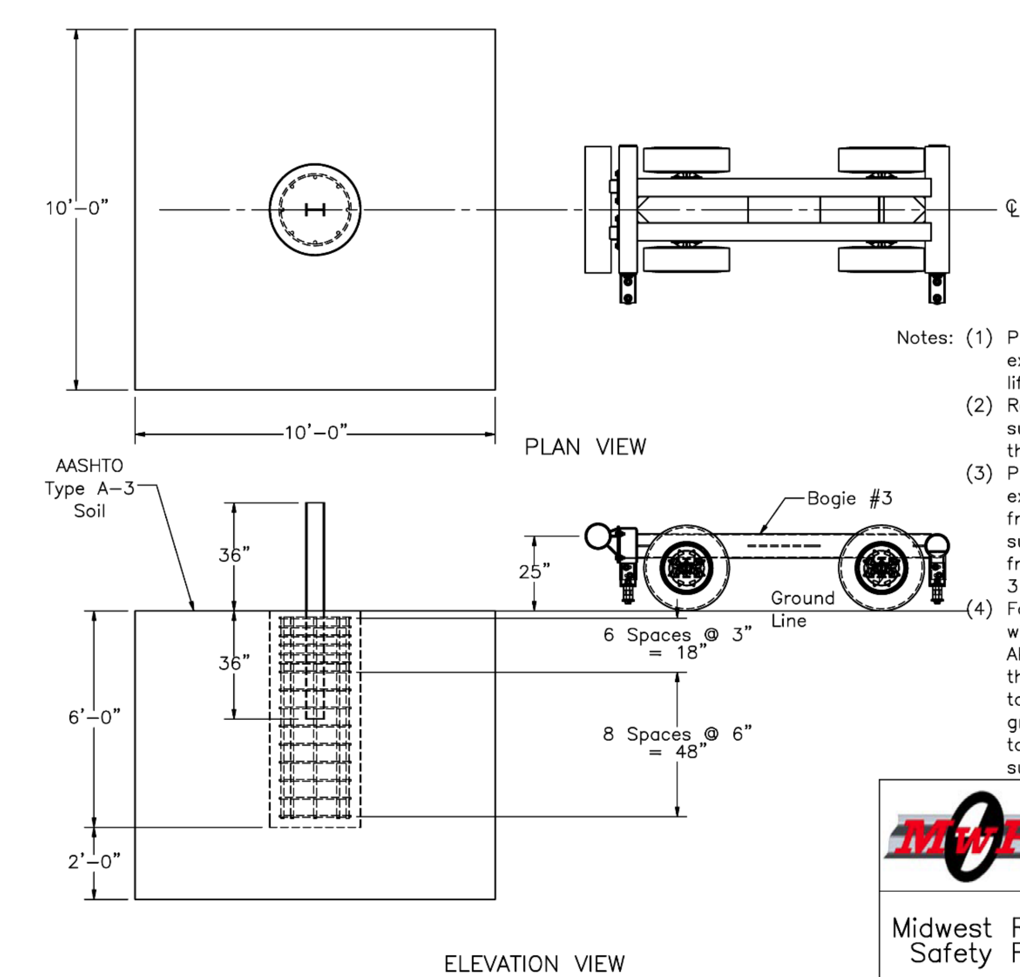

Notes: (1) Place soil in 8" lifts for the full height of the excavation, with 3 passes of piston tamper at each lift.
(2) Remove and replace foundation for this and each subsequent test. Place soil loose (no compaction) for the full height of the specimen.
(3) Place soil in 8" lifts for the full height of the excavation. Compact with 1 pass of a piston tamper from a depth of 6 ft up to 2 ft from the ground surface. Compact with 3 passes of a piston tamper from a depth of 2 ft up to the ground surface. Test 3 to be conducted with saturated soil conditions.
(4) For AKLP-4, remove AKLP-3 foundation and replace with AKLP-2 foundation oriented 180 degrees from AKLP-2. Place soil in 8" lifts for the full height of the excavation. Compact with 1 pass of a piston tamper from a depth of 6 ft up to 2 ft from the ground surface. Compact with 3 passes of a piston tamper from a depth of 2 ft up to the ground surface.

Midwest Roadside Safety Facility

Alaska DOT Light Poles
Test No. AKLP 1–4

Test Layout

SHEET: 1 of 5
DATE: 4/12/2024
DRAWN BY: SBW/GHR/MM
DWG. NAME. AKLP-1-4_R7
SCALE: 1:50
UNITS: in.
REV. BY: JSS/CSS

Figure 5.1 Bogie Testing Matrix and Setup, Test Nos. AKLP-1 through AKLP-4

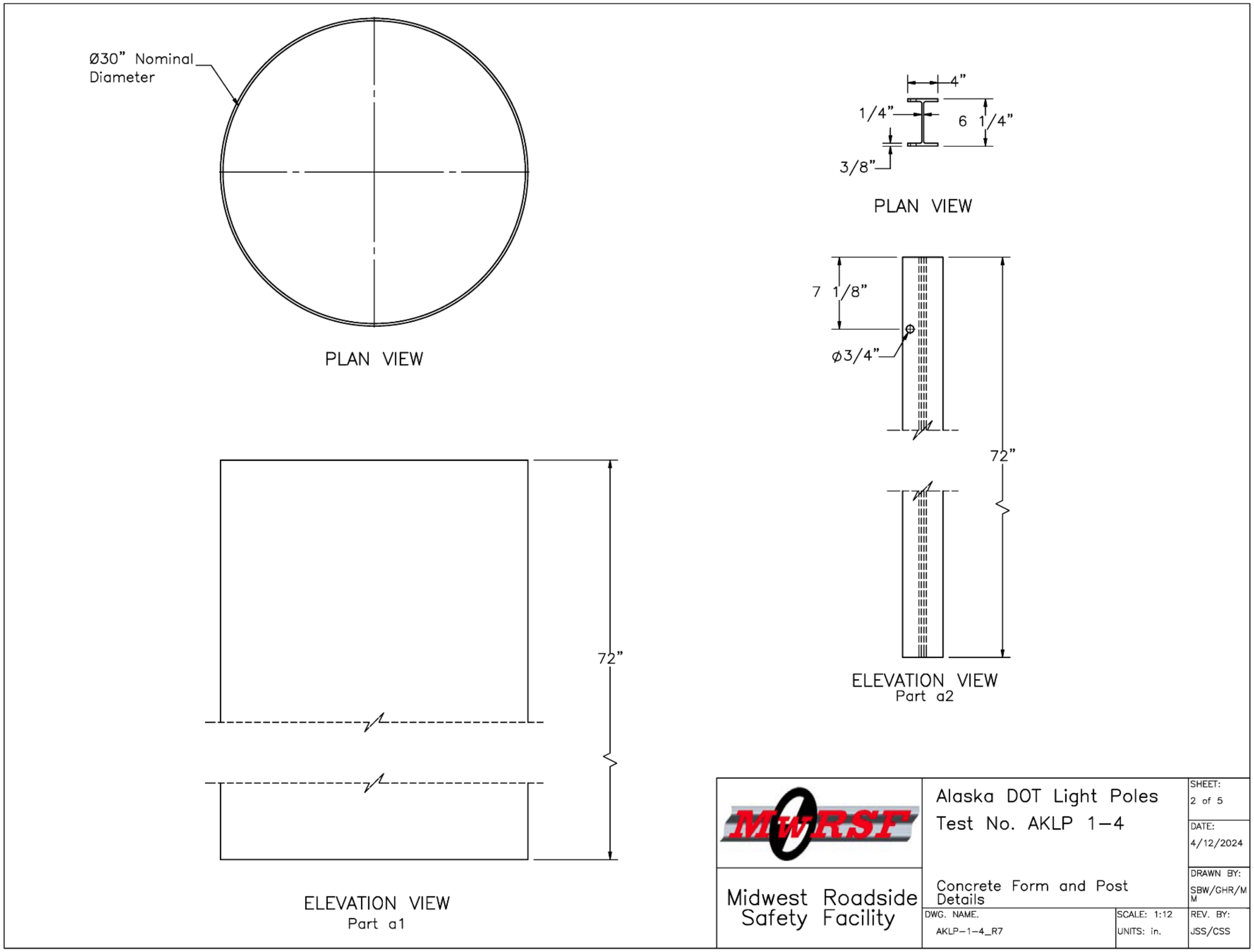

Figure 5.2 Concrete Form and Post Details, Test Nos. AKLP-1 through AKLP-4

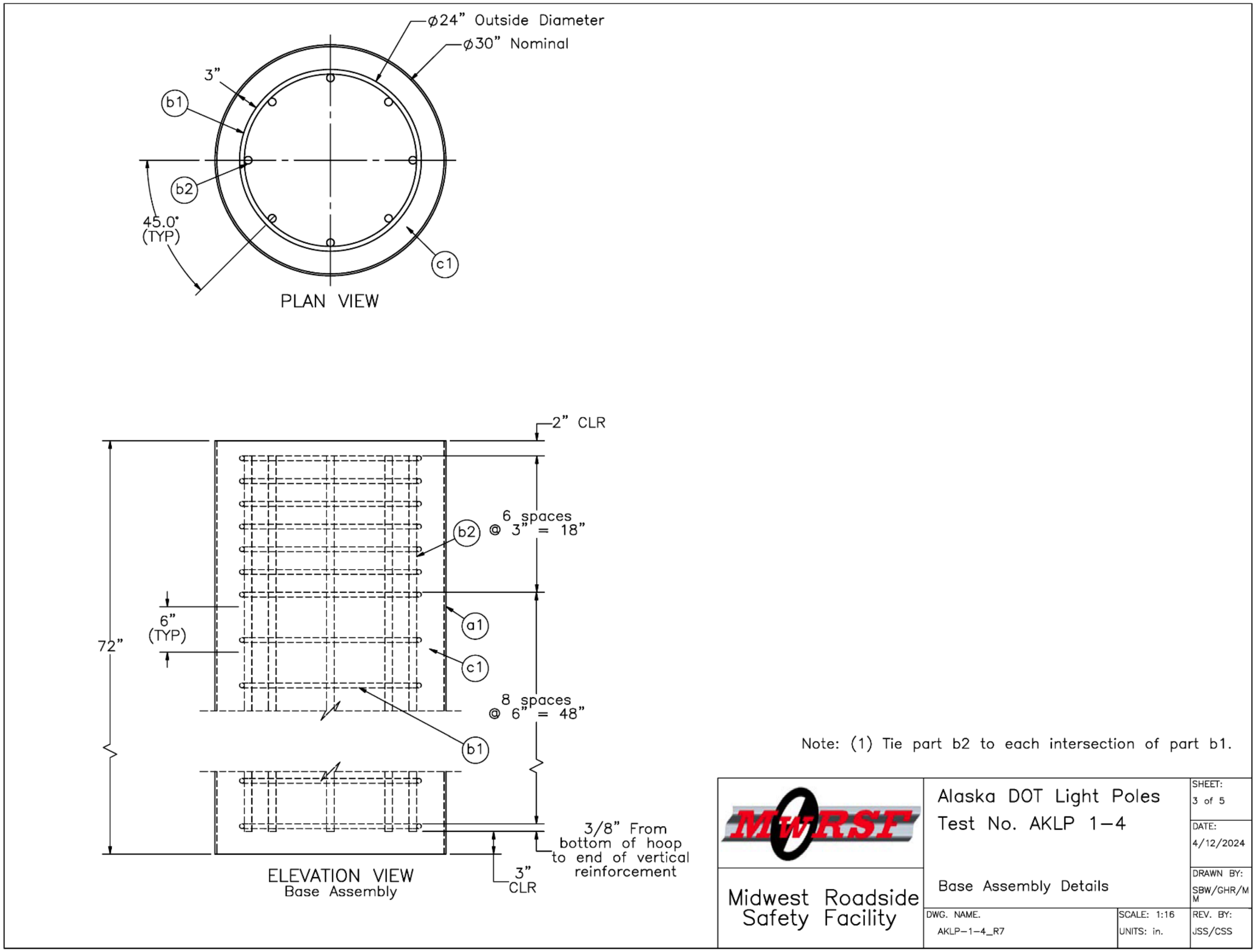

Figure 5.3 Base Assembly Details, Test Nos. AKLP-1 through AKLP-4

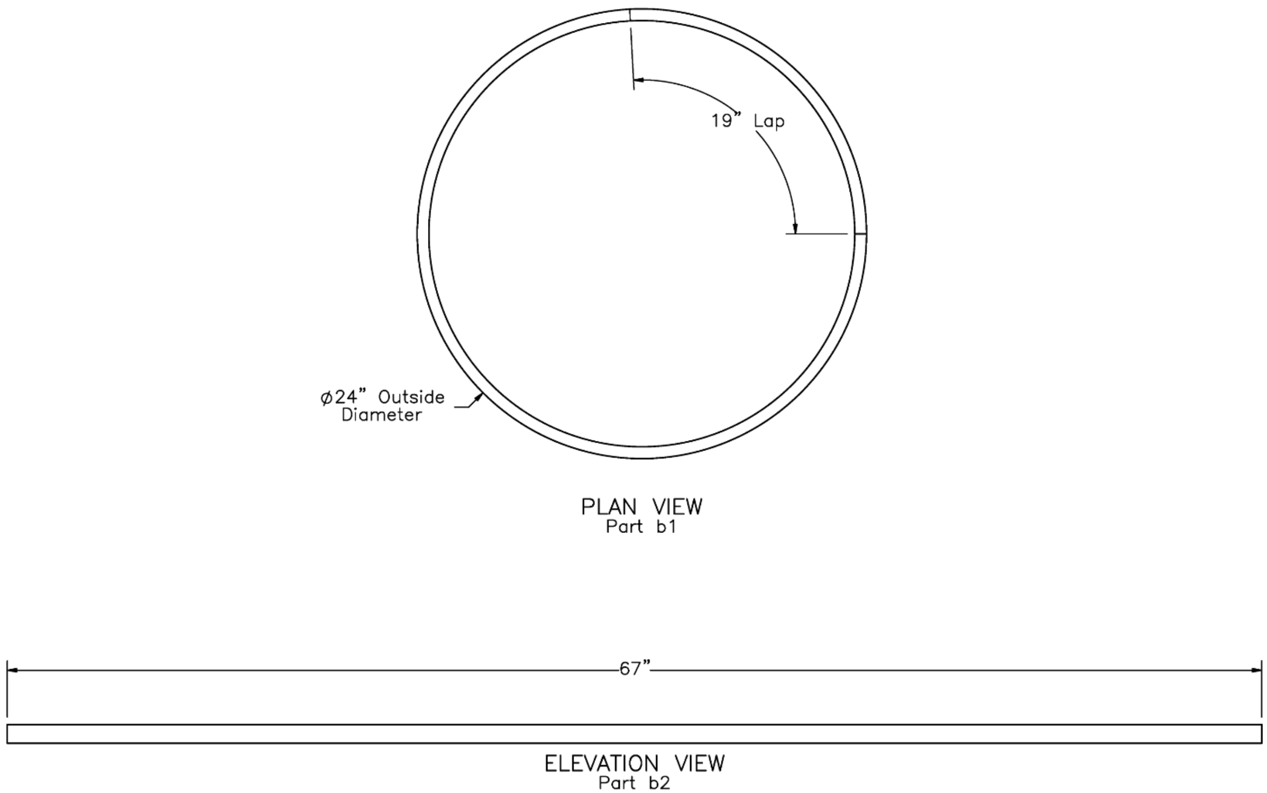

Notes: (1) Tie vertical reinforcing steel to each intersection of the tranverse and longitudinal reinforcing steel.

* Epoxy coating is optional for testing purposes.

Bill of Bars

Bar	QTY.	Size	Total Unbent Length	Material Specification	Treatment Specification
b1	15	#5	95”	ASTM A615 Gr. 60	*Epoxy–Coated (ASTM A775 or ASTM A934)
b2	8	#8	67”	ASTM A615 Gr. 60	*Epoxy–Coated (ASTM A775 or ASTM A934)

Midwest Roadside Safety Facility

Alaska DOT Light Poles
Test No. AKLP 1–4

Rebar Details

SHEET: 4 of 5
DATE: 4/12/2024
DRAWN BY: SBW/GHR/MM
DWG. NAME. AKLP–1–4_R7
SCALE: 1:8
UNITS: in.
REV. BY: JSS/CSS

Figure 5.4 Rebar Details, Test Nos. AKLP-1 through AKLP-4

Item No.	QTY.	Description	Material Specification	Treatment Specification	Hardware Guide
a1	1	30" Diameter Sonotube	–	–	–
a2	1	W6x16, 72" Long Steel Post	ASTM A992	–	–
b1	15	#5 Bar, 95" long, Circular Hoop Tie	ASTM A615 Gr. 60	*Epoxy–Coated (ASTM A775 or A934)	–
b2	8	#8 Bar, 67" Long	ASTM A615 Gr. 60	*Epoxy–Coated (ASTM A775 or A934)	–
c1	–	Concrete	AKDOT & PF Class A or Equivalent, f'c=4000 psi	–	–
d1	–	Clean, Fine Sand	AASHTO Type A–3	–	–

* Epoxy coating is optional for testing purposes.

Notes: (1) Quantites listed herein are only for 1 system installation.

Midwest Roadside Safety Facility

Alaska DOT Light Poles
Test No. AKLP 1–4

Bill of Materials

SHEET: 5 of 5

DATE: 4/12/2024

DRAWN BY: SBW/GHR/MM

DWG. NAME. AKLP–1–4_R7

SCALE: 1:96
UNITS: in.

REV. BY: JSS/CSS

Figure 5.5 Bill of Materials, AKLP-1 through AKLP-4

Figure 5.6 Construction Photographs, Test No. AKLP-1

Figure 5.7 Sand Compaction In-Progress, Test No. AKLP-1

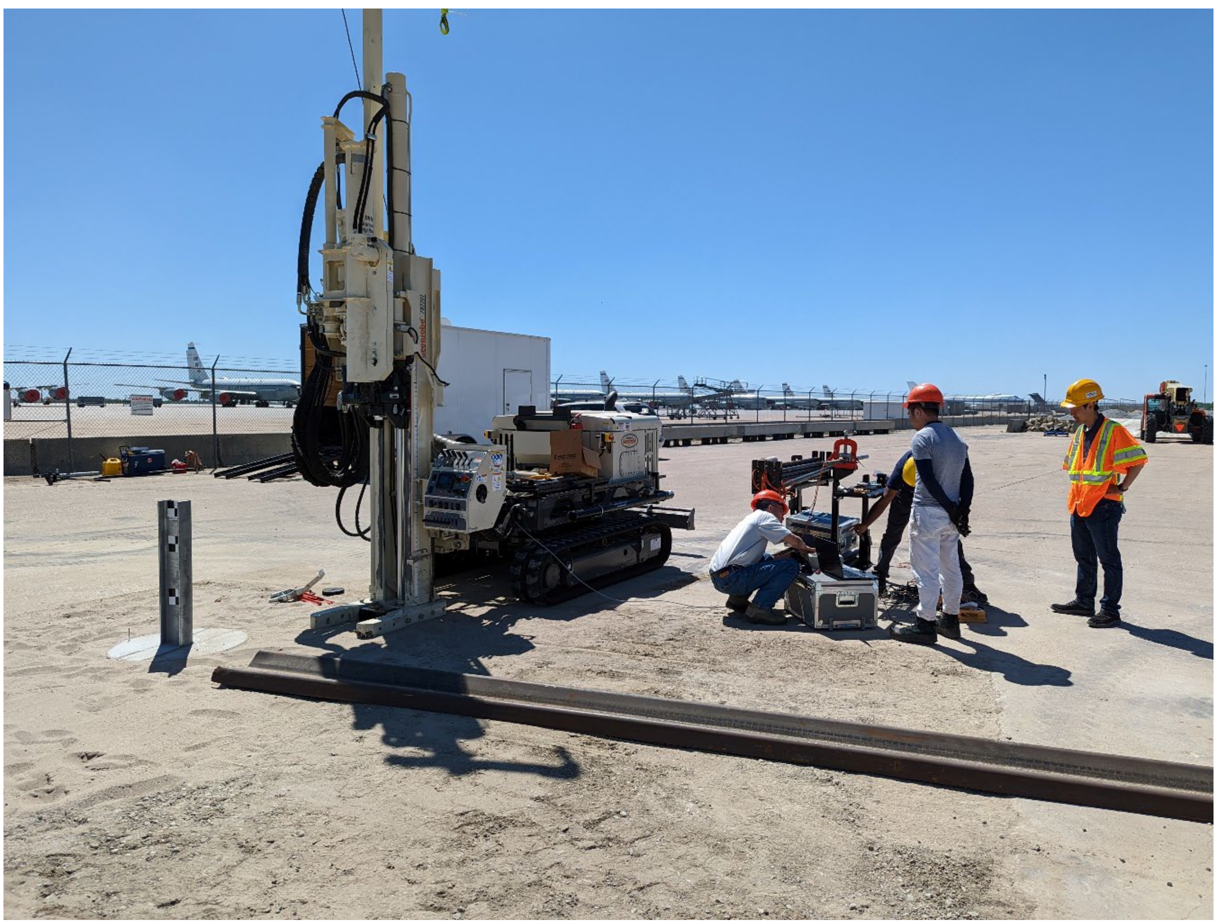

Figure 5.8 GeoProbe Preparing for Soil Testing, Test No. AKLP-1

Figure 5.9 GeoProbe Sampler for SPT Testing, Test No. AKLP-1

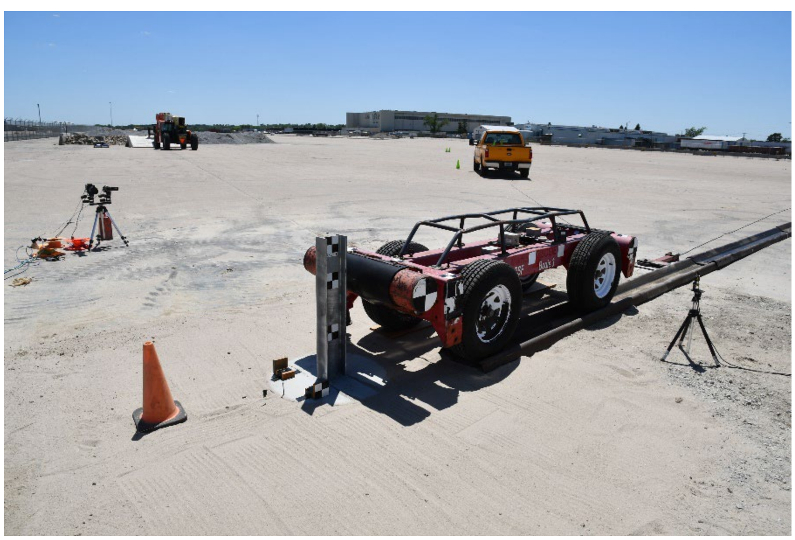

Figure 5.10 Pre-Test Photos, Test No. AKLP-1

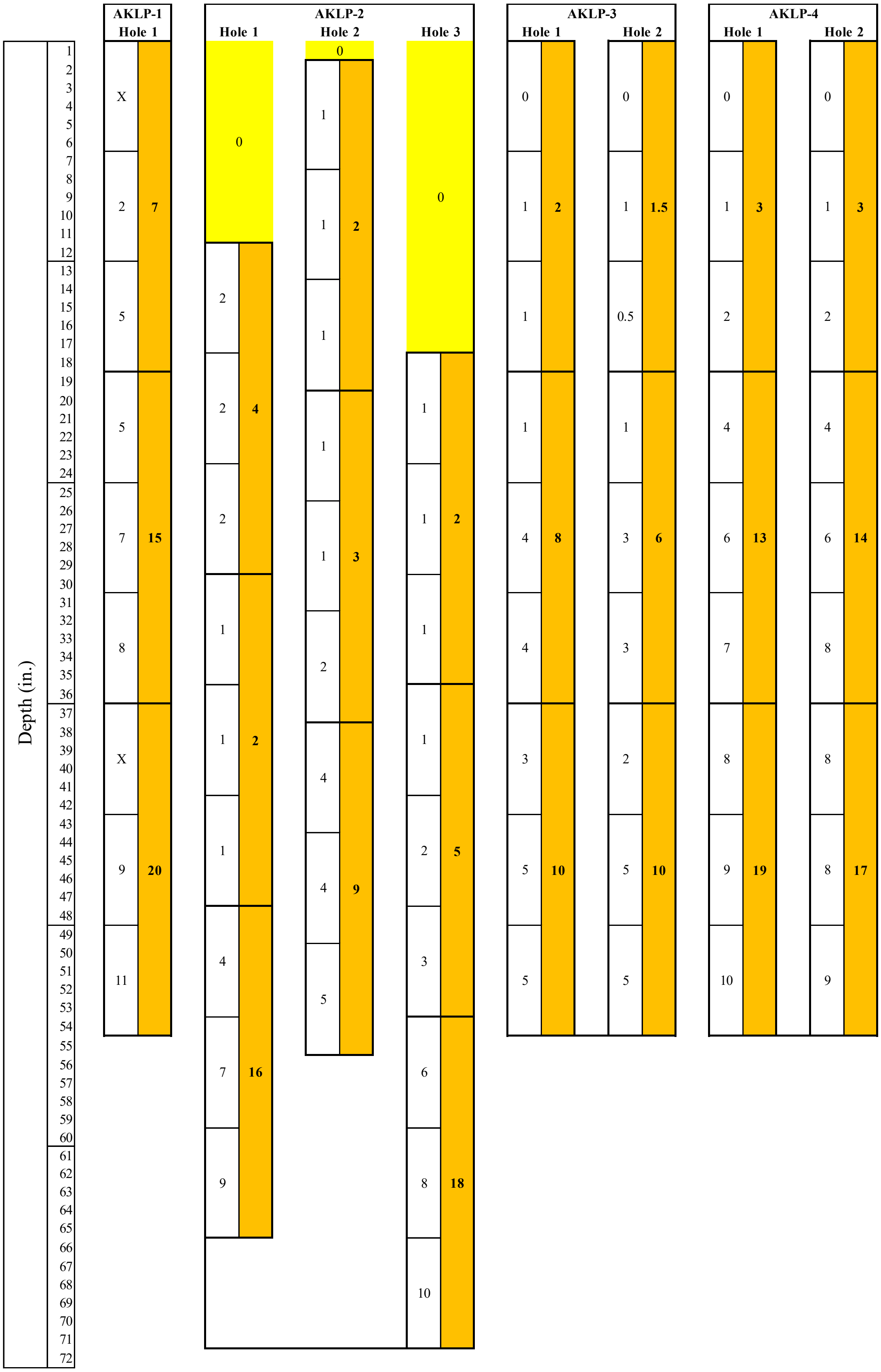

Figure 5.11 Measured SPT Blow Counts As-Installed for Test Nos. AKLP-1 through AKLP-4

Chapter 6 COMPONENT TESTING – FOUNDATIONS WITH EMBEDDED STEEL POSTS

6.1 Purpose

Tests on foundations with embedded steel posts were performed to assess the foundations' mechanical response during simulated impact events. Key performance characteristics included force versus displacement, energy versus displacement, and force versus lateral deflections. The intent of the tests was focused on cost-effectively investigating soil properties and behavior prior to performing tests on full-scale light poles, as the resistive forces offered by soil and the consequent displacements experienced by foundations during impact events were expected to be significantly influenced by soil stiffness.

6.2 Scope

Four bogie tests were conducted on three foundation specimens, as detailed in Chapter 5. Soil stiffness is correlated with soil compaction, density, and SPT blow counts. Tests varied compaction protocols, and included a comparative case of dry versus wetted soils. A matrix of test conditions is available in Chapter 5, in Figure 5.1.

6.3 Foundations with Embedded Posts Results

Through component testing, the performance of each foundation in varying soil conditions was evaluated in terms of the impact force as a function of displacement, the energy dissipated as a function of displacement, and the displacement of the foundation. Peak forces were desired to be at least as large as the Transpo breakaway couplings' activation threshold. Residual displacements would ideally be less than or equal to 1.8 in., although greater displacements did not necessarily disqualify a foundation as a candidate for light pole testing. The elongated impulse imposed on the foundation by plastic hinging of the embedded post was expected to produce greater displacements for the embedded post than would occur with breakaway couplings, as observed in preliminary modeling (recall Chapter 1).

Accelerometer data was used to ascertain the impact force. Displacements determined from the accelerometer data pertain to the motion of the bogie and section of the post in contact with the bogie, while the displacements recorded by the string potentiometer indicate foundation top surface displacement. Given that these displacements correspond to distinct components, the magnitudes and corresponding times of initial motion are anticipated to differ, with greater displacement at the bogie contact location than at the top surface of the foundation, as well as initiating earlier due to inertial activation of the foundation delaying foundation displacement.

The acceleration data was obtained at approximately the center of gravity of the bogie. This introduced a degree of error into the data, attributed to the bogie's lack of perfect rigidity and passages of vibratory stress waves within the bogie. Filtering procedures were applied to the data to mitigate errors associated with vibrations along the bogie frame. Although the bogie experienced slight rotations (pitching) during impact, the rotations were found to be insignificant. The data was deemed to be valid for representing the impact force applied between the bogie head and post.

6.3.1 Test No. AKLP-1

During test no. AKLP-1, a 1,860-lb bogie struck the post and foundation assembly traveling at a velocity of 18.9 mph. The bogie impacted the post flange at 25 in. above the ground line, causing strong-axis bending in the post. Upon impact, post hinging and rotation were observed prior to visible motion of the foundation through the soil. The bogie's forward momentum was arrested at approximately the 0.042-second mark following contact. The bogie pitched backward, sliding upward along the post flange, and losing contact with the post assembly at approximately the 0.100-second mark following contact. The post exhibited plastic deformation at its base. Cracking was observed at the top surface of the concrete, extending from the outer edges of the steel post flexural tension flange. Time-sequential and component damage photographs are provided in Figures 6.1 and 6.2.

The contact force rose smoothly to a peak force of 38.3 kips coinciding with an approximately 2.5-in. displacement of the post at the impact height. Following the peak value, the force plateaued at approximately 37.1 kips up to a displacement of 8.0 in. Beyond this displacement, the bogie's momentum was depleted and the bogie came to rest against the test article. Article rebound from its peak displacement was negligible. During the impact, the post, foundation, and soil absorbed a total energy of 266.3 kip-in., equal to the kinetic energy of the bogie immediately before impact, and reflecting that the bogie's forward motion was fully arrested. Force versus displacement and energy versus displacement plots, derived from accelerometer data, are depicted in Figure 6.3.

Data obtained via a string potentiometer indicated that the top of the reinforced concrete foundation attained maximum dynamic and permanent set deflections of approximately 1.5 in. and 0.9 in., respectively, as shown in Figure 6.4.

Impact

0.050 sec

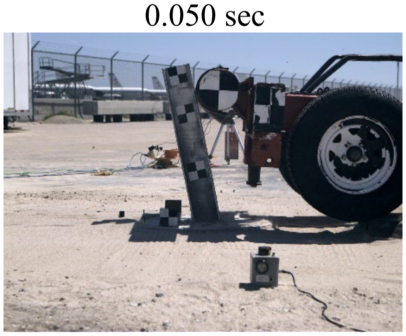

0.100 sec

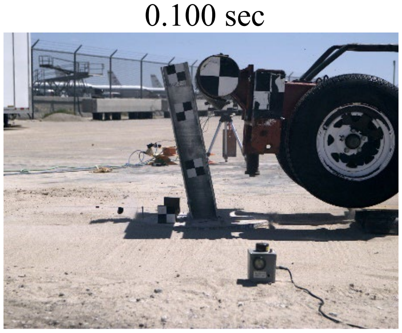

0.150 sec

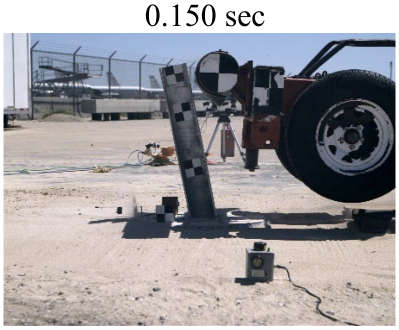

0.200 sec

Figure 6.1 Time-Sequential and Damage Photographs, Test No. AKLP-1

Impact

0.050 sec

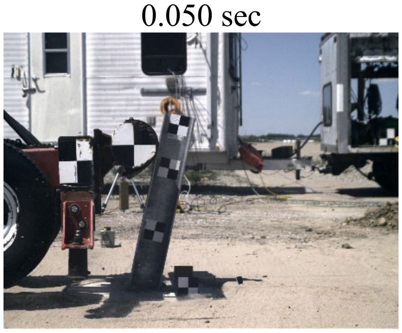

0.100 sec

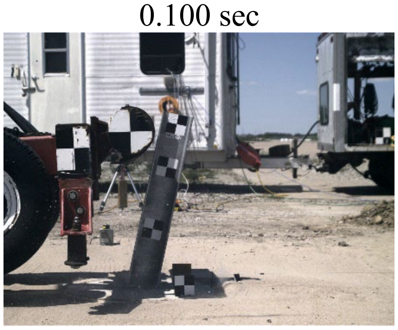

0.150 sec

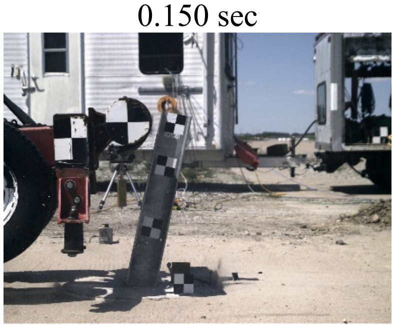

0.200 sec

Figure 6.2 Additional Time-Sequential and Damage Photographs, Test No. AKLP-1

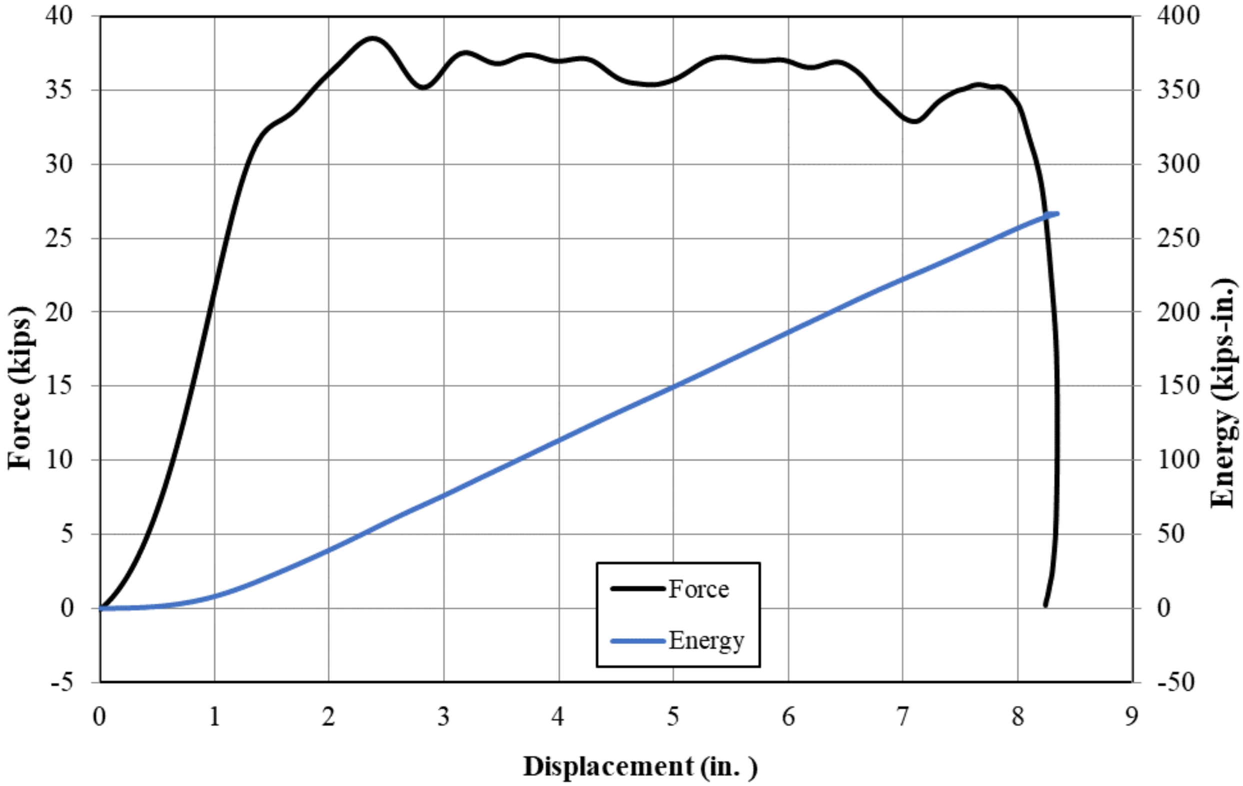

Figure 6.3 Force vs. Displacement and Energy vs. Displacement Response, Test No. AKLP-1

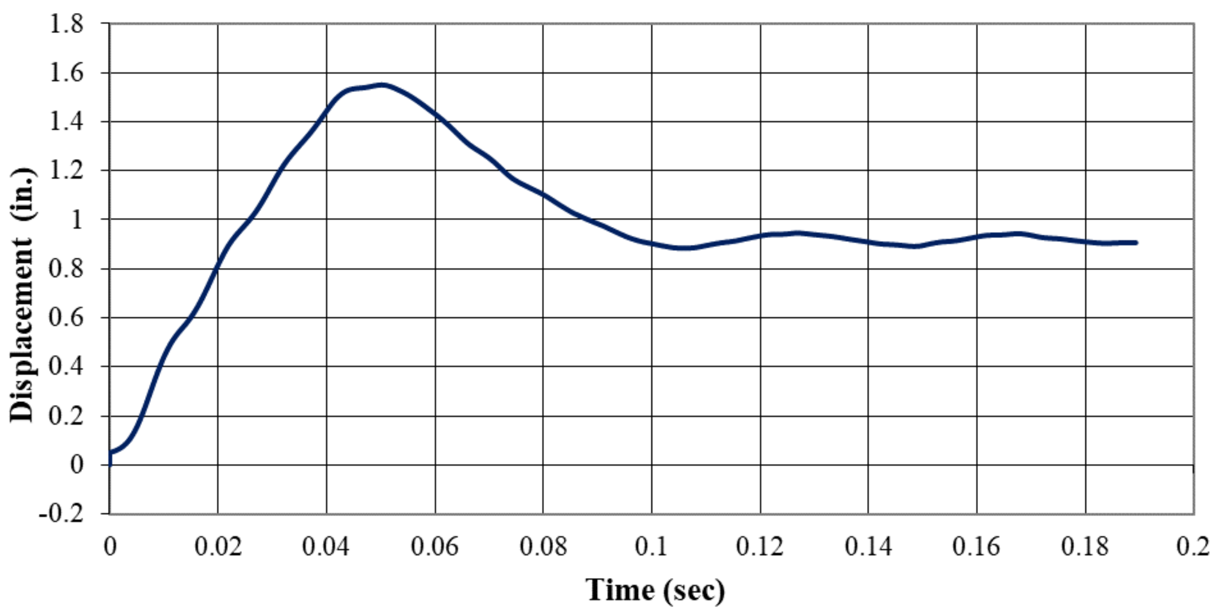

Figure 6.4 Displacement of the Foundation, Test No. AKLP-1

6.3.2 Test No. AKLP-2

During test no. AKLP-2, a 1,860-lb bogie struck the post and foundation assembly traveling at a speed of 19.0 mph. The bogie impacted the post flange at 25 in. above the ground line, causing strong-axis bending in the post. Upon impact, post hinging and rotation were observed prior to visible motion of the foundation through the soil. The bogie's forward momentum was arrested at approximately the 0.194-second mark following contact, at which time the foundation had undergone a large rotation in the soil. Bogie pitch was minor. Upon arrest of forward momentum, the bogie head slid down the face of the post until the bogie came to rest. The post exhibited plastic deformation at its base, evident by slight curvature of the compression flanges slightly above the concrete surface and flaking of the galvanizing coating. Plastic hinging was more clearly evident following excavation of the test article from the pit due to the tilt of the post when viewed in profile. Cracking was observed at the top surface of the concrete, extending from the outer edges of the steel post flexural tension flange. Time-sequential and component damage photographs are included in Figures 6.5 and 6.6.

The contact force rose smoothly to a peak force of 36.9 kips, corresponding with an approximately 2.3-in. displacement of the post at the impact height. The bogie lost contact with the post between 0.040 and 0.060 seconds, corresponding to a bogie post-impact displacement of about 7.1 in., due to foundation rotation through the loose sand fill. Loss of contact is evident in the accelerometer data with contact force dropping to zero. The bogie regained contact with the post and the impact force climbed to a secondary peak of 14.8 kips before falling again and plateauing at around 5 kips to a bogie post-impact displacement of approximately 25.2 in. before coming to rest. The post and foundation assembly absorbed a total energy of 267.9 kip-in. during the impact event, equal to the kinetic energy of the bogie immediately before impact, and reflecting that the bogie's forward motion was fully arrested. Force versus displacement and energy versus displacement plots obtained from accelerometer data are displayed in Figure 6.7.

Recorded data from the string potentiometer indicated a maximum and permanent set displacement of 12.4 in. for the top of the reinforced concrete foundation, as depicted in Figure 6.8. String pot displacements represent relative motion between the instrument housing, mounted to the tarmac at the edge of the test pit opposite the impact side of the post, and a reference attachment point for the string – a screw affixed to and projecting upward from the top surface of the concrete at the leading edge of the foundation. Notably, as shown in Figure 6.6, the attachment reference was subsumed in the loose sand fill. The string from the instrument housing to the attachment reference was also partially subsumed and went slack when the cable tension was not adequate to retract the cable at the same speed as the foundation top surface travel during the test. Therefore, the reliability of displacement data beyond about 60 ms may be compromised and should be viewed as approximate.

Impact

0.050 sec

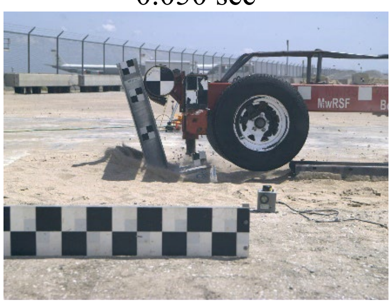

0.100 sec

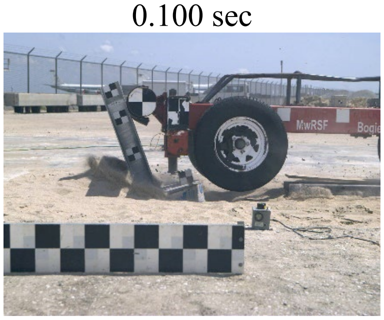

0.150 sec

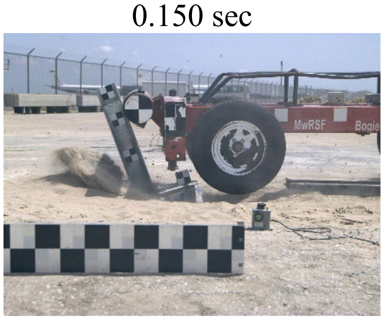

0.250 sec

Figure 6.5 Time-Sequential and Damage Photographs, Test No. AKLP-2

Impact

0.050 sec

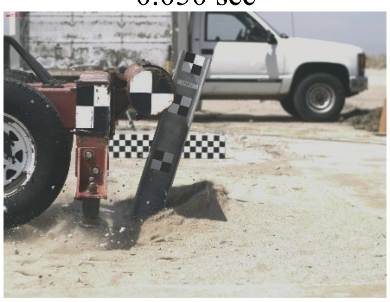

0.100 sec

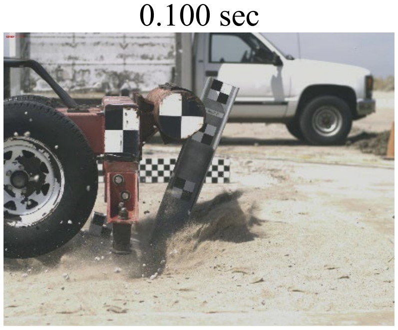

0.150 sec

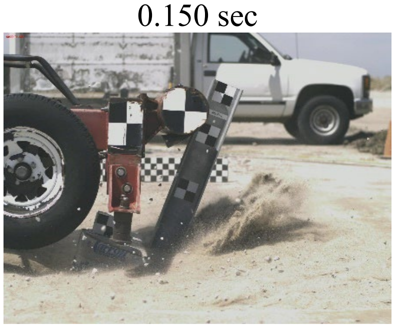

0.250 sec

Figure 6.6 Additional Time-Sequential and Damage Photographs, Test No. AKLP-2

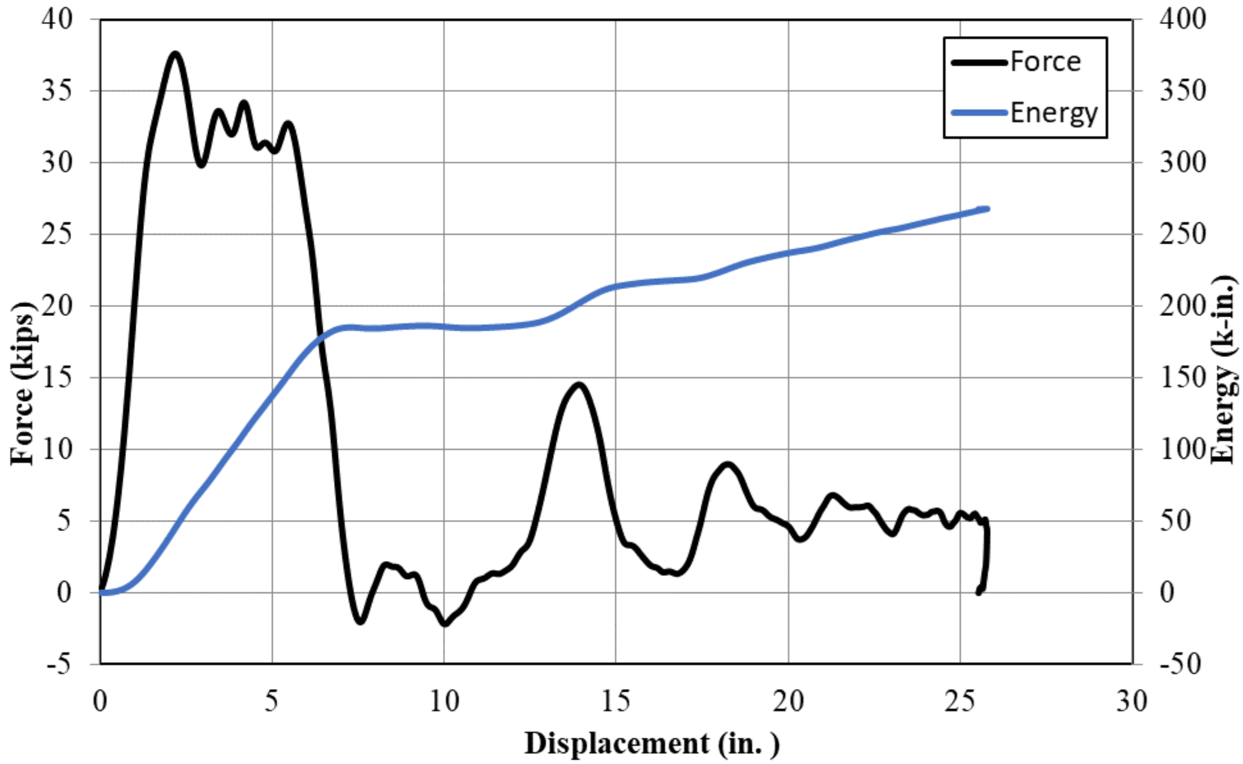

Figure 6.7 Force vs. Displacement and Energy vs. Displacement Response, Test No. AKLP-2

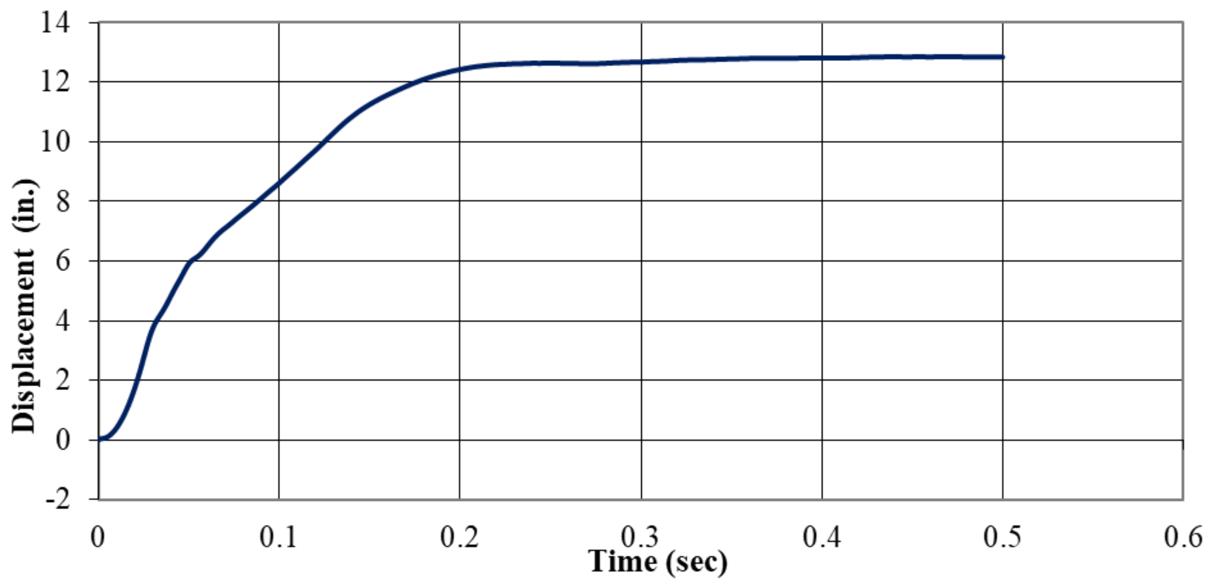

Figure 6.8 Displacement of the Foundation, Test No. AKLP-2

6.3.3 Test No. AKLP-3

During test no. AKLP-3, a 1,871-lb bogie struck the post and foundation assembly traveling at a velocity of 18.9 mph. The soil had been wetted the day before and the morning prior to the test, resulting in a moisture content approximately 5% to 8% in the sandy soil fill. The bogie's momentum was mostly arrested and the bogie pitched backward, sliding upward along the post flange, at approximately the 0.020-second mark following contact. The bogie head overrode the post and came to rest on the top of the post at approximately the 0.462-second mark following contact. The post exhibited plastic deformation at its base. Minor surface spalling was observed at the top surface of the concrete adjacent forward of the steel post flexural tension flange. Time-sequential and component damage photographs are provided in Figures 6.9 and 6.10.

The contact force rose smoothly to a peak force of 34.8 kips coinciding with an approximately 2.2-in. displacement of the post at the impact height. Following the peak value, the force plateaued at approximately 30.5 kips up to a displacement of 8.7 in. At that point, the bogie's momentum had been depleted and the bogie came to rest atop the test article. During the impact, the post, foundation, and soil absorbed a total energy of 268.0 kip-in, equal to the kinetic energy of the bogie immediately before impact, and reflecting that the bogie's forward motion was fully arrested. Force versus displacement and energy versus displacement plots, derived from accelerometer data, are depicted in Figure 6.11.

Data obtained via a string potentiometer indicated that the top of the reinforced concrete foundation attained maximum dynamic and permanent set deflections of approximately 1.8 in. and 1.2 in., respectively, as shown in Figure 6.12.

Impact

0.050 sec

0.100 sec

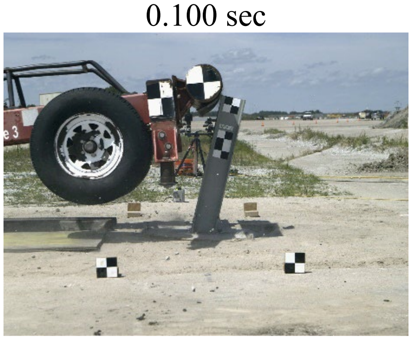

0.150 sec

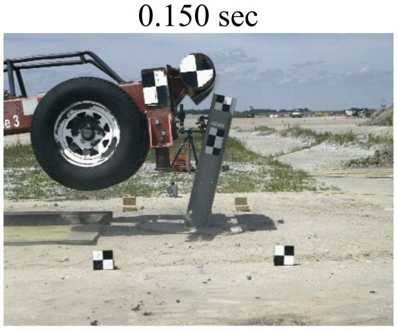

0.200 sec

Figure 6.9 Time-Sequential and Damage Photographs, Test No. AKLP-3

Impact

0.050 sec

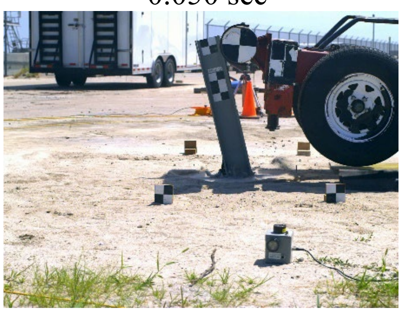

0.100 sec

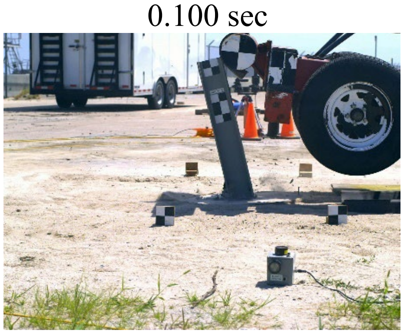

0.150 sec

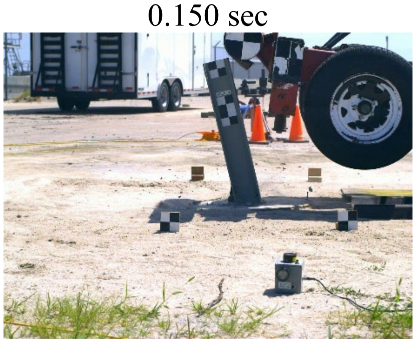

0.200 sec

Figure 6.10 Additional Time-Sequential and Damage Photographs, Test No. AKLP-3

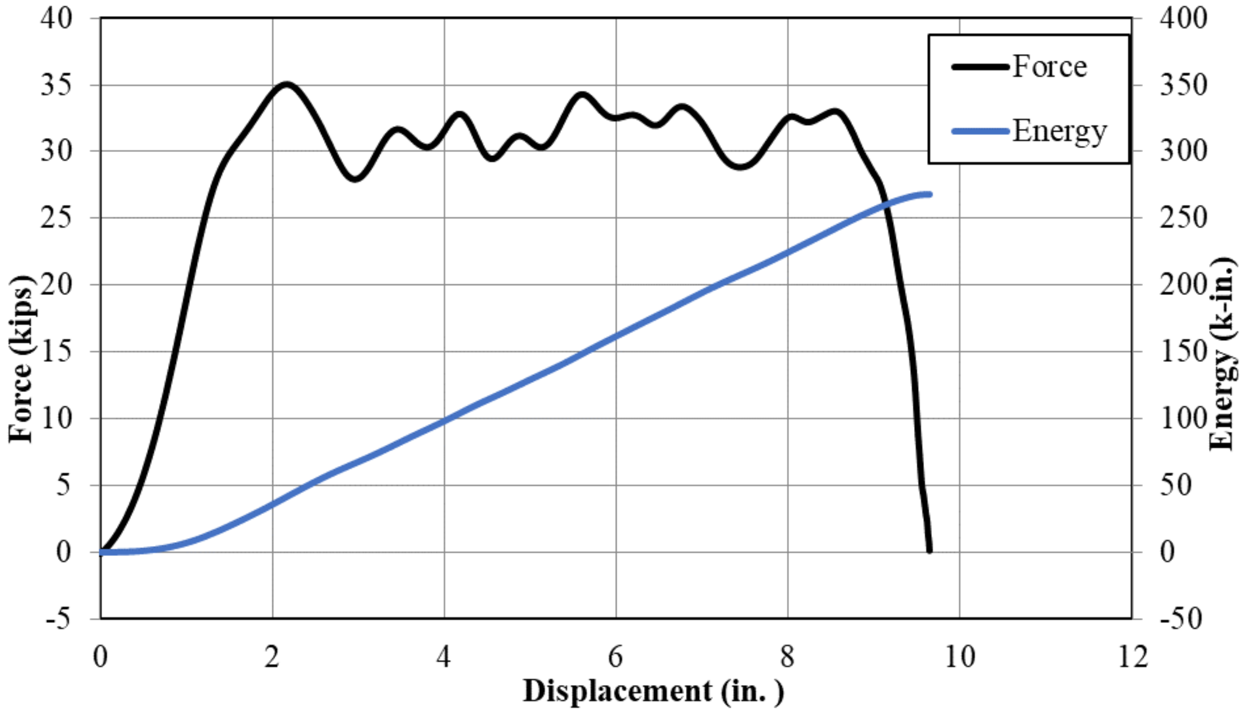

Figure 6.11 Force vs. Deflection and Energy vs. Deflection Responses, Test No. AKLP-3

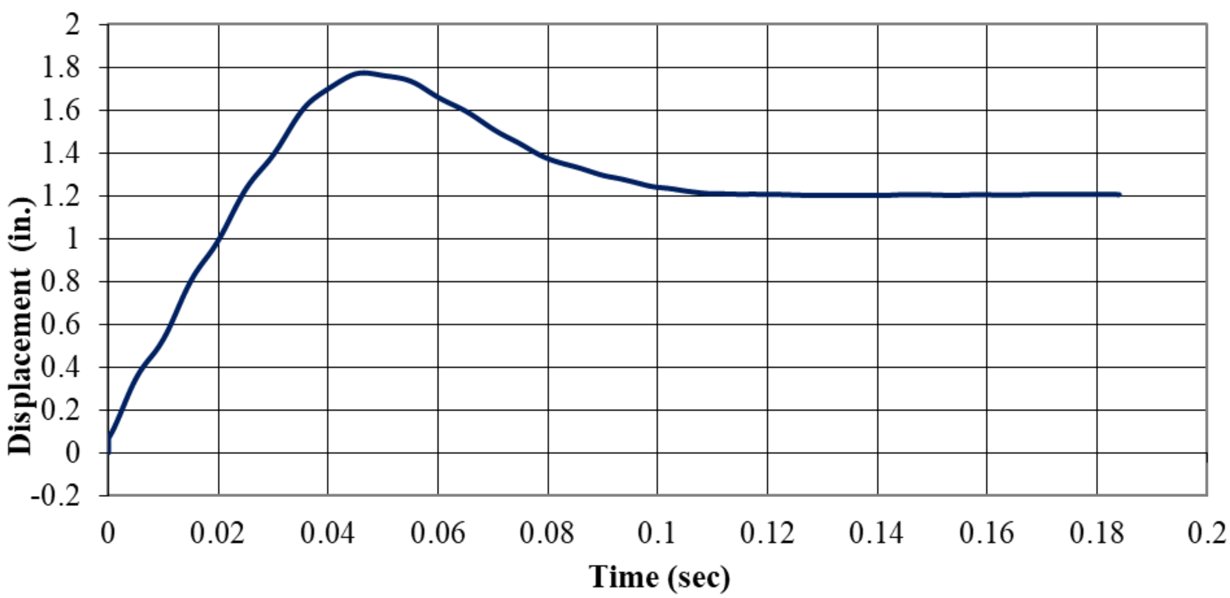

Figure 6.12 Displacement of the Foundation, Test No. AKLP-3

6.3.4 Test No. AKLP-4

The test article used previously with loose fill (no compaction) in test no. AKLP-2 had experienced less significant plastic deformation than other tests as a result of greater foundation movement in the loose soil. Its reuse was therefore deemed appropriate to obtain soil characterization test data in test no. AKLP-4 by installing the test article rotated 180 degrees from the orientation used in test no. AKLP-2. Soil placement and compaction procedures were identical to test no. AKLP-3, except that the soil was protected from weather for test no. AKLP-4 to ensure dry conditions, similar to test nos. AKLP-1 and AKLP-2.

During test no. AKLP-4, a 1,860-lb bogie struck the post and foundation assembly traveling at a velocity of 19.8 mph. The bogie impacted the post flange at 25 in. above the ground line, causing strong-axis bending in the post. Upon impact, post hinging and rotation were observed prior to visible motion of the foundation through the soil. The bogie's forward momentum was arrested at approximately the 0.044-second mark following contact. The bogie pitched backward, sliding upward along the post flange. The post exhibited plastic deformation at its base. Cracking and minor surface spalling were observed at the top surface of the concrete, extending from the outer edges of the steel post flexural tension flange. Time-sequential and component damage photographs are provided in Figures 6.13 and 6.14.

The contact force rose smoothly to a peak force of 35.8 kips coinciding with an approximately 2.5-in. displacement of the post at the impact height. Following the peak value, the force plateaued at approximately 35.2 kips up to a displacement of 8.9 in. Beyond this displacement, the bogie's momentum was depleted and the bogie came to rest against the test article. Article rebound from its peak displacement was minor. During the impact, the post, foundation, and soil absorbed a total energy of 291.7 kip-in., equal to the kinetic energy of the bogie immediately before impact, and reflecting that the bogie's forward motion was fully arrested. Force versus displacement and energy versus displacement plots, derived from accelerometer data, are depicted in Figure 6.15.

Data obtained via a string potentiometer indicated that the top of the reinforced concrete foundation attained maximum dynamic and permanent set deflections of approximately 1.6 in. and 0.9 in., respectively, as shown in Figure 6.16.

Impact

0.050 sec

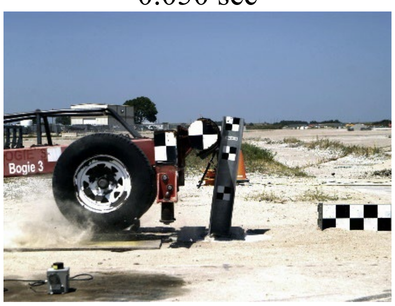

0.100 sec

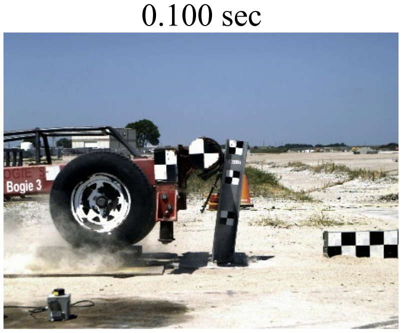

0.150 sec

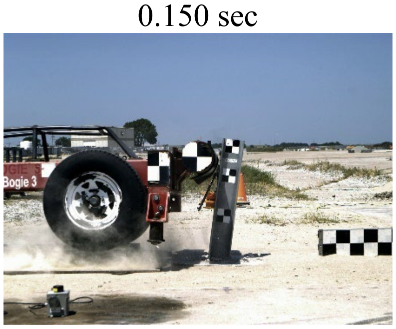

0.250 sec

Figure 6.13 Time-Sequential and Damage Photographs, Test No. AKLP-4

Impact

0.050 sec

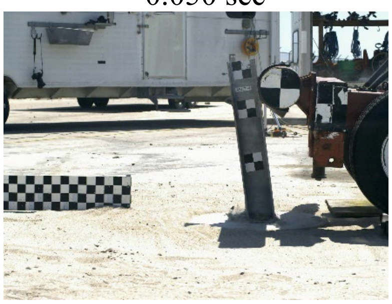

0.100 sec

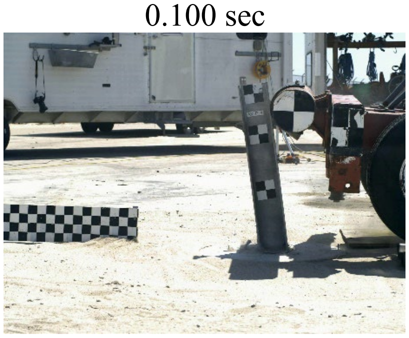

0.150 sec

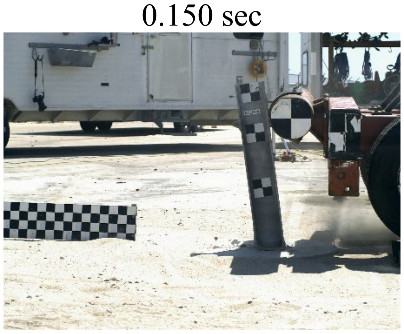

0.250 sec

Figure 6.14 Additional Time-Sequential and Damage Photographs, Test No. AKLP-4

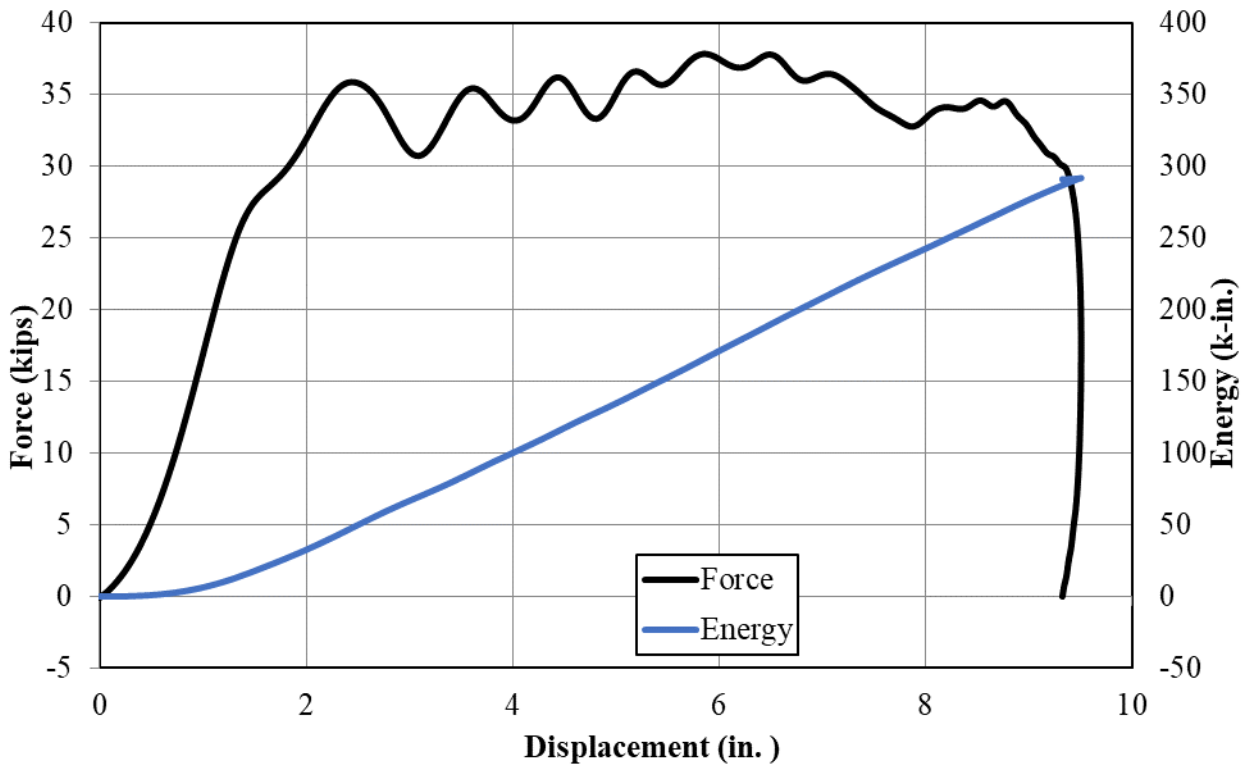

Figure 6.15 Force vs. Deflection and Energy vs. Deflection Responses, Test No. AKLP-4

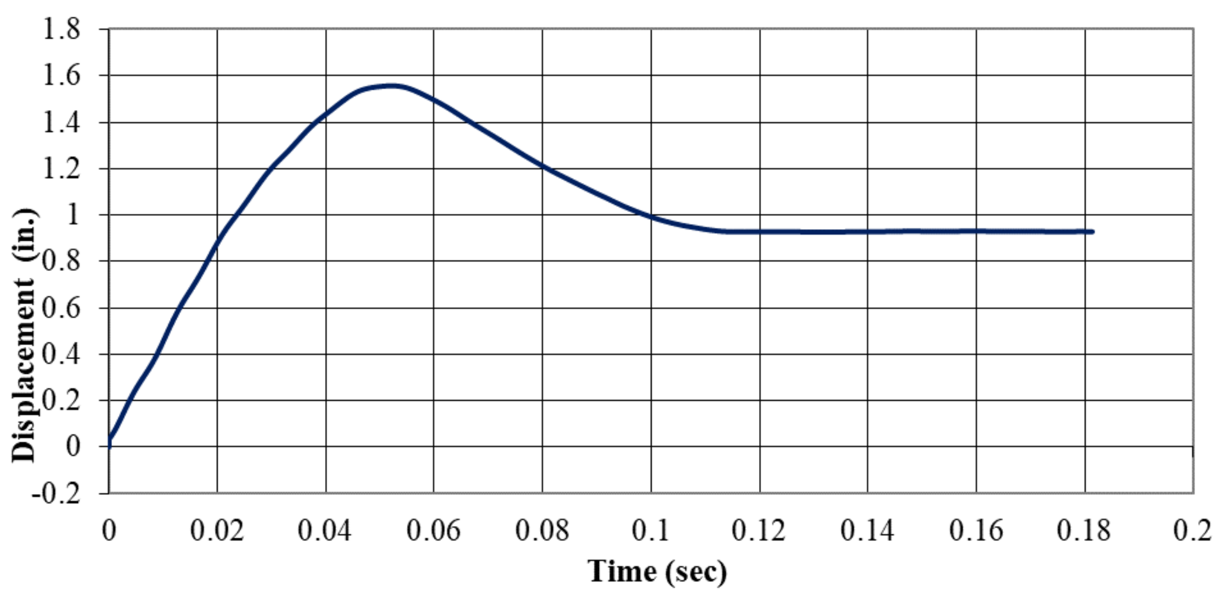

Figure 6.16 Displacement of the Foundation, Test No. AKLP-4

6.4 Summary of Bogie Tests on Embedded Posts

The results of the four bogie tests are summarized in Table 6.1. Additional data is available in Appendix G and Appendix H.

Table 6.1 Dynamic Testing Results

Test No.	Impact Velocity, mph	Peak Force, kips	Total Energy, kips-in.	Permanent Set Deflection, in.	Soil Condition
AKLP-1	18.9	38.3	266.3	0.9	Dry
AKLP-2	18.9	36.9	267.9	(±, ≥) 12.4	Dry
AKLP-3	18.9	34.8	268.0	1.2	Partially Saturated
AKLP-4	19.8	35.8	291.7	0.9	Dry

These tests were executed under similar impact parameters, which included:

- Utilization of a consistent W6x16 steel post section with an overall length of 72 in. and embedment depth measuring 36 in.
- Employment of an identical bogie impact head
- A constant impact height set at 25 in. above the ground line
- Implementation of a consistent concrete foundation having a diameter of 30 in. and an embedment depth of 72 in. (6 ft)
- Use of a surrogate bogie vehicle typically weighing 1,860 lb
- Impact velocities in close proximity to the predetermined target velocity of 19 mph

Test no. AKLP-1 was conducted with a 1,860-lb bogie and an impact velocity of 18.9 mph, resulting in a peak force of 38.3 kips. The total energy absorbed by the post and foundation assembly was 266.3 kip-in., and the permanent set deflection recorded was 0.9 in. This test was carried out under dry soil conditions with SPT blow counts ranging from 7 at 1.5 ft depth to 20 at 4.5 ft depth.

In test no. AKLP-2, the bogie weight was identical and impact velocity was nearly identical to that of test no. AKLP-1, at 1,860 lb and 19.0 mph, respectively. However, the peak force registered was slightly lower at 36.9 kips. The total energy absorption increased marginally to 267.9 kip-in., reflecting the slight increase in impact velocity, and there was a significant increase in the permanent set deflection, which was recorded at 12.4 in. Note that, due to interference from the soil, the foundation deflection should be considered approximate. Like test no. AKLP-1, this test was also conducted under dry soil conditions. SPT values were measured at three locations. Because the soil was placed loose, SPT values were much lower than in test no. AKLP-1, with the static hammer weight causing a penetration to almost 1.5 ft at one location, an SPT value of 2 at about a 4 ft depth at one location, and values of 5 and 9 at about 4.5 ft depths at two other locations.

Test no. AKLP-3 was conducted with a 1,871-lb bogie and an impact velocity of 18.9 mph. The peak force was 34.8 kips, and the total energy absorbed by the post and foundation assembly was 268.0 kip-in., comparable to test no. AKLP-2 with due to offsetting slightly increased mass and decreased impact velocity. The permanent set deflection was measured at 1.2 in. Soil was placed in a modified protocol from that used in test no. AKLP-1, resulting in intermediate SPT results between test nos. AKLP-1 and AKLP-2. Additionally, this test was carried out after wetting the soil. SPT blow counts ranged from 2 at 1.5 ft depth to 10 at 4.5 ft depth.

The final test, test no. AKLP-4, was conducted with a 1,860-lb bogie and a higher impact velocity of 19.8 mph compared to previous tests. The peak force recorded was 35.8 kips and the total energy dissipated was 291.7 kip-in, increasing in comparison to previous tests due to the higher impact velocity. The permanent set deflection was similar to test no. AKLP-1, measuring 0.9 in. Soil compaction procedures were identical to test no. AKLP-3, but the test pit was protected to ensure dry conditions. SPT blow counts ranged from 3 at 1.5 ft depth to an average of 18 at 4.5 ft depth for two hole locations. It is not known to what extent the difference in SPT blow counts for test nos. AKLP-3 and AKLP-4 is due to moisture conditions versus sensitivity of installation personnel compaction procedures.

Summary force versus displacement and energy versus displacement plots are provided in Figures 6.17 and 6.19, and Figures 6.18 and 6.20, respectively. Placing soil to achieve a uniform SPT value along the depth proved challenging, but the results indicate that the foundation response was largely insensitive to the soil compactness and moisture content for foundation displacements up to about 8 in. Test no. AKLP-2 exhibited much greater displacement with loose soil fill compared to other tests, but the duration of impulse and momentum transfer to the foundation with an embedded steel post unrepresentatively severe in comparison to the foundation demands that will be imposed by breakaway couplings when a light pole is subjected to a full-scale vehicle impact.

The theoretical peak shear expected for the posts was 23.4 kips based on a moment arm from the top of the foundation to the impact point 25 in. above. Confinement from the concrete surrounding the flange shifted the plastic hinge to occur about 2 in. above top of the foundation. Additionally, the mill certification for the steel post reported a yield stress of 57.5 ksi. Accounting for both of these effects, the shear corresponding to the plastic hinge increased to about 29.3 kips. Calculated peak forces during tests exceeding this value reflect additional inertial resistance from the steel post above the hinge. The testing series confirmed that the Transpo coupling breakaway activation maximum load of 22 kips could be developed solely by the mass of a concrete foundation with a typical diameter of 30 in. and a depth of only 6 ft, shallower than currently allowed under AK DOT& PF Standard Plan L-30.11.

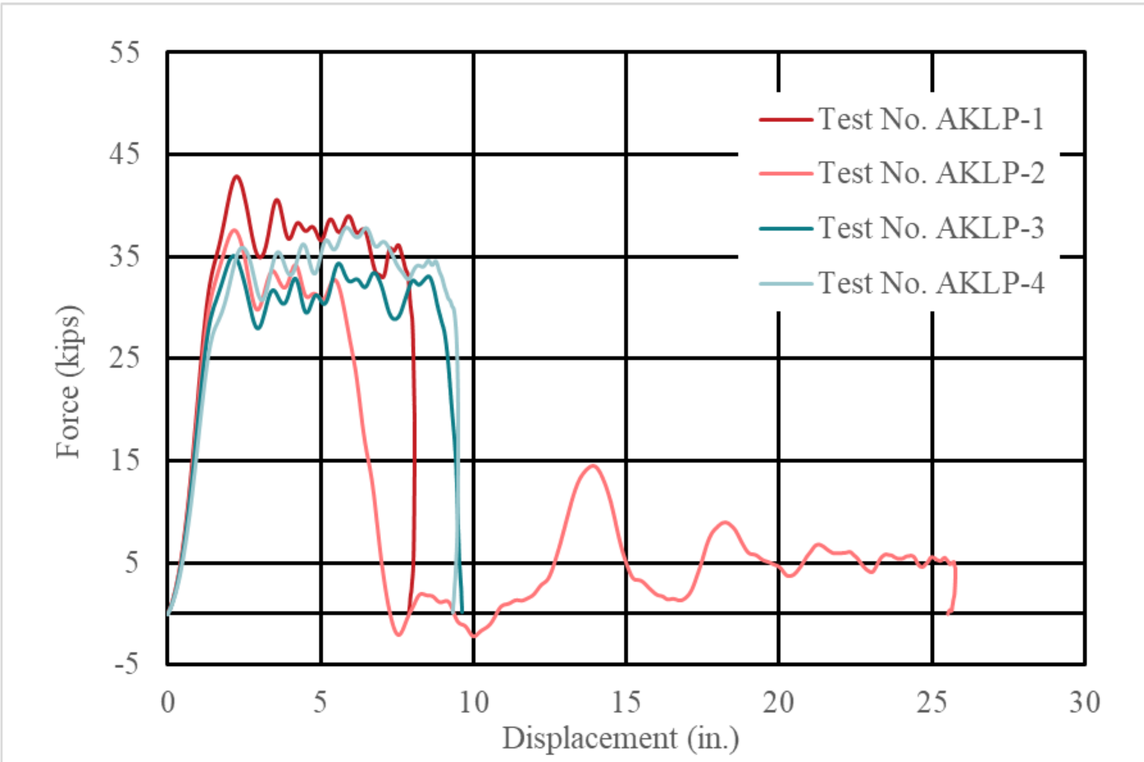

Figure 6.17 Force vs. Deflection Comparison, All Foundations with Embedded Steel Posts

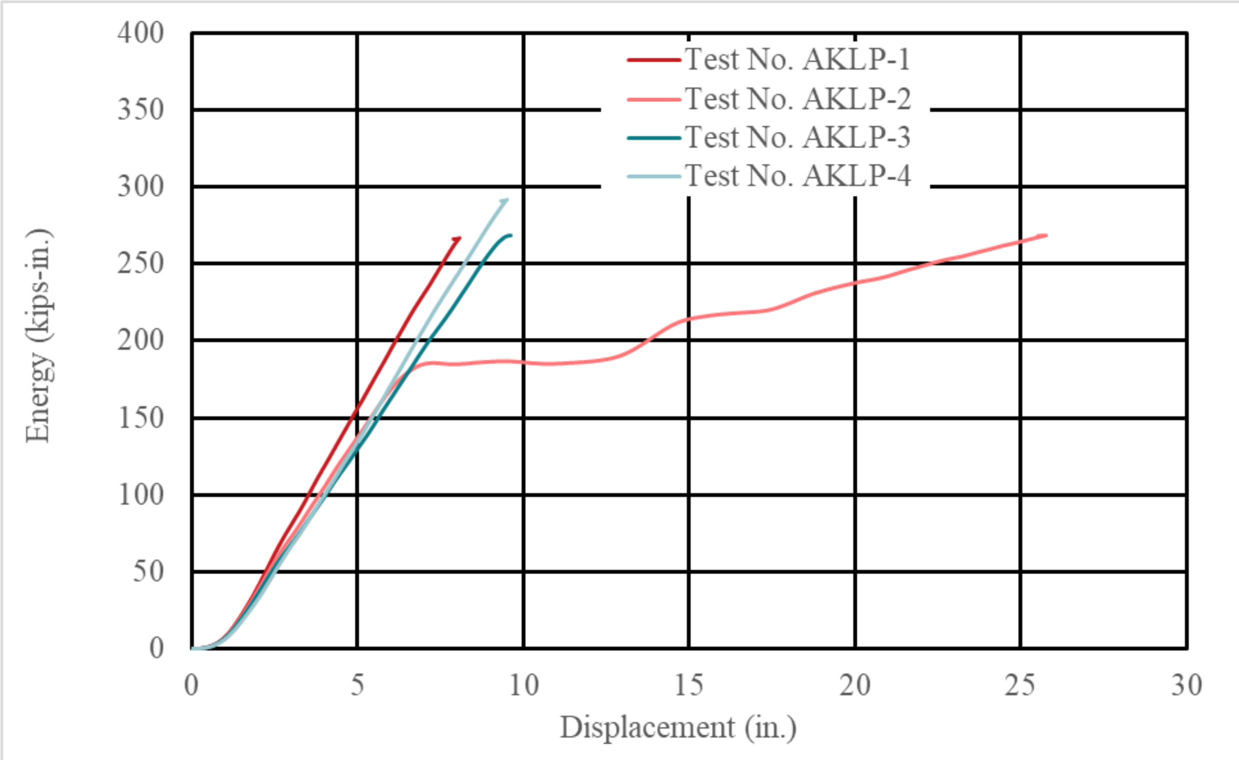

Figure 6.18 Energy vs. Deflection Comparison, All Foundations with Embedded Steel Posts

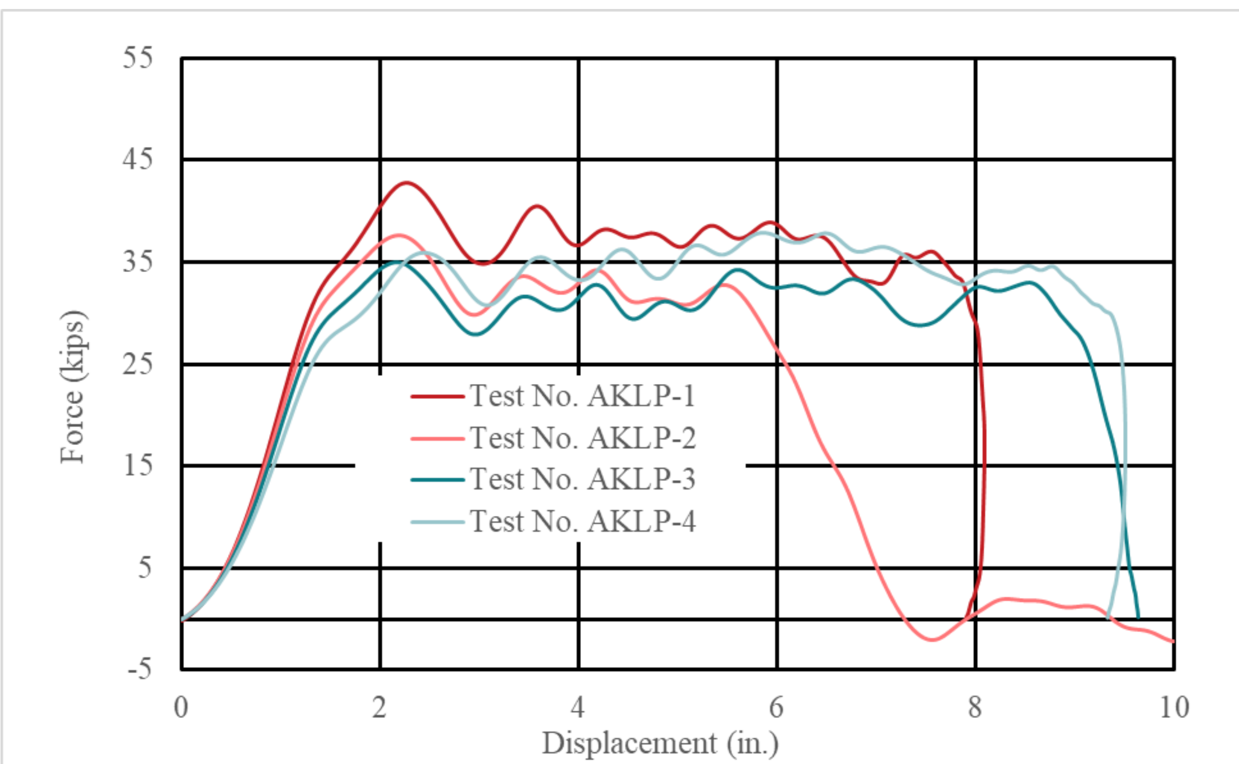

Figure 6.19 Force vs. Deflection Comparison, All Foundations with Embedded Steel Posts

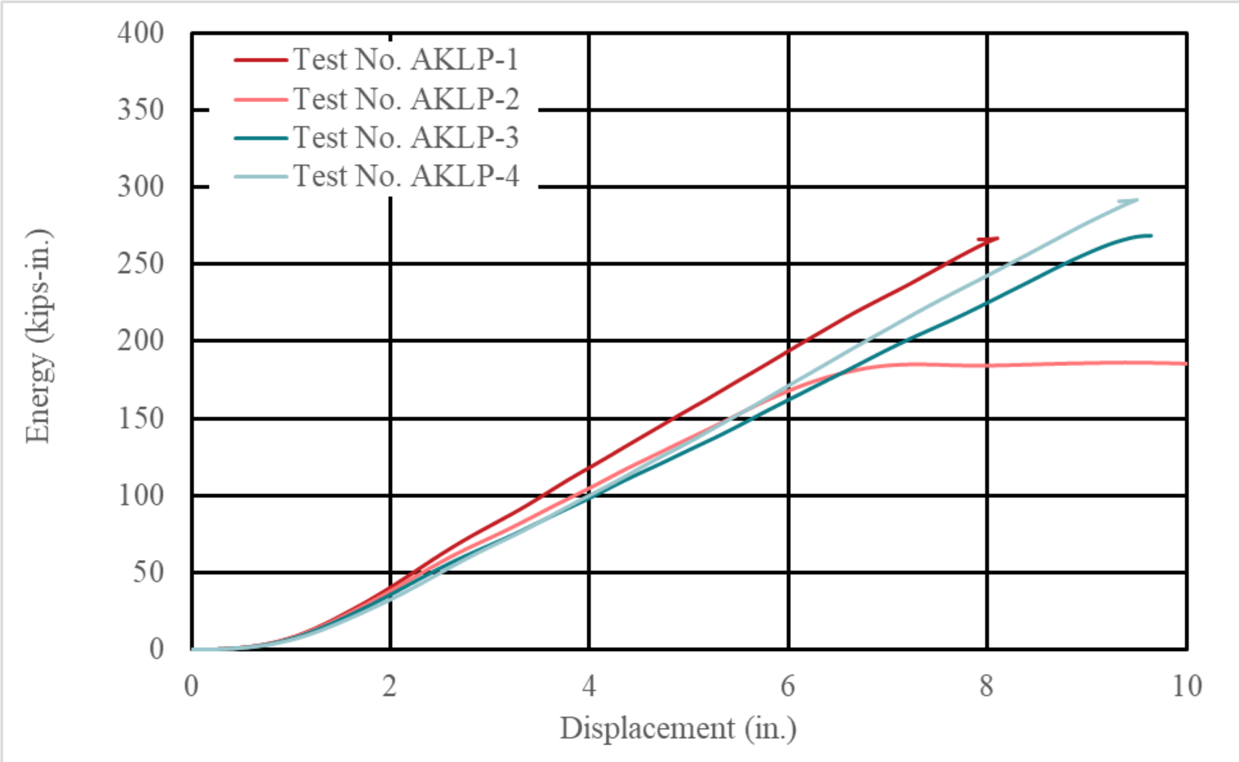

Figure 6.20 Energy vs. Deflection Comparison, All Foundations with Embedded Steel Posts

Chapter 7 Design Details – Foundations with Breakaway Steel Poles

Two bogie tests were conducted to investigate breakaway activation for steel light poles mounted to concrete foundations. Both foundations were embedded in weak soils. One test was performed with dry soils and one test with saturated soils. Test no. AKLP-2 demonstrated that a foundation surrounded by loose soils was able to develop a peak force at least as great as the maximum Transpo coupling breakaway activation threshold of 22 kips by relying primarily on the inertia of the foundation rather than soil stiffness. Therefore, foundations supporting steel poles with Transpo couplings were installed with loose sandy fill for both tests. SPT blow counts were 2 or less to depths of about 6 ft in both tests, as shown in Figure 7.1. Soil was dry for test no. AKLP-5 and saturated for test no. AKLP-6.

The test article for each test comprised a light pole with a height of 35.5 ft, a mast arm extending 20 ft, a coupling base, and a reinforced concrete foundation with a depth of 6 ft and a diameter of 30 in. The light pole specifications and details conformed to a recent order by AK DOT&PF, ensuring representativeness for the light pole inventory in Alaska. Concrete foundations were identical to those used in test nos. AKLP-1 through AKLP-4, except that ties were spaced at 12 in. throughout the height (i.e., the additional ties near the top of the foundation were not included for test nos. AKLP-5 and AKLP-6). Four Transpo Type B female anchors were embedded at the top surface of the foundations to receive Pole-Safe Model No. 5100 couplings. Soil was AASHTO Type A-3, identical to that used in test nos. AKLP-1 through AKLP-4. Both test nos. AKLP-5 and AKLP-6 were performed with a nominally 1,850-lb rigid bogie vehicle impacting the pole at an angle of 0 degrees, simulating a “head-on” or full-frontal collision, with a target velocity of 19 mph and with the bogie impact head centered at a height of 25 in. above the ground line. Design details for test nos. AKLP-5 and AKLP-6 are provided in Figures 7.2 through 7.19, and sample representative photographs documenting the construction and installation of the foundations are shown in Figures 7.20 through 7.26. Material specifications, mill certifications, and certificates of conformity for the materials used in the tests are shown in Figures 7.18 and 7.19.

Recalling that a significant portion of the water added to the fill soil for test no. AKLP-3 had partially run out into the native soil surrounding the pit, an impermeable liner was used to ensure saturated conditions for AKLP-6. The pit was fully excavated following test no. AKLP-5, then a liner was spread over the pit opening on the tarmac and the previously excavated fill was placed on the liner, as shown in Figure 7.23. The foundation was set level at the center of the pit on an initial loose fill depth of 2 ft. On the day of the test for test no. AKLP-6, a truck delivered water to the site and an approximate volume of 1,700 gallons of water was added to the test pit until saturation was achieved with visible standing water, as shown in Figure 7.24. Test no. AKLP-6 was unique in that the GeoProbe was not available from Drs. Song and Kim. Therefore, Terracon was hired to perform SPT and nuclear density testing. According to test results reported by Terracon, the moisture contents measured at two locations were 18.6% and 21.7%, reaching the nominal target of 18% selected to match the HNS boring log provided by AK DOT&PF. A small amount of soil was added to mitigate standing water and facilitate bogie testing, as shown in the bottom right panel of Figure 7.24.

Both tests employed an identical light pole system configuration. The light pole, a cylindrical steel structure, was constructed with a 10-gauge wall thickness and outside diameters that tapered from 10.5 in. at the bottom to 5.53 in. at the top along a length of 35.5 ft, as noted in Figure 7.5. The luminaire's nominal mounting height was set at 40 ft above ground level. The mounting point for the mast arm attachment was 34.5 ft above ground level. The base plate measured 1⅜ in. in thickness and had dimensions of 15.5 in. square, as illustrated in Figure 7.4, with a bolt circle spanning 15.5 in. in diameter.

The light pole was equipped with a single mast arm, extending 20 ft in length, as shown in Figure 7.5. This mast arm was attached to the light pole utilizing an attachment assembly comprising an 8¾-in. x 8-in. x 1-in. mounting plate on the pole side and an 8¾-in. x 6-in. x ¾-in. mounting plate on the mast arm side, as presented in Figure 7.8. To simulate the weight of a luminaire, ballast consisting of a steel plate weighing approximately 50 lb was mounted at the terminal end of the mast arm. The light pole system was anchored using four 1-in. diameter Model No. 5100 Double-Neck Pole-Safe steel breakaway couplings manufactured by Transpo Industries, Inc. Installed conditions for the couplings for test nos. AKLP-5 and AKLP-6 are visible in Figures 7.22 and 7.26, respectively.

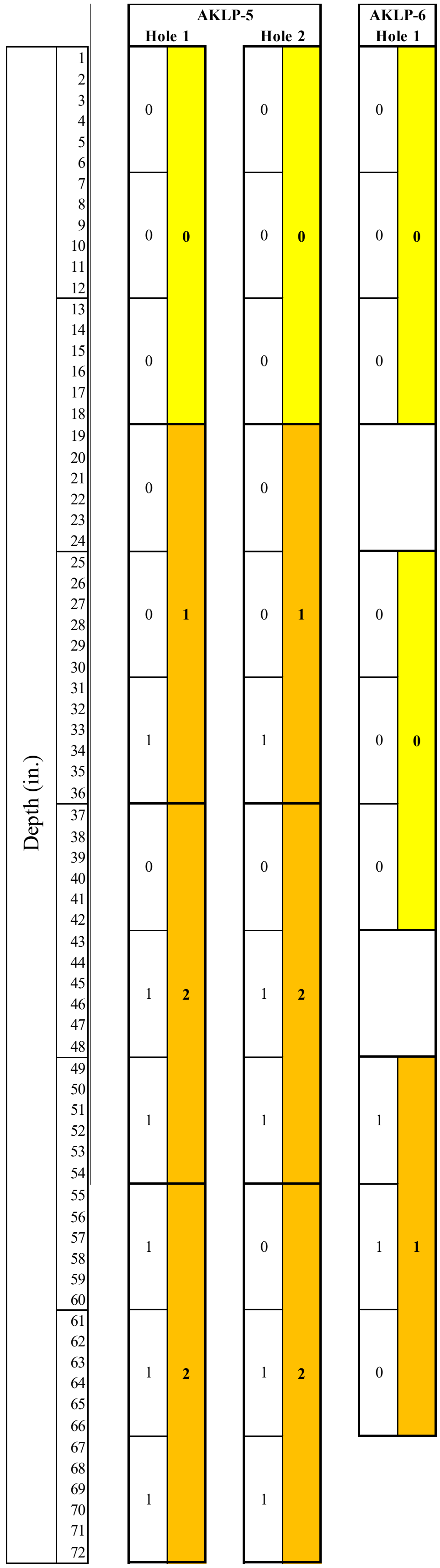

Figure 7.1 Measured SPT Blow Counts As-Installed for Test Nos. AKLP-5 and AKLP-6

Test No.	Impact Speed (mph)	Impact Orientation	Soil Condition	Luminaire Pole Height (ft.)	Bogie Weight (lbs)	Embedment Depth (in.)	Impact Height (in.)
AKLP-5	19	0°	Dry, See Note 1	35.5	1850	72	25
AKLP-6	19	0°	Saturated, See Note 2	35.5	1850	72	25

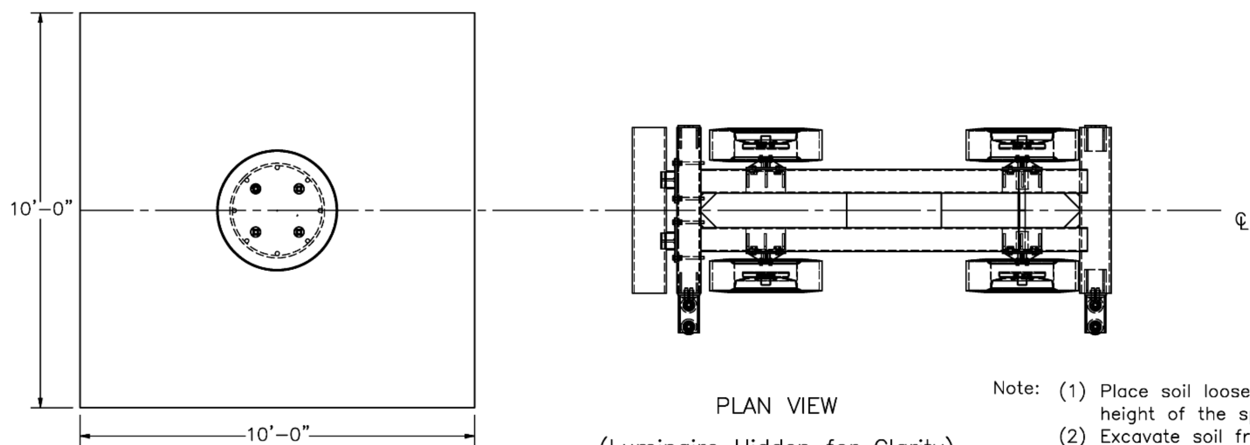

PLAN VIEW

(Luminaire Hidden for Clarity)

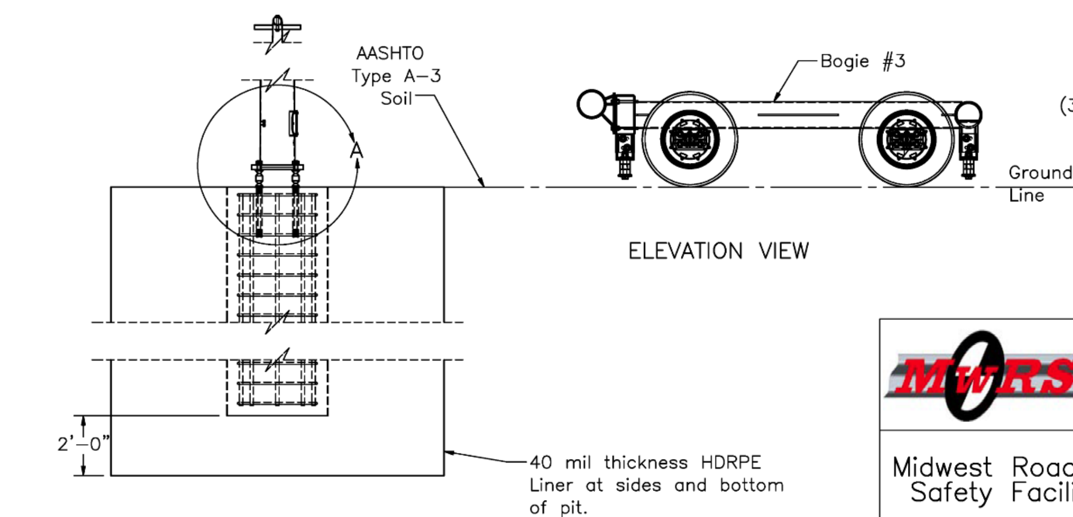

ELEVATION VIEW

Note:
(1) Place soil loose (no compaction) for the full height of the specimen.
(2) Excavate soil from around foundation, ensure foundation is set plumb or replace if damaged, and replace soil with soil placed loose (no compaction). Test to be performed with at least 15% moisture content. Add approximately 1700 gallons of water or until standing water overflows at surface.
(3) Tighten each nut on to pole base plate. Pole–Safe couplings must be held with an additional wrench on the upper wrench flats to prevent an induced torque stress across the necked portion of the couplings. Nuts shall be tightened using the turn–of–nut method in accordance with American Inisitute of Steel Constructurion (AISC) procedures (for ASTM A325 and A490 anchor bolts, 1/3 rotation past "snug tight").

Midwest Roadside Safety Facility	Alaska DOT Light Poles Test Nos. AKLP 5–6 Test Layout		SHEET: 1 of 18 DATE: 5/28/2024 DRAWN BY: CAO/GSK/MM
	DWG. NAME. AKLP–5–6_R7	SCALE: 1:45 UNITS: in.	REV. BY: JSS

Figure 7.2 Bogie Testing Layout, Test Nos. AKLP-5 and AKLP-6

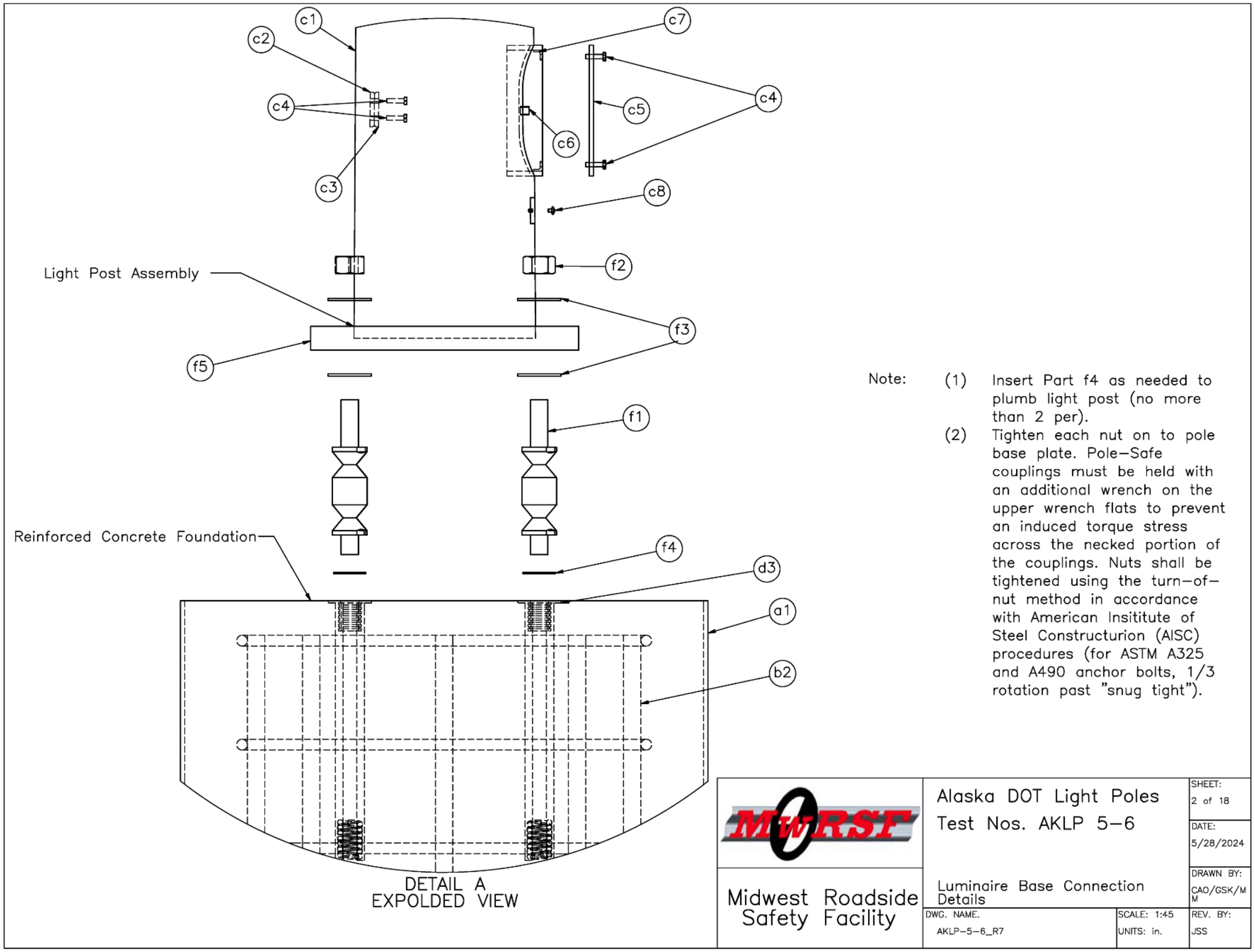

Figure 7.3 Luminaire Base Connection Details, Test Nos. AKLP-5 and AKLP-6

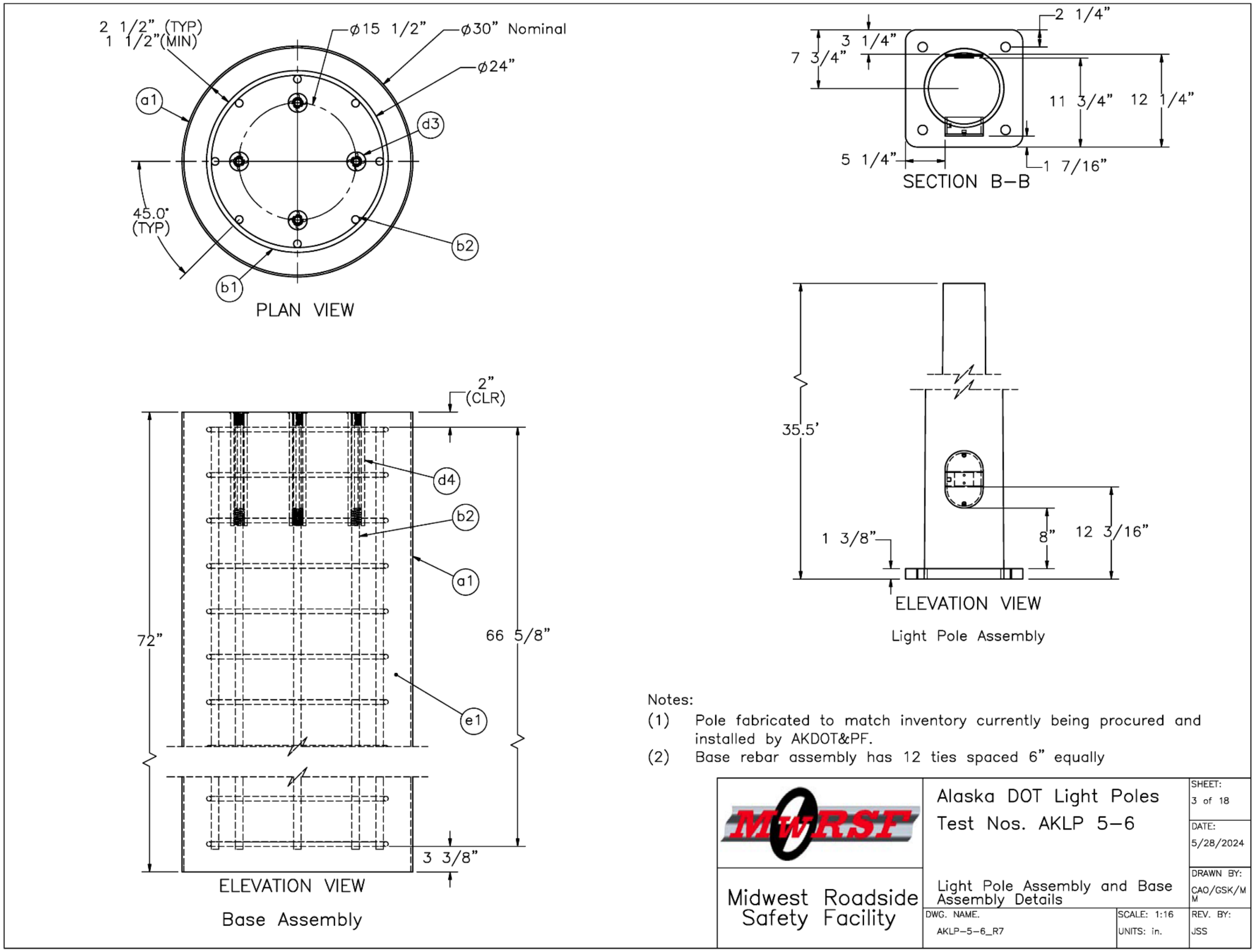

Figure 7.4 Light Pole Assembly and Base Assembly Details, Test Nos. AKLP-5 and AKLP-6

Pole Tube					Luminaire Arm					
Pole No.	Base Dia. (in)	Top Dia. (in)	Length (ft)	Gauge or Thick	Span "L" (ft)	Mounting Height (ft)	Fixed End Dia. (in)	Free End Dia. (in.)	Rise Height "R" (ft)	Gauge or Thick
141	10.50	5.53	35.50	10 Gauge	20.00	40.00	5.35	2.40	5.50	11 Gauge

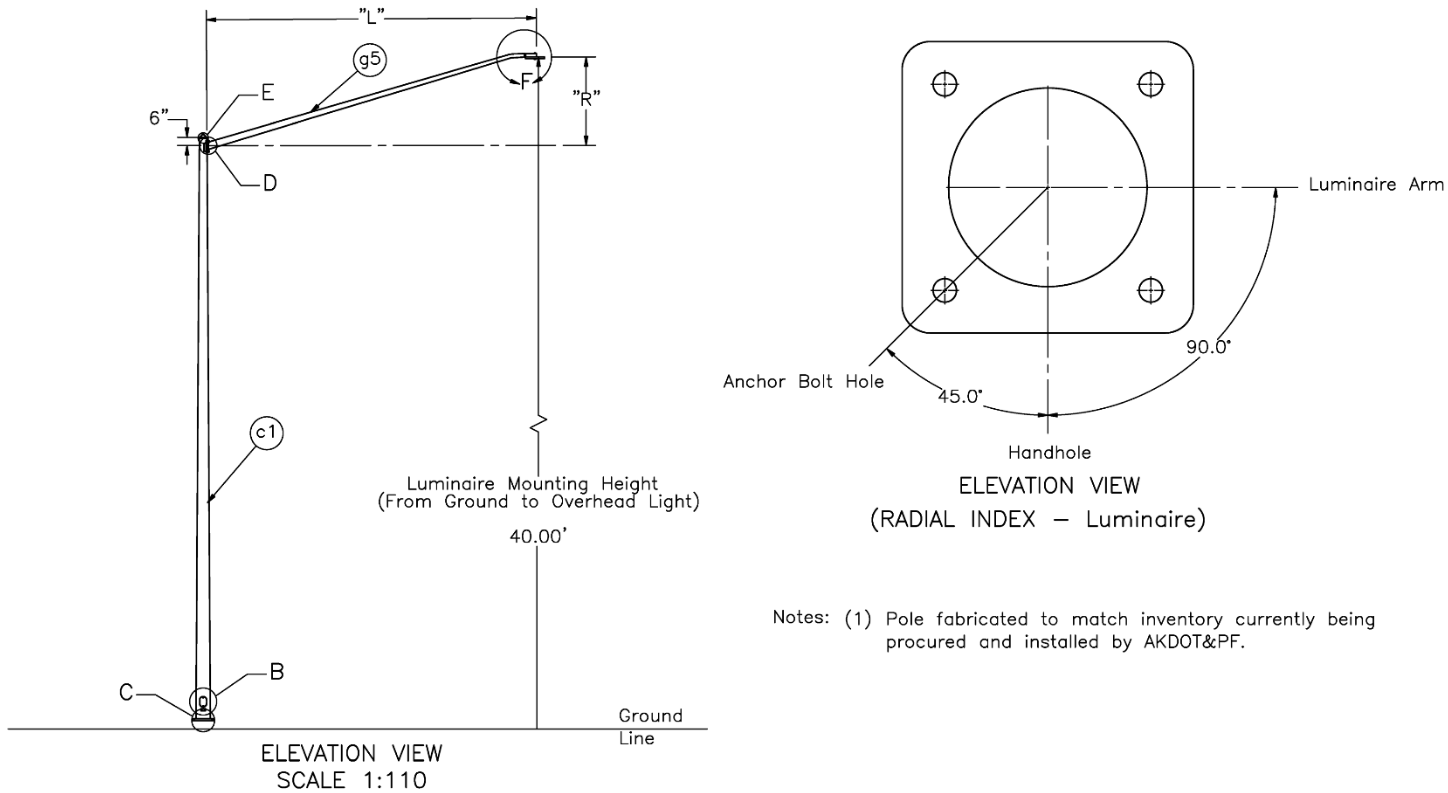

Notes: (1) Pole fabricated to match inventory currently being procured and installed by AKDOT&PF.

Item No.	QTY.	Description	Material Specification	Treatment Specification
c1	1	Pole Shaft	A595 Gr. A	A123
g5	1	Lum. Arm Shaft	A595 Gr. A	A123
g2, g3	2	Arm Connecting Plates	A709 ZONE 3	A123
g1	2	Gussets	A36	A123
g4	3	Lum. Arm Con. Bolts	A325	A123
f5	1	Base Plate	A709 ZONE 3	A123
–	–	Galvanizing – HWR	A153	A123

Midwest Roadside Safety Facility	Alaska DOT Light Poles Test Nos. AKLP 5–6 Luminaire Assembly		SHEET: 4 of 18 DATE: 5/28/2024 DRAWN BY: CAO/GSK/MM
	DWG. NAME. AKLP-5-6_R7	SCALE: 1:8 UNITS: in.	REV. BY: JSS

Figure 7.5 Luminaire Assembly, Test Nos. AKLP-5 and AKLP-6

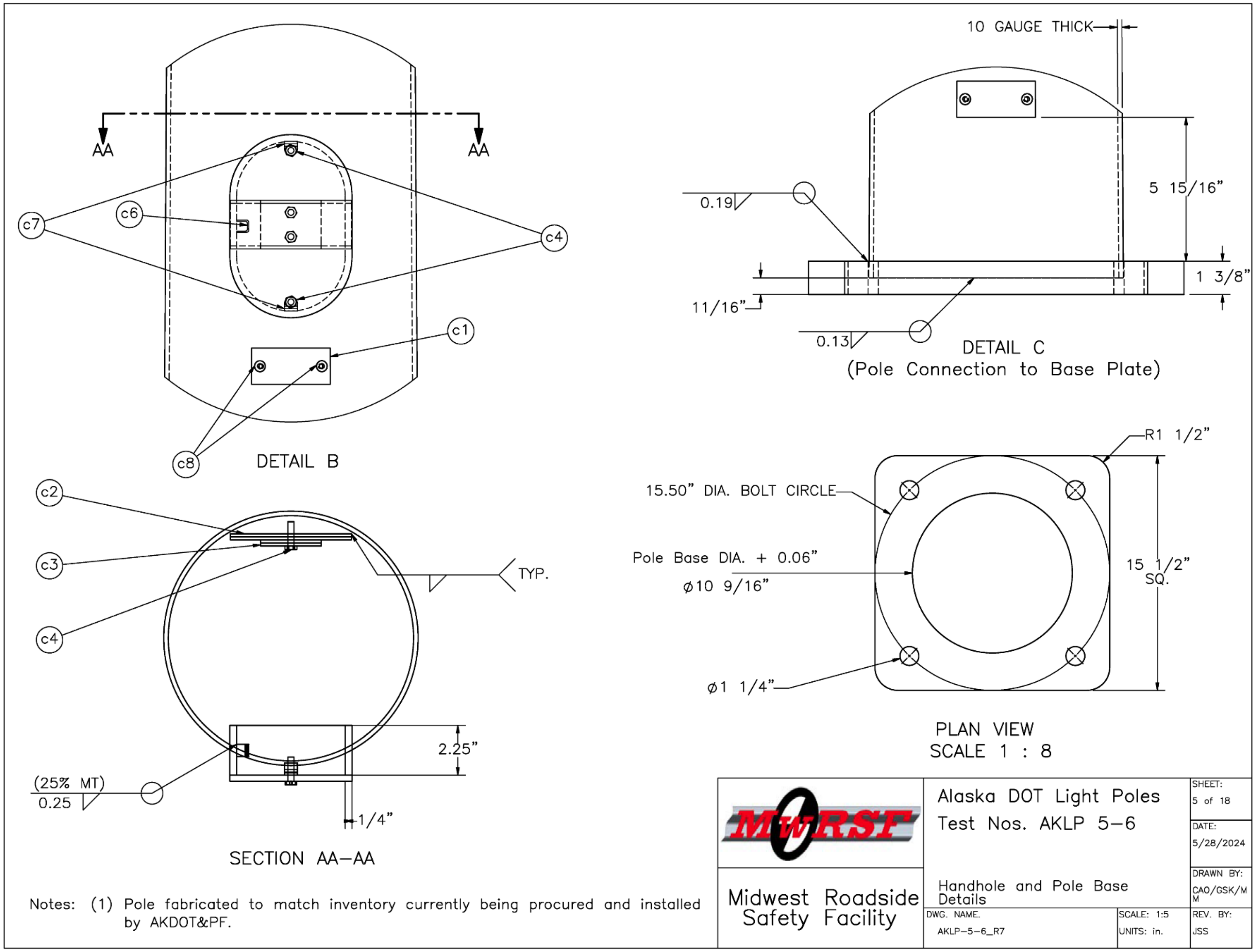

Figure 7.6 Handhole and Pole Base Details, Test Nos. AKLP-5 and AKLP-6

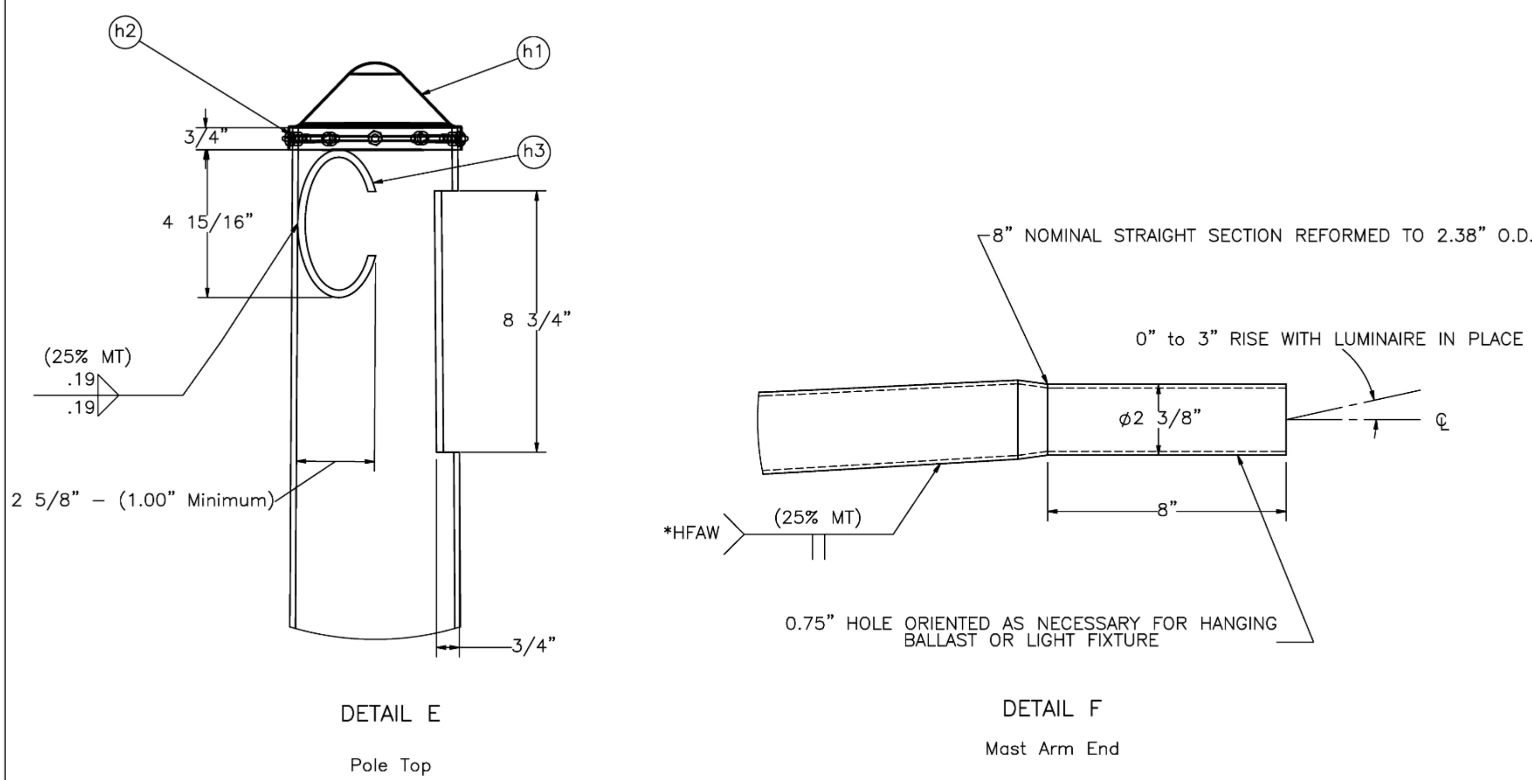

Notes: (1) Pole fabricated to match inventory currently being procured and installed by AKDOT&PF.
(2) Hole is drilled on top or as necessary to hand ballast and/or cobra light head.
(3) End of tube to be squared up and chamfered inside and out.

Midwest Roadside Safety Facility	Alaska DOT Light Poles Test Nos. AKLP 5–6	SHEET: 6 of 18
		DATE: 5/28/2024
	Pole and Mast Arm Details	DRAWN BY: CAO/GSK/MM
	DWG. NAME. AKLP–5–6_R7 / SCALE: 1:5 UNITS: in.	REV. BY: JSS

Figure 7.7 Pole and Mast Arm Details, Test Nos. AKLP-5 and AKLP-6

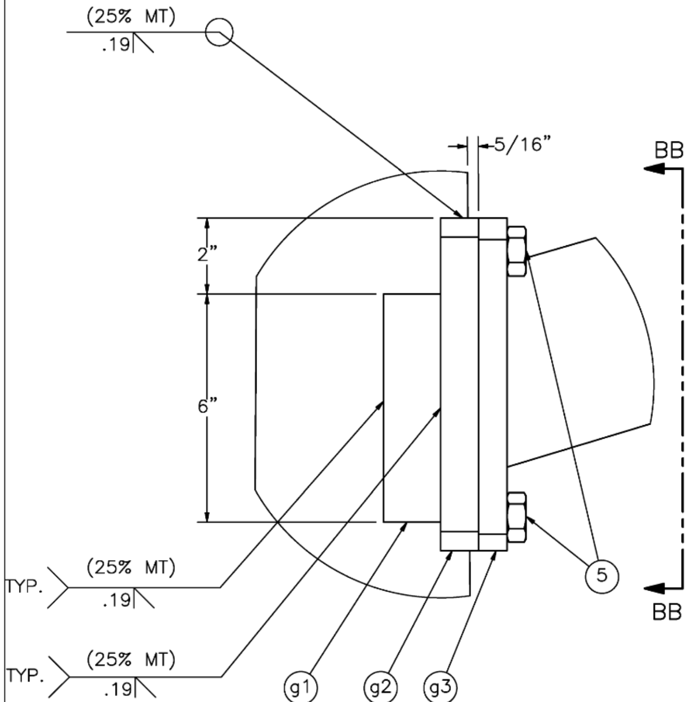

DETAIL D

Mast Arm Connection

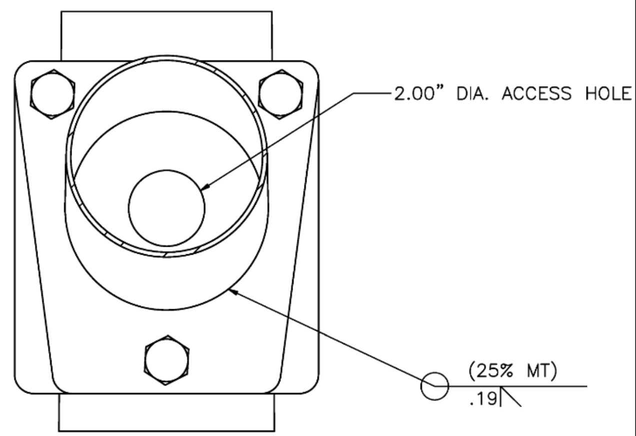

SECTION BB–BB

Notes: (1) Pole–to–mast arm connections fabricated to match inventory currently being procured and installed by AKDOT&PF.

MwRSF Midwest Roadside Safety Facility	Alaska DOT Light Poles Test Nos. AKLP 5–6 Mast Arm Connection Details	SHEET: 7 of 18
		DATE: 5/28/2024
		DRAWN BY: CAO/GSK/MM
	DWG. NAME. AKLP–5–6_R7 / SCALE: 1:4 UNITS: in.	REV. BY: JSS

Figure 7.8 Mast Arm Connection Details, Test Nos. AKLP-5 and AKLP-6

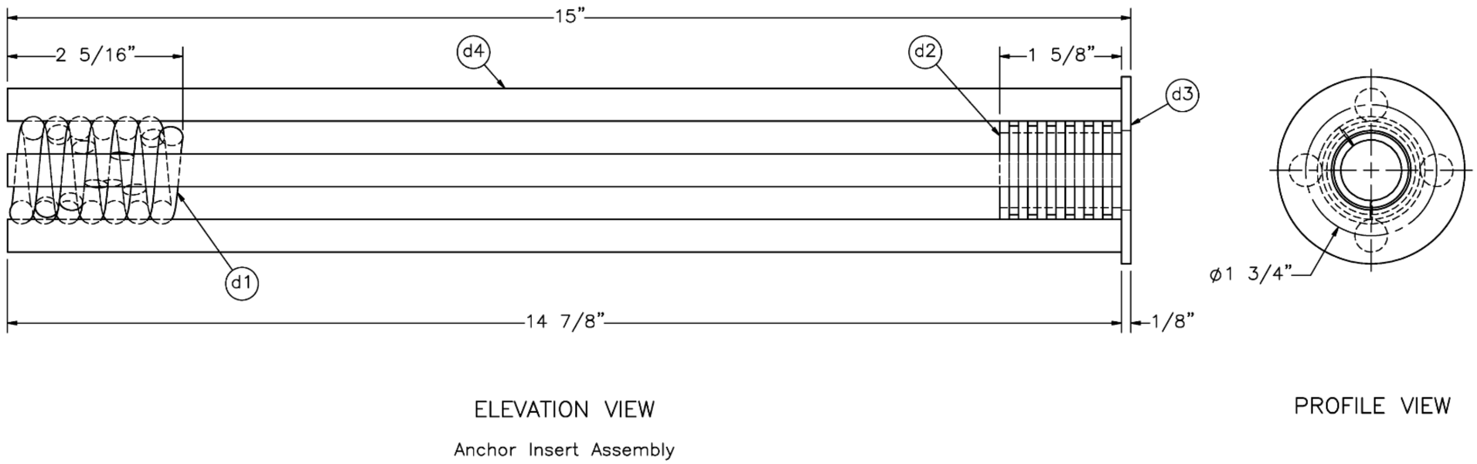

Item No.	QTY.	Description	Material Specification	Treatment Specification
f1	4	Anchor Insert Assembly (Pole–Safe type B Anchor)	As Supplied	As Supplied
d1	1	Closed Wire Coil	ASTM A153 or AASHTO M232	ASTM A123/M111
d2	1	Threaded ferrule	See Assembly	See Assembly
d3	1	Anchor Insert Washer	ASTM A153 or AASHTO M232	ASTM A123/M111
d4	4	Anchor Insert Wire	See Assembly	#4 AWG

Midwest Roadside Safety Facility

Alaska DOT Light Poles
Test Nos. AKLP 5–6

Anchor Insert Assembly Details

SHEET:	8 of 18
DATE:	5/28/2024
DRAWN BY:	CAO/GSK/MM
DWG. NAME.	AKLP–5–6_R7
SCALE:	1:2
UNITS:	in.
REV. BY:	JSS

Figure 7.9 Anchor Insert Assembly Details, Test Nos. AKLP-5 and AKLP-6

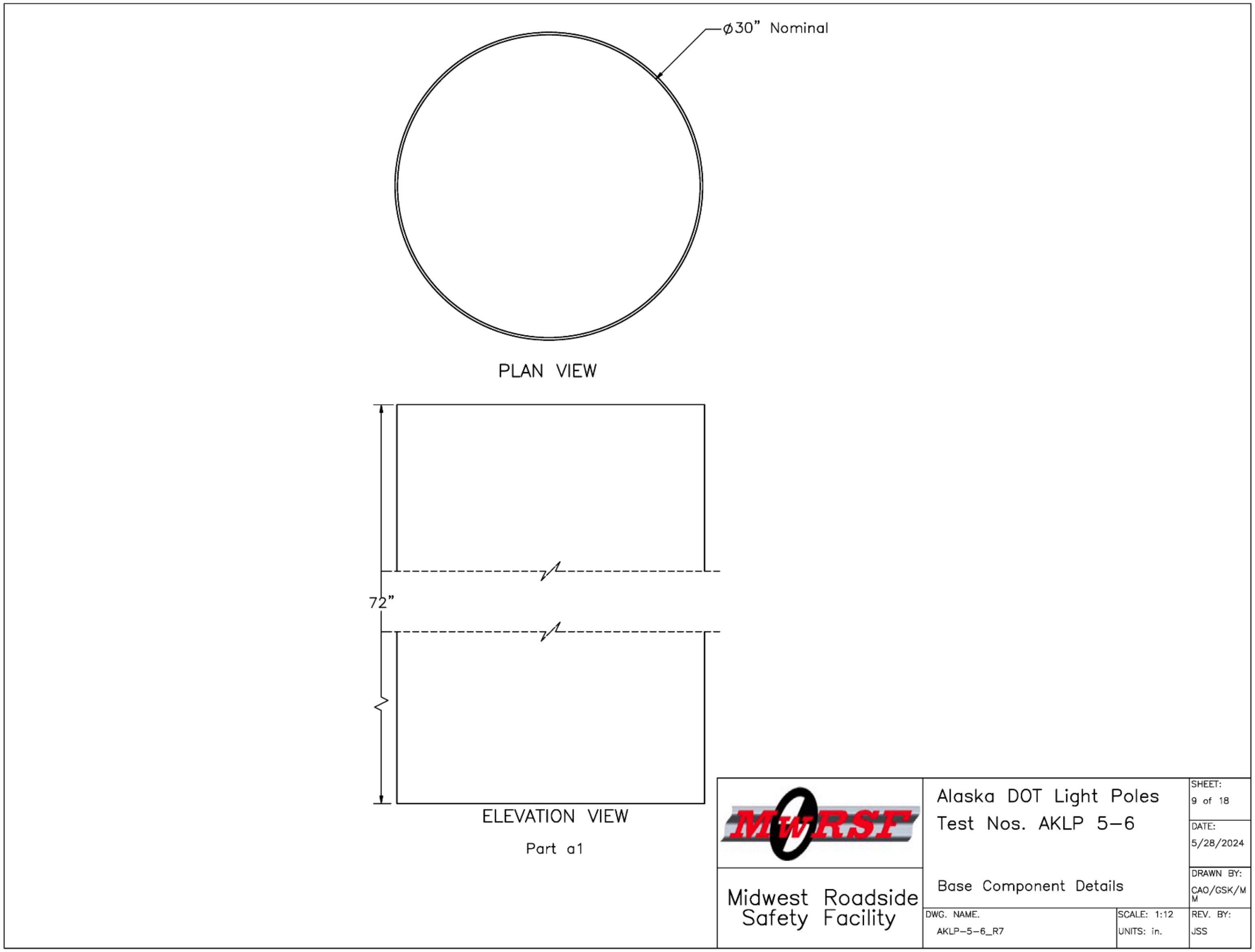

Figure 7.10 Base Component Details, Test Nos. AKLP-5 and AKLP-6

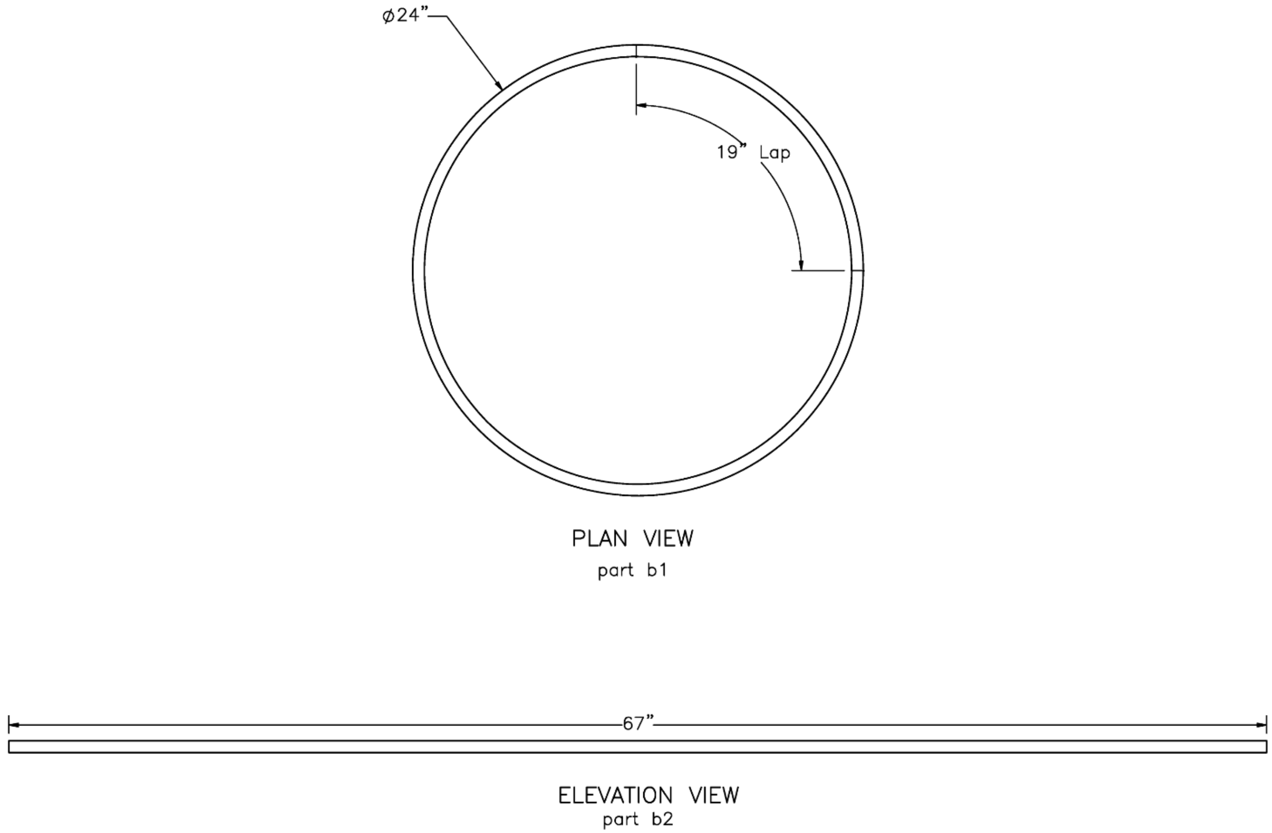

Notes: (1) Tie vertical reinforcing steel to each intersection of the part b1 spaced 6" apart.

Bill of Bars

Bar	QTY.	Size	Total Unbent Length	Material Specification	Treatment Specification
b1	12	#5	95"	ASTM A615 Gr. 60	Epoxy-Coated (ASTM A775 or ASTM A934)
b2	8	#8	67"	ASTM A615 Gr. 60	Epoxy-Coated (ASTM A775 or ASTM A934)

Midwest Roadside Safety Facility

Alaska DOT Light Poles
Test Nos. AKLP 5-6

Base Rebar

SHEET: 10 of 18
DATE: 5/28/2024
DRAWN BY: CAO/GSK/MM
DWG. NAME. AKLP-5-6_R7
SCALE: 1:8
UNITS: in.
REV. BY: JSS

Figure 7.11 Base Rebar, Test Nos. AKLP-5 and AKLP-6

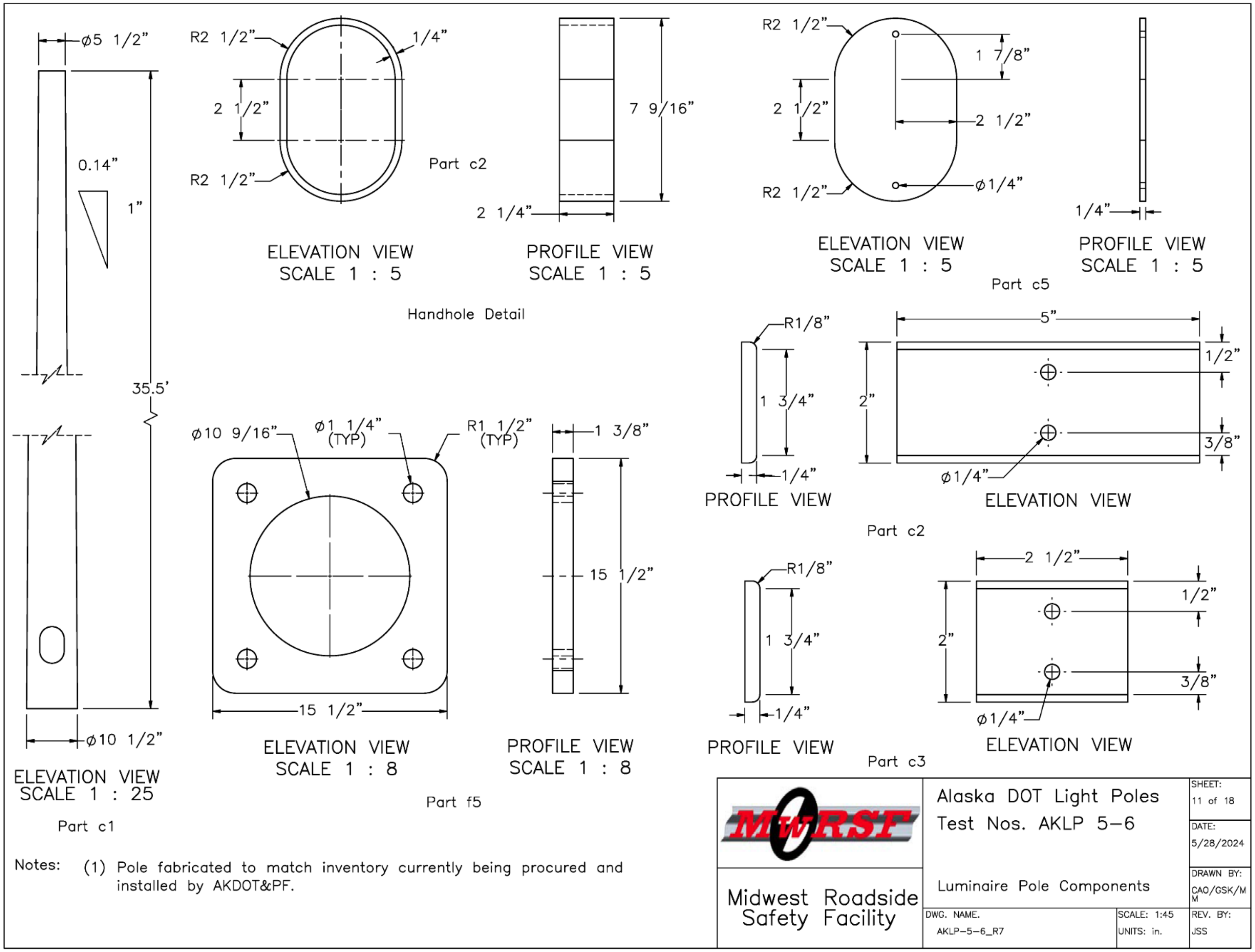

Figure 7.12 Light pole Components, Test Nos. AKLP-5 and AKLP-6

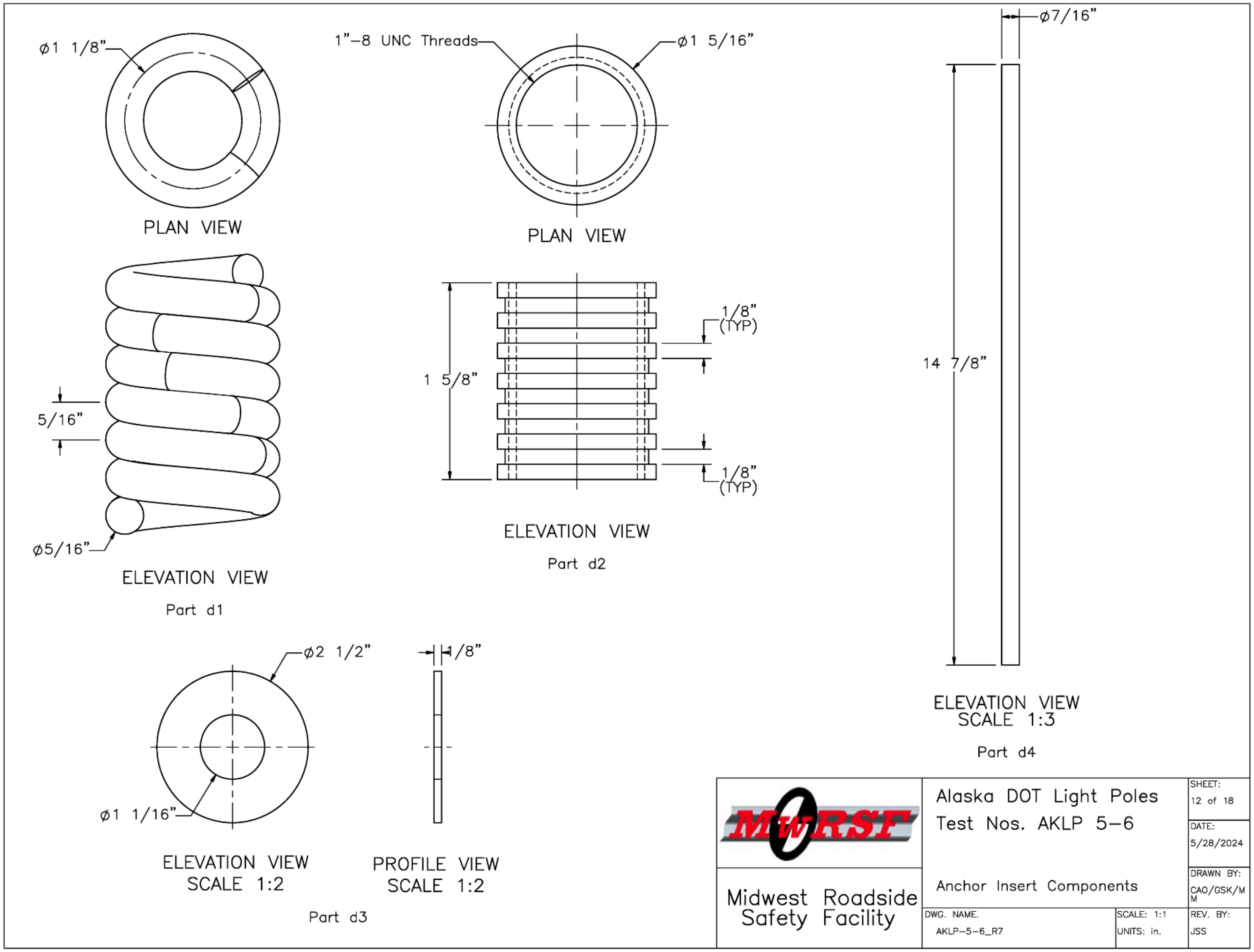

Figure 7.13 Anchor Insert Components, Test Nos. AKLP-5 and AKLP-6

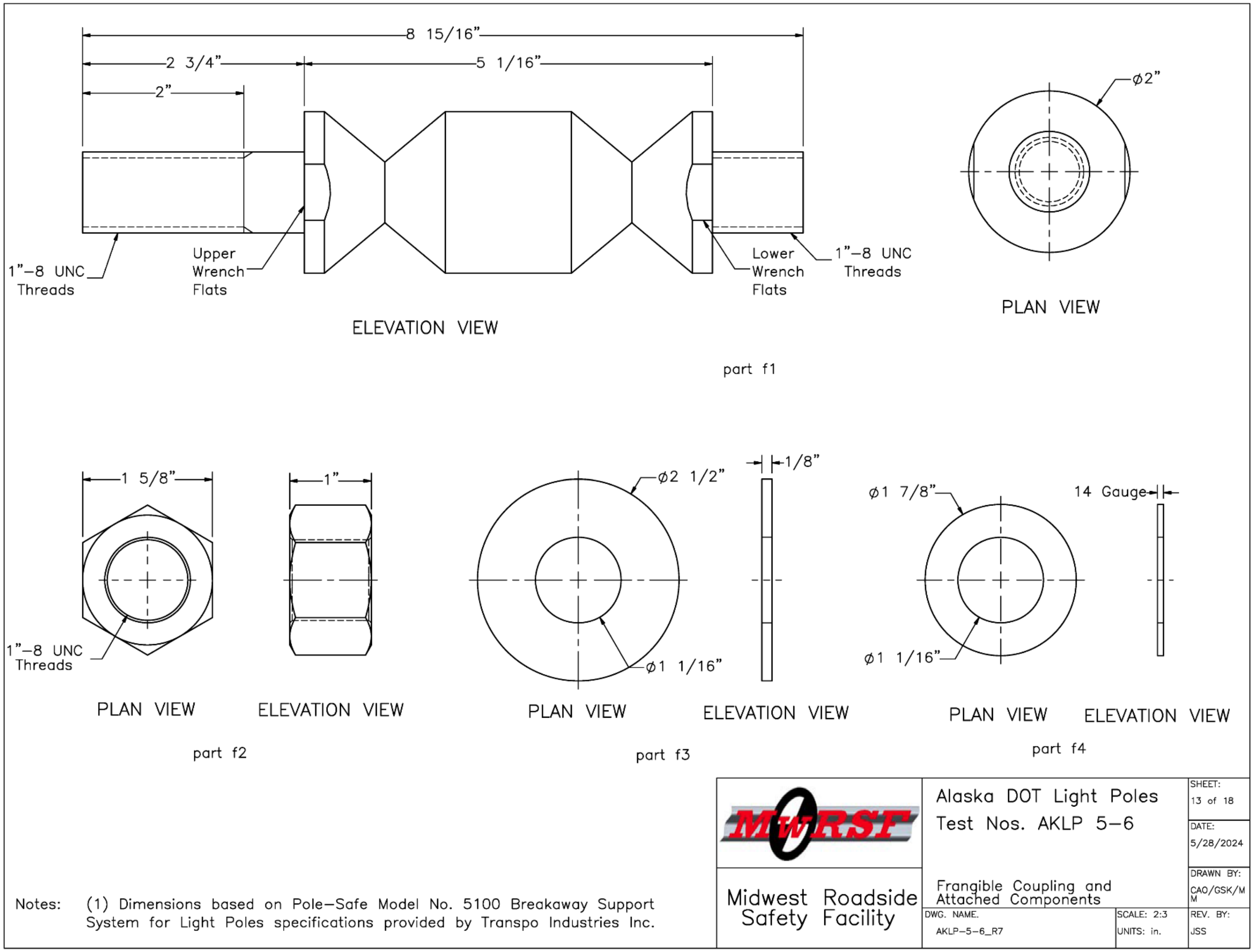

Figure 7.14 Frangible Coupling and Attached Components, Test Nos. AKLP-5 and AKLP-6

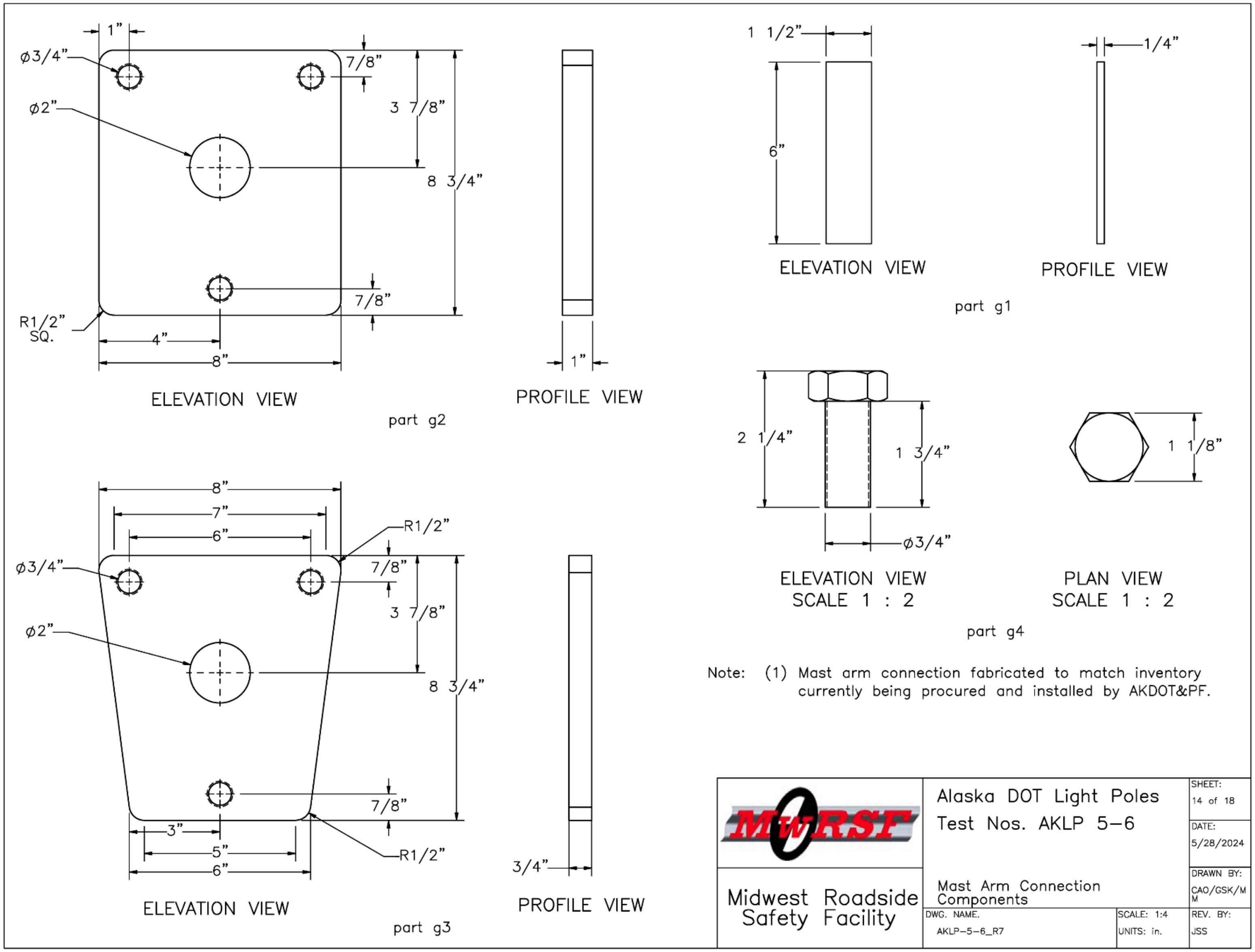

Figure 7.15 Mast Arm Connection Components, Test Nos. AKLP-5 and AKLP-6

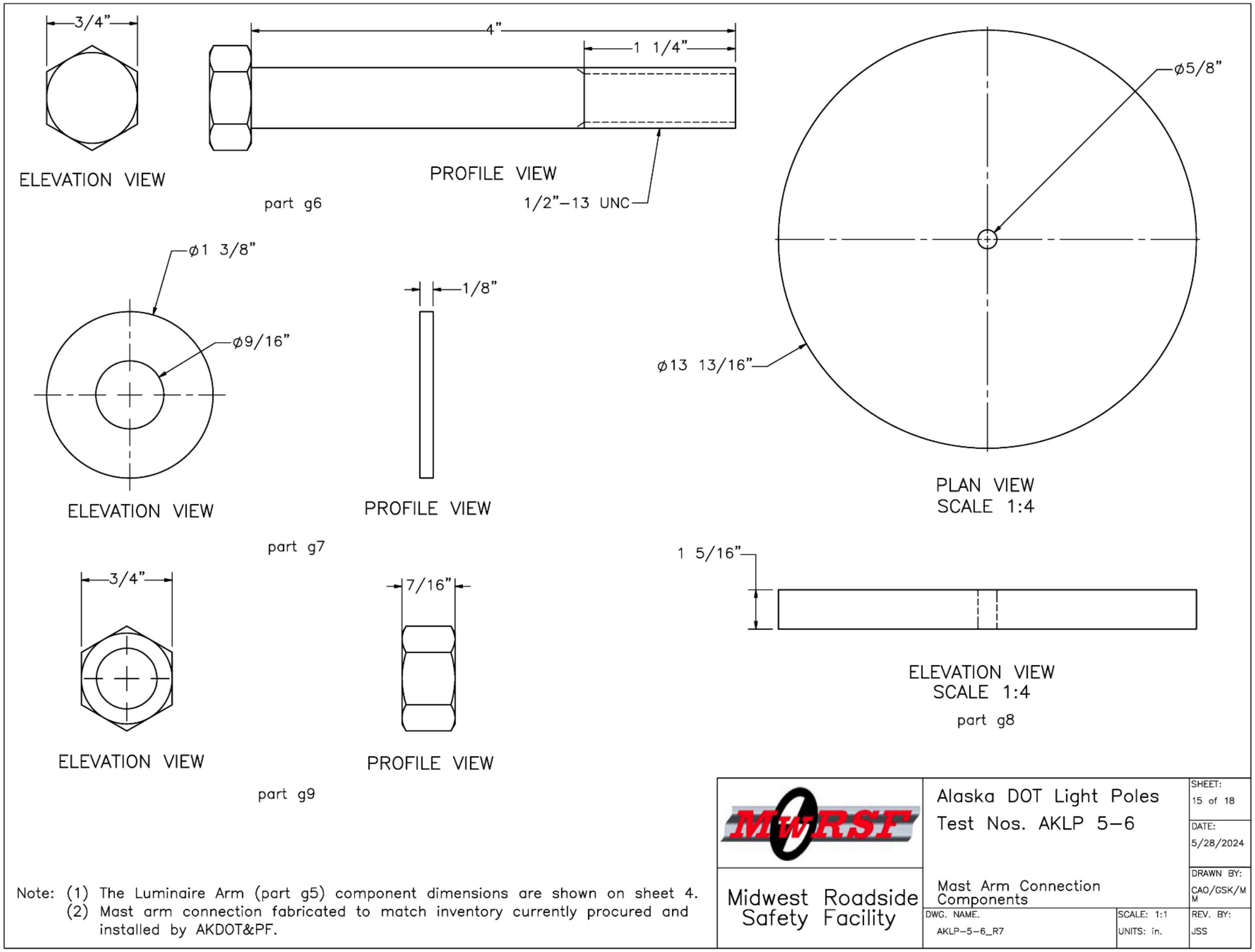

Figure 7.16 Mast Arm Connection Components, Test Nos. AKLP-5 and AKLP-6

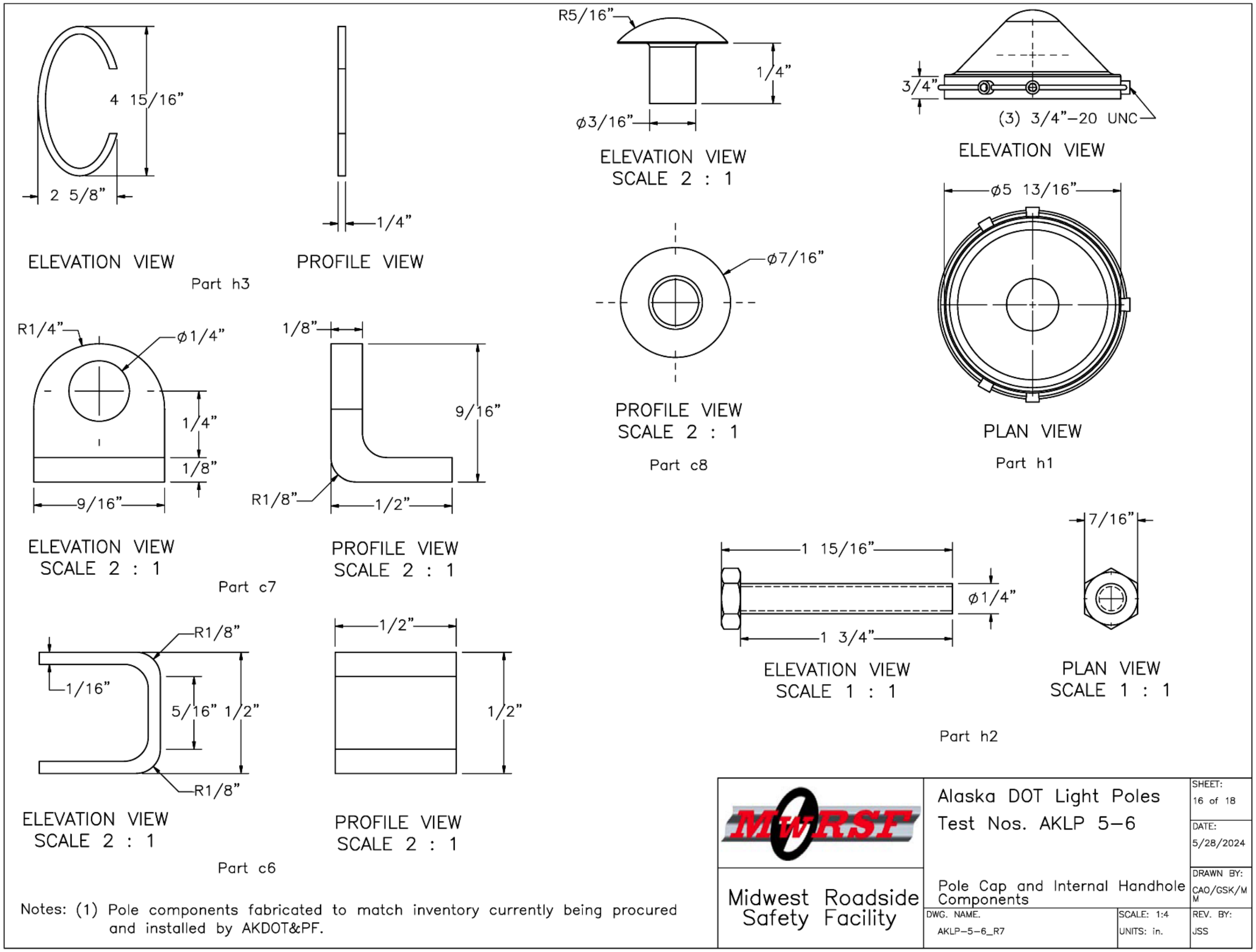

Figure 7.17 Pole Cap and Internal Handhole Components, Test Nos. AKLP-5 and AKLP-6

Item No.	QTY.	Description	Material Specification	Treatment Specification	Hardware Guide
a1	1	30" Diameter Sonotube	–	–	–
b1	12	#5 Bar, 95" long, Circular Hoop Tie	ASTM A615 Gr. 60	*Epoxy–Coated (ASTM A775 or A934)	–
b2	8	#8 Bar, 67" Long	ASTM A615 Gr. 60	*Epoxy–Coated (ASTM A775 or A934)	–
c1	1	Luminaire Pole, 35.5' Long, 10.5" Base Dia., 5.53 Top Dia., 10 Gauge Thick	ASTM A595 Gr. A	ASTM A123	–
c2	1	Pole Inner Bracket Back Plate	ASTM A153 or AASHTO M232	ASTM A123/M111	–
c4	4	1/4" Dia. – 20UNC, 1" Long Hex Screw	ASTM A153	ASTM A123	–
c5	1	Handhole Cover, Rim formed from 6" Std. Black Pipe	ASTM A595 Gr. A	ASTM A123	–
c6	1	0.5" Nut Holder	ASTM A153 or AASHTO M232	ASTM A123/M111	–
c7	2	Cover Mounting Clip	ASTM 153 or AASHTO M232	ASTM A123/M111	–
c8	2	0.19"x0.25"x0.25" Rivet Bolt	ASTM A153	ASTM A123	–
c9	1	1.50" x 3.25" Identification Tag	Aluminum	–	–
d1	4	Closed Wire Coil	ASTM A153 or AASHTO M232	ASTM A123/M111	–
d2	4	Threaded ferrule	See Assembly	See Assembly	–
d3	4	Anchor Insert Washer	ASTM A153 or AASHTO M232	ASTM A123/M111	–
d4	16	Anchor Insert Wire	See Assembly	#4 AWG	–
e1	–	Concrete	AKDOT & PF CLASS A or Equivalent, f'c=4000 psi	–	–
f1	4	Double–Neck Pole–Safe Coupling, Model No. 5100	ASTM A449 or NCHRP 350 TL3	ASTM A153	–
f2	4	1"–8 UNC Heavy Hex Nut	ASTM A563DH or Equivalent	ASTM A153 or B695 Class 55 or F2329	FNX24b
f3	8	1" Dia. Plain USS Washer	ASTM F436	A153	FWC24a
f4	4	Galvanized Steel Shim	ASTM A568	ASTM A653	–
f5	1	Light Post Base Plate	ASTM A709 ZONE 3 or AASHTO M270 F3	ASTM A123/M111	–
g1	2	6"x1 1/2"x1/4" Gusset	ASTM A36	ASTM A123	–
g2	1	8 3/4"x8"x1" Mounting Plate	ASTM A709 ZONE 3 or AASHTO M270 F3	ASTM A123	–
g3	1	8 3/4"x6"x1" Mounting Plate	ASTM A709 ZONE 3 OR AASHTO M270 F3	ASTM A123/M111	–
g4	3	3/4" Dia. UNC, 1 3/4" Long Hex Screw	ASTM A325	ASTM A123	–
g5	1	Luminaire Mast Arm, 20' Span, 11 Gauge Thick, 5.5' Rise	ASTM A595 Gr. A	ASTM A123	–
g6	1	1/2"–13 UNC, 4" Long Hex Bolt	ASTM A325	–	–

Notes:
(1) Quantities listed herein are only for 1 system installation.
(2) For testing purposes part e1 used NE Mix 47B1S/1PF4000HW.
(3) This arm designed for finished luminaire end angle rise of 3 degrees.

Midwest Roadside Safety Facility

Alaska DOT Light Poles
Test Nos. AKLP 5–6

Bill of Materials

SHEET: 17 of 18
DATE: 5/28/2024
DRAWN BY: CAO/GSK/MM
DWG. NAME. AKLP–5–6_R7
SCALE: 1:96
UNITS: in.
REV. BY: JSS

Figure 7.18 Bill of Materials, Test Nos. AKLP-5 and AKLP-6

Item No.	QTY.	Description	Material Specification	Treatment Specification	Hardware Guide
g7	2	1/2" Dia. Plain Round Washer	ASTM A153 or AASHTO M232	–	–
g8	1	13 13/16" Dia. x 1 5/16" Thick Ballast Plate	ASTM A36	–	–
g9	1	1/2" Dia. UNC Heavy Hex Nut	ASTM A563DH	–	–
h1	1	Luminaire Pole Cap	ASTM B86	ASTM A123/M111	–
h2	3	1/4" Dia. UNC, 1 3/4" Long Hex Bolt	ASTM A153	ASTM A123	–
h3	1	"C" Hook	ASTM A153 – Commercial grade hot rolled bar	ASTM A123	305354

Notes: (1) Quantities listed herein are only for 1 system installation.

Midwest Roadside Safety Facility

Alaska DOT Light Poles
Test Nos. AKLP 5–6

Bill of Materials

SHEET: 18 of 18
DATE: 5/28/2024
DRAWN BY: CAO/GSK/MM
DWG. NAME. AKLP–5–6_R7
SCALE: 1:45
UNITS: in.
REV. BY: JSS

Figure 7.19 Bill of Materials, Test Nos. AKLP-5 and AKLP-6

Figure 7.20 Construction Photographs, Test No. AKLP-5

Figure 7.21 Test Installation Photographs, Test No. AKLP-5

Figure 7.22 Test Installation Photographs, Test No. AKLP-5

Figure 7.23 Construction Photographs, Test No. AKLP-6

Figure 7.24 Construction and Soil Testing Photographs, Test No. AKLP-6

Figure 7.25 Test Installation Photographs, Test No. AKLP-6

Figure 7.26 Test Installation Photographs, Test No. AKLP-6

Chapter 8 Component Testing – Foundations with Breakaway Steel Poles

8.1 Purpose

Tests on foundations with breakaway steel poles were performed to investigate frangible coupling activation and foundation permanent set resulting from simulated vehicle impacts. Key performance characteristics included force versus time, force versus displacement, energy versus displacement, and foundation lateral deflection. The intent of the tests was focused on verifying breakaway activation for light poles mounted to foundations surrounded by weak soils at a favorable price point compared to full-scale crash tests.

8.2 Scope

Two bogie tests were conducted on two foundation specimens, as detailed in Chapter 1. The tests represent extreme soil conditions by placing soil loose around foundations, without any compaction, and testing soils in dry and saturated conditions. As a rigid bogie head was used in testing, the scope of results is limited to peak contact forces between the bogie and pole and associated foundation displacements. The tests do not represent occupant risk in terms of Occupant Impact Velocity (OIV) or Occupant Ridedown Acceleration (ORA) due to the lack of a crushable nose.

8.3 Dynamic Test No. AKLP-5

8.3.1 Test Description

The light pole system, comprised of a 35.5-ft tall steel pole with an attached single mast arm, ballasted to simulate luminaire weights, and anchored to a reinforced concrete foundation in dry, uncompacted sand via four 1-in. diameter Model No. 5100 Transpo couplings, was subjected to an impact from a 1,858-lb bogie vehicle. The bogie vehicle impacted the light pole at an impact height of 25 in. and a velocity of 20.4 mph. Sequential photographs for the test are shown in Figures 8.1 and 8.2. A sequential description of impact events is summarized in Table 8.1.

Table 8.1 Sequential Description of Impact Events, Test No. AKLP-5

Time (s)	Event Description
0.00	Initial contact between bogie vehicle and light pole.
0.01	Cracking at the upper neck was observed in both rear couplings; the light pole sustained a dent.
0.02	Complete fractures at neck locations manifested in all four couplings. Breakaway activation achieved.
0.03	The bogie vehicle's head lost contact with the light pole.
0.30	Light pole's base section established contact with the ground surface.
0.51	A secondary impact occurred between the bogie vehicle and the light pole.

8.3.2 System Damage

Damage to the steel light pole and the four Transpo couplings is photographically documented in Figures 8.3 and 8.4. The steel pole was dented at the impact location. All four couplings fractured, with the left-front coupling exhibiting fracture at the upper neck section, resulting in a 4-in. stub height, while the remaining three couplings fractured at the lower neck sections, leaving 1.5-in. stub heights. Disturbance of the soil surrounding the foundation was negligible.


0.000 sec


0.010 sec


0.020 sec


0.030 sec


0.040 sec


0.300 sec

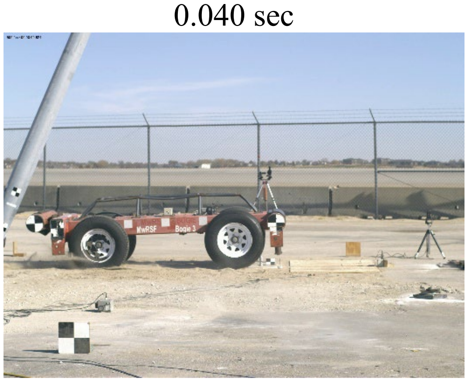
0.400 sec

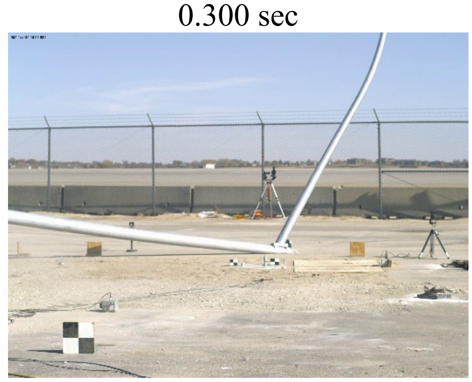
1.460 sec

Figure 8.1 Time-Sequential Photographs, Test No. AKLP-5

0.000 sec

0.010 sec

0.050 sec

0.100 sec

0.460 sec

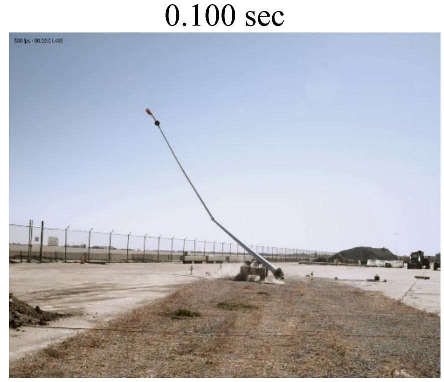

1.220 sec

2.140 sec

3.060 sec

Figure 8.2 Additional Time-Sequential Photographs, Test No. AKLP-5

Figure 8.3 System Damage Photographs, Test No. AKLP-5

Figure 8.4 Additional System Damage Photographs, Test No. AKLP-5

8.3.3 Impact Force and Foundation Displacement

Force versus displacement and energy versus displacement curves were determined from recorded accelerometer data, as depicted in Figure 8.5. The peak recorded force value was 27.8 kips at a bogie displacement of 4.6 in. This force magnitude is similar to the maximum shear strength of the Transpo couplings as a group, 22 kips, but larger due to mass activation and inertial resistance of the light pole system. The light pole and foundation assembly collectively absorbed a total energy of 115.3 kip-in. throughout the duration of the impact. Data collected from the string potentiometer indicated that the top of the reinforced concrete foundation experienced a peak dynamic deflection of 1.18 in. and slightly rebounded, coming to rest at a permanent deflection of 0.96 in., as illustrated in Figure 8.6.

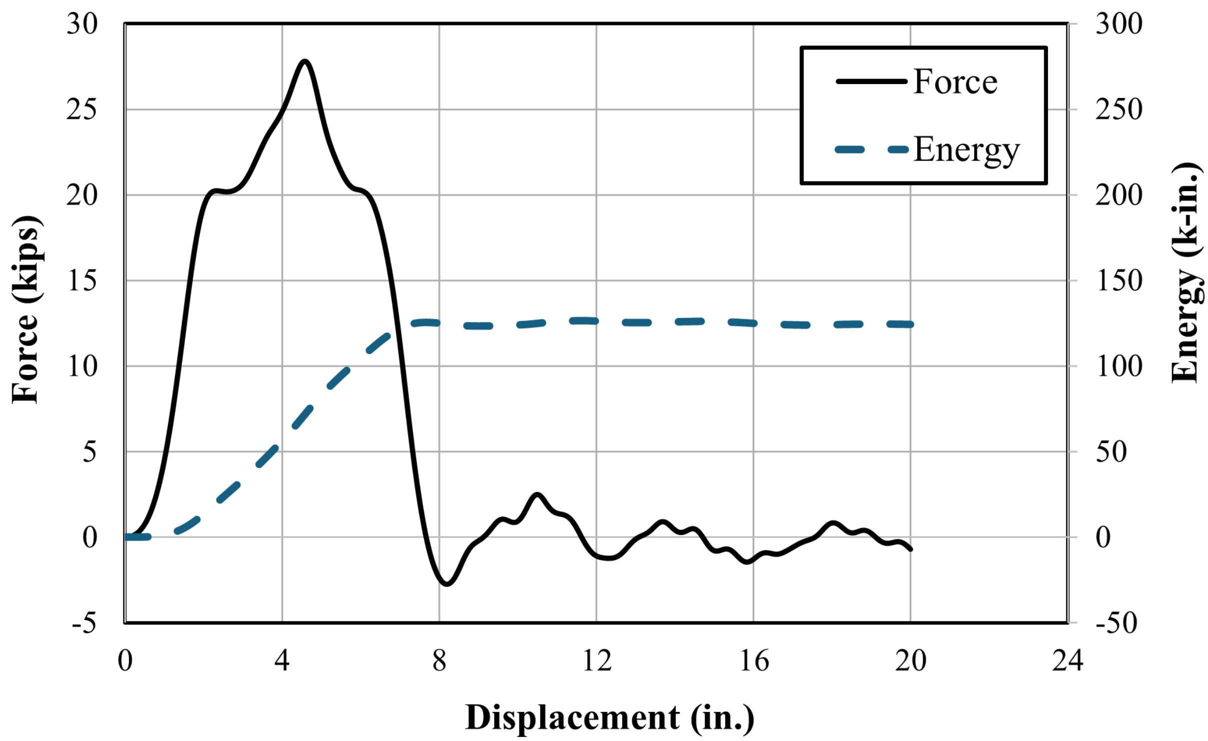

Figure 8.5 Force vs. Deflection and Energy vs. Deflection, Test No. AKLP-5

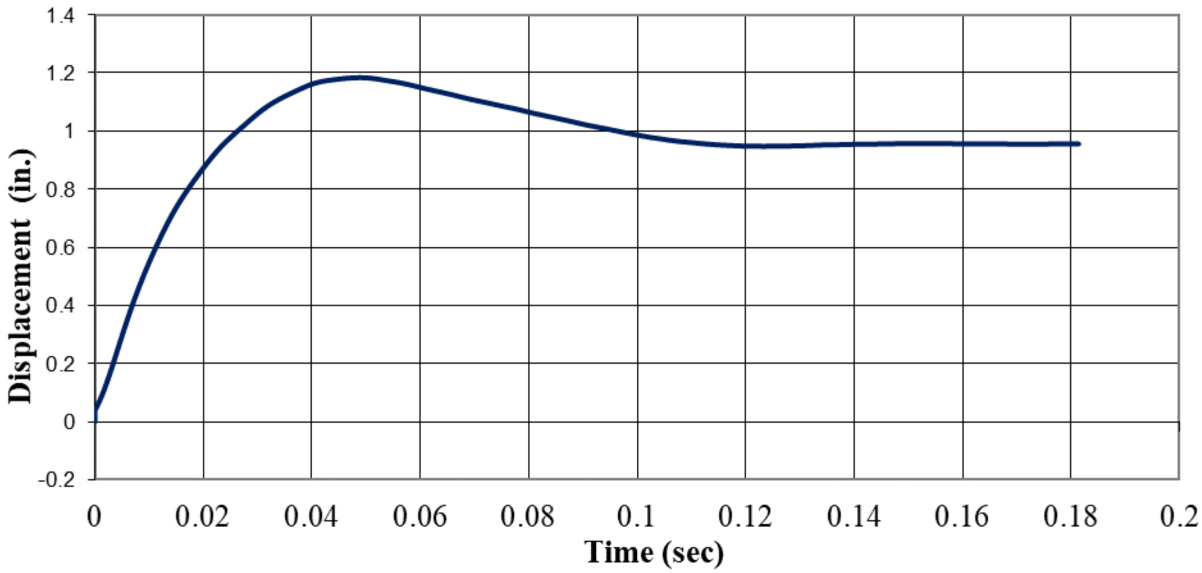

Figure 8.6 Foundation Displacement, Test No. AKLP-5

8.3.4 Discussion

The analysis of the results from test no. AKLP-5 revealed that the light pole system, composed of a 35.5-ft tall steel pole with a 20-ft long single mast arm, securely anchored to a 6-ft deep, 30-in. diameter reinforced concrete foundation embedded in dry, non-compacted sandy soil by four Model No. 5100 Transpo breakaway couplings, exhibited a controlled and predictable breakaway behavior. Stub heights complied with the 4-in. threshold set by *AASHTO's Standard Specifications for Structural Supports for Highway Signs, Luminaires, and Traffic Signals*. The couplings and foundation mass were able to provide crashworthy breakaway activation, without causing objectionable foundation displacement. Similar impacted light poles in service could therefore reasonably be expected activate predictably, and also to be able to be reinstalled on a foundation with any dry, sandy soil fill surrounding the foundation, regardless of soil in-situ SPT value, and without requiring removal or repair of the foundation.

8.4 Dynamic Test No. AKLP-6

8.4.1 Test Description

The light pole system, comprised of a 35.5-ft tall steel pole with an attached single mast arm, ballasted to simulate luminaire weights, and anchored to a reinforced concrete foundation in saturated, uncompacted sand via four 1-in. diameter Model No. 5100 Transpo couplings, was subjected to an impact from a 1,782-lb bogie vehicle. The bogie vehicle impacted the light pole at an impact height of 25 in. and a velocity of 20.0 mph. Sequential photographs for the test are shown in Figures 8.7 and 8.8. A sequential description of impact events is summarized in Table 8.2.

Table 8.2 Sequential Description of Impact Events, Test No. AKLP-6

Time (s)	Event Description
0.00	Initial contact between bogie vehicle and light pole.
0.01	Upper neck fractures occurred in both front couplings; the light pole sustained a dent.
0.02	The breakaway mechanism was activated due to the fracture of all four couplings.
0.03	The bogie vehicle’s head lost contact with the light pole.
0.31	The base section of the light pole established contact with the ground surface.
0.41	A secondary impact occurred between the bogie vehicle and the light pole.

8.4.2 System Damage

Damage to the steel light pole and the four Transpo couplings is photographically documented in Figures 8.9 and 8.10. The steel pole was dented at the impact location. All four couplings fractured at lower neck sections, leaving 1.5-in. stub heights. Disturbance of the soil surrounding the foundation was negligible.


0.000 sec


0.010 sec


0.020 sec


0.030 sec

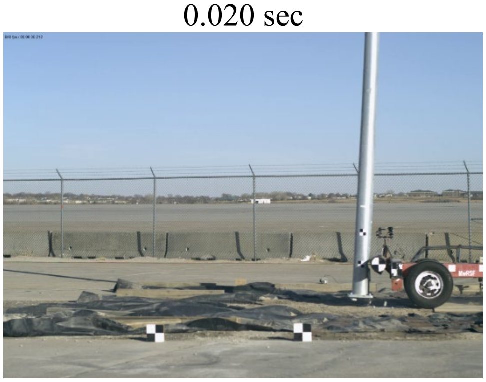
0.040 sec

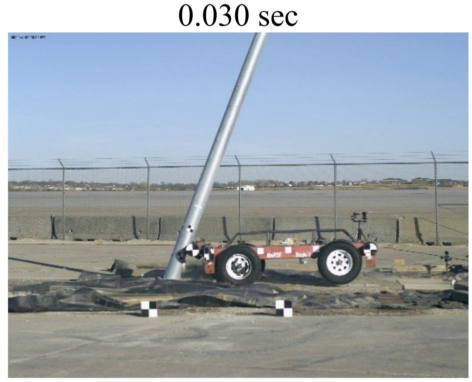
0.400 sec

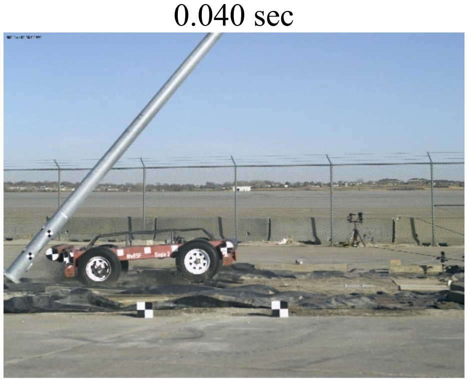
0.800 sec

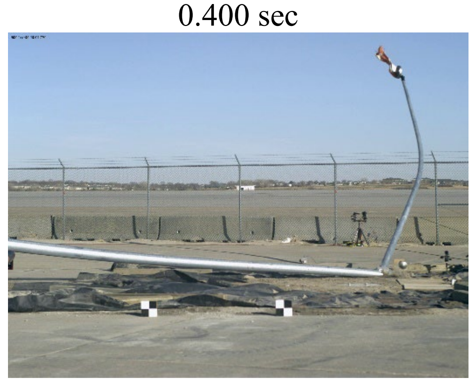
1.500 sec

Figure 8.7 Time-Sequential Photographs, Test No. AKLP-6

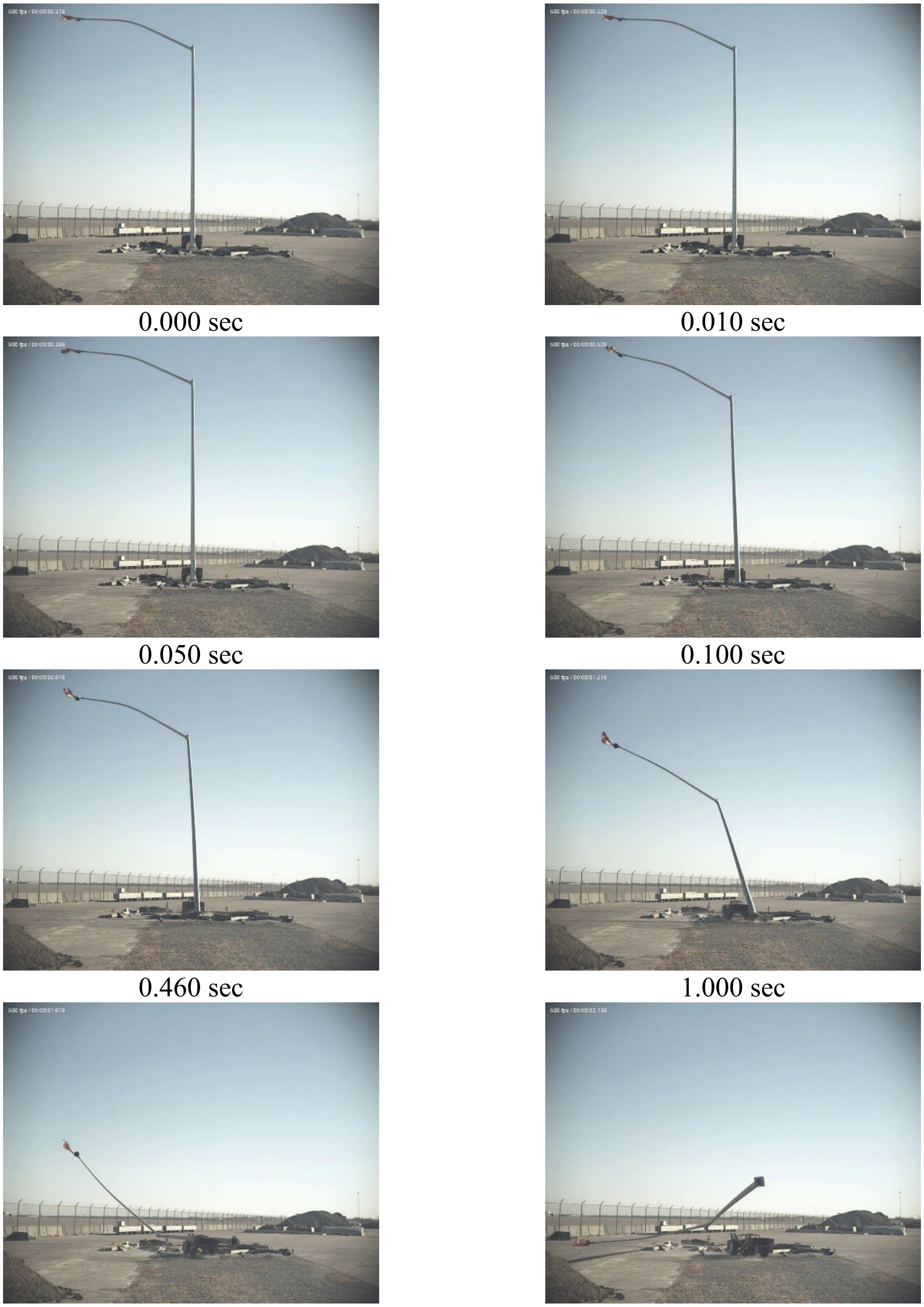

0.000 sec | 0.010 sec

0.050 sec | 0.100 sec

0.460 sec | 1.000 sec

1.500 sec | 1.920 sec

Figure 8.8 Additional Time-Sequential Photographs, Test No. AKLP-6

Figure 8.9 System Damage Photographs, Test No. AKLP-6

Figure 8.10 Additional System Damage Photographs, Test No. AKLP-6

8.4.3 Impact Force and Foundation Displacement

Force versus displacement and energy versus displacement curves for test no. AKLP-6 were determined from recorded accelerometer data, as depicted in Figure 8.11. The peak recorded force value was 27.5 kips at a bogie displacement of 2.7 in. Similar to test no. AKLP-5 in dry soil, this force magnitude is near to and slightly greater than the 22-kip maximum shear strength of the Transpo couplings as a group, with the excess recorded force attributed to mass activation and inertial resistance of the light pole system. The light pole and foundation assembly collectively absorbed a total energy of about 96.9 kip-in. Data collected from the string potentiometer indicated that the top of the reinforced concrete foundation experienced a peak dynamic deflection of 0.32 in. and slightly rebounded, coming to rest at a permanent deflection of 0.12 in., as illustrated in Figure 8.12.

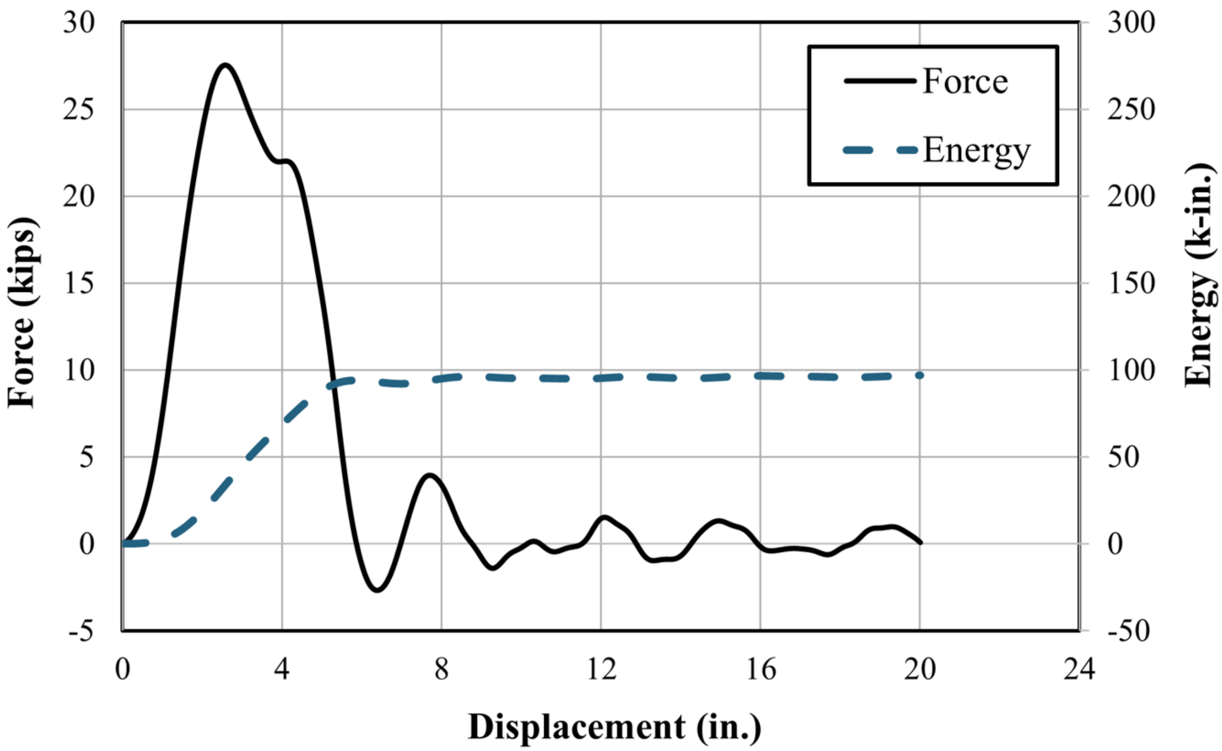

Figure 8.11 Force vs. Deflection and Energy vs. Deflection, Test No. AKLP-6

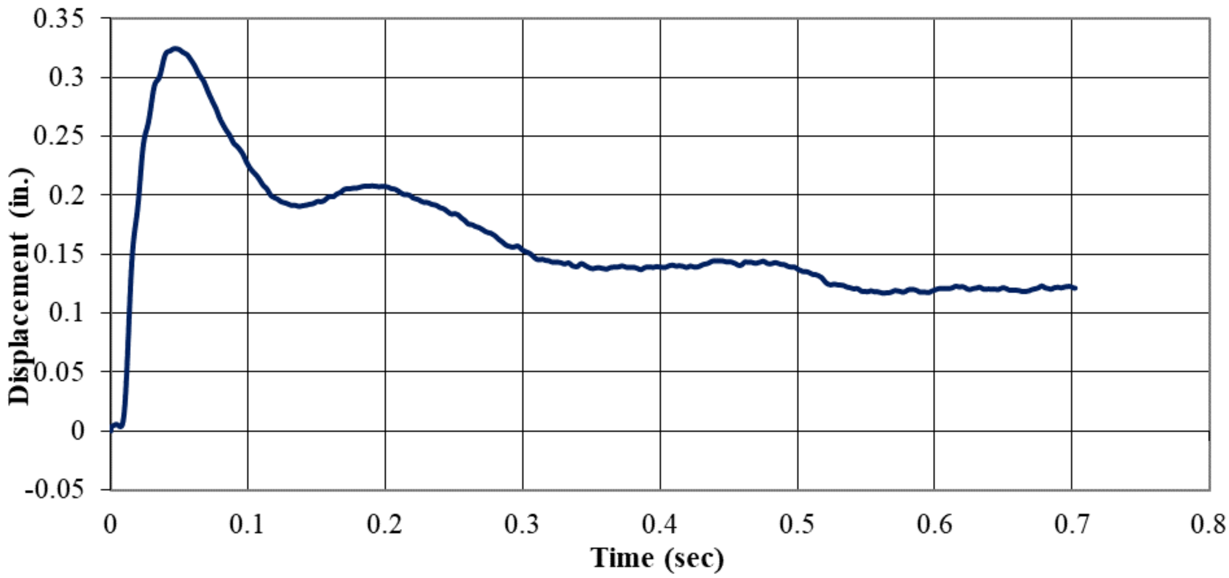

Figure 8.12 Foundation Displacement, Test No. AKLP-6

8.4.4 Discussion

The analysis of the results from test no. AKLP-6 revealed that the light pole system, composed of a 35.5-ft tall steel pole with a 20-ft long single mast arm, securely anchored to a 6-ft deep, 30-in. diameter reinforced concrete foundation embedded in saturated, non-compacted sandy soil by four Model No. 5100 Transpo breakaway couplings, exhibited a controlled and predictable breakaway behavior. Stub heights complied with the 4-in. threshold set by *AASHTO's Standard Specifications for Structural Supports for Highway Signs, Luminaires, and Traffic Signals*. The couplings and foundation mass were able to provide crashworthy breakaway activation, without causing objectionable foundation displacement. Similar impacted light poles in service could therefore reasonably be expected activate predictably, and also to be able to be reinstalled on a foundation with any sandy soil fill surrounding the foundation, regardless of soil in-situ SPT value or moisture content, and without requiring removal or repair of the foundation.

8.5 Summary of Bogie Tests on Breakaway Steel Poles

Two simulated vehicle impact tests were performed on steel light poles fabricated identically to others recently ordered by AK DOT&PF, mounted to concrete foundations similar to the detail shown in AK DOT&PF Standard Plan L-30.11, and anchored with four Transpo Model No. 5100 frangible couplings, also as shown in AK DOT&PF Standard Plan L-30.11. Similar bogie vehicles weighing approximately 1,800 lb impacted each pole at a height of 25 in. and a velocity of approximately 20 mph. Exact values for each test are summarized in Table 8.3, and additional data is available in Appendix G and Appendix H.

Table 8.3 Dynamic Testing Results, Test Nos. AKLP-5 and AKLP-6

Test No.	Pole Height (ft.)	Impact Angle	Bogie Weight (lb)	Impact Height (in.)	Impact Speed (mph)	Soil Condition	Peak Force (kips)	Total Energy (kip-in.)	Peak Foundation Displacement (in.)	Failure Mechanism
AKLP-5	35.5	0° (Long.)	1,858	25	20.35	Dry	27.8	115.3	1.18	Coupling fracture
AKLP-6	35.5	0° (Long.)	1,782	25	18.96	Saturated	27.6	96.9	0.36	Coupling fracture

In both tests, the frangible couplings activated reliably. A plot showing force versus time for both tests is shown in Figure 8.13. Additionally, foundation movement was minor in both tests, as shown in Figure 8.14. Greater peak and residual displacements were observed for the dry condition, potentially due to reduced interparticle friction and resulting greater density for the saturated condition. While elastic rebound and foundation rock-back are subject to a high degree of uncertainty, the results were highly favorable, considering that the peak displacement for both tests was only about 66% of the target threshold likely to allow impacted pole replacement without replacing the foundation (1.18 in. compared to 1.8 in., recall Section 3.4).

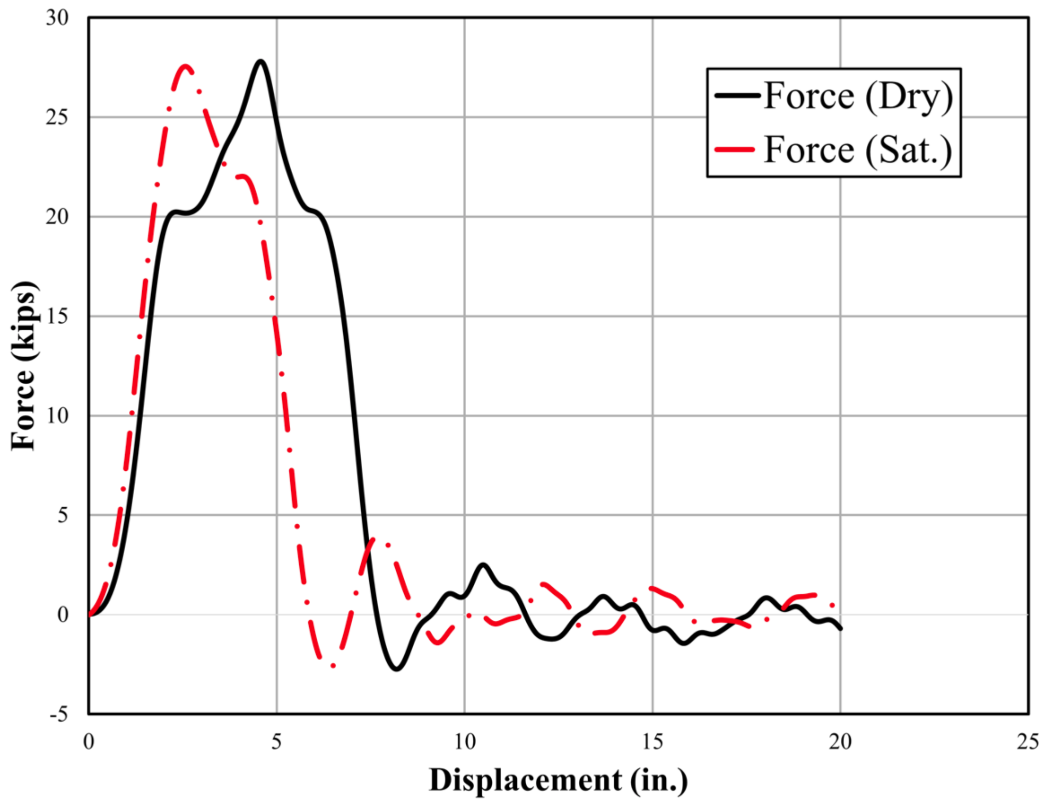

Figure 8.13 Force vs. Time, Test Nos. AKLP-5 and AKLP-6

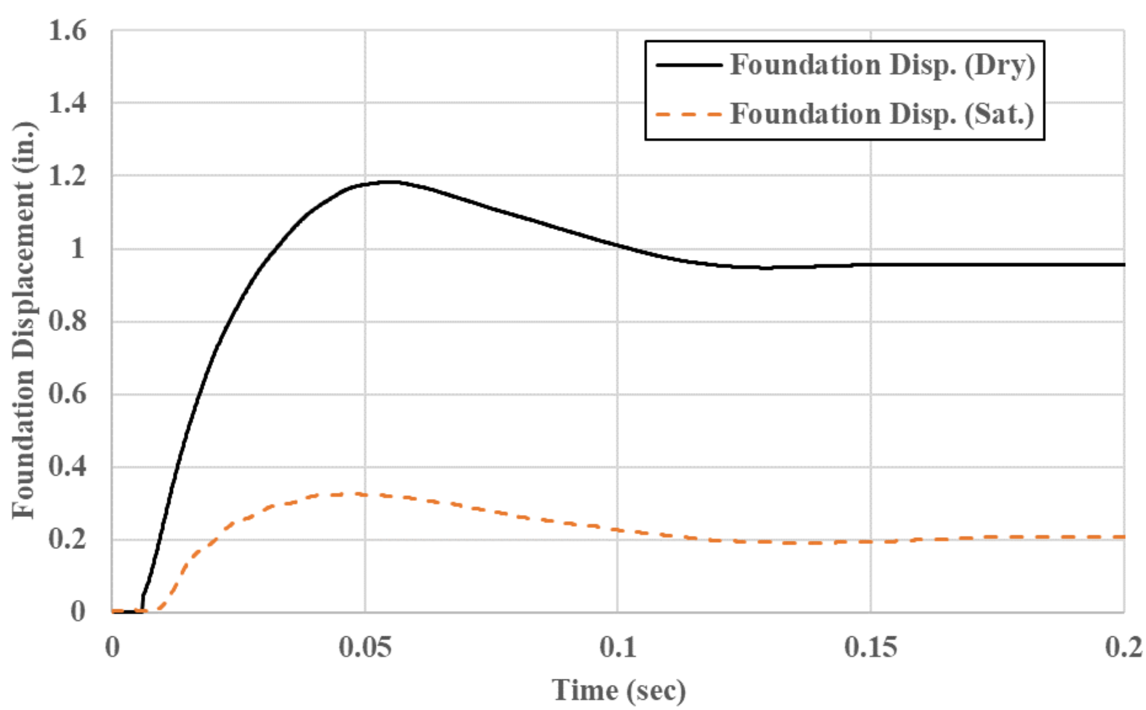

Figure 8.14 Force vs. Foundation Displacement, Test Nos. AKLP-5 and AKLP-6

Chapter 9 Hybrid Fem+Ale Simulation for a Laterally Impacted Light Pole Foundation in Sand

9.1 Introduction

Modeling soil-foundation interaction problems involving large soil deformations remains a crucial area of research in geotechnical engineering and geomechanics [40-42]. Applications of the traditional Lagrangian Finite Element Method (FEM) often encounter issues, such as mesh distortion and element entanglement during large deformations, which can lead to the premature termination of analyses. To address these challenges, advanced techniques and novel numerical methods have been developed, including the Arbitrary Lagrangian-Eulerian (ALE) formulation. The ALE has demonstrated reasonable accuracy in modeling and simulating large deformation geotechnical problems [41-42].

This study employed a hybrid FEM+ALE method to simulate dynamic soil-foundation interaction. This approach utilizes FEM to model the foundation and ALE to handle large soil deformations. This is the first application of this formulation to large-scale, dynamic impact soil-pole foundation interaction problems documented in the literature. Additionally, this research represents one of the few computational efforts aimed at modeling and capturing soil-structure interaction under vehicle impact and large dynamic deformations in both the foundation and the surrounding soil.

9.2 Material Model of Sand, Light pole Foundation, Steel Post, and Air

Regardless of the computational method employed to simulate the impact dynamics of light pole foundation-soil systems subjected to vehicular impacts, the assignment of suitable soil, concrete, and steel constitutive models is crucial. This is particularly important for accurately modeling and investigating the dynamics of impact events on light pole foundations embedded in sand.

9.2.1 Sand Constitutive Model

The Soil and Crushable Foam (SCF) model within the LS-DYNA simulation platform was utilized for the ALE soil domain. It is important to note that, during the preliminary modeling discussed in Chapter 3 of this report, the Jointed Rock model was initially used to simulate the soil. However, the Jointed Rock model is not compatible with the ALE method in the LS-DYNA simulation platform. Consequently, the SCF model, being the most convenient soil model available in LS-DYNA for use with the ALE approach, was selected for this research.

Conveniently, the SCF model's constitutive parameters can be tailored to align with those of the Drucker-Prager (D-P) model, a model noted for its successful application to the dynamic interaction between structures and granular media in several studies [43]. Additionally, the D-P model's constitutive parameters can be associated with soil properties, such as the cohesion coefficient and friction angle, which can be determined from conventional geotechnical laboratory tests or approximately correlated to SPT blow count. This section will discuss the determination of SCF model parameters, based on laboratory and field geotechnical tests.

The mean stress p is expressed as:

Here σ_1, σ_2, and $\sigma_3$denote the principal stress values.

The deviator stress $s_{ij}$is given by:

$$s_{ij} = \sigma_{ij} - p\delta_{ij} \tag{4}$$

Where σ_{ij}signifies the Cauchy stress tensor and $\delta_{ij}$is the second order identity tensor.

The SCF model's yield criterion is described in terms of the second invariant of the deviator stress, $J_2 = \frac{1}{2}s_{ij}s_{ij}$, and the mean stress, as follows:

$$J_2 = a_0 + a_1 p + a_2 p^2 \tag{5}$$

Here a_0, a_1, and $a_2$are the constitutive parameters.

The first invariant of the stress tensor, I_1, is defined as:

$$I_1 = \sigma_1 + \sigma_2 + \sigma_3 = -3p \tag{6}$$

Introducing I_1 in Equation (5) yields:

$$J_2 = a_0 - \frac{1}{3}a_1 I_1 + \frac{1}{9}a_2 I_1^2 \tag{7}$$

The D-P yield criterion is expressed by:

$$\sqrt{J_2} = -\alpha I_1 - k \tag{8}$$

Here α and k represent D-P model constitutive parameters.

Squaring both sides of Equation (8) provides:

$$J_2 = \alpha^2 I_1^2 - 2k\alpha I_1 + k^2 \tag{9}$$

By equating the coefficients of Equation (7) from Equation (9), the SCF model parameters $a_0 = k^2$, $a_1 = -6\alpha k$, and $a_2 = 9\alpha^2$can be determined. Using the D-P model yield surface that circumscribes the Mohr-Coulomb (M-C) yield surface of the soil proves beneficial because the two surfaces match at the compression corners, an advantage when simulating dynamic soil compression during lateral light pole foundation impact. The circumscribed D-P yield surface parameters are [44]:

$$\alpha = \frac{2 \sin \phi}{\sqrt{3}(3 - \sin \phi)} \tag{10}$$

$$k = \frac{6c \cos \phi}{\sqrt{3}(3 - \sin \phi)} \tag{11}$$

where c is the cohesion coefficient and ϕ is the friction angle.

The cohesion coefficient values for the compacted and uncompacted sand were determined based on the Standard Penetration Test (SPT) N values obtained prior to the crash testing program. In the absence of specific data on the sand's friction angle in dynamic bogie tests, the friction angle was assumed to be equal to the angle of repose. These cohesion and friction angle values were initially utilized to compute the D-P model parameters, i.e., α and k and subsequently, the SCF model parameters a_0, a_1, and $a_2$were calculated based on the D-P model parameters using the aforementioned relations.

The density of the uncompacted sand was set as 86.8 pcf, while the density of compacted sand was set at 103.1 pcf. The sand's shear modulus G and bulk modulus K values were established based on Young's modulus obtained using the SPT N values and from a range of values suggested by Wright [45] for modeling dry sand under dynamic loading environments. The SCF model parameters for compacted and uncompacted sand are presented in Tables 9.1 and 9.2.

Table 9.1 SCF Model Input Parameters for Compacted Sand Utilized in Test No. AKLP-1

Item	Soil Parameter	Value (SI Unit)	Value (US Unit)
Basic parameter	Density of soil, ρ_{soil}	1.65e-06 kg/mm^3	103.10 pcf
Elasticity parameters	Bulk modulus, K	11.64	1.68 ksi
	Shear modulus, G	5.24 MPa	0.76 ksi
Yield surface parameters	Yield surface parameter, a_0	2.19e-09	2.19e-09
	Yield surface parameter, a_1	7.66e-05	7.66e-05
	Yield surface parameter, a_2	0.671	0.671

Table 9.2 SFC Model Parameters for Uncompacted Sand Used in Test No. AKLP-2

Item	Soil Parameter	Value (SI Unit)	Value (US Unit)
Basic parameter	Density of soil, ρ_{soil}	1.39e-06 kg/mm^3	86.80 pcf
Elasticity parameters	Bulk modulus, K	9.47 MPa	1.37 ksi
	Shear modulus, G	2.62 MPa	0.38 ksi
Yield surface parameters	Yield surface parameter, a_0	8.5e-10	8.5e-10
	Yield surface parameter, a_1	4.78e-6	4.78e-6
	Yield surface parameter, a_2	0.671	0.671

9.2.2 Reinforced Concrete Foundation Model

In this study, the Continuous Surface Cap Model (CSCM), a standard model in LS-DYNA, was utilized to simulate the concrete foundation. This isotropic, elasto-plastic material model employs a yield surface to distinguish between elastic and plastic domains. Extensive information regarding the theoretical underpinnings and numerical implementation of the CSCM is accessible in prior works [46-47].

The CSCM's efficacy in accurately replicating experimental outcomes and predicting the performance of reinforced concrete (RC) structural components under impact or blast loading has been verified by numerous researchers [48-50]. This model enables the definition of concrete properties via a parameter initialization function grounded on the concrete's compressive strength and maximum aggregate size, which is particularly useful when detailed data is unavailable.

For the purpose of this research, the compressive strength of the concrete was set at 4.1 ksi, and the maximum aggregate size was specified to be 0.75 in., enabling the derivation of the CSCM parameter sets. In the CSCM, a parameter *'d'* is introduced to quantify damage accumulation, applicable to concrete damage in both tension and compression.

$$d(\tau_b) = \frac{0.999}{D_c}\left[\frac{1+D_c}{1+D_c\,exp^{-C_c(\tau_b-r_{0b})}} - 1\right] \tag{12}$$

$$d(\tau_b) = \frac{d_{max}}{D_c\left[\frac{1+B_c}{1+B_c\,exp^{-A_c(\tau_d-r_{0d})}} - 1\right]} \tag{13}$$

Equations (12) and (13) determine the tensile damage accumulation from the maximum principal strain and the compressive damage accumulation from the total strain components. Parameters A_c, B_c, C_c, and D_c define the softening curve shape, whereas τ_b and τ_d correspond to the brittle and ductile energy terms, respectively, defined from the total strain's accumulation. r_{0b} and r_{0d} represent the initial tensile and compressive thresholds, while d_{max} denotes the maximum damage level as a function of confining pressure.

Concrete damage is thus represented by the damage parameter, ranging from 0 to 1. As the damage parameter approaches 1, a reduction in the strength and stiffness of the concrete element occurs, eventually leading to concrete cracking. Furthermore, the CSCM considers rate effects, which simulate an increase in the strength of concrete corresponding with an increase in strain rate. The specific concrete properties used in deriving the CSCM material parameter sets for simulating concrete under impact loading are outlined in Table 9.3.

Table 9.3 CSCM Parameter for Concrete Used in Test Nos. AKLP-1 and AKLP-2

Parameters	Value (SI Unit)	Value (US Unit)
Mass density (kg/mm^3)	2.380 e-06 kg/mm^3	148.62 pcf
Compressive strength (MPa)	28 MPa	4.10 ksi
Aggregate size (mm)	19 mm	0.75 in.

9.2.3 Steel Post and Reinforcement Bars Model

The Piecewise-Linear Plasticity model, a commonly selected material model in LS-DYNA for simulating metals in dynamic impact environments, was employed to model the stress-strain response of the steel post [51-52]. The deviator stress in the piecewise-linear plasticity model is determined to satisfy the yield function as follows:

$$f = \frac{1}{2} s_{ij} s_{ij} - \left(\frac{\sigma_y}{\sqrt{3}}\right)^2 \leq 0 \tag{14}$$

Where s_{ij} represents the deviator stress tensor and

$$\sigma_y = \beta\left[\sigma_0 + f_h\left(\varepsilon_{eff}^p\right)\right] \tag{15}$$

In this equation, β signifies a strain rate factor accounting for strain-rate effects, σ_0 represents the initial yield stress, and $f_h\left(\varepsilon_{eff}^p\right)$ is the post-yield hardening stress increase as a function of ε_{eff}^{p}, the effective plastic strain. The hardening function can be specified either in a tabular form or as linear hardening of the form $f_h\left(\varepsilon_{eff}^{p}\right) = E_P(\varepsilon_{eff}^{p})$ with E_P as the plastic hardening modulus.

In this elastoplastic model, the deviator stresses are updated elastically, and the yield function is evaluated. If the yield function is satisfied, the deviator stresses are accepted. Otherwise, the plastic strain increment is computed using Equation (16):

$$\Delta\varepsilon_{eff}^{p} = \frac{\left(\frac{3}{2}\tilde{s}_{ij}\tilde{s}_{ij}\right)^{\frac{1}{2}} - \sigma_y}{E_P + 3G} \tag{16}$$

Here E_P stands for the current hardening modulus, and Grepresents the shear modulus. The trial deviator stress state, $\tilde{s}_{ij}$is scaled back as illustrated in Equation (17):

$$s_{ij}^{n+1} = \frac{\sigma_y}{\left(\frac{3}{2}\tilde{s}_{ij}\tilde{s}_{ij}\right)^{\frac{1}{2}}}\tilde{s}_{ij} \tag{17}$$

The Cowper-Symonds model [53] scales the yield stress using a factor β, calculated via Equation (18):

$$\beta = 1 + \left(\frac{\dot{\varepsilon}_p}{c}\right)^{\frac{1}{p}} \tag{18}$$

In this equation, $\dot{\varepsilon}_p$ represents the effective plastic strain rate, and c and $p$are Cowper-Symonds strain rate parameters. These parameters cannot be determined from tensile tests, but values of 40.4 and 5 for c and p, respectively, have demonstrated reasonable agreement with experimental data for mild steel [54].

Material properties for the steel post were derived from tensile tests conducted at MwRSF-UNL and reported by Schrum et al. [55]. The specific material input parameters for the steel post are tabulated in Tables 9.4 and 9.5.

Table 9.4 Piecewise Linear Plasticity Material Model Input Parameters for Steel (SI units) [55]

Material parameter	**Value**							
Density (kg/mm^3)	7.86e-06							
Young's modulus (GPa)	200							
Poisson's ratio	0.30							
Effective plastic strain	ep1	ep2	ep3	ep4	ep5	ep6	ep7	ep8
	0.000	0.0160	0.0470	0.0890	0.1170	0.1410	0.1850	2.0000
Effective stress (GPa)	es1	es2	es3	es4	es5	es6	es7	es8
	0.439	0.4730	0.5200	0.5610	0.5860	0.6010	0.6210	1.8000

Table 9.5 Piecewise Linear Plasticity Material Model Input Parameters for Steel (US units) [55]

Material parameter	**Value**							
Density (pcf)	490.7							
Young's modulus (ksi)	29007							
Poisson's ratio	0.30							
Effective plastic strain	ep1	ep2	ep3	ep4	ep5	ep6	ep7	ep8
	0.000	0.0160	0.0470	0.0890	0.1170	0.1410	0.1850	2.0000
Effective stress (ksi)	es1	es2	es3	es4	es5	es6	es7	es8
	63.67	68.60	75.42	81.37	84.99	87.17	90.07	261.07

Reinforcement of the concrete foundation was achieved through eight #8 longitudinal steel reinforcing bars and #5 circular hoops at 6-in. intervals. The reinforcement was comprised of American Society of Testing Materials (ASTM) A615 material, with a yield strength of 60 ksi (413.7 MPa). Reinforcing bar material behavior was simulated with a computationally efficient elasto-plastic model, using MAT Plastic Kinematic. This model is suitable for modeling isotropic and kinematic hardening plasticity, incorporating strain rate effects. The yield strength of steel reinforcement was set to 60 ksi, consistent with nominal properties of material used in the physical impact tests. The specific material input parameters utilized for modeling the reinforcement bars are presented in Table 9.6.

Table 9.6 Material Properties for Reinforcement Bars within the MAT Plastic Kinematic Model

Material Property	Value (SI Unit)	Value (US Unit)
Density	7.86e-06 (kg/mm3)	490.7 (pcf)
Young's modulus	200 (GPa)	29007.5 (ksi)
Poisson's ratio	0.30	0.30
Yield strength	0.4137 (GPa)	60.0 (ksi)
Tangent modulus	20 (GPa)	2900.7 (ksi)
Cowper-Symonds Strain rate parameter, *C*	40 (-)	40 (-)
Cowper-Symonds Strain rate parameter, *p*	5 (-)	5 (-)

9.2.4 Constitutive Model and Equation of State for Air Material

The implemented hybrid FEM and ALE computational model for the light pole foundation-soil encompasses three components: (1) the air domain; (2) the soil domain; and (3) the light pole foundation. Prior research often simulated the air domain within coupled fluid-structure interaction (FSI) impact and contact problems using "void materials." However, the use of "void materials" to represent air may not accurately reflect the physics of FSI impact scenarios, potentially resulting in excessive impact forces [56].

In this study, MwRSF researchers modeled the air domain using material properties and a governing equation of state (EOS), specifically utilizing the Null material model. This model accommodates minimal shear strength and necessitates an EOS. Consequently, the air domain elements were assigned the null hydrodynamic material type with a Linear Polynomial type EOS.

In the Linear Polynomial EOS, the initial thermodynamic state of the material and pressure are defined by Equation (19):

$$p = C_0 + C_1\zeta + C_2\zeta^2 + C_3\zeta^3 + (C_4 + C_5\zeta + C_6\zeta^2)\tilde{E} \tag{19}$$

In this equation C_0, C_1, C_2, C_3, C_4, C_5 and C_6 are user defined constants, $\tilde{E}$ signifies the initial energy per volume, and ζ is a volumetric variable, which can be expressed as follows:

$$\zeta = \frac{1-V_o}{V_o} \tag{20}$$

Here V_o denotes the relative volume as described by Equation (21):

$$V_o = \frac{\rho_0}{\rho} \tag{21}$$

In this equation ρ_0 represents the reference or initial mass density, and ρ is the current mass density of the material.

Air material and EOS properties were determined from the previous studies [57-58] and are summarized in Table 9.7.

Table 9.7 Input Data: ALE Air Material and EOS (kg, mm, ms) [57-58]

MAT_NULL	Mass density [ρ_0]		Pressure cutoff [PC]			Dynamic viscosity [μ]		
	1.23e-09		0			0		
EOS_LINEAR_ POLYNOMINAL	C_0	C_1	C_2	C_3	C_4	C_5	C_6	E
	-1e-04	0	0	0	0.4	0.4	0	2.5e-4

9.3 Numerical Modeling

9.3.1 Model Configuration

A hybrid FEM and ALE model was constructed in LS-DYNA [51] with to simulate the lateral impact response of a light pole foundation and embedded steel post assembly, with the foundation surrounded by sand, and subjected to a bogie (surrogate vehicle) collision. The LS-DYNA hydrocode was specifically chosen for its proven effectiveness in solving transient dynamic events characterized by intricate contact interactions and nonlinear material behavior, such as large strains and deformations.

The overall geometric model of this system was partitioned into three distinct regions, each representing the light pole foundation, the soil, and the surrounding air materials. The various model elements are depicted in Figure 9.1. This figure illustrates the domain where the ALE soil mesh size varies from 100 mm to 335 mm in the circumferential direction, and 100 mm to 115 mm in the radial direction. Throughout the Z-direction, the mesh size remains consistently at 100 mm.

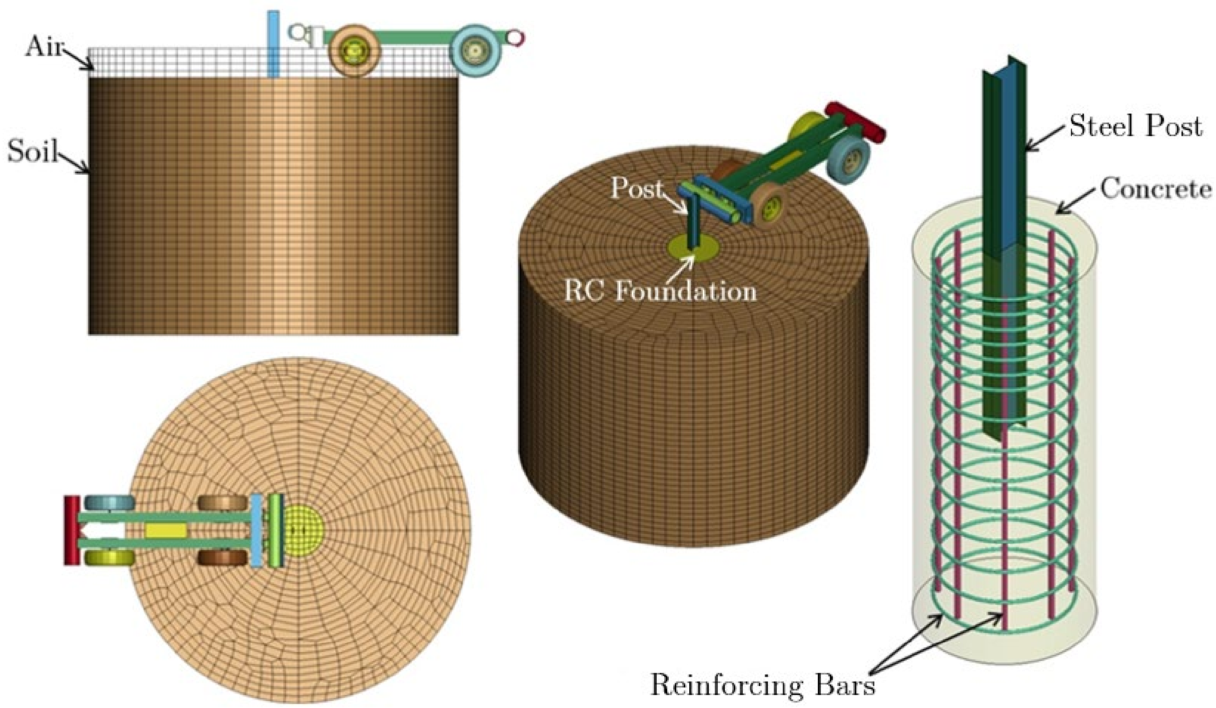

Figure 9.1 Hybrid ALE+ FEM Model Setup and Geometry of a Laterally Impacted Light pole Foundation in Sand

The ALE soil domain was configured as 3h in plan and 1.5h in depth to ensure that the boundaries of the soil domain were situated outside the region of significant deformation or the plastic zone, where h represents the embedment depth of the light pole foundation. The light pole foundation itself was embedded at a depth, h, of 72 in. and had a diameter of 30 in.

Both soil and air domains were modeled with one-point quadrature hexahedral ALE elements. The mesh size of the soil varied in the X-Y plane, contingent on the distance from the light pole foundation, as illustrated in Figure 9.1. Noting that large deformation and plastic flow of the soil occur in the vicinity of the foundation, a fine soil mesh size was adopted in the adjacent area (i.e., the near-field soil domain) of the foundation to precisely model the rapid and large deformation of the soil during post impact.

The near-field soil domain spanned a diameter of 100 in. and a depth of 90 in., dimensions that were deduced from observations gleaned from high-speed video footage of numerous soil-foundation system physical impact tests conducted at the Midwest Roadside Safety Facility (MwRSF) at the University of Nebraska-Lincoln (UNL).

Lagrangian meshes were employed to model the reinforced concrete foundation and the post. The W6x16 post was simulated using fully integrated shell elements. A constant-stress solid element with an incorporated Flanagan-Belytschko stiffness-based hourglass control was used to simulate foundation concrete. This hourglass control, which had an hourglass coefficient set to 0.1 [51-52], was chosen to curtail non-physical modes of deformation during impact loading. Both longitudinal and hoop reinforcement bars were represented using a two-node Hughes-Liu beam element.

Sand and air materials were defined using LS-DYNA's multi-material functionality, specifically through the adoption of the ALE_Multi-Material_Group. A requisite for the ALE formulation is an advection scheme, which serves to facilitate material transport. Given the array of advection schemes available in LS-DYNA, we elected to utilize the second-order accurate

Van Leer technique in the current study. This choice was driven by the technique's capacity to mitigate nonphysical energy dissipation, enhancing the accuracy of the simulation [51-52].

The surrogate vehicle model, or bogie, as depicted in Figure 9.2, was created by researchers at MwRSF-UNL to approximately represent the mass of a small car as a near-rigid, robust, and reuseable impact testing device. MwRSF's extensive research and development have culminated in the development of numerous surrogate vehicle models designed to simulate physical impact testing [59]. Rigid material assigned to Belytschko-Tsay shell elements was used to simulate all steel components of the surrogate vehicle, including the two longitudinal frame tubes, frame gussets and frame plate, and both the front and rear frame tubes, as well as the impact head.

The rear neoprene pad was modeled with solid elements and rigidly constrained to the bogie vehicle since it does not contact the post. Deformable solid elements with CRUSHABLE_FOAM material definition was utilized to model the neoprene pad. The frame tubes and impact head were rigidly secured to the frame tubes via the *Constrained_Rigid_Bodies command.

The surrogate vehicle tires were defined using elastic material and incorporated an internal airbag definition to simulate tire pressure. The interaction between the surrogate vehicle and the ground was simulated using a friction coefficient of 0.05. More extensive details regarding the surrogate vehicle model can be referenced in [59-61].

For this study, modifications to the bogie vehicle model consisted of updating the impact velocity and mass to what was used in actual dynamic impact testing and changing the height of the impact head.

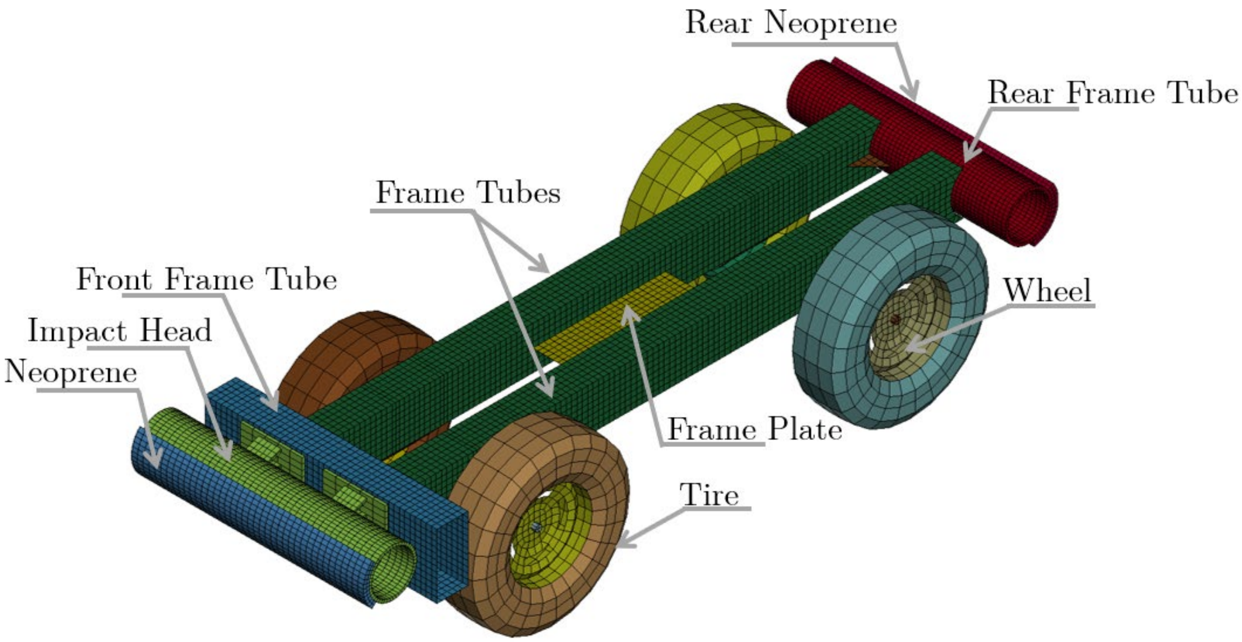

Figure 9.2 A Bogie (Surrogate) Vehicle Simulation Model

9.3.2 Dynamic Contacts and Couplings

9.3.2.1 Modeling Bogie Vehicle and Steel Post Contact

The Automatic Node to Surface contact mechanism was used to model the dynamic interaction between the surrogate vehicle's neoprene impact head and the steel post. This particular contact method facilitates the transfer of compressive and tangential loads between the slave nodes (of the post) and master segments (of the bogie vehicle's impact head). The Automatic Node to Surface contact is a penalty-based algorithm which restricts penetration between the interacting parts by exerting a force proportionate to the penetration depth whenever such penetration is detected [51].

Moreover, to account for the friction interaction at the interfaces, a Coulomb friction formulation is incorporated in the sliding contact. A static and dynamic friction coefficient of 0.1 was adopted in our study to model the friction interaction between the neoprene impact head and the post, drawing from the values ascertained from friction tests performed on rubber and steel materials in the research of Deladi [62]. In dynamic impact simulations, it is generally preferable to equalize the static and dynamic friction coefficients to circumvent potential numerical instabilities and higher frequency contact [51-52].

9.3.2.2 Concrete and reinforcement bars coupling

The concrete and reinforcement bars were modeled distinctly, necessitating a coupling mechanism to represent the interaction between the steel reinforcement and surrounding concrete. To achieve this, we employed the Constrained-Beam-in-Solid keyword available in LS-DYNA, facilitating the coupling of reinforcement bars with the concrete matrix.

In this formulation, beam node velocity and accelerations are compelled to equate with those of the concrete solid elements housing them. The application of the Constrained-Beam-in-Solid formulation in this study successfully rectified energy imbalances that were observed in the previously favored Constrained-Lagrange-in-Solid formulation, which had been typically used for constraining rebar in concrete [63].

9.3.2.3 ALE soil and Lagrangian light pole foundation coupling

A critical component of coupled soil-light pole foundation impact analysis is the successful interaction of the foundation with the soil. This dynamic soil-foundation interaction is facilitated by a coupling algorithm, which enables a suitable connection between the ALE soil and the Lagrangian light pole foundation, thus accurately capturing the dynamic soil-light pole foundation interaction during lateral impact loading.

We used a penalty-based coupling algorithm, Constrained-Lagrangian-in-Solid [51-52], to achieve dynamic soil-light pole foundation interaction. In this method, the foundation is embedded within the ALE (soil) mesh, which includes both the foundation and the ALE soil that flows through the fixed mesh as the advection scheme updates the history variables and velocity. This coupling algorithm ensures the conservation of momentum and energy [51-52].

Several key parameters within the Constrained-Lagrangian-in-Solid coupling algorithm were essential for modeling the foundation-soil impact interaction: Multi-material Coupling (MCOUP), Number of Coupling Points (NQUAD), Constraint Type (CTYPE), Coupling Direction (DIREC), and Penalty Factor (PFAC). MCOUP determines the Lagrangian component (i.e., the post) that interacts with the ALE material (i.e., the soil). NQUAD signifies the number of coupling points in the foundation; for instance, when NQUAD=2 is defined, there will be 4 coupling points on the foundation. As specifying a larger value of NQUAD could lead to a computationally costly coupling and excessively large contact forces, NQUAD=2 was used for coupling the foundation and soil in this study.

CTYPE was set to 4, in line with use of a penalty-based algorithm for coupling the foundation and soil. For this study, we used DIREC=2, considering only normal direction coupling as it offers robustness and stability [52]. The segment normals of the Lagrangian (post) shell segments, used in the slave side for the soil and foundation (structure) coupling, were directed towards the soil (ALE) material with which they are coupled. When using a penalty-based coupling algorithm (i.e., CTYPE=4), defining an appropriate coupling stiffness is crucial for achieving satisfactory post-soil coupling. Therefore, we used the default penalty stiffness, PFAC=0.1. This default value yields accurate simulations and serves as an appropriate starting point [64].

9.3.3 Boundary Condition

The dynamic impact loading of the soil-light pole foundation interaction problem involves shocks and dynamic waves generated by the vehicle's impact on the soil-foundation system. Given these conditions, the most suitable boundary condition to be applied to the four exterior faces and the bottom surface of the baseline model is the Boundary Non-Reflecting (BNR) boundary condition.

In contrast to standard boundary constraints, where rotations and displacements are fixed, the BNR condition does not restrict rotations and displacements. Rather, the solver internally defines conditions and equations to depict the computational domain as an infinite medium [51-52]. Consequently, we used the BNR boundary condition on the computational domain for the baseline model simulation.

9.3.4 Impact Load Application

In this study, the process of load application to the computational model of the soil-light pole foundation system was split into two stages to simultaneously address the static geo-stress in the soil due to gravity and the transient load from impact. In the first stage, we implemented the explicit dynamic relaxation feature to gradually introduce gravity to the soil-foundation system prior to the initiation of transient loading. Following this dynamic relaxation or initialization phase, the soil-foundation systems were brought to an appropriate initial state of stress.

Once the dynamic relaxation or initialization stage was completed, the model attained stability, and we proceeded to apply the transient impact load to the computational model of the soil-foundation system. This approach facilitated an effective coupling of static and dynamic forces acting on the soil-light pole foundation system.

9.4 Validation of the Numerical Model

The validation of the computational model entailed comparing the outcomes from its simulations against empirical data obtained from impact tests on a light pole foundation embedded in both compacted and uncompacted sand. The experiments designated test no. AKLP-1 and test no. AKLP-2 were selected for this comparative analysis. For both tests, a 72-

in. long ASTM A992 W6x16 steel post was embedded 36 in. into a 6-ft deep, 30-in. diameter reinforced concrete light pole foundation. The foundation was impacted at a point 25 in. above ground level.

The sand fill around the concrete foundation conformed to the American Association of State Highway and Transportation Officials (AASHTO) Type A-3 soil. In test no. AKLP-1, sand was layered in 8-inch lifts throughout the full depth of the excavation, and each layer was subjected to three rounds of compaction with a piston tamper. In test no. AKLP-2, sand was placed loose around the foundation, with no compaction other than the natural influence of self-weight overburden.

The dynamic impact evaluations were performed using a bogie vehicle fitted with accelerometers and a mountable head, weighing a total of 1,876 pounds, at an impact velocity of 19 mph. High-speed video recording equipment was employed to capture the impact tests, and an accelerometer attached to the central point of gravity on the bogie vehicle frame recorded lateral accelerations during the collision. The time-history of the impact force was computed by multiplying the measured lateral accelerations by the bogie vehicle's mass. The displacement of the post at the point of impact was calculated using the bogie vehicle's speed and integrated accelerations and velocity changes. The energy absorbed by the post and light pole foundation assembly-soil system was ascertained by integrating the area under the force versus displacement curve.

The acquisition of acceleration data from the computational model was critical to permit a direct comparison with the dynamic impact test data. Accordingly, model acceleration data was gathered from a node situated at the bogie vehicle model's center of gravity and processed in an analogous manner to the physical impact test data. Quantitative comparisons focused on the force versus displacement, and energy versus displacement responses, with displacements measured at the point of impact. Qualitative assessments were also undertaken, concentrating on damage and plastic deformation of the light pole foundation system ascertained from the simulated and physical impact tests.

This comparative approach facilitated the evaluation of the accuracy and robustness of the proposed modeling methodology, specifically, the hybrid FEM and ALE method as a practical tool for engineering design and analysis of foundation systems under impact loading. Of greater significance, the stress distribution in the sand during lateral impacts on the light pole foundation was examined. The stress distribution in the soil along the light pole foundation during lateral post impact incidents, utilizing the hybrid FEM and ALE method, was a novel contribution to domain knowledge for soil-embedded articles subject to dynamic loads.

9.4.1 Comparison to Dynamic Bogie Test No. AKLP-1

9.4.1.1 Force vs. Displacement and Energy vs. Displacement Responses

Figures 9.3 and 9.4 present a comparison between the impact force versus displacement and energy versus displacement responses, respectively, as obtained from both the hybrid FEM and ALE numerical analysis and test no. AKLP-1. The post and light pole foundation assembly cross-section, the embedment depth, and other impact variables such as the velocity and mass of the bogie vehicle were kept consistent between test no. AKLP-1 and the numerical model.

As depicted in Figure 9.3, the force versus displacement curves from both the simulated and physical impact tests exhibited similarities in shape and magnitude. A minor discrepancy was noted with the simulated test recording slightly lower impact forces than the experimentally measured values. Despite this, the peak force derived from the simulation correlated well with the peak force from the dynamic test. The simulated peak force was within 8.7% of the experimentally determined peak force.

Furthermore, the energy versus displacement curves for the simulation and the physical impact test demonstrated similar patterns in shape and magnitude. Differences were negligible (less than 5.3%) for the first four-inch bogie displacement following contact. Between 4 and 8 in. of post displacement, the energy absorbed by the post and light pole foundation assembly-soil system in the simulated test was marginally lower than that of the physical impact test. However, the total absorbed energies were similar, with the simulation's total energy deviating by only 2.1% compared to the dynamic impact test's total energy.

Considering that simulated dynamic impact results within 20% of test results are generally accepted as reasonable [65], these outcomes can be considered satisfactory according to the accepted standards in this field of research and testing. The favorable outcome for this particular test was expected, as the peak force and accumulated energy were primarily dictated by plastic deformation of the embedded steel post.

The soil modeling resulted in a slight overprediction of the peak displacement during unloading, but ultimately predicted the final position of the foundation at rest with negligible error.

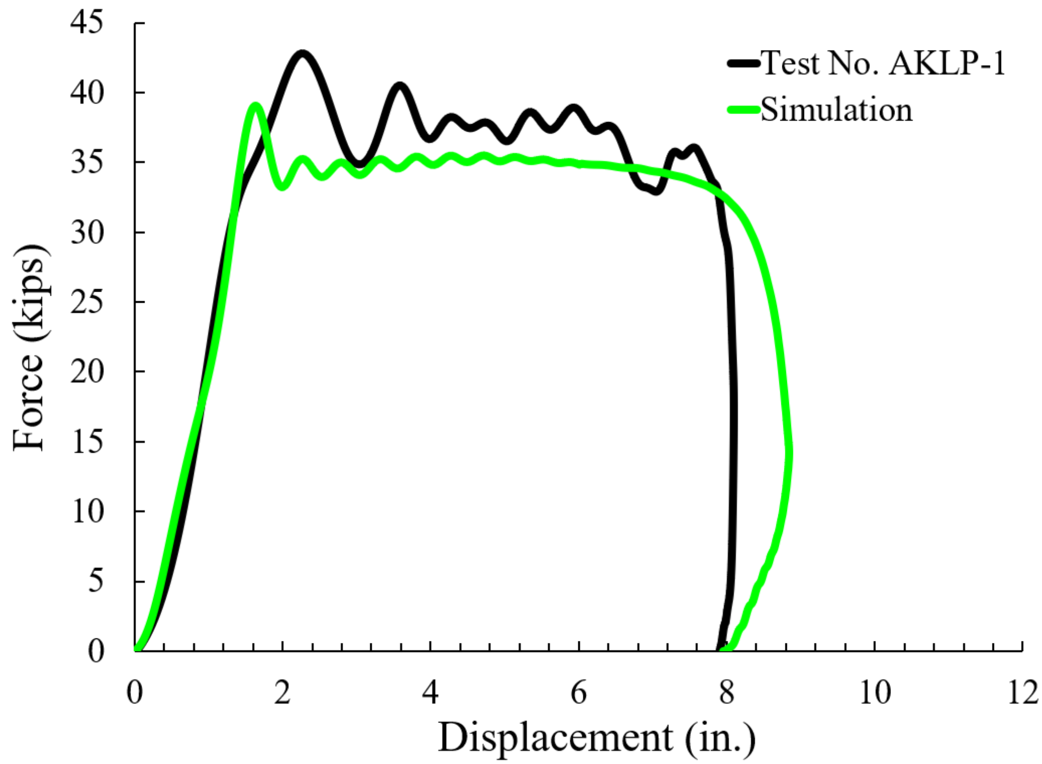

Figure 9.3 Comparison Force vs. Displacement Response of Simulated and Test No. AKLP-1 Results

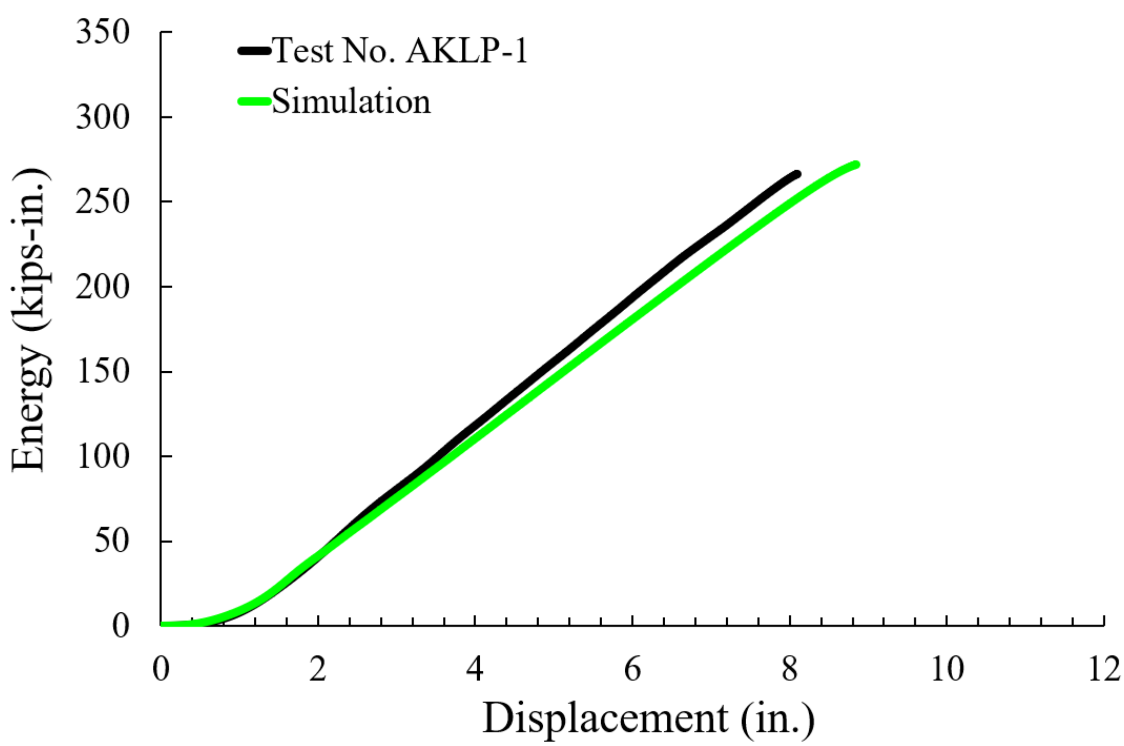

Figure 9.4 Comparison of Energy vs. Displacement Plots from Simulated and Test No. AKLP-1 Results

9.4.1.2 Foundation Displacement

A comparative analysis of the lateral displacement at the top of the reinforced concrete foundation was performed, as obtained from a linear displacement transducer, otherwise known as a string potentiometer, in test no. AKLP-1. Time was referenced to the initiation of foundation motion, which was slightly delayed from bogie contact on the steel post, as transmitted forces needed to achieve sufficient momentum transfer to overcome foundation inertia. This analysis was compared with the hybrid FEM+ALE simulation result, as illustrated in Figure 9.5.

The general shape of the response curve is similar for simulated and physical test results, although the simulation appears to predict more rapid foundation movement than was recorded in the physical test. It is important to note that the simulated results are tracking the motion of a particular node in the model, whereas the physical test data represent recorded rotation of a wire spool at a string potentiometer. Although the string potentiometer was a high-tension model intended for use during dynamic testing, the placement of the sensor on the opposite side of the test article from the impact side may have resulted in slack in the wire during the impact event, and so may not have perfectly measured the velocity of the test article.

The simulation slightly overpredicted peak displacement and underpredicted post-peak displacements and permanent set. The test recorded a peak displacement of 1.55 in., whereas the simulation predicted a peak displacement of 1.62 in., a difference of +4.52%. The plot in Figure 9.5 is truncated at the end of the simulation, but additional data for physical test displacement was recorded beyond that shown. The test displacement ultimately settled at 0.91 in., while the simulation predicted a permanent set of 0.73 in., a difference of -19.78%. The simulated permanent set displacement was underpredicted. However, it was believed that potential errors arising from displacement transducer vibrations during the impact event could contribute to this discrepancy.

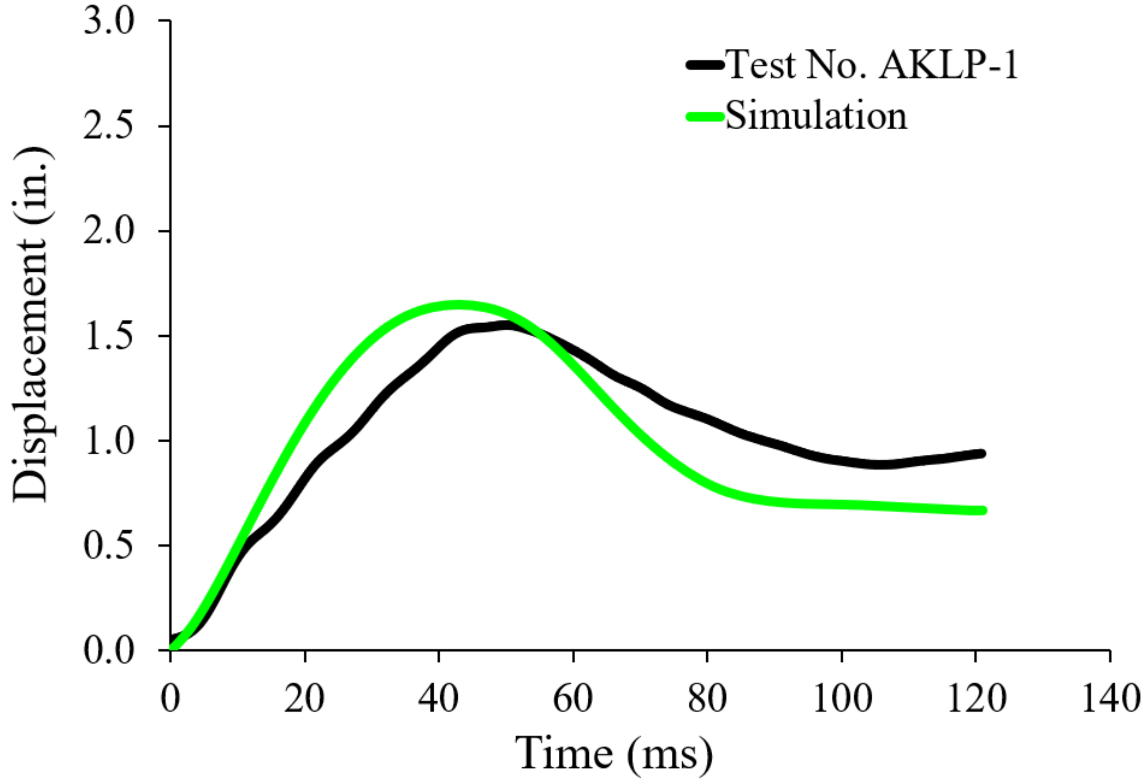

Figure 9.5 Foundation Lateral Displacement Comparison Between Simulated Test and Test No. AKLP-1

9.4.1.3 Qualitative Comparisons

The qualitative analysis focused on the deformation patterns of the light pole foundation during the bogie vehicle's impact and the damage observed post test no. AKLP-1. High-speed video footage was compared with simulation images for comparison. As illustrated in Figure 9.5, the computational model was found to offer a qualitatively accurate prediction of the global behavior. When the final deformed shape of the post and foundation assembly was compared with the model's predictions, similarities were noted in terms of damage and localized plastic deformations.

As shown in Figure 9.6, the inertial resistance generated by the light pole foundation-soil system during the lateral impact event surpassed the post's yield capacity. As depicted in Figure

9.7, a plastic hinge formed due to the bogie impact. Therefore, the lateral impact force resistance of the light pole foundation embedded in compacted sand was primarily governed by the mechanical properties of the post.

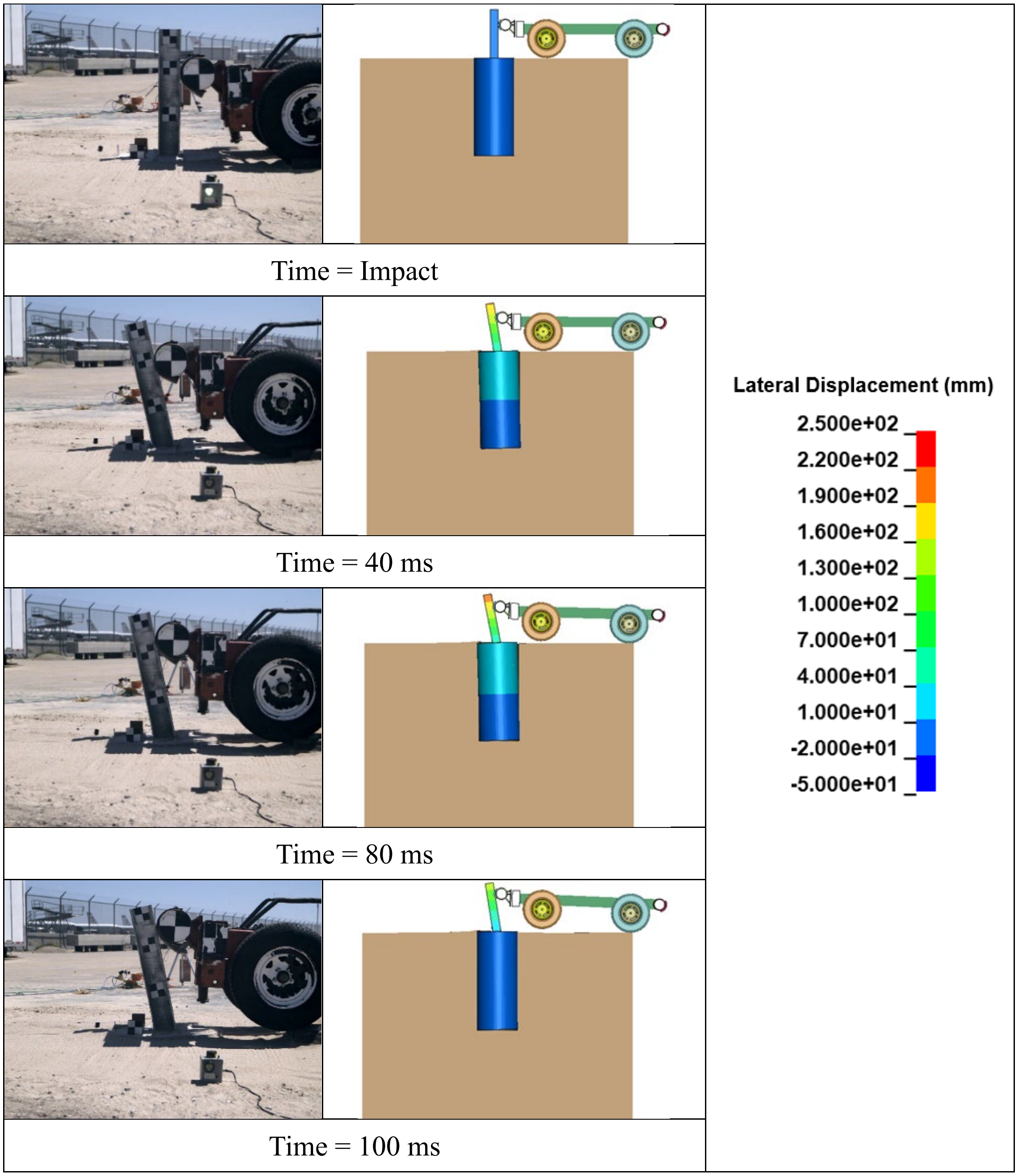

Figure 9.6 Comparison of Time Sequential Images Between Dynamic Impact Test (i.e., test no. AKLP-1) and Simulated Impact Test Using the Hybrid FEM+ALE Method for a Post and Light Pole Foundation Assembly Embedded in Compacted Sand

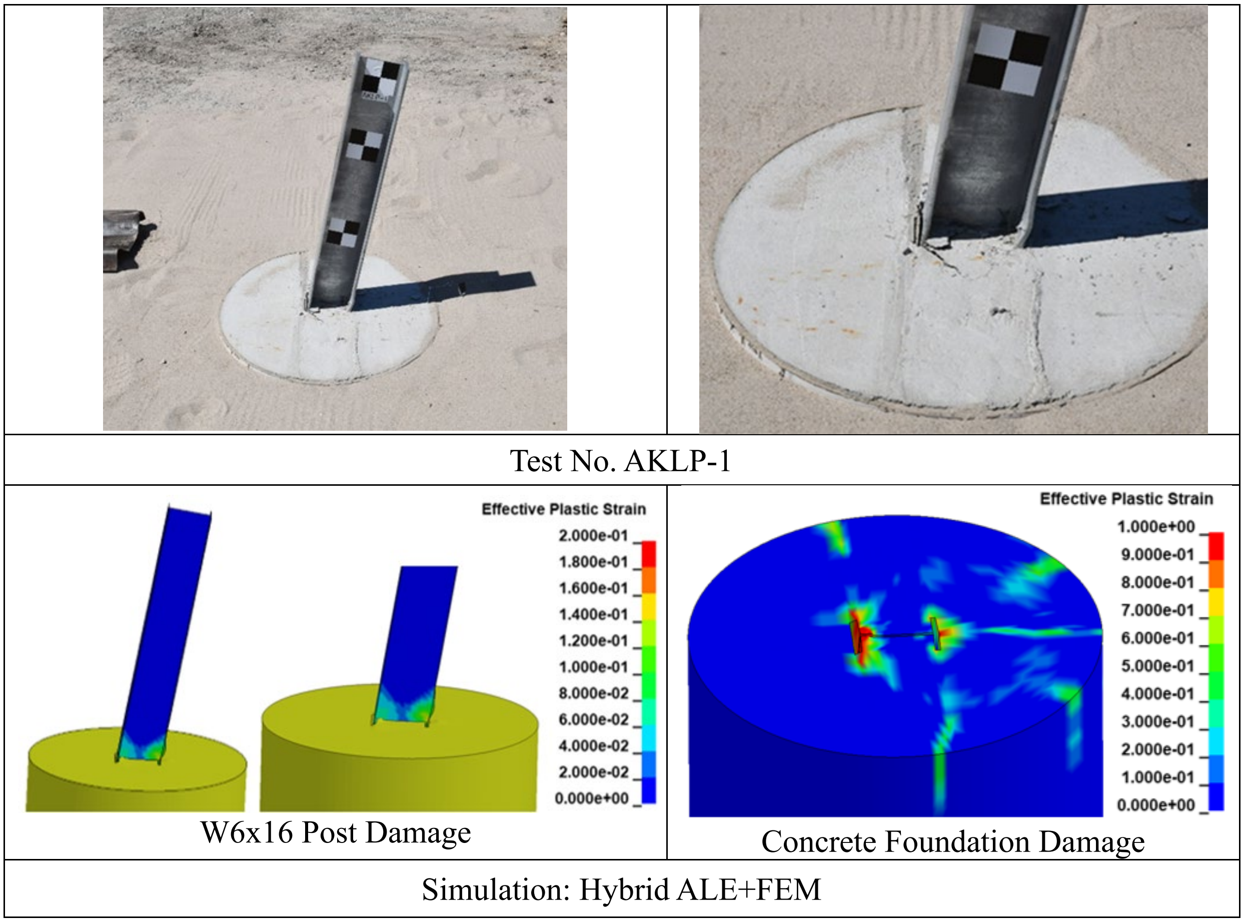

Figure 9.7 Post-Impact Photographs of Post and Light Pole Foundation Assembly Simulation Using Hybrid FEM+ALE Method and Test No. AKLP-1

9.4.1.4 Soil Response during Lateral Impact

Figure 9.8 reveals that the soil's compressive and shear resistance exceeded the post section's yield moment. Consequently, the lateral impact capacity of the light pole foundation system, embedded in compacted sand, was primarily dictated by the post's properties rather than soil behavior. As demonstrated in Figure 9.7, the formation of a plastic hinge further suggests that the impact resistance of the light pole foundation-soil system is dependent on the post's dynamic yield moment. This yield moment is typically achieved prior to full mobilization of dynamic soil resistance.

The von Mises stress contours within the soil at various time points, as illustrated in Figure 9.8, indicate that soil plastic deformation predominantly occurs near the ground surface. Additional plastic deformation was observed at the base of the light pole foundation, correlating with slight rotations of the light pole foundation within the compacted sand. This suggests that the soil below provides substantial impact resistance, inhibiting any substantial rotation of the light pole foundation. Despite the deformation of the upper W6x16 post, as shown in Figure 9.8, the light pole foundation remained vertical.

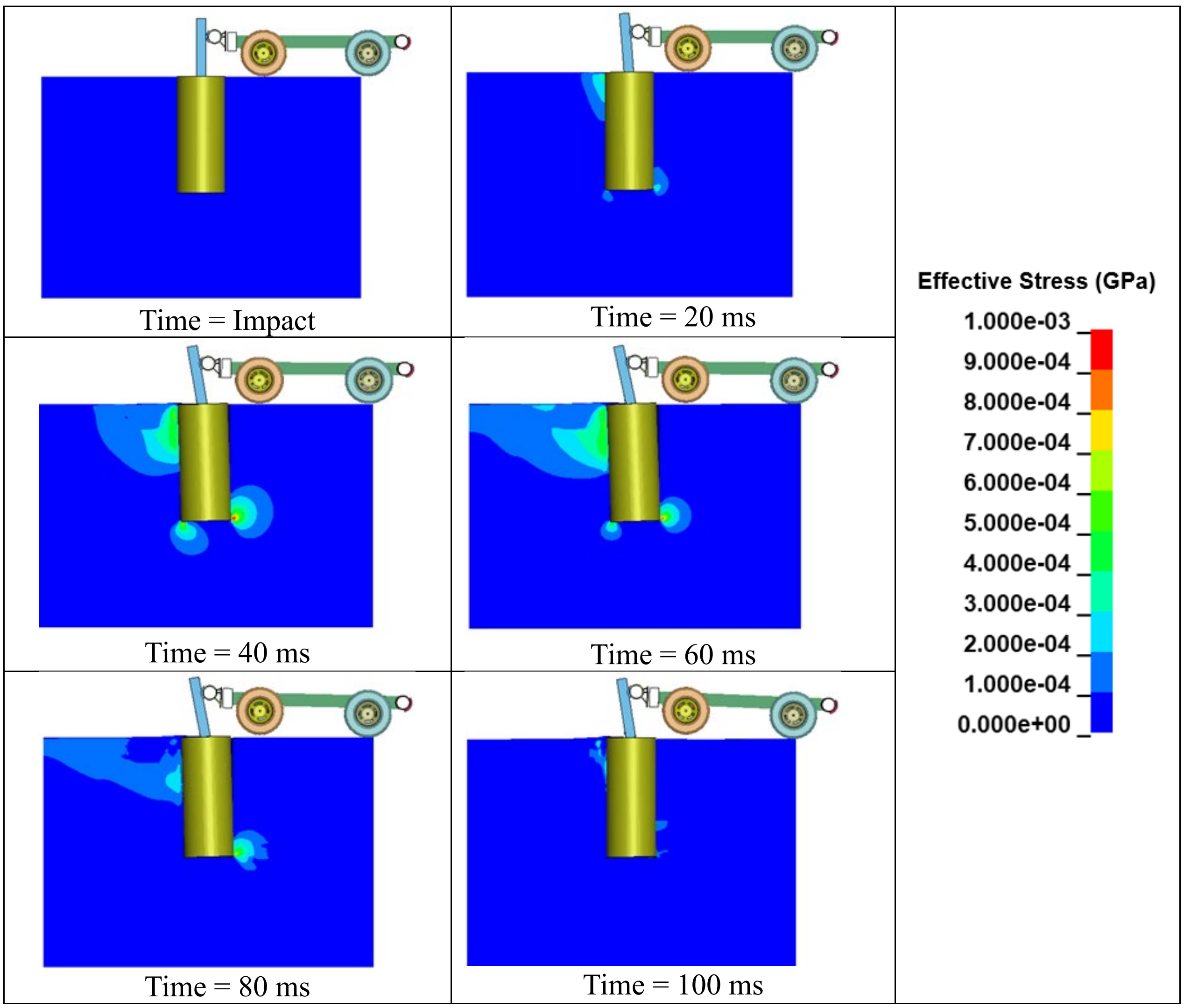

Figure 9.8 Von Mises Stress Distribution Within Compacted Sand/Soil in Laterally Impacted Post and Light pole Foundation Assembly in Compacted Sand

9.4.2 Comparison to Dynamic Bogie Test No. AKLP-2

9.4.2.1 Force vs. Displacement and Energy vs. Displacement Responses

Figures 9.9 and 9.10 present a comparison between the impact force versus displacement and energy versus displacement responses, respectively, as obtained from both the Hybrid ALE+FEM numerical analysis and test no. AKLP-2, which was conducted with loose, non-compacted sand fill surrounding the concrete foundation. As depicted in Figure 9.9, the force versus displacement curves from both the simulated and physical impact tests exhibited similarities in shape and magnitude through a total bogie post-impact displacement of more than 20 in., despite large rotation of the foundation through the soil. The simulated force results were within 10% of the experimentally determined forces for a significant portion of the performance range. The largest relative discrepancies between simulated and physical test results occurred when approaching the maximum displacement, in the range of 23 to 25 in. The root cause of this minor discrepancy remains unclear due to the dynamic complexity of the impact process, but the discrepancy itself is insignificant with respect to the modeling objectives focused on peak forces and primary energy dissipation that occurred in the range of 0 to 7 in.

Figure 9.10 demonstrates that the energy versus displacement response predicted by the computational model exhibited excellent accuracy both in shape and magnitude. The maximum relative error was 5.6% and occurred in the range of approximately 7 to 12 in. of bogie displacement. The computational model thus successfully represented the experimentally observed responses in terms of both force and energy with respect to displacement, for a post and light pole foundation assembly embedded in loose, uncompacted sandy soil. Modeling accuracy was demonstrated despite large soil displacement with SPT values approximately 5 or less. The discrepancies between the simulation and the physical impact test data fell well within the expected variation range observed across similar post-soil impact tests.

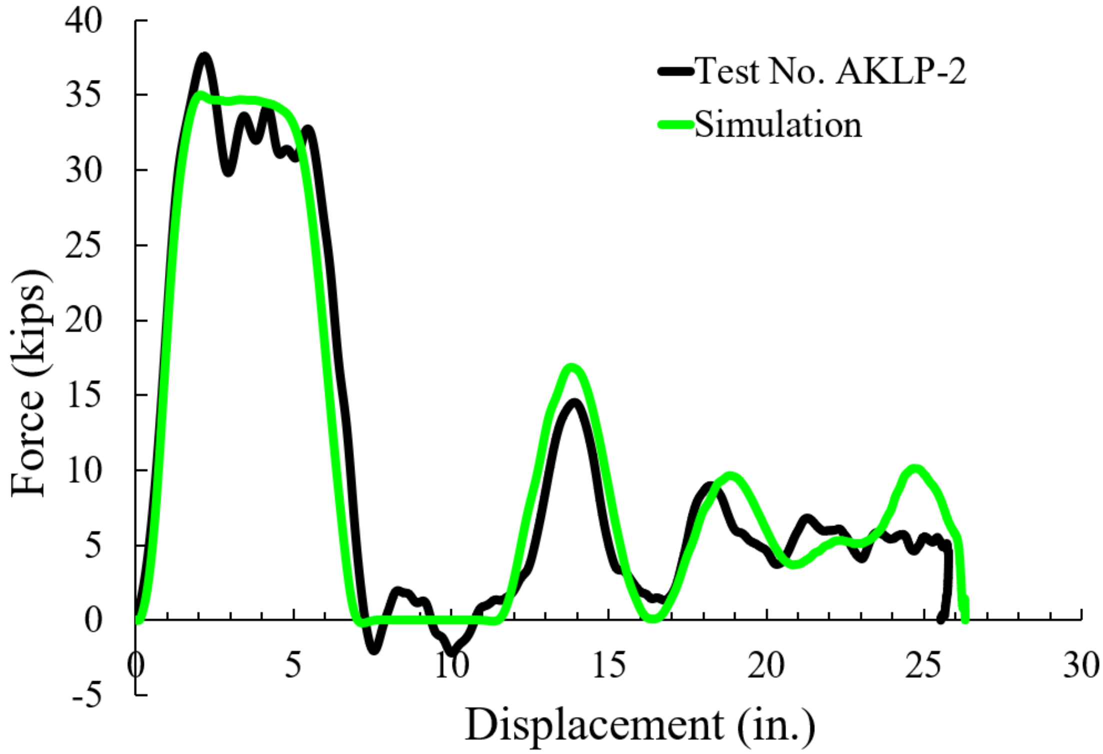

Figure 9.9 Comparison Force vs. Displacement Response of Simulated and Test No. AKLP-2 Results

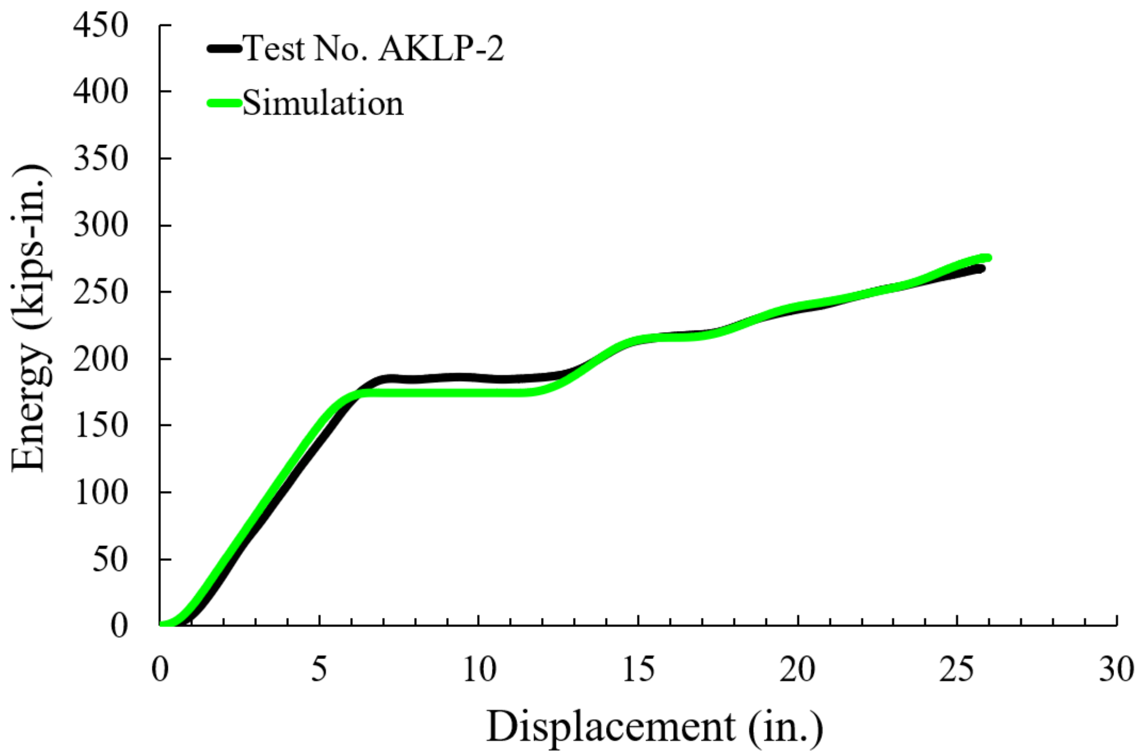

Figure 9.10 Comparison of Energy vs. Displacement Plots from Simulated and Test No. AKLP-2 Results

9.4.2.2 Comparative Analysis of Foundation Displacement

Similar to Section 9.4.1.2, a comparative analysis of the lateral displacement at the top of the reinforced concrete foundation was performed, as obtained from a linear displacement transducer, otherwise known as a string potentiometer, in test no. AKLP-2. Time was referenced to the initiation of foundation motion, which was slightly delayed from bogie contact on the steel post, as transmitted forces needed to achieve sufficient momentum transfer to overcome foundation inertia. This analysis was compared with the hybrid FEM+ALE simulation result, as illustrated in Figure 9.12.

The analysis considered only the initial 60 ms of the impact event, as the potentiometer string (physically a metal wire) became fully immersed in displaced sand as a direct result of the impact event. This immersion raised concerns regarding the accuracy and reliability of displacement data beyond this timeframe. The results demonstrate a significant level of agreement between the two distinct data sets, with a maximum error of 16.21%. Furthermore, quantitative discrepancies do not necessarily indicate errors in the simulation, as the physical test data may be influenced by slackening of the potentiometer string during retraction.

Impact

0.050 sec

Figure 9.11 Test No. AKLP-2 Photos at Beginning and End of Simulation Displacement Comparison

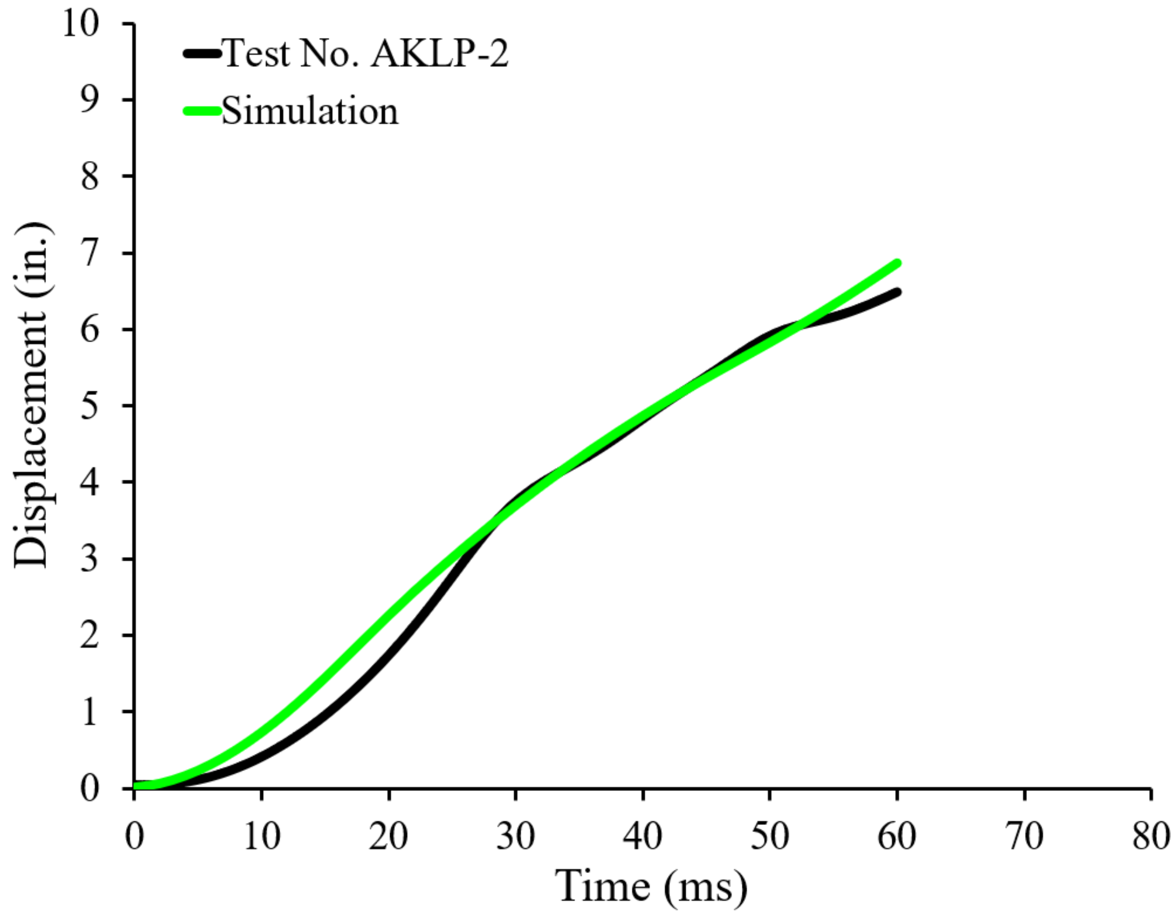

Figure 9.12 Foundation Lateral Displacement Comparison Between Simulated Test and Test No. AKLP-2

9.4.2.3 Qualitative comparisons

Figures 9.13 and 9.14 illustrate the lateral impact response of the post and foundation assembly-soil system. These figures provide a comparative analysis, comparing simulation sequential and post displacement contours with high-speed video footage obtained from the physical test no. AKLP-2. The presented data show that the numerical model was qualitatively able to predict the global impact behavior of the post and foundation assembly-soil system. The simulation accurately reflects both the formation of plastic hinging in the steel post prior to significant foundation movement, and also the induced soil wave and foundation movement at the top of the soil following momentum transfer from the bogie.

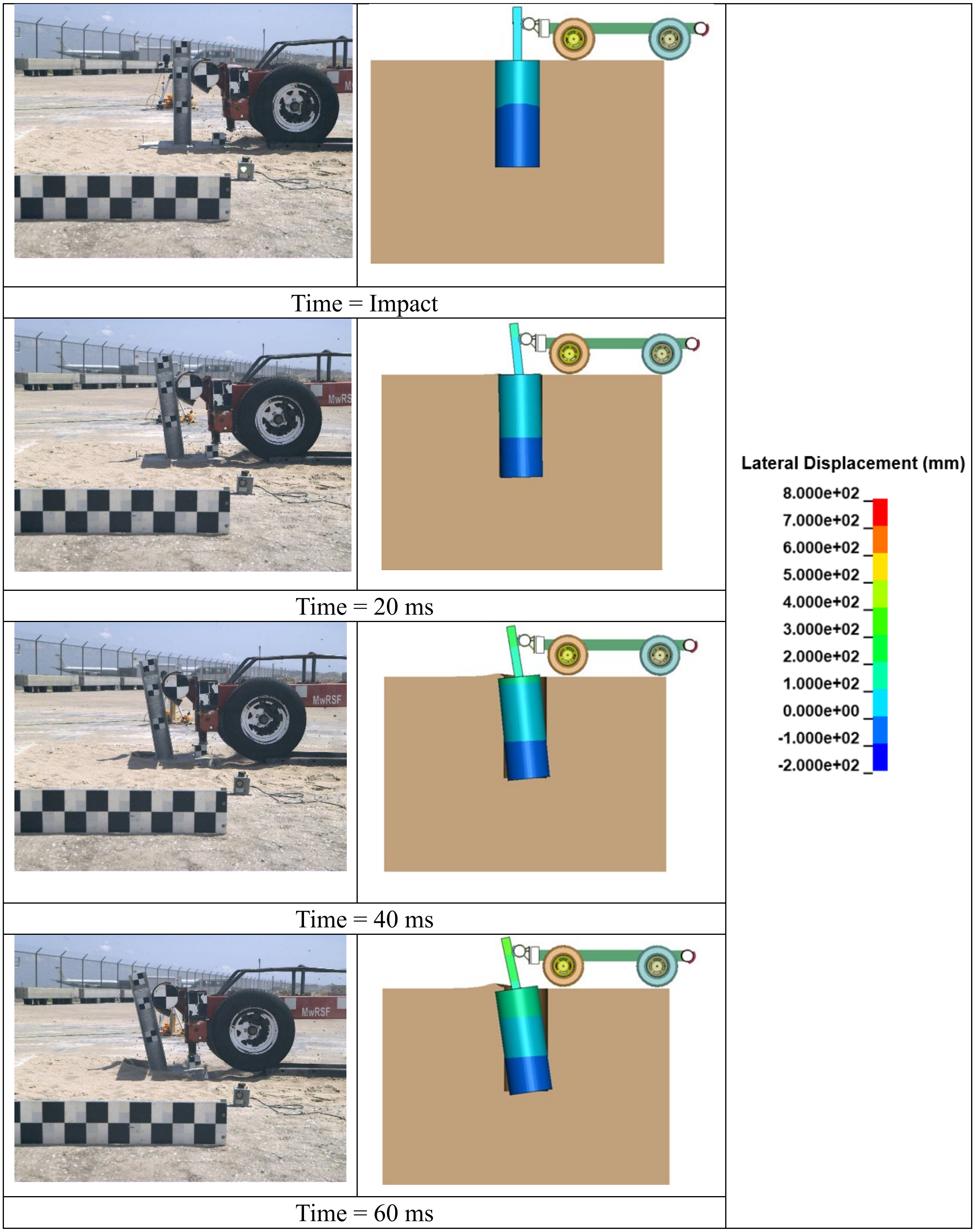

Figure 9.13 Comparison of Time Sequential Images Between Dynamic Impact Test (i.e., Test No. AKLP-2) and Simulated Impact Test Using the Hybrid FEM+ALE Method for a Post and Light pole Foundation Assembly Embedded in Loose, Uncompacted Sand

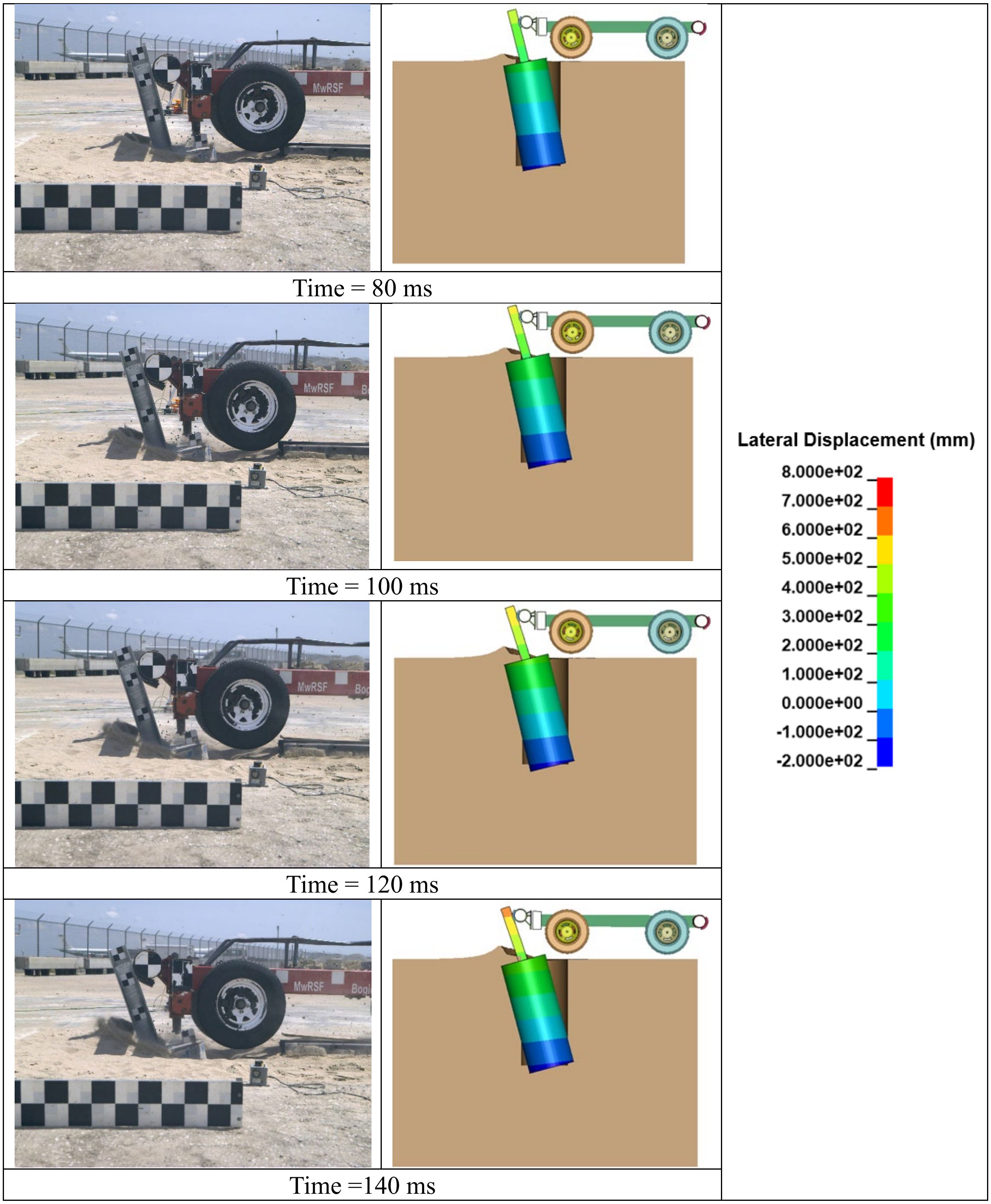

Figure 9.14 Comparison of Time Sequential Images Between Dynamic Impact Test (i.e., Test No. AKLP-2) and Simulated Impact Test Using the Hybrid FEM+ALE Method for a Post and Light pole Foundation Assembly Embedded in Loose, Uncompacted Sand

Figure 9.15 presents the post-impact condition of the post and foundation assembly, acquired from both the physical impact test and the hybrid FEM+ALE method simulation. The images confirm that plastic hinging occurred in both the physical test and simulation, despite extreme soil deformations due to loose, uncompacted soil.

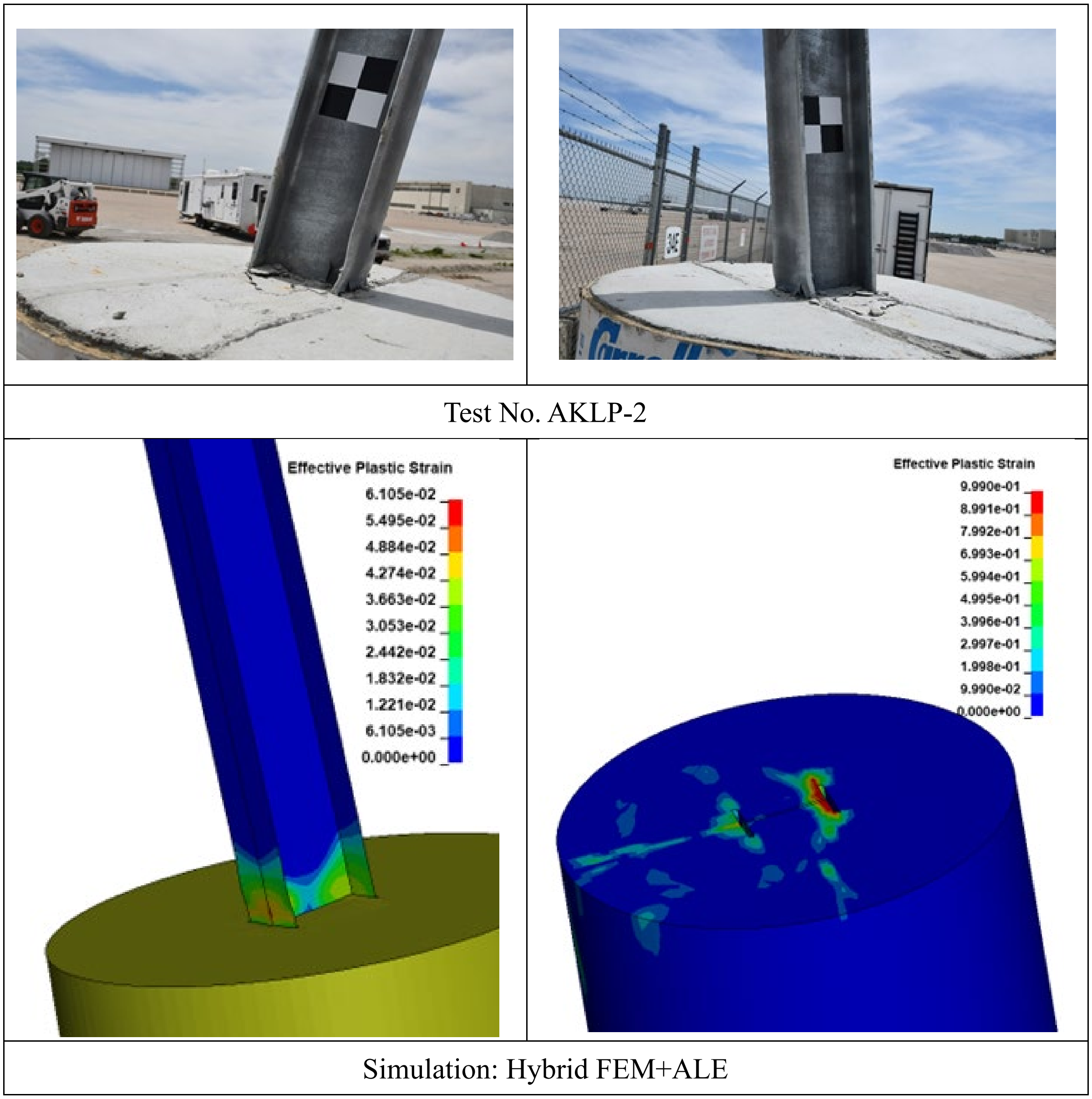

Figure 9.15 Post-Impact Photographs of Post and Light pole Foundation Assembly Simulation Using Hybrid FEM+ALE Method and Test No. AKLP-2

9.4.2.4 Soil Response to Lateral Impact on Post and Foundation Assembly

Figure 9.16 provides a visual representation of the von Mises stress distribution within the soil. This illustration elucidates the particular geometry of the post and foundation assembly rotation, which necessitates the largest deflection at both the ground line and the base of the reinforced concrete foundation. Consequentially, this prompts observable plastic soil deformation in the vicinity of the ground line and the foundation base. The evolution of von Mises stress within the soil, depicted in Figure 9.16, further illuminates these observations.

Despite the soil strength parameters – such as internal friction angle and cohesion – being assumed as constants with respect to depth, it is noteworthy that dynamic soil resistance exhibits an increasing trend with depth. Additionally, the soil resistance exhibits a shear component acting at the foundation base. This shear-induced von Mises stress is markedly pronounced at the foundation base and remains salient throughout the majority of the impact event, as evident in Figure 9.16. This finding underlines the significance of the shear component at the foundation base for light pole foundation systems embedded in extremely weak soil conditions, suggesting its necessary incorporation in future analytical studies of laterally impacted light pole foundations embedded in weak soil.

As shown in Figure 9.16, the rotation resistance of the post and foundation assembly is solely dictated by the strength and stiffness properties of the soil adjacent to the embedded portion of the foundation. This adjacent soil essentially governs the behavior of post and foundation assemblies embedded in loose, non-compacted sand. The impact performance and behavior of these assemblies are predominantly contingent on the lateral dynamic soil resistance.

Soil failure is occurred when the ultimate lateral dynamic resistance of the soil along the length of the foundation is surpassed, as depicted in Figure 9.16. This leads to the post and foundation assembly rotating around a rotation point, thereby creating dynamic soil resistance in front of the foundation below the pivot point, and behind the foundation above the rotation point. This process culminates in the failure of the post and foundation assembly by rotation, once the dynamic impact resistance of the soil above and below the rotation point is exceeded.

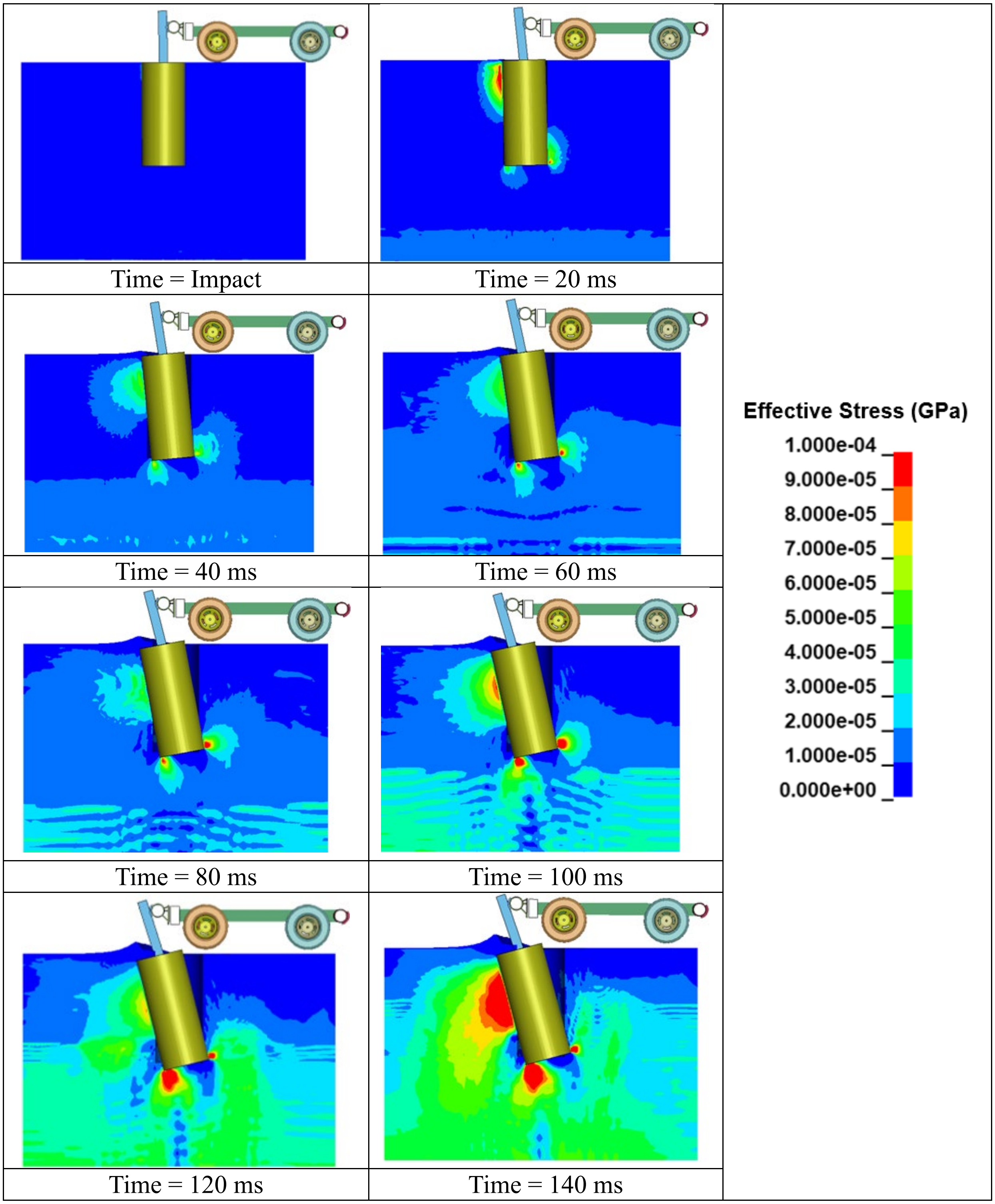

Figure 9.16 Von Mises Stress Distribution Within Compacted Sand Soil in Laterally Impacted Light pole Foundation in Loose, Uncompacted Sand

9.5 ALE Mesh Density Study

9.5.1 Methodology

This study evaluated the influence of mesh sizes on the dynamic interaction between post and light pole foundation assemblies and soil when subjected to impact loading, using test no. AKLP-2 as a reference case to represent extremely loose soil conditions. More specifically, the study examined the implications of ALE soil mesh density surrounding the light pole foundation, representing the large deformation region, during lateral vehicular impacts. To our current knowledge, no previous research has been conducted to explore the effects of ALE soil mesh density on the simulation outcomes concerning dynamic impact soil-structure interaction.

The primary goal was to illuminate the role of ALE soil mesh density on the dynamic performance and behaviors of the post and light pole foundation assembly-soil system, with a focus on resistive force versus displacement and energy versus displacement responses. To analyze the effect of mesh density, soil mesh size was varied while maintaining constant soil, post, and light pole foundation constitutive laws, input parameters, and soil domain size. The broader aim was to establish guidelines for appropriate soil mesh sizes for use in LS-DYNA hybrid FEM+ALE foundation-soil impact simulations, significantly contributing to existing knowledge and practice in this field.

Five distinct ALE models were configured, each characterized by varying soil mesh sizes: (1) 15 mm (0.6 in.); (2) 20 mm (0.8 in.); (3) 25 mm (1 in.); (4) 50 mm (2 in.); and (5) 100 mm (4 in.). These models are illustrated in Figures 9.17 through 9.21. The study focused on a laterally impacted post and light pole foundation assembly embedded within loose, non-compacted sand. Particular attention was paid to the large deformation soil zone (near-field soil domain) surrounding the light pole foundation, a decision driven by observations from physical impact test no. AKLP-2.

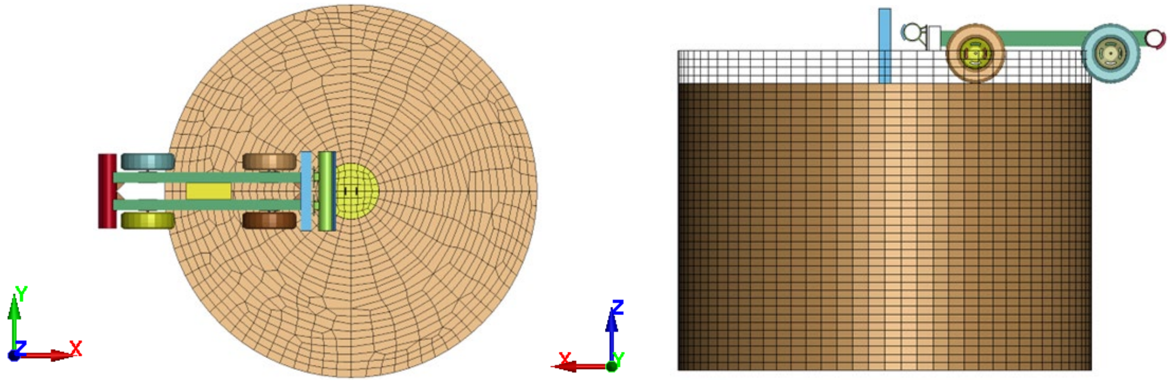

Figure 9.17 Representation of the 100 mm ALE Mesh Size

This figure illustrates the domain where the ALE mesh size varies from 100 mm to 335 mm in the circumferential direction, and 100 mm to 115 mm in the radial direction. Throughout the Z-direction, the mesh size remains consistently at 100 mm. This domain, defined by these mesh sizes, is designated as the 100 mm mesh size domain.

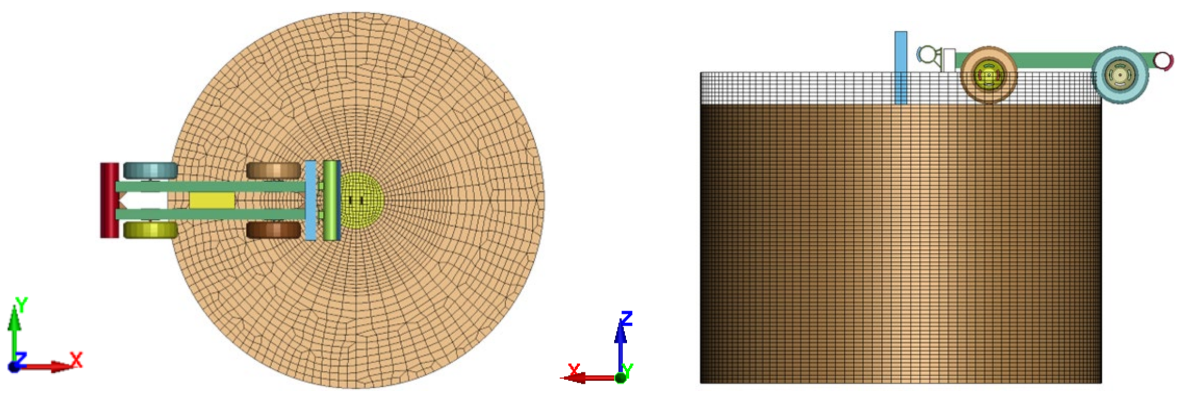

Figure 9.18 Depiction of the 50 mm ALE Mesh Domain

This figure displays the region where the ALE mesh size extends from 50 mm to 170 mm in the circumferential direction and from 50 mm to 58 mm in the radial direction. In the Z-direction, a consistent mesh size of 100 mm is maintained. This region, delineated by these mesh dimensions, is termed as the 50 mm mesh size domain.

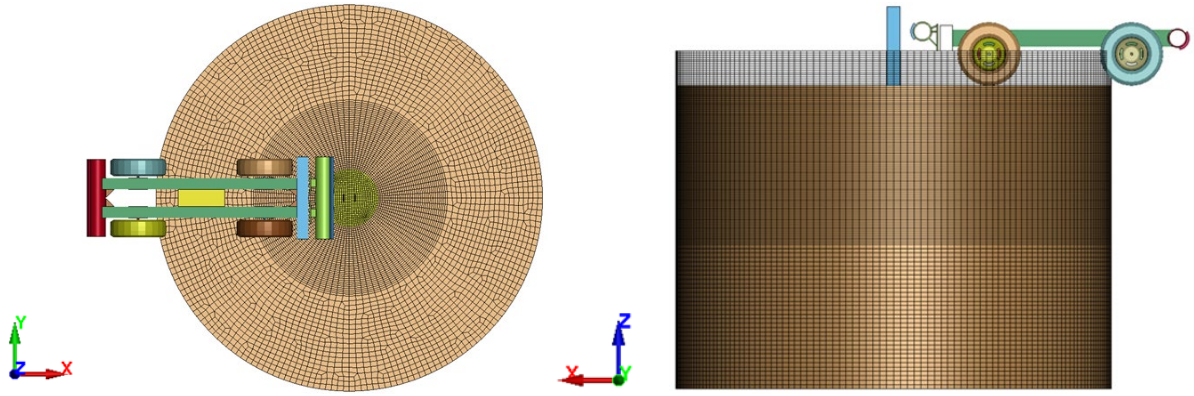

Figure 9.19 Illustration of the 25 mm ALE Mesh Domain

The figure delineates a domain in which the ALE mesh size ranges from 25 mm to 85 mm in the radial direction, while maintaining a consistent size of 25 mm in both the circumferential and Z-directions. This defined area, characterized by these particular mesh dimensions, is identified as the 25 mm mesh size domain.

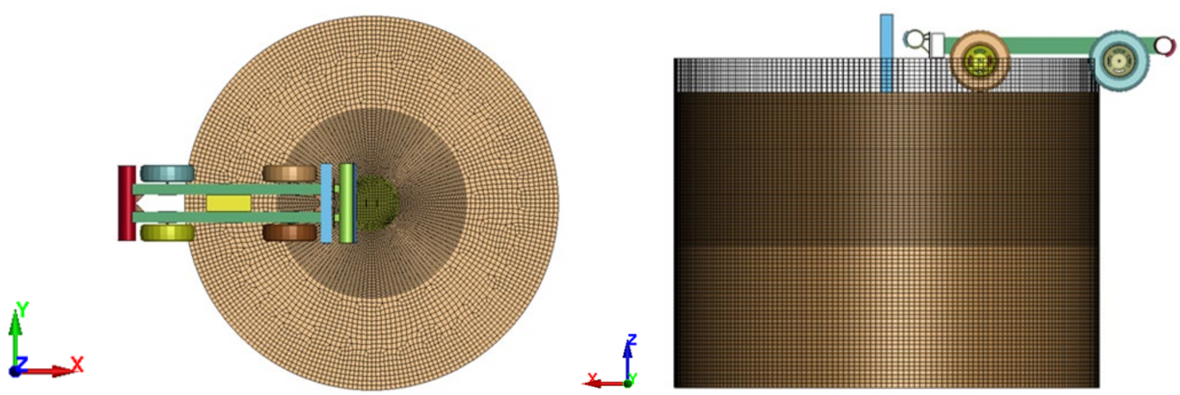

Figure 9.20 Description of the 20 mm ALE Mesh Domain

The figure presents a domain where the ALE mesh size extends from 20 mm to 65 mm in the radial direction, while remaining uniform at 20 mm in both the circumferential and Z-directions. This specifically outlined region, defined by these mesh sizes, is recognized as the 20 mm mesh size domain.

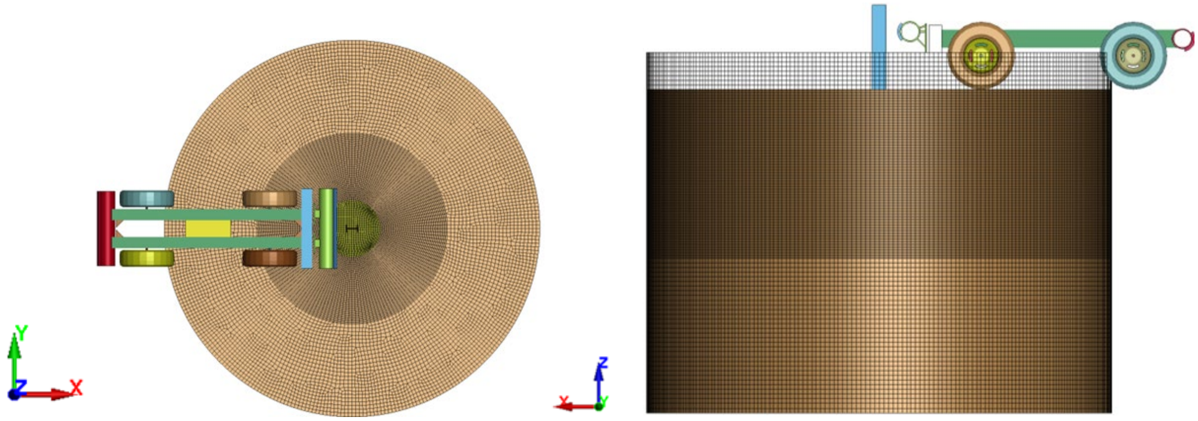

Figure 9.21 Representation of the 15 mm ALE Mesh Domain

The figure illustrates a domain where the ALE mesh size ranges from 15 mm to 50 mm in the radial direction, while maintaining a consistent size of 15 mm in the circumferential and Z-directions. This region, demarcated by these specific mesh dimensions, is designated as the 15 mm mesh size domain.

9.5.2 Results and Discussion

The effect of soil mesh size was investigated by observing the sensitivities of predicted forces versus bogie displacement at the point of impact, as well as the correlation between predicted energy dissipated and bogie displacement. Figures 9.22 and 9.23 present a comparison between force versus displacement and energy versus displacement curves derived from five distinct hybrid FEM+ALE soil-foundation system models, and those obtained from test no. AKLP-2. Simulation results were practically identical among mesh refinement options for displacements up to approximately 11 in. At larger displacements, force response progressively drifted farther from the physical test results with increasing mesh resolution. Thus, the optimal resolution among those considered was the coarsest option in terms of force versus displacement response.

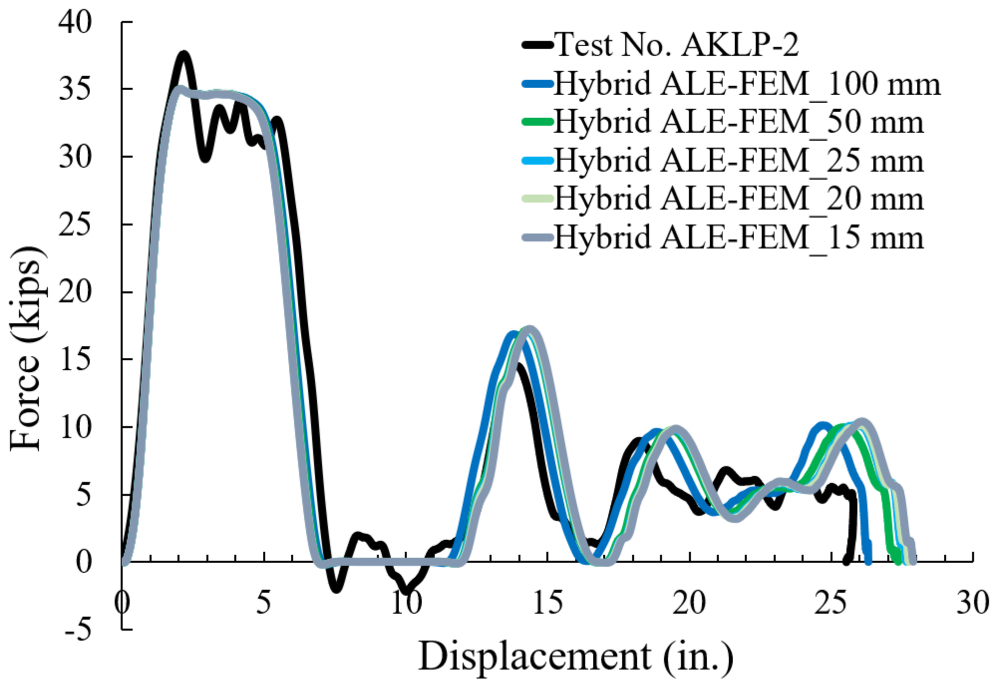

Figure 9.22 Comparison of Force vs. Displacement Curves Between Simulated Test for Various ALE Soil Mesh Sizes and Physical Impact Test Result

Similarly, Figure 9.23 illustrates that the energy versus displacement responses displayed essentially no sensitivity to mesh refinement among the considered cases. The maximum percent differences relative to the baseline physical test data were 3.6%, 6.9%, 7.9%, 8.1%, 8.2% for meh sizes of 100 mm, 50 mm, 25 mm, 20 mm, and 15 mm, respectively, occurring within the displacement range of 6 to 13 inches.

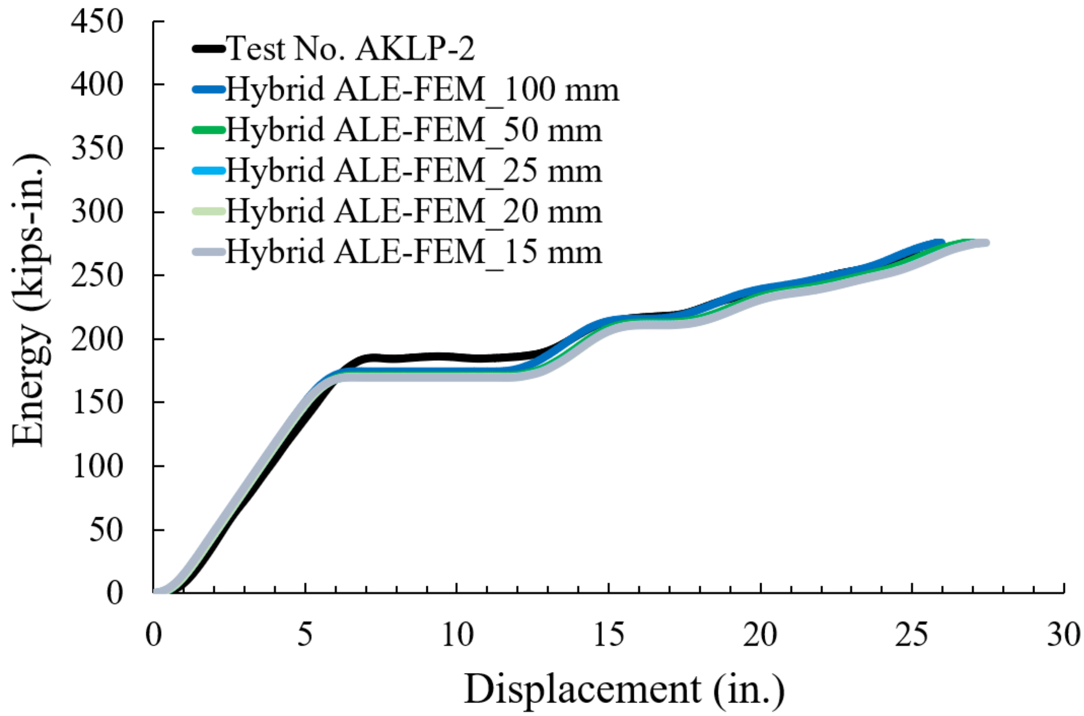

Figure 9.23 Comparison of Energy vs. Displacement Curves Between Simulated Test for Various ALE Soil Mesh Sizes and Physical Impact Test Result

A computational efficiency analysis was conducted on the aforementioned post and light pole foundation assembly-soil systems, each featuring different soil mesh sizes. The researchers posit that this performance analysis, combined with the mesh sensitivity studies discussed earlier, equips roadside safety researchers and engineers with the insights necessary to strike a balance in selecting an optimum mesh size for precise and efficient hybrid FEM+ALE soil-foundation impact simulations.

All simulations in this study were conducted utilizing the MMP LS-DYNA hydrocode, version R13.1.0, on the University of Nebraska's Crane supercomputer cluster, equipped with Intel Xeon E5-2670 2.6GHz processors and utilizing 32 cores per simulation. Figure 9.24 depicts the CPU execution time for the post and light pole foundation assembly-soil impact simulation, varying the ALE mesh sizes.

Figure 9.24 shows that, as anticipated, the hybrid FEM+ALE method computational time demand increased significantly with the number of elements or finer spatial discretization. Computational time ratios between different mesh sizes were: 15 mm (0.6 in.) and 20 mm (0.8 in.) at 1.65, 20 mm (0.8 in.) and 25 mm (1.0 in.) at 1.40, 25 mm (1.0 in.) and 50 mm (2.0 in.) at 1.24, and 50 mm (2.0 in.) and 100 mm (4 in.) at 1.52, respectively. These ratios provide practical insights into the performance trade-offs associated with different mesh sizes.

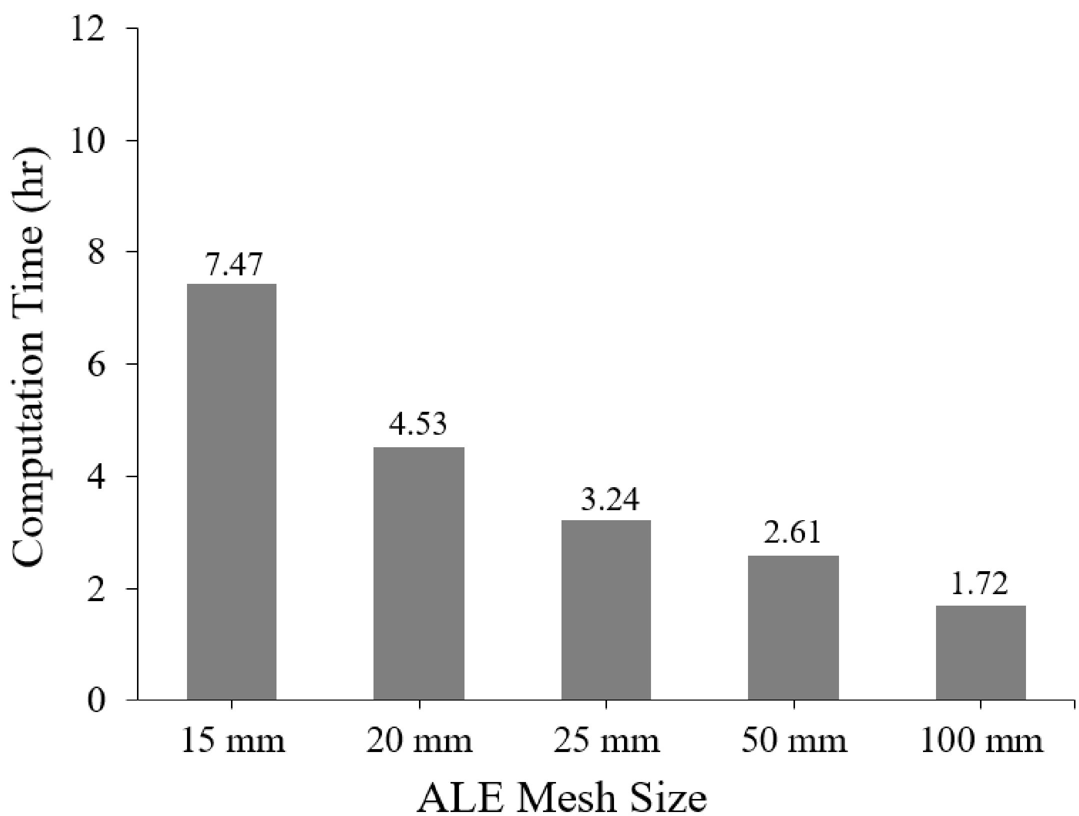

Figure 9.24 Performance Comparison of ALE Post-Soil Impact Simulation using 32 Cores Per Simulation

Chapter 10 Numerical Simulation of Light Pole-Foundation Systems

10.1 Introduction

Models were developed to simulate the bogie tests impacting steel light poles mounted to concrete foundations in loose soils with Transpo couplings. Validating models with respect to observed test behaviors facilitates extended modeling efforts with full-scale vehicle impacts.

10.2 Light pole System LS-DYNA Model

Models were developed and results compared to physical test data from test nos. AKLP-5 and AKLP-6. The modeling effort investigated the hybrid FEM+ALE method's capability to capture results from these breakaway tests and develop models which could provide preliminary predictions for MASH full-scale crash test outcomes. Both models included a 35.5-ft high light pole, frangible couplings, and a concrete foundation embedded in uncompacted sand, consistent with the bogie crash test articles. The comparisons of simulated to physical test results included force versus time histories, impulse versus time histories, damage, and displacement of the top of the reinforced concrete foundation.

10.2.1 System Geometry and Element Formulation

The modeled light pole system was composed of a light pole, a 20-ft long mast arm, a coupling base, a 6-ft deep reinforced concrete (RC) foundation, soil domain, and an air volume. A visual representation of these computer models can be found in Figure 10.1.

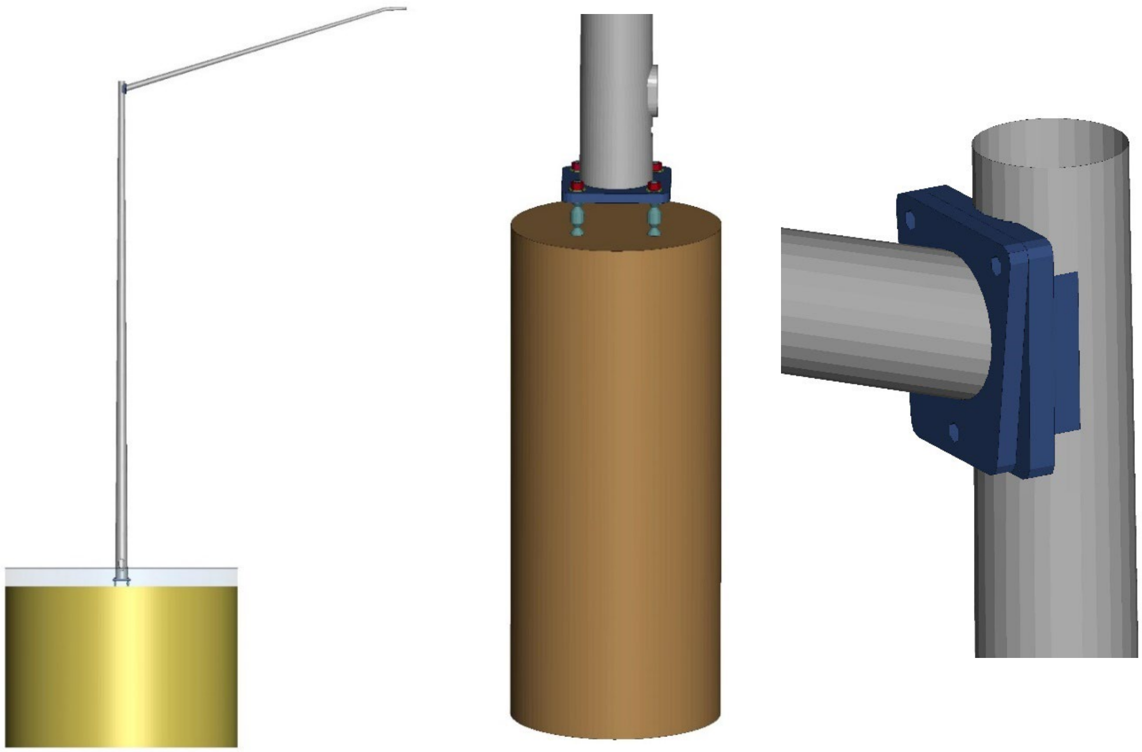

(a) (b) (c)
Figure 10.1 Computer Models for Light pole Systems: (a) Light pole System; (b) RC Foundation; (c) Mast Arm-to-Pole Connection

The light pole system was anchored by a 2.5-ft diameter reinforced concrete (RC) foundation, embedded in sand, with a depth of 6 ft. The concrete foundation was reinforced with eight #8 longitudinal steel reinforcing bars and #5 circular hoops at 6-in. intervals. Steel reinforcement was ASTM A615 steel, with a minimum yield strength of 60 ksi. Concrete strength was set at 4 ksi, per material specifications. Concrete was modeled using eight-node solid elements, while the steel reinforcement was simulated employing two-node, Hughes-Liu beam elements. The interaction between the reinforcements and the enveloping concrete was simulated using the Constrained Beam in the Solid option in LS-DYNA.

In order to simulate the large deformation and dynamics of the soil-foundation system during vehicle impact, the hybrid FEM+ALE approach was used. The model also included a 16.5-ft soil domain constructed to replicate the interactions between the soil and the RC foundation, with a soil depth of 11.5 ft. An air volume with a depth of 1.5 ft was placed above the soil domain. The soil and air were simulated using one-node, ALE multi-material, solid elements. The hourglass coefficient for the ALE solid element was set to 1×10^{-6}, in line with the LS-DYNA manual and precedent studies. Table 10.1 details the simulation model parts and corresponding LS-DYNA modeling parameters.

Table 10.1 List of Simulation Model Parts and LS-DYNA Parameters

Part Name	**Element Type**	**Element Formulation**	**Material Type**	**Material Formulation**
Light pole	Shell	Belytschko-Tsay	ASTM A595 Grade A	Piecewise Linear Plasticity
Mast arm	Shell	Belytschko-Tsay	ASTM A595 Grade A	Piecewise Linear Plasticity
Light pole base plate	Solid	Constant stress	ASTM A709	Piecewise Linear Plasticity
Hex nut	Solid	Constant stress	ASTM A563 Grade DH	Rigid
Flat washer	Solid	Constant stress	ASTM A153	Rigid
Double-neck light pole-safe coupling	Solid	Constant stress	ASTM A449 (approximate)	Piecewise Linear Plasticity
Mounting plate	Solid	Constant stress	ASTM A709	Piecewise Linear Plasticity
Luminaire mass	Shell	Belytschko-Tsay	ASTM A595 Grade A	Rigid
Concrete	Solid	Constant stress	4, 000 psi Concrete	CSCM Concrete
Reinforcement	Beam	Hughes-Liu	ASTM A615	Plastic Kinematic
Soil	Solid	ALE	Dry & Saturated	Soil and Foam
Air	Solid	ALE	Air	Null

10.2.2 Material Properties and Models

The light pole system's material response, which includes components such as the light pole, mast arm, mounting plates, base plate, couplings, nuts, and washers, was simulated using the MAT Piecewise Linear Plasticity model. This model accommodates elasto-plastic behaviors, accounting for yielding, hardening, plastic-strain-based failure, and strain-rate effects. The steel's elastic modulus was set at 2.9×10^4 ksi, with a Poisson's ratio of 0.3. The yield strength for ASTM A595 and ASTM A449 steel was specified as 55 ksi and 43.5 ksi, respectively, consistent with materials used in component test nos. AKLP-5 and AKLP-6. The Cowper and Symonds model was used to incorporate strain-rate-dependent strength increase, scaling the yield stress with coefficients $C = 40.4$ and $p = 5$. A plastic failure strain was set in the material model for couplings, to facilitate the breakaway mechanism during impact loading. This enabled elements to be deleted from the simulation to mimic steel fracture when the plastic strain reached a predetermined value. After considering prior studies and systematic simulation trials, the plastic failure strain was set at 0.2 to achieve an accurate representation of coupling fractures' locations and timing.

Cohesion coefficients for dry, noncompacted sand (test no. AKLP-5) and saturated noncompacted sand (test no. AKLP-6) were derived from Standard Penetration Test (SPT) N values, acquired in the preliminary stages of the crash testing program. Given the lack of detailed data regarding the sand's dynamic friction angle during bogie testing, an equivalence was posited between the friction angle and the angle of repose. The initial computational steps involved the determination of Drucker-Prager (D-P) model parameters using the cohesion and friction angle values. In subsequent calculations, the Soil and Crushable Foam (SCF) model parameters were derived from the D-P parameters through established relations (as explained in the preceding chapter).

For test no. AKLP-5, the dry noncompacted sand, was characterized by a density of 86.8 pcf. Conversely, the saturated noncompacted sand in test no. AKLP-6 was assigned a density of 124.1 pcf,. Additionally, values for the shear modulus and bulk modulus were determined with reliance on Young's modulus—derived from SPT N values—and a range of values suggested by Wright [45] and Lee [66] tailored to the modeling of dry and saturated sands, respectively, under dynamic loading conditions. SCF model parameters corresponding to the dry (noncompacted) and saturated (noncompacted) sands are documented in Tables 9.1 and 9.2.

For a comprehensive understanding of the constitutive models and input parameters pertaining to soil, concrete, and reinforcement bars, readers are encouraged to refer to the previous chapter, where these aspects are extensively discussed, or to technical documentation available for LS-DYNA. Additionally, the previous chapter provides a detailed exploration of the material properties and governing equation of state for the air material.

10.2.3 Contact Models and Boundary Conditions

The Automatic General contact type was employed to model the interaction between the bogie vehicle and the light pole. The Contact Automatic General, a penalty-based contact algorithm, counters penetration among interacting parts by exerting a force proportional to the depth of penetration. The algorithm was adjusted to use a soft constraint penalty formulation (SOFT = 1), an approach particularly effective when materials of different mesh densities and stiffness come into contact. A Coulomb friction formulation was used to account for the frictional interaction during sliding contact. Static and dynamic friction was implemented with a coefficient of 0.1 to simulate the frictional interaction between the impact head and the light pole.

The light pole system components, including the light pole, mast arm, couplings, nuts, washers, and base plate, were assigned a segment-based contact algorithm via the Contact Automatic Single Surface, with static and dynamic friction coefficients set to 0.1. A penalty-based contact algorithm was used to model the interaction between the couplings and the concrete foundation using the Contact Automatic Surface to Surface, with both static and dynamic friction coefficients set at 0.57, values derived from relevant literature [67-68].

The connections between the light pole and attachment complex and between the mast arm and attachment complex were simulated as rigid constraints to save computational time. In this model, the soil and air were represented using an MM-ALE mesh, while a Lagrangian mesh was used for the RC foundation. The dynamic soil and foundation interaction was achieved using a penalty-based coupling algorithm via the Constrained Lagrangian in Solid keyword.

The boundaries of the soil domain and air volume were restrained to prevent the movement of exterior surfaces during the impact event. A Boundary Non-Reflecting (BNR) boundary condition was applied to the four exterior faces and the bottom surface of the models. Bolt preload of 15.5 kips was applied to the couplings using the Initial Stress Section keyword in LS-DYNA to simulate the effect of installation torque.

10.3 Baseline Simulation and Validation

Baseline simulations corresponding to test nos. AKLP-5 and AKLP-6 involved a bogie vehicle model of 1,850 lb mass impacting the light pole model at a velocity of 20.4 mph and 20.0 mph, respectively, maintaining an impact angle of 0 degrees. The simulated initial impact mirrored the physical impact tests, occurring 25 in. above the ground. In both simulations, the single mast arm was set perpendicular to the direction of impact to match test conditions.

10.3.1 Simulation of Test No. AKLP-5

The evaluation of the test no. AKLP-5 simulation incorporated both qualitative and quantitative considerations. Quantitative considerations included impact force versus time histories, impulse versus time histories, and foundation displacement relative to the experimental data from test no. AKLP-5. Impulse time histories were computed by integrating force versus time curves.

Figures 10.2 and 10.3 show that the simulation results accurately represented physical test no. AKLP-5 behavior and events, including light pole release, light pole rotation, light pole-bogie interaction, and concrete foundation response. Simulated breakaway coupling base fractures initiated in the two rear couplings at 10 ms, followed by a full breakaway mechanism at 20 ms, with fractures observed in all four couplings at both neck locations. Post-impact analyses identified light pole buckling and coupling fracture, with the MM-ALE computational model accurately capturing both global behavior and local outcomes, such as deformed shapes and areas of local buckling and plastic material response.

The simulation predicted the peak impact force with an error margin of 9.4% relative to the physical impact test, as illustrated in Figure 10.4. This tolerance was deemed acceptable considering the inherent complexities of dynamic impact simulations involving a light pole-foundation-soil system. However, the model overpredicted the force for initial softening by 9.4%, potentially due to lack of detailed material data for the proprietary couplings, and/or limitations of the steel material model and associated parameters in accurately predicting the shear-based fracture of the couplings. The simulation generated an impulse versus time history that closely aligned with the experimental data, exhibiting a maximum 8.9% difference in the maximum impulse.

The baseline test no. AKLP-5 simulation also produced an acceptably accurate representation of the dynamic soil-foundation interaction and the foundation's response during the impact event. The peak lateral displacement at the foundation top was slightly lower (12%) in the simulation than in test no. AKLP-5 (Figure 10.5).

Despite minor impact force and foundation displacement discrepancies, the baseline simulation corresponding to test no. AKLP-5 offered reasonable predictions of light pole system behavior and damage under impact loading. These differences were within an acceptable range, thus justifying the model's validity for other analyses, such as full-scale MASH test simulations.

t = 0 ms

t = 10 ms

t = 20 ms

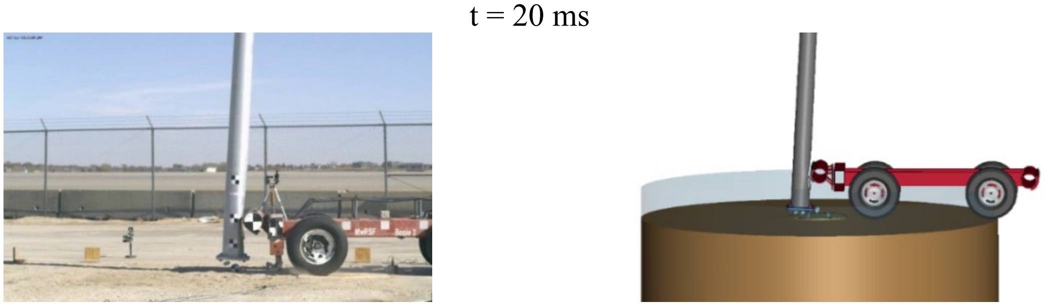

t = 40 ms

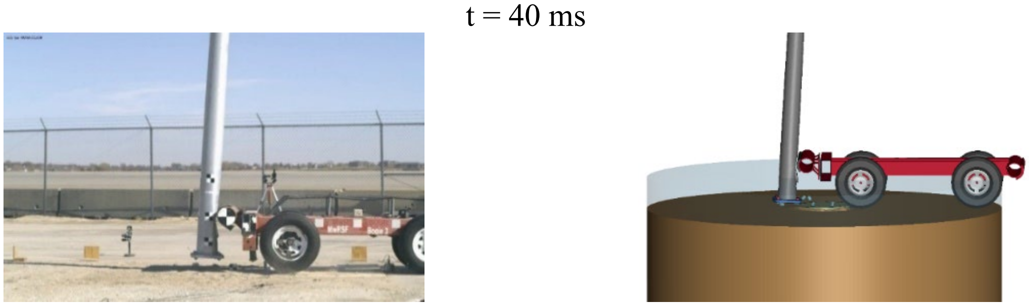

t = 80 ms

Figure 10.2 Sequential Views, Test No. AKLP-5 and Simulation

(a) Light Pole Damage

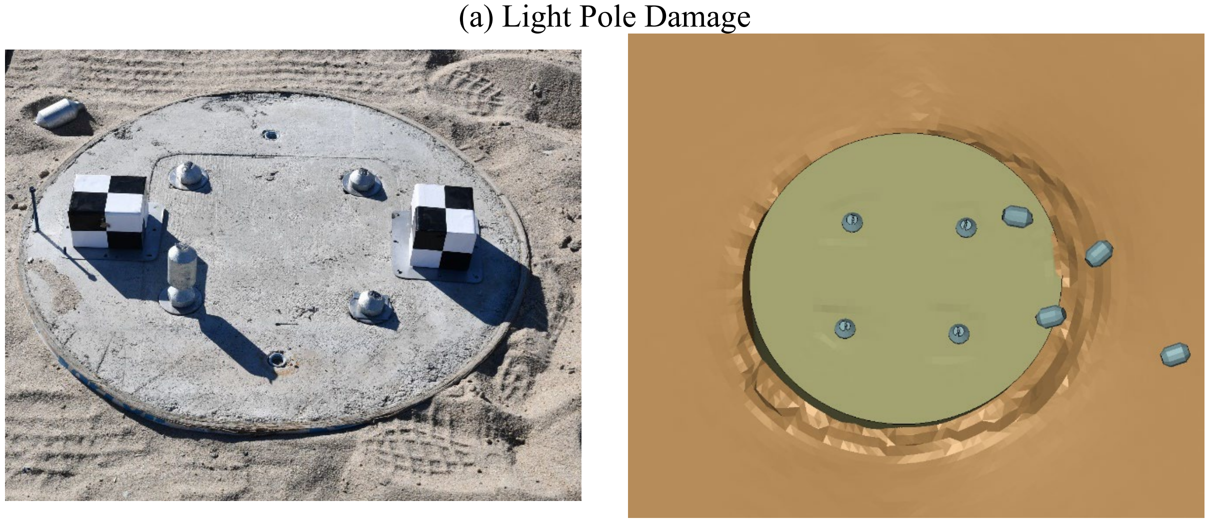

(b) Coupling Breakaway

Figure 10.3 Test No. AKLP-5 Test versus Simulation Damage: (a) Light pole and (b) Foundation and Couplings

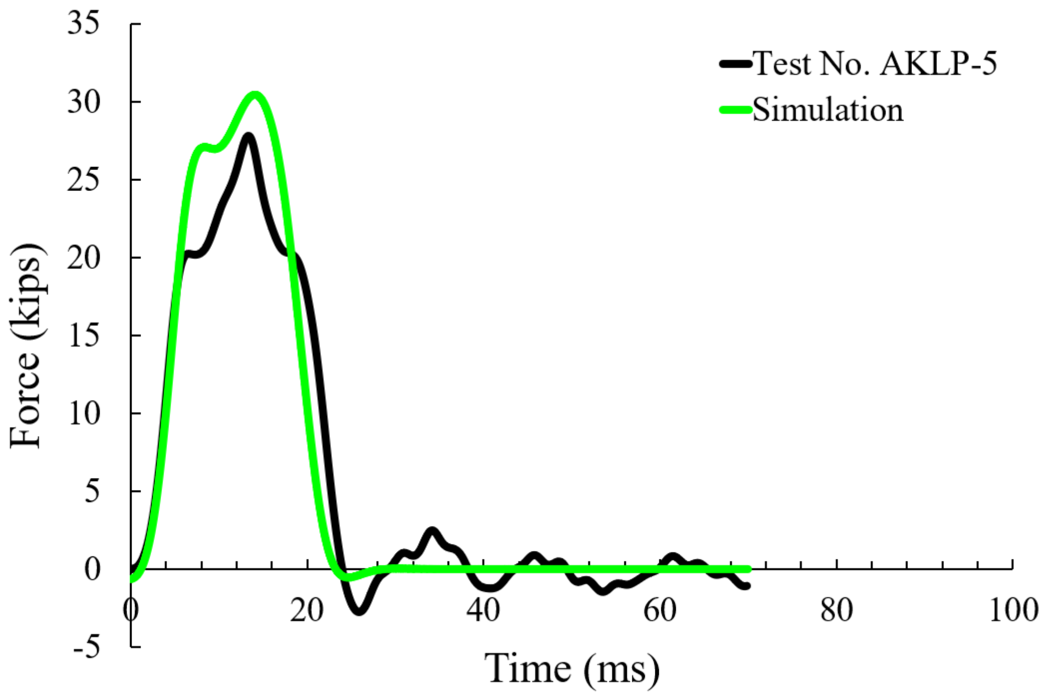

(a) Impact Force Time Histories

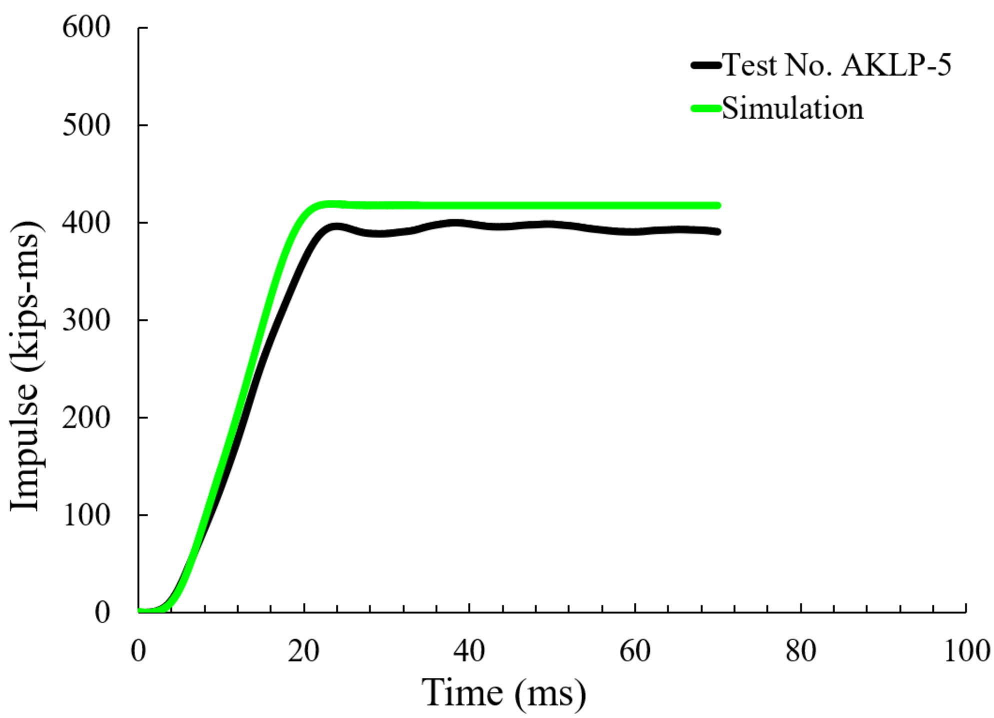

(b) Impulse Time Histories

Figure 10.4 Impact Force and Impulse, Test No. AKLP-5 and Simulation: (a) Impact Force Time Histories and (b) Impulse Time Histories

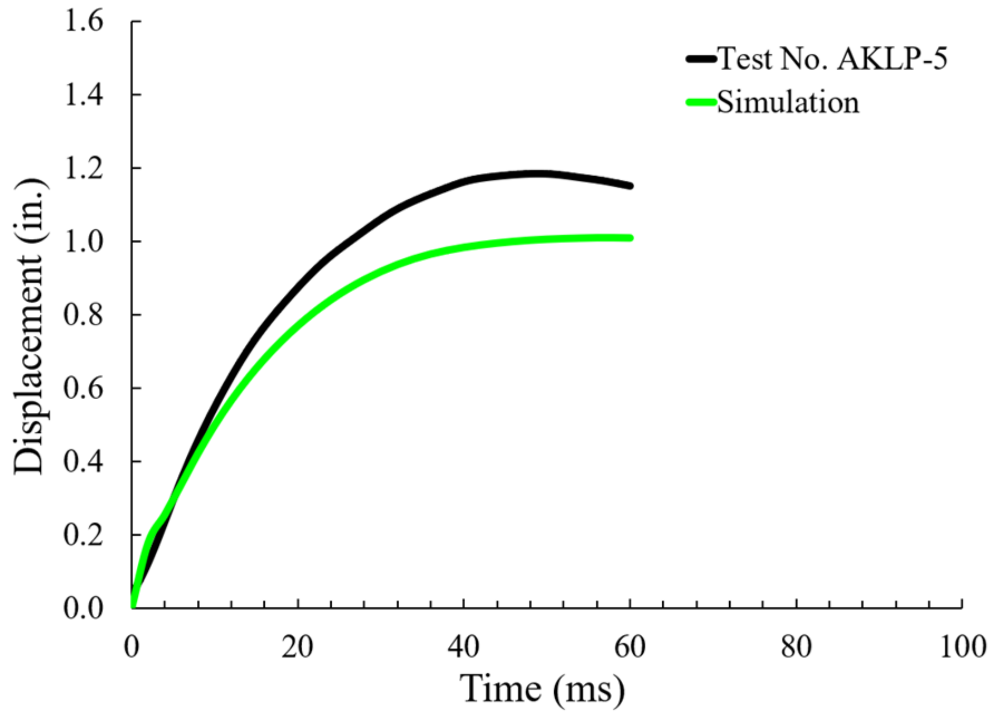

Figure 10.5 Foundation Displacement, Test No. AKLP-5 and Simulation

10.3.2 Simulation of Test No. AKLP-6

A numerical simulation was additionally performed to assess the fidelity of the developed models in replicating and evaluating the dynamic response of a 35.5-ft steel light pole system under impact loading with saturated, loose sand conditions. The simulation modeled a bogie vehicle impacting the system at a speed of 19.98 mph. The soil moisture content was maintained at 26%. Qualitative and quantitative comparisons were conducted against the data from test no. AKLP-6, concentrating on post-impact crash analysis and metrics such as impact force versus time histories, impulse versus time histories, and lateral foundation displacement.

Graphical representations of the results from the simulation and test no. AKLP-6, as illustrated in Figure 10.6, displayed similar light pole release timing, light pole rotation, and coupling breakaway behavior. The initial impact in both scenarios occurred with the light pole centerline aligned with the bogie center point. The two front couplings on the impact side first exhibited cracking at t = 10 ms, with a full coupling breakaway ensuing at t = 15 ms due to the failure of all four couplings at both neck locations. The light pole rotated around its center of gravity and translated with the bogie in the direction of impact before losing contact at t = 40 ms.

Qualitative assessments involved post-impact analysis of light pole plastic deformation and fracturing of couplings. A comparison between the simulation and test no. AKLP-6, presented in Figure 10.7, suggested that the computational model accurately predicts locations of plastic behavior by examining deformed shapes. The light pole was dented similarly for both the physical test and the model at the impact height, as shown in Figure 10.7(a). Furthermore, all four couplings fractured at both neck locations during the impact event, achieving the desired breakaway mechanism for the light pole system in both the simulation and test no. AKLP-6.

Figure 10.8 illustrates the comparison between the simulation and test no. AKLP-6 for impact force-time histories and impulse-time histories. The simulation accurately captured the initial loading branch and the peak load experienced between the bogie and pole, which primarily reflected the Transpo couplings' resistance. The simulation predicted a similar maximum force of 27.1 kips at 7.2 ms, compared to the test peak force of 27.8 kips at 7.5 ms, a difference in the simulation of 2.5%. Following this local peak in the force versus time simulation response, the simulation reached a second local peak, also the maximum peak in the simulation, of 27.6 kips at 12.7 ms, which approximately corresponded to a short leveling of the recorded forces in the physical test data. This difference in simulated and physical test responses is likely due to the fracture mechanism of the proprietary, double-neck, frangible Transpo couplings, with brittle fracture at necked sections of couplings in the test represented by a more ductile loss of strength in the simulation. As the objective was to reasonably approximate the activation of the proprietary components, the simulation exhibited excellent agreement with the physical test in general, only excepting an overestimated impulse of approximately 17% due to the precise nature of the Transpo couplings' fracture mechanics.

A comparison of lateral displacements at the foundation top in the simulation and test no. AKLP-6 is presented in Figure 10.9. The peak displacements, corresponding to the activation of the breakaway mechanism for the coupling base, were 0.34 in. in the simulation and 0.30 in. in the test. This 13% discrepancy is within the acceptable margin, which could result from the simplified representation of saturated soil conditions and the model's inability to accurately predict the coupling fracture under bogie impact.

In conclusion, the simulation provided satisfactory predictions of light pole system behavior, coupling base breakaway mechanism, dynamic soil-foundation interaction, and bogie behavior under impact conditions. The model can be expected to produce approximately accurate but slightly conservative outcomes for other potential simulations, such as slightly overestimated occupant risk and foundation displacement if simulated for full-scale vehicle impacts.

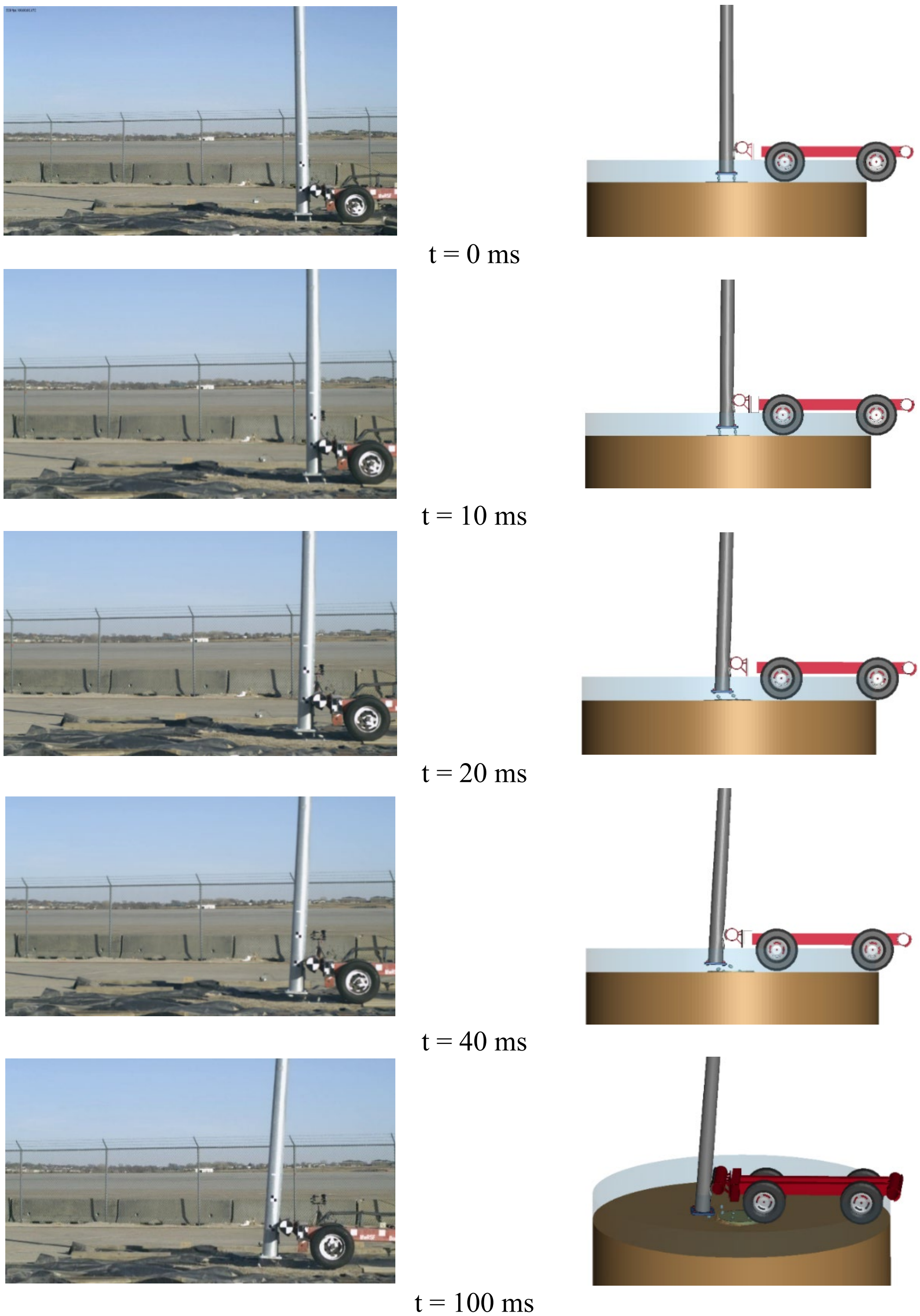

Figure 10.6 Sequential Views, Test No. AKLP-6 and Simulation

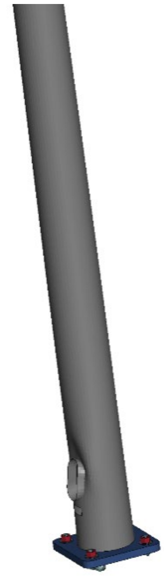

(a) Light pole Damage

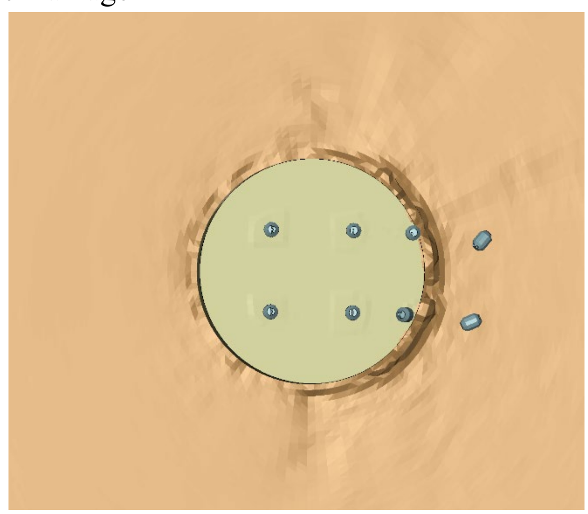

(b) Coupling Breakaway

Figure 10.7 Test No. AKLP-6 Test versus Simulation Damage: (a) Light pole and (b) Foundation and Couplings

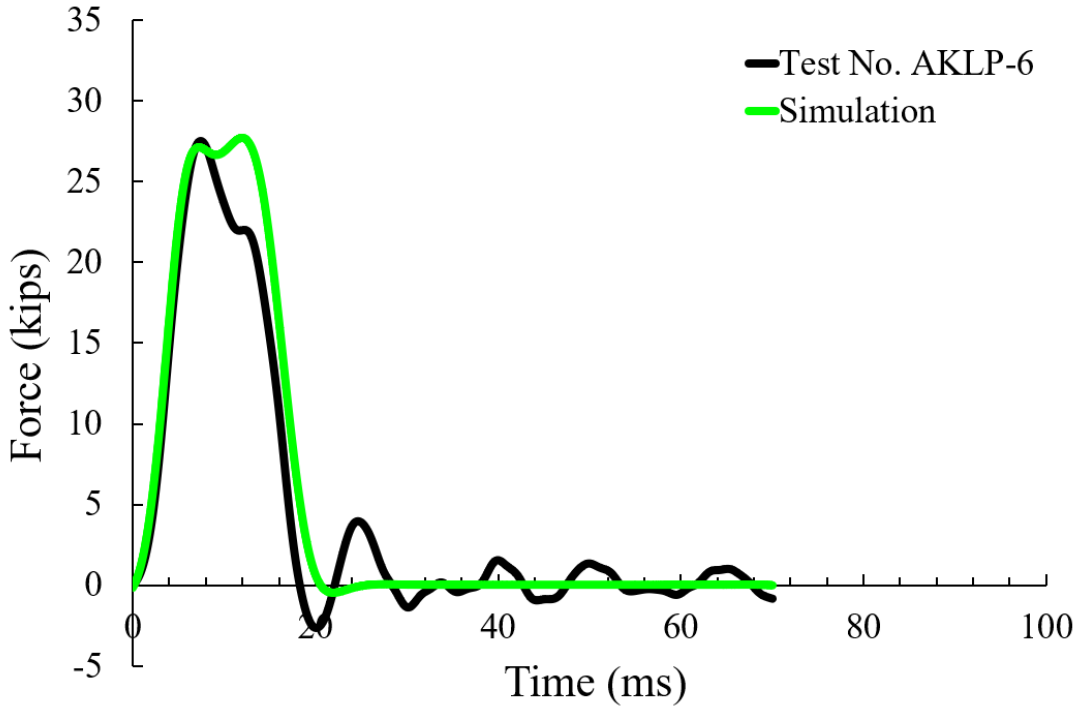

(a) Impact Force Time Histories

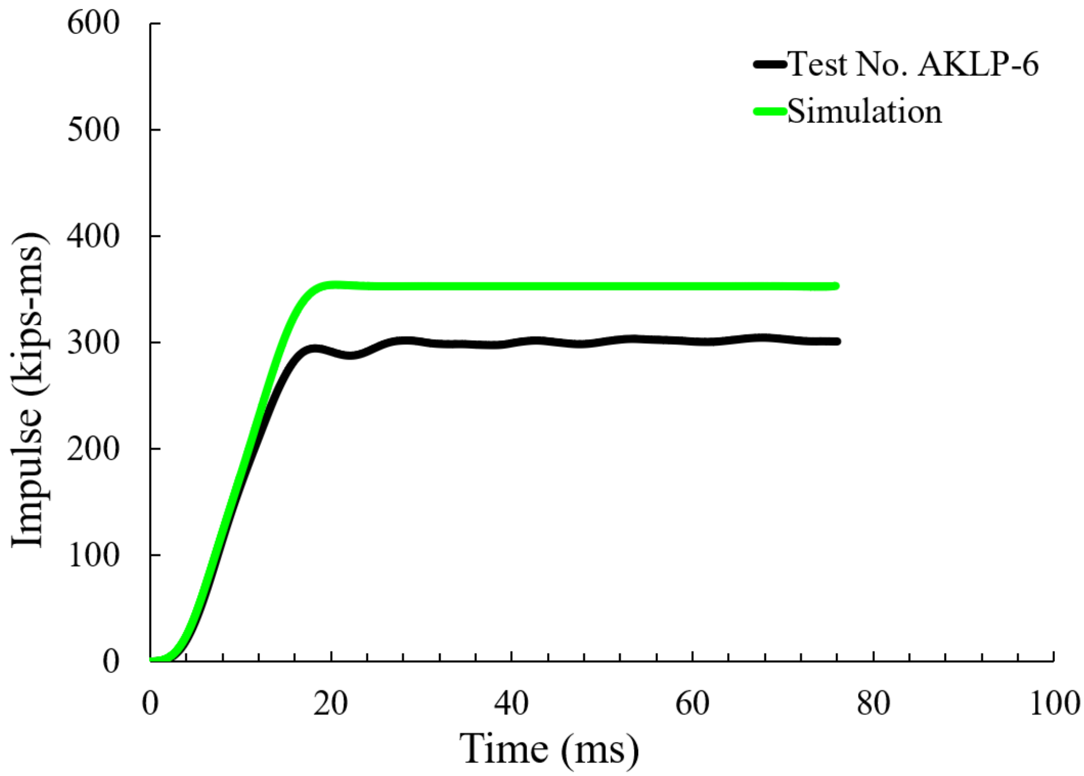

(b) Impulse Time Histories

Figure 10.8 Impact Force and Impulse, Test No. AKLP-6 and Simulation

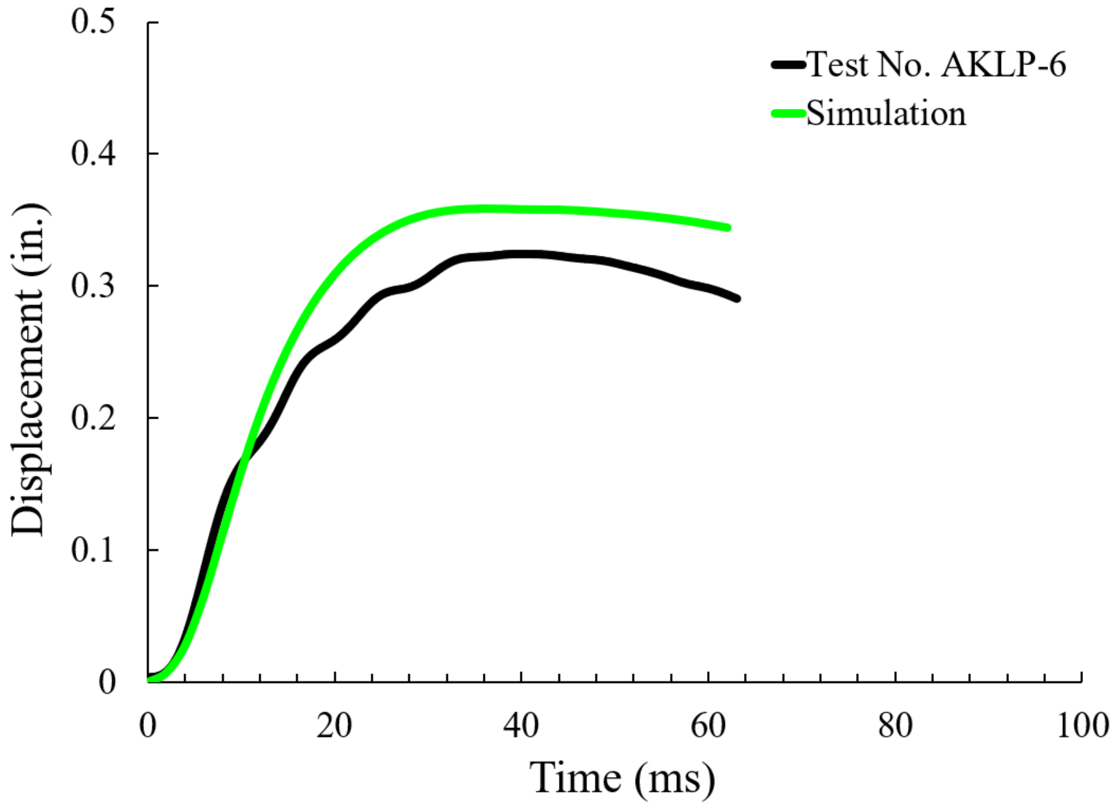

Figure 10.9 Foundation Displacement, Test No. AKLP-6 and Simulation

Chapter 11 Mash Evaluation of Light Pole-Foundation System

11.1 Overview

Simulations were performed to investigate the potential outcomes for full-scale vehicle impacts as an extension to the previous modeling performed to simulate weak soil conditions. Transpo Model 5100 couplings activated as intended in physical impact test nos. AKLP-5 and AKLP-6, and foundation permanent sets were within target thresholds to allow reusing foundations for pole replacements after impacts. While these results are encouraging, crash safety requires additional considerations to ensure adequate safety for motorists. LS-DYNA computational simulations, replicating the conditions of for a portion of Manual for Assessing Safety Hardware (MASH) Test Level 3 (TL-3) [9], were conducted to preliminarily confirm anticipated breakaway activation and investigate occupant risk metrics.

11.2 MASH TL-3 Requirements and Evaluation Criteria

MASH TL-3 prescribes three distinct full-scale crash tests for breakaway luminaire support systems: test designation nos. 3-60, 3-61, and 3-62. Test designation no. 3-60 involves an 1100C test vehicle impacting the pole at 19 mph, primarily assessing the kinetic energy needed for breakaway mechanism activation, the reliability of breakaway activation for low-speed impacts, and the potential risks of occupant interaction with the vehicle (Occupant Impact Velocity (OIV), Occupant Ridedown Acceleration (ORA)), and occupant compartment intrusion (roof and windshield crush) resulting from vehicle interaction with the pole during and after breakaway occurs and potential vehicle instability such as uncontrolled yaw and rollover. Test designation nos. 3-61 and 3-62 focus on high-speed impacts with similar metrics. Table 11.1 summarizes the parameters for MASH TL-3 tests.

Table 11.1 MASH Test Matrices for Breakaway Luminaire Supports [9]

Test Article	**Test Designation No.**	**Test Vehicle**	**Vehicle Weight (lb)**	**Impact Conditions**		**Impact Point**	**Evaluation Criteria** [1]
				Speed (mph)	**Angle (deg)**		
Luminaire Support Structures	3-60	1100C	2,425	19	CIA	CIP	B, D, F, H, I, N
	3-61	1100C	2,425	62	CIA	CIP	B, D, F, H, I, N
	3-62	2270P	5,000	62	CIA	CIP	B, D, F, H, I, N

[1]Evaluation criteria explained in Table 11.2.

Prior research [69-71] indicated the heightened criticality of tests 3-60 and 3-61 with 1100C small cars over 3-62 with a 2270P pickup truck, given the risks of occupant compartment intrusion and longitudinal OIV breaches. Consequently, this study focused on evaluating the crashworthiness of the light pole supported by a concrete foundation through breakaway couplings in alignment with MASH test designation nos. 3-60 and 3-61.

MASH requires that safety be evaluated by impacting at a Critical Impact Angle (CIA), to be determined for each test system. Generally, roadside devices should be tested at a CIA selected between 0 and 25 degrees. For crash testing, critical angles may be determined from analyses or engineering judgement with reference to past testing practices and outcomes for similar systems. Ideally, simulations such as those described in this section would be performed to examine multiple test conditions, so that physical testing can be limited to investigate only the most critical conditions.

In addition to CIP, MASH requires that a Critical Impact Point (CIP) be selected, and recommends testing single support structures like light poles with the support centerline aligned with either the left-front or right-front quarter point of the impacting vehicle. This historical recommendation was based on potential risk of vehicle instability. However, recent findings from

NCHRP Project 03-119 [72] highlighted center impacts as more critical due to increased severity of occupant compartment intrusion from pole contact with the vehicle roof. Accordingly, the vehicle was simulated as centered on the pole at impact.

Full-scale crash testing evaluation criteria encompass three key areas: structural adequacy, occupant risk, and post-collision vehicle trajectory. Structural adequacy requires predictable activation of the test article through breakaway, fracturing, or yielding. Occupant risk assessment evaluates hazards to vehicle occupants, while post-impact vehicle trajectory considers the likelihood of secondary collisions. These criteria are detailed in Table 11.2.

Table 11.2 MASH 2016 Evaluation Criteria for Support Structures [9]

<table>
<tr><td>Structural Adequacy</td><td>B.</td><td colspan="3">Test article should readily activate in a predictable manner by breaking away, fracturing, or yield.</td></tr>
<tr><td rowspan="11">Occupant Risk</td><td>D.</td><td colspan="3">Detached elements, fragments or other debris from the test article should not penetrate or show potential for penetrating the occupant compartment, or present an undue hazard to other traffic, pedestrians, or personnel in a work zone. Deformations of, or intrusions into, the occupant compartment should not exceed limits set forth in Section 5.2.2 and Appendix E of MASH 2016.</td></tr>
<tr><td>F.</td><td colspan="3">The vehicle should remain upright during and after collision. The maximum roll and pitch angles are not to exceed 75 degrees.</td></tr>
<tr><td rowspan="4">H.</td><td colspan="3">Occupant Impact Velocity (OIV) (see Appendix A, Section A5.2.2 of MASH 2016 for calculation procedure) should satisfy the following limits:</td></tr>
<tr><td colspan="3">Occupant Impact Velocity Limits</td></tr>
<tr><td>Component</td><td>Preferred</td><td>Maximum</td></tr>
<tr><td>Longitudinal and Lateral</td><td>10 ft/s
(3.0 m/s)</td><td>16 ft/s
(4.9 m/s)</td></tr>
<tr><td rowspan="4">I.</td><td colspan="3">The Occupant Ridedown Acceleration (ORA) (see Appendix A, Section A5.2.2 of MASH 2016 for calculation procedure) should satisfy the following limits:</td></tr>
<tr><td colspan="3">Occupant Ridedown Acceleration Limits</td></tr>
<tr><td>Component</td><td>Preferred</td><td>Maximum</td></tr>
<tr><td>Longitudinal and Lateral</td><td>15.0 g’s</td><td>20.49 g’s</td></tr>
<tr><td></td><td></td><td></td></tr>
<tr><td></td><td>N.</td><td colspan="3">Vehicle trajectory behind the test article is acceptable.</td></tr>
</table>

11.3 1100C Vehicle Model

Simulations were performed using a modified 1100C Toyota Yaris vehicle model, developed by the Center for Collision Safety and Analysis (CCSA) and further refined by Midwest Roadside Safety Facility (MwRSF) researchers [59]. It should be noted that this model omits failure mechanisms in suspension parts and lacks tire deflation and windshield failure capabilities. Figure 11.1 presents the 1100C Toyota Yaris vehicle model for full-scale simulations.

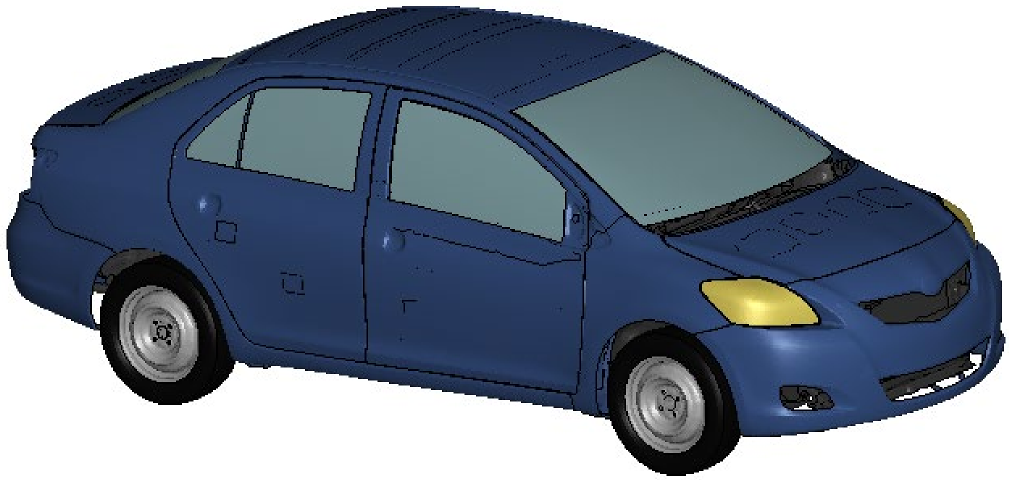

Figure 11.1 1100C Toyota Yaris Vehicle Model

11.4 MASH TL-3 Evaluation of Light pole – Concrete Foundation System

The simulation findings were analyzed to assess the impact safety performance of the light pole and foundation system against MASH safety criteria. This evaluation examined occupant compartment deformation, occupant risk measures (OIVs and ORAs), and vehicle instability indicators such as roll, pitch, or yaw angles.

11.4.1 Full-Scale Crash Simulation: MASH Test Designation No. 3-60 Evaluation

To simulate MASH test designation no. 3-60, an 1100C vehicle was modeled to collide with a light pole-concrete foundation system at 19 mph. The simulations consistently demonstrated that the light pole disengaged from its couplings within 0.1 seconds of impact, regardless of soil stiffness or impact angle. Following detachment, the pole exhibited rotation about its center of mass, leading to subsequent contact with the vehicle's windshield and roof, as illustrated in Figure 11.2. All four frangible couplings exhibited fractures at their lower necked sections, producing a residual stub height of approximately 1.5 in.

The vehicular damage, detailed in Figure 11.3, revealed significant deformations within the occupant compartment for each simulated scenario. Note that the color map has been configured so that red corresponds to a deformation of 4 in., the maximum permissible roof deformation according to MASH. Any red regions therefore indicate expected MASH violations. Occupant compartment deformation results are tabulated in Table 11.3. The damage was predominantly localized at the vehicle's front and roof, corresponding with the impact regions. In simulations involving the light pole foundation embedded in soft soil (SPT = 7), the maximum roof deformation reached 11.5 in. and 8.6 in. for 0-degree and 25-degree impacts, respectively. In contrast, for foundations in very soft soil conditions (SPT = 3), the maximum roof deformations reached 6.1 in. and 9.8 in. for the respective impact angles. Furthermore, the simulations predicted windshield deformations surpassing the MASH limit of 3 in., indicating a high likelihood of windshield shattering upon impact. These deformations notably exceeded the MASH deformation thresholds, indicating unlikelihood of full-scale tests to satisfy established safety criteria for light poles and foundations in both soft and very soft soil conditions.

In terms of occupant safety metrics, the OIVs and the maximum 0.010-second average ORAs in both longitudinal and lateral directions were within the acceptable limits as stipulated in MASH 2016. These findings are presented in Table 11.3.

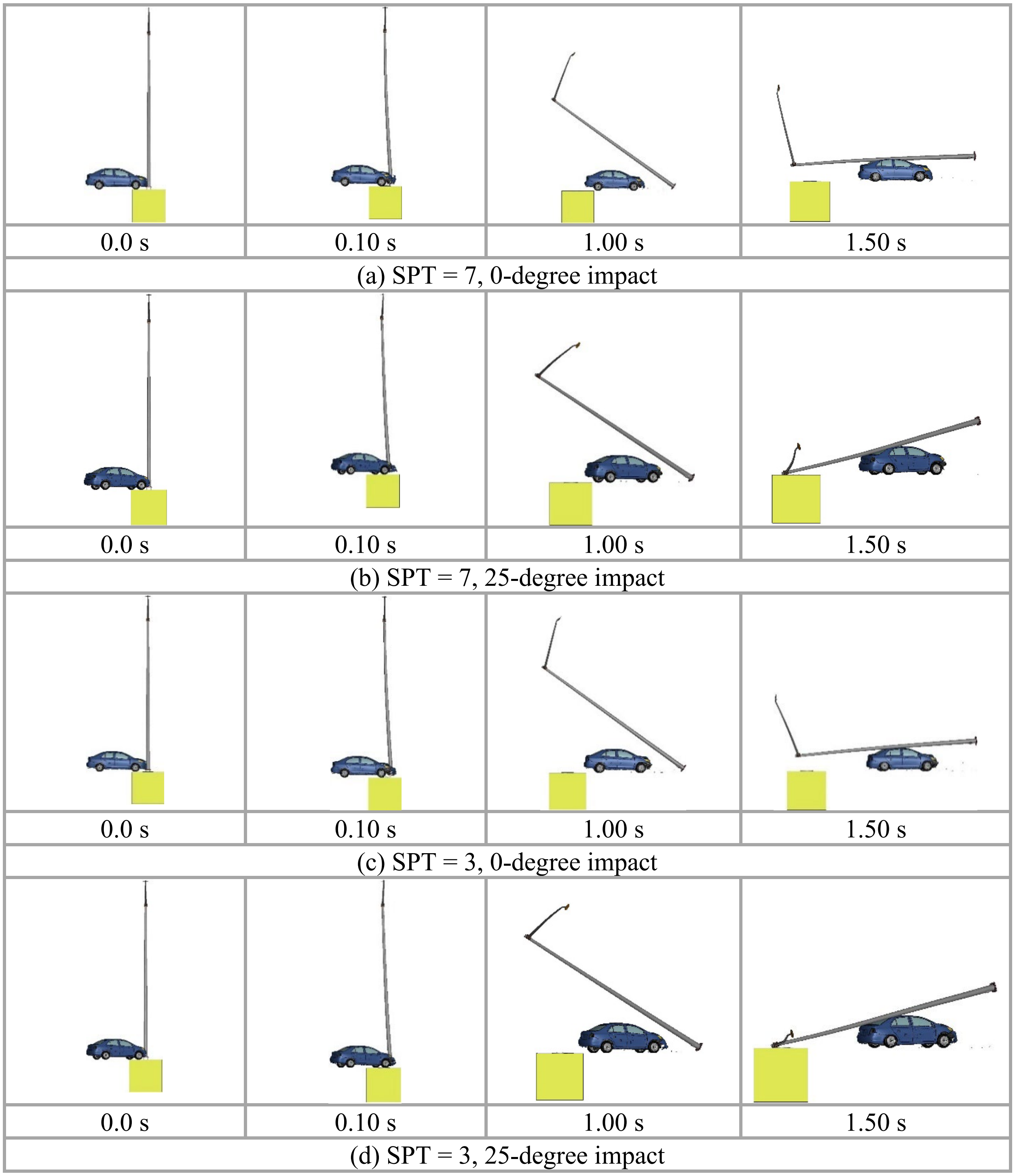

Figure 11.2 Sequential Views, MASH Test Designation No. 3-60

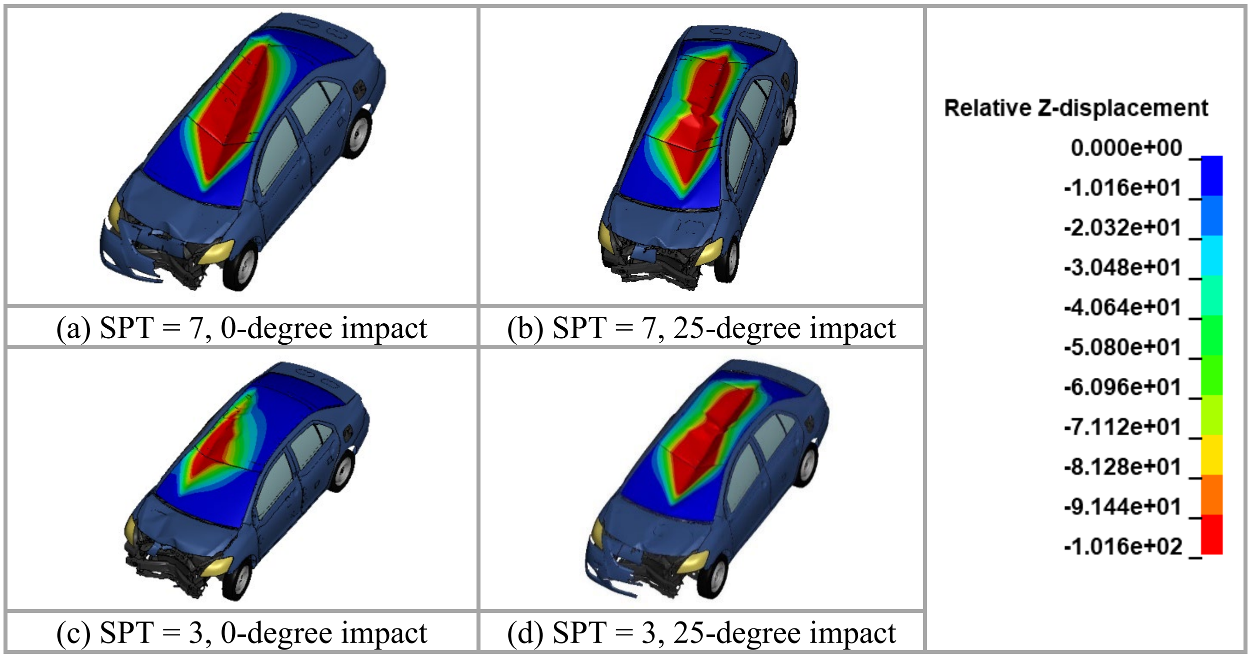

(a) SPT = 7, 0-degree impact
(b) SPT = 7, 25-degree impact
(c) SPT = 3, 0-degree impact
(d) SPT = 3, 25-degree impact

Figure 11.3 Occupant Compartment Deformations, MASH Test Designation No. 3-60

Table 11.3 Summary of OIV, ORA, Maximum Angular Displacement, and Occupant Deformation Results from MASH 3-60 Impact Simulations

MASH Evaluation Criteria		Soft Soil (SPT = 7)		Very Soft Soil (SPT = 3)		MASH limit
Impact Vehicle		1100C		1100C		
Impact Velocity		19 mph		19 mph		
Impact Angle		0°	25°	0°	25°	
OIV (ft/s)	Longitudinal	12.25	10.4	10.7	9.73	±16
	Lateral	0.28	0.23	0.11	0.07	not required
ORA (g's)	Longitudinal	0.59	0.74	0.82	0.70	±20.49
	Lateral	0.55	0.52	0.77	0.44	±20.49
Maximum Angular Displacement (degree)	Roll	1.89	0.70	4.54	0.36	±75°
	Pitch	2.12	2.83	2.13	2.71	±75°
Occupant Compartment Deformation (in.)	Roof	11.5	8.6	6.1	9.8	4.0
	Front windshield	8.6	7.9	5.3	8.9	3.0

11.4.2 Full-Scale Crash Simulation: MASH Test Designation No. 3-61 Evaluation

For MASH test designation no. 3-61, simulation parameters were identical to test designation no. 3-60, except that the 1100C small vehicle was initialized with a higher-velocity in accordance with MASH criteria. The systems under examination were embedded in varying soil conditions: soft (SPT = 3) and very soft (SPT = 7), and with the vehicle traveling at 62 mph upon impact. The light pole rapidly disengaged from its couplings consistently in all simulations, occurring within a mere 0.02 seconds post-impact. Subsequently, the pole underwent rotational motion around its center of mass, and the vehicle traversed underneath the airborne pole, as depicted in Figure 11.4. The fracturing of all four couplings resulted in a uniform stub height of 1.5 in.

An analysis of vehicular damage is presented in Figure 11.5, delineating the occupant compartment deformations for each simulated case. Table 11.4 compares these maximum deformations against the MASH-prescribed limits for occupant compartment deformation. The damage was primarily localized to the vehicle's front, correlating with the impact zone. It should be noted that none of the deformations breached the MASH criteria for occupant compartment deformation, as evidenced in Figure 11.5 and summarized in Table 11.4. Furthermore, the vehicle's roll and pitch angular displacements were observed to be within safe limits, not exacerbating occupant risk nor leading to vehicular rollover. Vehicle yaws were similarly deemed unlikely to result in instability. OIVs and ORAs were calculated, and while OIVs were higher than for test 3-60, the results still fell safely with the thresholds established in MASH 2016.

The simulations thus indicated that the light pole and concrete foundation system, when embedded in soft and very soft soil conditions, exhibited a high likelihood of satisfying MASH safety criteria with test designation no. 3-61.

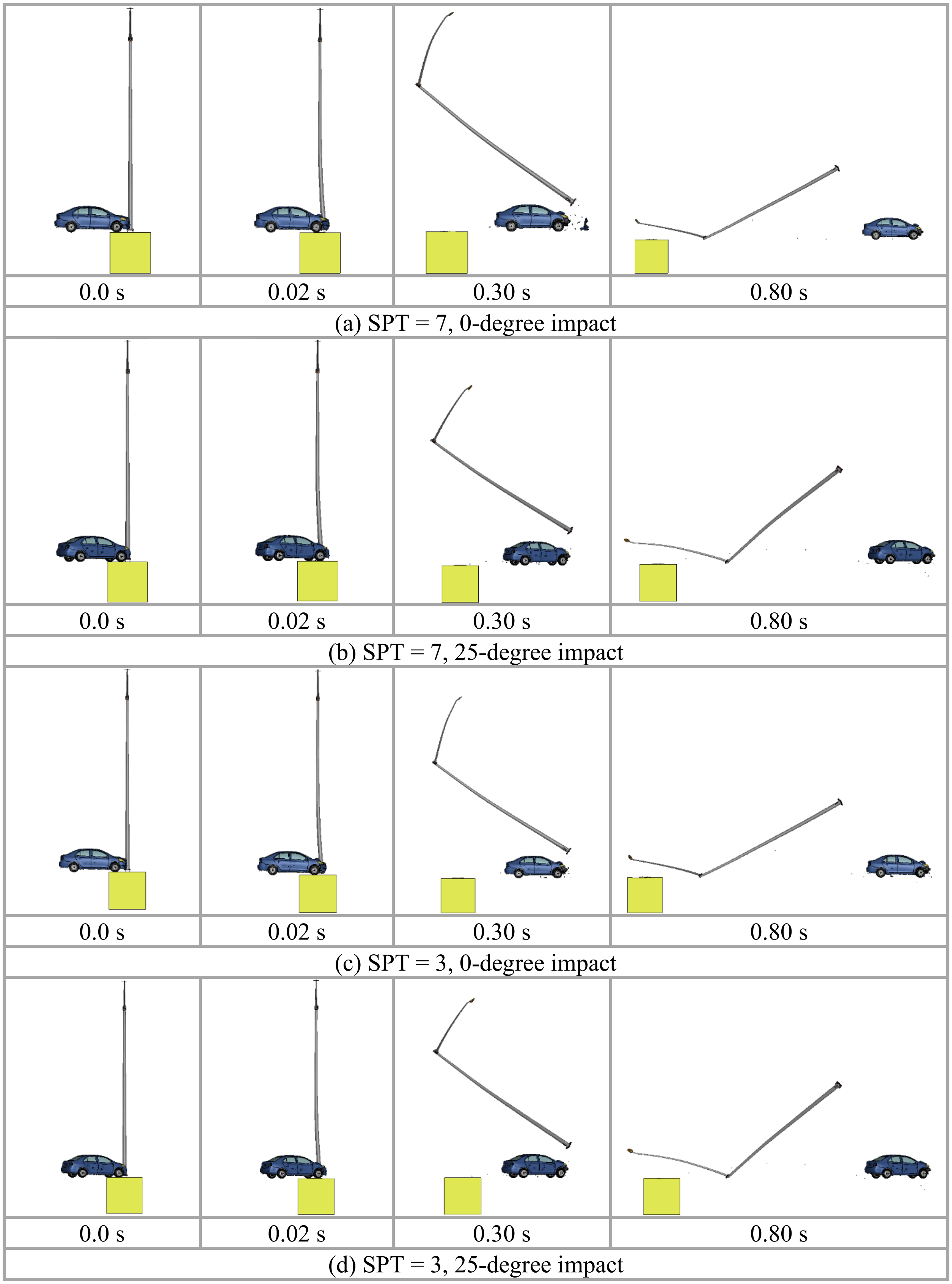

Figure 11.4 Sequential Views, MASH Test Designation No. 3-61

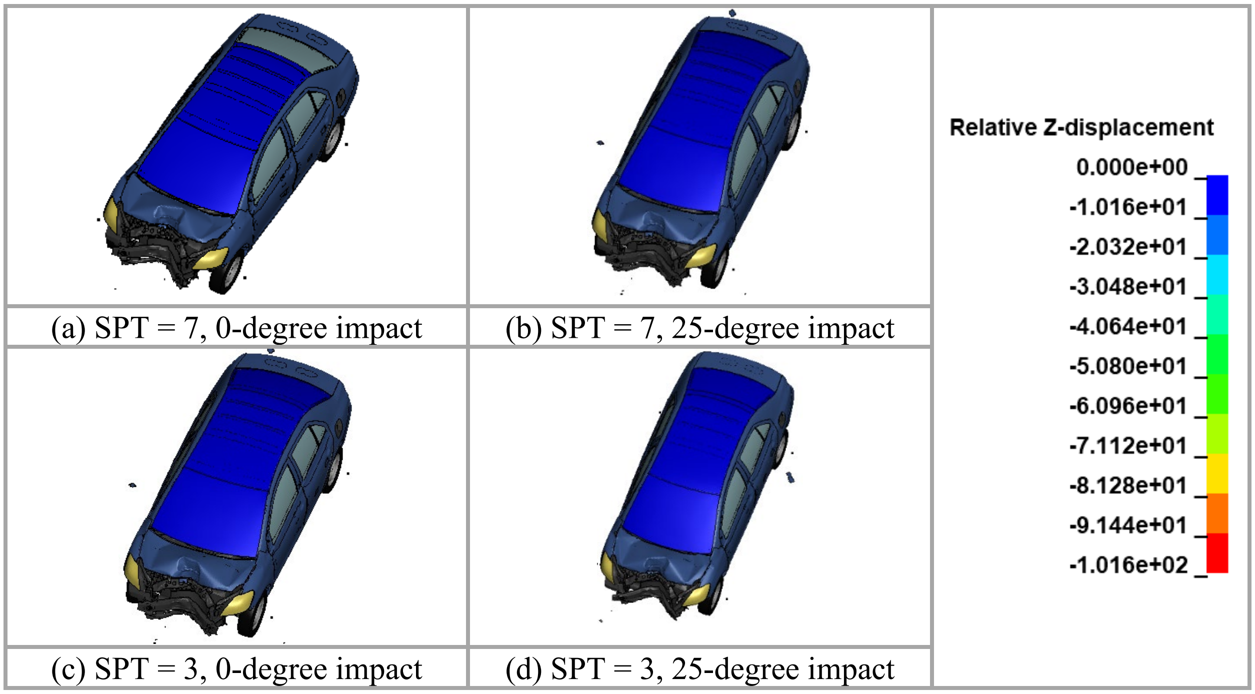

Figure 11.5 Occupant Compartment Deformations, MASH Test Designation No. 3-61

Table 11.4 Summary of OIV, ORA, Maximum Angular Displacement, and Occupant Deformation Results from MASH 3-61 Impact Simulations

MASH Evaluation Criteria		Soft soil (SPT = 7)		Very soft soil (SPT = 3)		MASH limit
Impact Vehicle		1100C		1100C		
Impact Velocity		62 mph		62 mph		
Impact Angle		0°	25°	0°	25°	
OIV (ft/s)	Longitudinal	-14.7	-13.9	-14.5	-13.8	±16
	Lateral	0.39	0.19	0.31	0.19	not required
ORA (g's)	Longitudinal	-1.03	-0.85	-1.21	-0.85	±20.49
	Lateral	0.74	0.70	1.10	0.67	±20.49
Maximum Angular Displacement (degree)	Roll	0.39	0.79	0.47	0.79	±75°
	Pitch	-1.96	-1.51	-1.87	-1.51	±75°
Occupant Compartment Deformation (in.)	Roof	0	0	0	0	4.0
	Front windshield	0	0	0	0	3.0

11.4.3 Discussion of Results

Full-scale simulations of MASH test designation nos. 3-60 and 3-61 were conducted using the LS-DYNA simulation platform. Similar to test nos. AKLP-5 and AKLP-6, the simulated approximate Transpo couplings provided predictable breakaway activation in all simulations of 35.5-ft tall light poles, supported by 6-ft deep foundations with 30-in. diameters, in soft and very soft soil conditions. Frangible coupling activation was achieved primarily through inertial foundation resistance and therefore insensitive to modeled soft to very soft soil conditions.

Simulation results should be interpreted with consideration of their preliminary nature and the related potential implications for full-scale physical testing. The simulations predicted a higher breakaway activation force and resulting impulse compared to data recorded from test nos. AKLP-

5 and AKLP-6. Therefore, it is conceivable that the model used in these simulations might conservatively overestimate foundation displacements, OIVs, and ORAs. The simulations indicated minimal damage to the concrete foundation, which was also observed in physical testing, suggesting that foundations may be reused when poles and frangible couplings are replaced post-impact.

Despite the successful demonstration of breakaway activation in both bogie tests and full-scale simulations, a significant concern was the interaction of the light pole with the vehicle post-activation. The pole's contact with the vehicle roof and front windshield led to excessive deformations within the occupant compartment. The crashworthiness of the light pole, thus, was largely influenced by factors such as the impact angle, vehicle type, pole configuration, geometric properties, and the type of breakaway support. In the context of MASH safety requirements, this interaction predicted a low potential for test designation no 3-60 to meet MASH impact safety performance criteria due to substantial occupant compartment deformations caused by the pole collapsing onto the vehicle post-activation.

Chapter 12 Conclusions

Four tests were performed with surrogate vehicles (bogies) approximately simulating small cars impacting steel posts embedded in concrete foundations, and two subsequent tests were performed with bogies impacting steel posts mounted to foundations with Transpo frangible couplings, consistent with AK DOT&PF Standard Plans. The bogie impacts on embedded steel posts demonstrated that foundation inertia alone, regardless of surrounding soil stiffness, was adequate to develop shear forces sufficient to activate typical breakaway couplings used by AK DOT & PF.

Although the displacement was unacceptably large for the foundation with an embedded steel post and surrounded by loose soil, the displacement was significantly less and within the desirable range for permanent set when the foundation supported a steel pole connected by frangible couplings. This difference in behavior illustrates the significance of loading duration, and highlights the inapplicability and unnecessary overconservativism of static methods such as Broms' Method for addressing vehicle impacts.

Furthermore, small foundation permanent sets were observed for foundations with frangible couplings in both dry and fully saturated conditions. Thus, foundations consistent with the current AK DOT&PF Standard Plan L-30.11, using Transpo Pole-Safe Model No. 5100 couplings, with depths of at least 6 ft, provide compliance with previously accepted crashworthiness standards predating the *Manual for Assessing Safety Hardware, Second Edition (MASH 2016)*, regardless of surrounding soil stiffness and moisture content.

MASH compliance differs from predating standards by including additional requirements restricting occupant compartment deformation. Preliminary LS-DYNA simulations for full-scale MASH testing with small cars impacting poles commonly used by AK DOT&PF indicate that the poles are unlikely to demonstrate acceptable crashworthiness, regardless of the favorable breakaway mechanism and insensitivity to soil conditions surrounding foundations, due to excessive roof and windshield deformations.

Chapter 13 Recommendations for Future Research

13.1 Breakaway Steel Couplings Modeling

The present study utilized a representative steel material model, specifically, the MAT Piecewise Linear Plasticity model in LS-DYNA, to simulate the fracture dynamics and overall behavior of the couplings under impact loading conditions. This model accommodates a range of steel properties, encompassing yielding, plastic hardening, failure based on plastic strain, and strain-rate effects, while offering the capacity to incorporate a stress versus strain curve.

A complex interplay of factors, including nonlinear material properties, inertial effects, and the interaction of stress waves, contribute to fracture initiation and propagation in the steel couplings under impact conditions. These complexities may not be entirely encapsulated by the Piecewise Linear Plasticity constitutive model adopted for simulating steel fracture in this study.

The couplings were proprietary products, so it is unsurprising that detailed data was not readily available from the manufacturer. If detailed material data is deemed necessary, research efforts should anticipate needing to perform material tests on supplied couplings to obtain additional characterization data, as needed. For the study presented herein, the research team estimated the stress versus strain curve for the couplings from previous studies and the team's collective experience. Furthermore, a plastic failure strain was defined within the Piecewise Linear Plasticity material model to simulate coupling fracture. Upon reaching this predefined plastic strain, the associated element was removed from the numerical simulation to emulate a steel fracture. This plastic failure strain value was ascertained via a series of systematic numerical experiments.

The Extended Finite Element Method (XFEM) has shown promising potential for fracture modeling, encompassing both initiation and propagation. This approach has been specifically executed for modeling shell elements in LS-DYNA. Upon functionalization of the explicit version of XFEM in LS-DYNA for solid elements, it is recommended to explore its utility for simulating the fracture of breakaway steel couplings.

13.2 Soil Dynamics Modeling

The dynamic behavior of light pole foundations is primarily governed by soil properties, notably compaction and moisture content, significantly influencing soil behavior. Consequently, two parameters emerge as pivotal: the void ratio and degree of saturation, both playing a crucial role in modulating the impact of soil moisture content on deformation characteristics. Importantly, compaction is directly linked to the void ratio, while moisture content correlates strongly with excess pore water pressure.

Our investigation employed the Soil and Crushable Foam (SCF) model to simulate dynamic soil-foundation interaction. However, it is noteworthy that this model does not intrinsically consider the generation of excess pore water pressure or a biphasic (solid-liquid) soil system. This underlines the necessity for future studies to integrate soil models capable of accommodating both excess pore water pressure and moisture effects. Such models could enable a more thorough analysis of the dynamic impact response and overall performance of light pole foundations within saturated granular soils. Using such soil constitutive models could also pave the way for evaluating potential soil liquefaction under dynamic impact loading conditions.

References

1. *AASHTO LRFD Bridge Design Specifications, Eighth Edition*, American Association of State Highway and Transportation Officials (AASHTO), Washington, D.C., 2017.

2. *LRFD Specifications for Structural Supports for Highway Signs, Luminaires, and Traffic Signals, First Edition*, American Association of State Highway and Transportation Officials (AASHTO), Washington, D.C., 2017.

3. Broms, B.B., *Lateral Resistance of Piles in Cohesive Soils*, American Society of Civil Engineers Journal of the Soil Mechanics and Foundation Division, Vol. 90, Issue 2, March 1964, pages 27-63. https://doi.org/10.1061/JSFEAQ.0000611

4. Broms, B.B., *Lateral Resistance of Piles in Cohesionless Soils*, American Society of Civil Engineers Journal of the Soil Mechanics and Foundation Division, Vol. 90, Issue 3, March 1964, pages 123-156. https://doi.org/10.1061/JSFEAQ.0000614

5. *Geotechnical Design Manual M 46-03.16*, Washington State Department of Transportation, Olympia, WA, 2022. https://www.wsdot.wa.gov/publications/manuals/fulltext/M46-03/Geotech.pdf

6. Michie, J.D., *Recommended Procedures for the Safety Performance Evaluation of Highway Appurtenances*, National Cooperative Highway Research Program (NCHRP) Report 230, Transportation Research Board, Washington, D.C., 1981.

7. Ross, H.E., Sicking, D.L., Zimmer, R.A., and Michie, J.D., *Recommended Procedures for the Safety Performance Evaluation of Highway Features*, National Cooperative Highway Research Program (NCHRP) Report 350, Transportation Research Board, Washington, D.C., 1993.

8. *Manual for Assessing Safety Hardware (MASH), First Edition*, American Association of State Highway and Transportation Officials (AASHTO), Washington, D.C., 2009.

9. *Manual for Assessing Safety Hardware (MASH), Second Edition*, American Association of State Highway and Transportation Officials (AASHTO), Washington, D.C., 2016.

10. Rosenbaugh, S., Faller, R. K., Lechtenberg, K. A., Bielenberg, R. W., Sicking, D. L., and Reid, J. D., *Dynamic Evaluation of New York State's Aluminum Pedestrian Signal Pole System*, Report No. TRP-03-223-09, Midwest Roadside Safety Facility, University of Nebraska-Lincoln, Lincoln, Nebraska, December 22, 2009.

11. *Standard Specifications for Structural Supports for Highway Signs, Luminaires, and Traffic Signals, Fifth Edition*, American Association of State Highway and Transportation Officials (AASHTO), Washington, D.C., 2009.

12. Owings, R. P, Adair, J. W., and Cantor, C., *Safer Sign and Luminaire Supports – Task L – Final Report*, Report No. FHWA-RD-76-36, ENSCO, Inc., Springfield, Virginia, 1975.

13. Steinke, D. P., *FHWA Memorandum HNG-14 for Action: Identifying Acceptable Highway Safety Features*, Federal Highway Administration, Washington, DC, 1997.

14. Putjenter, J. G., Rosenbaugh, S. K., Lechtenberg, K. A., Faller, R. K., Reid, J. D., and Sicking, D. L., *Performance Evaluation of Brass Breakaway Couplings*, Report No. TRP-03-248-10, Midwest Roadside Safety Facility, University of Nebraska-Lincoln, Lincoln, Nebraska, 2011.

15. Rosenbaugh, S. K., Schmidt, T. L., Faller, R.K., and Reid, J. D., *Development of Socketed Foundations for S3x5.7 Posts*, Report No. TRP-03-293-15, Midwest Roadside Safety Facility, University of Nebraska-Lincoln, Lincoln, Nebraska, 2015.

16. Das, B. M., and Sobhan, K., *Principles of Geotechnical Engineering, Ninth Edition*, Cengage Learning, Boston, Massachusetts, 2018.

17. Liao, S., and Whitman, R. V. *Overburden Correction Factor for SPT in Sand*, ASCE Journal of Geotechnical Engineering, Vol. 112, No. 3, 1986, pages 373–377.

18. Skempton, A. W. *Standard Penetration Test Procedures and the Effect in Sands of Overburden Pressure, Relative Density, Particle Size, Aging and Overconsolidation*, Geotechnique, Vol. 36, No. 3, 1986, pages 425–447.

19. Seed, H. B., Arango, I., and Chan, C. K. *Evaluation of Soil Liquefaction Potential during Earthquakes*, Report No. EERC 75–28, Earthquake Engineering Research Center, University of California, Berkeley, Berkeley, California, 1975.

20. Peck, R. B., Hanson, W. E., and Thornburn, T. H., *Foundation Engineering, Second Edition*, Wiley, New York, New York, 1974.

21. Bazaraa, A. R., *Use of the Standard Penetration Test for Estimating Settlements of Shallow Foundations on Sand*, Ph.D. Dissertation, Civil Engineering Department, University of Illinois, Champaign–Urbana, Illinois, 1967.

22. D'Appolonia, D.J., D'Appolonia, E. and Brisette, R.F., *Closure to Discussion of Settlement of Spread Footings on Sand*, ASCE Journal of the Geotechnical Engineering Division, Vol. 96, SM2, 1970, pages 754-761.

23. Denver, H., *Modulus of Elasticity Determined by SPT and CPT*, Proceedings, Second European Symposium of Penetration Testing (ESOPT II), Amsterdam, Netherlands, Vol. 1, 1982, pages 35-40.

24. Imai, T. and Tonouchi, K., *Correlation of N Value with S-wave Velocity and Shear Modulus*, Proceedings, Second European Symposium of Penetration Testing (ESOPT II), Amsterdam, Netherlands, Vol. 1, 1982, pages 67-72.

25. Clayton, C. R. I., Matthews, M. C. & Simons, N. E., *Site Investigation, Second Edition*, Blackwell, Oxford, 1995.

26. Bowles, J.E., *Foundation Analysis and Design, Fourth Edition*, McGraw-Hill, New York, New York, 1988.

27. Wolff, T.F., *Pile capacity prediction using parameter functions*, ASCE Geotechnical Special Publication No. 23, 1989, pages 96-107.

28. Hatanaka, M. and Uchida, A., *Empirical correlation between penetration resistance and internal friction angle of sandy soils*, Soils and Foundations, Vol. 36, No. 4, 1996, pages 1-9.

29. Mayne, P.W., Christopher, B.R., and DeJong, J., *Manual on Subsurface Investigations*. National Highway Institute Publication No. FHWA NHI-01-031, Federal Highway Administration, Washington, D.C., 2001.

30. Japan Road Association (JRA), *Specifications for highway bridges*, Part IV. 1990.

31. LS-DYNA, Livermore Software Technology Corporation, Livermore, California, 2021.

32. Hallquist, J.O., *LS-DYNA Keyword User's Manual*, LS-DYNA R7.1, Livermore, CA: Livermore Software Technology Corporation, 2007.

33. Coon, B.A. and Reid, J.D., *Dynamic Impact Testing of Guardrail Posts Embedded in Soil*, Report No. TRP-03-77-98, Midwest Roadside Safety Facility, University of Nebraska-Lincoln, Lincoln, Nebraska, 1999.

34. Pajouh, M. A., Schmidt, J., Bielenberg, R. W., Reid, J. D., and Faller, R. K., *Simplified Soil-Pile Interaction Modeling under Impact Loading*, Geotechnical Earthquake Engineering and Soil Dynamics V, American Society of Civil Engineers, Reston, Virginia, 2018, pages 269-280.

35. Wu, W., and Thomson, R., *A Study of the Interaction between a Guardrail Post and Soil during Quasi-Static and Dynamic Loading*, International Journal of Impact Engineering, Vol. 34, Issue 5, 2007, pages 883–898. doi:10.1016/j.ijimpeng.2006.04.004

36. Bligh, R. P., Seckinger, N.R., Abu-Odeh, A.Y., Roschke, P.N., Menges, W.L., and Haug, R R., *Dynamic Response of Guardrail Systems Encased In Pavement Mow Strips*, Report No. FHWA/TX-04/0-4162-2, Texas Transportation Institute, College Station, Texas, 2004.

37. Asadollahi Pajouh, M., Bielenberg, R.W., Schmidt, J.D., Lingenfelter, J.L., Faller, R.K., and Reid, J.D., *Placement of Breakaway Light Poles Located Directly behind Midwest Guardrail System (MGS)*, Report No. TRP-03-361-17, Midwest Roadside Safety Facility, University of Nebraska-Lincoln, Lincoln, Nebraska, 2017.

38. *Construction Manual for Highway Construction*, American Association of State Highway and Transportation Officials (AASHTO), Washington, D.C., 1990.

39. Society of Automotive Engineers (SAE), *Instrumentation for Impact Test – Part 1 – Electronic Instrumentation*, SAE J211/1 MAR95, New York City, New York, July 2007.

40. Aubram, D., *Development and experimental validation of an arbitrary Lagrangian-Eulerian (ALE) method for soil mechanics*, Geotechnik, Vol. 38, Issue 3, 2015, pages 193-204.

41. Aubram, D., Rackwitz, F., and Savidis, S., *Contribution to the Non-Lagrangian Formulation of Geotechnical and Geomechanical Processes, Holistic simulation of geotechnical installation processes*, T. Triantafyllidis, Springer International Publishing, Cham, 2017, pages 53-100.

42. Wang, D., Bienen, B., Nazem, M., Tian, Y., Zheng, J., Pucker, T., and Randolph, M., *Large deformation finite element analyses in geotechnical engineering*, Computers and Geotechnics, Vol. 65, 2015, pages 104-114.

43. Agarwal, S., Senatore, C., Zhang, T., Kingsbury, M., Iagnemma, K., Goldman, D. I., and Kamrin, K., *Modeling of the interaction of rigid wheels with dry granular media*, Journal of Terramechanics, Vol. 85, 2019, pages 1–14.

44. Alejano, L., and Bobet, A., Drucker–Prager Criterion, *Rock Mechanics and Rock Engineering*, Vol. 45, Issue 6, 2012, pages 995–999.

45. Wright, A., *Tire/Soil Interaction modeling within a virtual proving ground environment*, Ph.D. Dissertation, Cranfield University, 2012.

46. Murray, Y., *Users manual for LS-DYNA concrete material model 159*, U.S. Department of Transportation, McLean, VA, 2007.

47. Murray, Y., Abu-Odeh, A., and Bligh, R., *Evaluation of LS-DYNA concrete material model 159*. U.S. Department of Transportation, McLean, VA, 2007.

48. AuYeung, S., and Alipour, A., *Evaluation of AASHTO Suggested Design Values for Reinforced Concrete Bridge Piers Under Vehicle Collisions*, Transportation Research Record: Journal of the Transportation Research Board (2592), 2016, pages 1-8.

49. Coughlin, A., Musselman, E., Schokker, A., and Linzell, D., *Behavior of portable fiber reinforced concrete vehicle barriers subject to blasts from contact charges*, International Journal of Impact Engineering, Vol. 37, Issue 5, 2010, pages 521-529.

50. Sharma, H., Gardoni, P., and Hurlebaus, S., *Probabilistic demand model and performance-based fragility estimates for RC column subject to vehicle collision*, Engineering Structures, Vol. 74, 2014, pages 86-95.

51. Hallquist, J., *LS-DYNA Theoretical Manual*, Livermore Software Technology Corporation, Livermore, CA, 10–82–10–102, 2014.

52. *LS-DYNA Keyword User's Manual (r:13107)*, Livermore Software Technology Corporation, Livermore, CA, 10–82–10–102, 2020.

53. Cowper, G., and Symonds, P., *Strain Hardening and Strain-Rate Effects in the Impact Loading of Cantilever Beams*, Report No. 28, Brown University Division of Applied Mathematics, Providence, Rhode Island, 1957.

54. Symonds, P. S., *Survey of methods of analysis for plastic deformation of structures under dynamic loading*, Division Engineering Report BU/NSRDC/1–67, Brown University, 1967.

55. Schrum, K., Sicking, D., Faller, R., and Reid, J., *Predicting the Dynamic Fracture of Steel via a Non- Local Strain Energy Density Failure Criterion*, Final Report to Federal Highway Administration, Report No. TRP-03-311-14, Midwest Roadside Safety Facility, University of Nebraska-Lincoln, Lincoln, Nebraska, 2014.

56. Challa, R., and Yim, S., *Finite Element and Smoothed Particle Hydrodynamics Modeling of Fluid–Structure Interaction Using a Unified Computational Methodology*, Journal of Offshore Mechanics and Arctic Engineering, Vol. 140, Issue 6, 2018.

57. Fang, C., Yosef, T., Linzell, D., and Rasmussen, J., *Residual Axial Capacity Estimates for Bridge Columns Subjected to Combined Vehicle Collision and Air Blast*, Journal of Bridge Engineering, Vol. 26, Issue 7, 2021.

58. Fang, C., Yosef, T., Linzell, D., and Rasmussen, J., *Computational modeling and dynamic response of highway bridge columns subjected to combined vehicle collision and air blast*, Engineering Failure Analysis, 125, 105389, 2021.

59. Reid, J., Bielenberg, R., and Ginger, C., *LS-DYNA Modeling Enhancement Support. Final Report to Midwest States Regional Pooled Fund Program*, Report No. TRP-03-357-17, Midwest Roadside Safety Facility, University of Nebraska-Lincoln, Lincoln, Nebraska, 2017.

60. Reid, J., Lechtenberg, K., and Stolle, C., *Developments of advanced Finite Element Models for Cable Barrier Wire Rope*, Final Report to Mid-America Transportation Center, Report No. TRP-03-233-10, Midwest Roadside Safety Facility, University of Nebraska-Lincoln, Lincoln, Nebraska, 2010.

61. Stolle, C., and Reid, J., *Development of a wire rope model for cable guardrail simulation*, International Journal of Crashworthiness, Vol. 16, Issue 3, 2011, pages 31-41.

62. Deladi, E., *Static friction in rubber-metal contacts with application to rubber pad forming processes*, Ph.D. Dissertation, University of Twente, 2006.

63. Chen, H., *An Introduction to *CONSTRAINED_BEAM_IN_SOLID*, Technical Memo, Livermore Software Technology Corporation, 2016.

64. Chatterjee, K., Choudhury, D., and Poulos, H., *Seismic analysis of laterally loaded post under influence of vertical loading using finite element method*, Computers and Geotechnics, Vol. 67, 2015, pages 172-186.

65. Mongiardini, M., Ray, M., Plaxico, C., and Anghileri, M., *Procedures for verification and validation of computer simulations used for roadside safety applications*. Final Report to the National Cooperative Highway Research Program (NCHRP), NCHRP Report No. W179, Project No. 22-24, Worcester Polytechnic Institute, 2010.

66. Lee, W., *Numerical modeling of blast-induced liquefaction*, Ph.D. Dissertation, Bingham Young University, Provo, Utah, 2006.

67. Yuan, Jian Song, and Muhammad NS Hadi, *Friction coefficient between FRP pultruded profiles and concrete*, Materials and Structures, 51.5, 2018, 120.

68. Rabbat, B. G., and H. G. Russell, *Friction coefficient of steel on concrete or grout*, Journal of Structural Engineering, 111.3, 1985, pages 505-515.

69. *Proposed AASHTO Guidelines for Implementation of MASH Sign Supports, Breakaway Poles, and Work Zone Traffic Control Devices, Interim Report No. 1*, NCHRP 22-43, University of Nebraska-Lincoln and George Mason University and, March 2021.

70. *Proposed AASHTO Guidelines for Implementation of MASH Sign Supports, Breakaway Poles, and Work Zone Traffic Control Devices, Interim Report No. 2*, NCHRP 22-43, University of Nebraska-Lincoln and George Mason University and, January 2022.

71. *Proposed AASHTO Guidelines for Implementation of MASH Sign Supports, Breakaway Poles, and Work Zone Traffic Control Devices, Interim Report No. 2*, NCHRP 22-43, University of Nebraska-Lincoln and George Mason University and, August 2023.

72. *Application of MASH Test Criteria to Breakaway Sign and Luminaire Supports and Crashworthy Work-Zone Traffic Control Devices, Interim Report No. 2*, NCHRP 03-119. George Mason University and University of Nebraska-Lincoln, January 2021.

Appendices

Appendix A General Design Guidelines State DOT Review

The data provided in this appendix was compiled by Mr. Taylor Drahota in partial fulfillment of his appointment in the University of Nebraska-Lincoln Undergraduate Creative Activities and Research Experiences (UCARE) program, and is supplementary to Sections 2.5.1 and 2.5.2.

Connecticut Data Source:

https://portal.ct.gov/DOT/CONNDOT/SECTION-M15#M.15.04

M.15.04—**Light Standards:** (anchor base and transformer base), (aluminum).

(a) General: Each light standard with appurtenances attached thereto shall be fabricated of aluminum alloy, designed and constructed in accordance with the plans and current requirements of AASHTO "Standard Specification for Structural Support for Highway Signs, Luminaires and Traffic Signals." Light standards with brackets and luminaires shall be designed to withstand a wind speed of 90 mph (145 kilometers per hour).

(b) Base: Light standard with transformer base shall conform to the breakaway requirements of the current AASHTO "Standard Specifications for Structural Support for Highway Signs, Luminaires and Traffic Signals" and shall be identified with visible markings. The transformer base shall be approximately 17 inches (430 millimeters) high with a door having an approximate opening of 9 inches x 12 inches (250 millimeters x 300 millimeters).

A bonding lug shall be provided in each transformer base and each anchor base shaft shall have the handhole frame or anchor base tapped for bonding. All castings shall be clean and smooth with all details well-defined and true to pattern. It shall be the Contractor's responsibility to verify existing bolt circle diameters by field checking that the bolt circle of the light standard base will match the anchor base on the foundation or structure.

Figure A.1 Connecticut DOT Light Standards

Delaware Data Source:

https://deldot.gov/Business/drc/pdfs/traffic/LightingPolicy.pdf?cache=1599176213610

5.A.1.d Foundations

The DelDOT standard Type 6 pole base shall be considered typical for the installation of DelDOT road level light poles. However, structural analysis should be completed for nonstandard longer arm lengths or pole heights. If soil conditions are known to be poor in the area, additional structural analysis is needed.

There is no standard for a high mast light pole foundation. As such, the foundation design for these poles shall be completed by a structural engineer and shall be coordinated with the DelDOT Bridge Section.

For poles that require foundation designs, the lighting designer shall coordinate with DelDOT's Geotechnical Engineer to determine if soil information is available for the project location. If soil data is not available for the project location, the lighting designer should submit a soil boring request to DelDOT's Geotechnical Engineer for any DelDOT projects. A sample of a soil boring request form can be found in **Appendix Y**. The number of soil borings necessary for the project should be coordinated with DelDOT's Geotechnical Engineer. The cost of the soil borings should be included in project estimates.

Figure A.2 Delaware DOT Type 6 Pole Base

Florida Data Source:

https://fdotwww.blob.core.windows.net/sitefinity/docs/default-source/roadway/ds/18/ids/ids-21200.pdf?sfvrsn=29e0f9eb_2

Design Assumptions and Limitations

Use this Index with Indexes 420, 422, 423, 425, 427, 428, 820, 821, 5210, and 5212 as appropriate.

Anchor Bolts were designed for Design Wind, Bridge Deck Height (above MLW), Luminaire Mounting Height, and Luminaire Arm Lengths of Standard (Index 17515), Light Poles.

Design of the additional bridge deck reinforcement is based on the minimum transverse top deck reinforcing required by the ***SDG***.

The pedestal and supporting deck are designed to accommodate Load Case 2; which is an Index 17515 Standard Light Pole with a 50 ft. mount height, 170 mph wind speed, located on a 75 ft. high bridge deck (above ground or MLW) with a 15 ft. arm. Load case 2 requires 4~1 ¼" diameter anchor bolts. Load Case 1 requires 4~1" diameter anchor bolts.

The working loads at the top of the pedestal for Load Case 2 are:

Axial Dead Load = 1.56 kip
Wind Load Moment about Transverse Axis = 40.6 kip-ft
Wind Load Moment about Longitudinal Axis = 28.3 kip-ft
Dead Load Moment about Longitudinal Axis = 1.69 kip-ft
Torsion about Pole Axis = 3.56 kip-ft
Maximum Shear = 1.38 kip

Locate pedestals near to substructure support to minimize vibration of the light poles due to traffic live loads. Locate the centerlines of pedestals a minimum 3'-10" away from centerlines of open joints in railings and ends of railings.

Commentary: Use of this Index with Index 424 (Corral Shape) Traffic Railings is not recommended because the Standard Corral Shape Railing cannot accommodate the required electrical conduit and embedded junction boxes (EJB's).

Figure A.3 Florida DOT Light Pole Design Assumptions

Illinois Data Source:

http://www.idot.illinois.gov/Assets/uploads/files/Doing-Business/Manuals-Split/Design-And-Environment/BDE-Manual/Chapter%2056%20Highway%20Lighting.pdf

56-3.01 Foundations and Mounting

In conventional highway lighting applications, luminaire assemblies generally are attached to davit or mast-arm poles mounted along the roadway either on ground foundations or atop bridge parapets or barriers. Foundations for conventional light poles may be either reinforced concrete or steel helix foundations and are constructed from typical designs. However, concrete foundations for light towers in high-mast lighting applications require special designs and soil analyses to determine adequate foundation depth. Depending on factors such as roadside location, most conventional light poles will be mounted on frangible devices (breakaway supports). Attach light poles that are mounted atop parapets and barriers or behind guardrail to foundations with high-strength, non-breakaway bolts. Use special vibration isolating materials to mount light poles on bridges. Where feasible at signalized intersections, a roadway luminaire may be mounted on a combination mast-arm assembly and pole using approved combination structures.

Luminaires mounted in underpasses and tunnels are either attached directly to the wall adjacent to or hung from vibration-dampening pendants at the edge of the travel lanes. Light sources that are used to externally illuminate overhead sign panels typically are fastened to the truss or cantilever support structure.

Waterway and aviation obstruction warning luminaires are attached directly to the structures representing the hazard. Ensure the location and installation of warning luminaires for waterway and aviation also meet the requirements of Section 56-2.11.

Figure A.4 Illinois DOT Foundations and Mounting General Notes

Foundation Height Relative to Final Grade. For other than light towers, ensure pole foundations are no more than 0.5 in (13 mm) higher than the high edge of the surrounding final grade and in compliance with Figure 56-5.J. This permits proper drainage around the foundation and reduces the likelihood of the foundation intensifying a collision. The foundation also is less likely to be destroyed during a collision. When located within the clear zone, ensure that the foundation and fractured breakaway support does not protrude more than 4 in (100 mm) above the finished grade within a 5 ft (1.5 m) chord as noted in 56-5.05(a)2(c) above. See Chapter 38 for additional information on clear zones.

Metal Foundations. The steel (i.e., helix screw-in type) foundation is one that is commonly used by the Department for conventional light poles. This foundation is placed in undisturbed earth using a clockwise rotation similar to a common screw. The metal tube is typically 8 in (200 mm) in diameter and 6 ft to 8 ft (1.8 m to 2.4 m) long. Shorter lengths may be appropriate for foundations in areas with shallow bedrock. The metal foundation will accommodate poles with 11.5 in and 15 in (292 mm and 381 mm) bolt circles for luminaire mounting heights up to 50 ft (15.2 m).

Light Tower Foundations. Foundations for light towers used in high-mast lighting applications typically require specialized designs and soil surveys to ensure adequate support. A 4-ft (1.2-m) diameter reinforced concrete foundation, to a depth as required by the soils analysis, usually is adequate for towers accommodating 80 ft to 110 ft (24.4 m to 33.5 m) luminaire mounting heights. The top 18 in (450 mm) of the foundation is formed. Below this depth, ensure that the foundation is poured monolithically against the undisturbed earth of the bored hole. Specify the foundation depth on the lighting plans. Additionally, include a level concrete work pad at the base of the tower.

Figure A.5 Illinois DOT Grade and Dimension Considerations

Kansas Data Source:

https://www.bpu.com/SearchResults.aspx?Search=Unified+Government+%26+Board+of+Public+Utilities+Street+Lighting+Equipment+%26+Material+Specifications

c. **Pole and Luminaire Erection On Concrete Foundations:** No sooner than five (5) days after construction of the foundation, a nut and washer shall be installed on each anchor bolt. The 30' or 35' pole will be mounted to a breakaway transformer base using nuts, bolts, and washers as recommended by the pole manufacturer. Using the lower nuts, the pole shall be brought into vertical alignment (plumb), the top nuts tightened, and the anchor bolt covers installed. The opening between the pole base and the foundation shall be taped and grouted. Transformer bases access doors shall be situated so that they are on the house side, or opposite side from the adjacent traffic. For poles installed in a median, the transformer doors should be oriented away from one direction of oncoming traffic, facing North or East.

Figure A.6 Kansas DOT Luminaire on Concrete Foundation

Louisiana Data Source:

http://wwwsp.dotd.la.gov/Inside_LaDOTD/Divisions/Engineering/Bridge_Design/BDEM_Guidelines/Guide%20to%20Constructing,%20Operating,%20and%20Maintaining%20Highway%20Lighting%20Systems.pdf

iii. Light Poles & Foundations-Light poles shall be manufactured from steel, aluminum, fiberglass or other corrosion resistant materials. Wood poles are not acceptable; however, lights may be installed on existing wood utility poles provided the system conforms to all illumination requirements of these standards; Poles and foundations shall be designed to withstand wind velocities for the area where the poles are installed. The design wind velocities shall be for the 25 year mean recurrence interval; Pole foundations shall be flush with the existing ground. On slopes, the longitudinal centerline shall be flush with the existing ground; A 6 foot diameter X 4" thick concrete mowing apron shall be placed around each light pole. The apron shall be constructed flush with the ground line; Light poles located within 40 feet of the roadway shall conform to AASHTO criteria for breakaway supports or shall be located such that they are protected from vehicular collision. The above may be excepted by the DOTD where a greater hazard would be created by falling poles.

Figure A.7 LaDOTD General Design Notes

Maine Data Source:

https://www.maine.gov/mdot/contractors/publications/standardspec/docs/2014/StandardSpecification-full.pdf

" No foundation design will be required for 18- and 24-inch diameter foundations for structures less than 30-feet tall and with no projecting arms. A foundation design prepared by a Professional Engineer licensed in accordance with the laws of the State of Maine will be required for all other foundations Precast foundations will be permitted for 18 and 24-inch diameter foundations for structures less than 30-feet tall and with no projecting arms. Where precast foundations are permitted flowable concrete fill shall be used as backfill in the annular space, and placed from the bottom up. Construction of precast foundations shall conform to the Standard Details and all requirements of Section 712.061 except that the concrete shall have a minimum permeability of 17 kOhm-cm and the use of calcium nitrite will not be required. "

Figure A.8 Maine DOT General Foundation Guidelines

634.024 Light Standards The terms "conventional standard" or "conventional light standard" shall mean the assembled metal base flange, transformer base or breakaway device, metal columnar shaft, metal overhanging bracket arm and incidental hardware.

The term "high mast pole" shall mean the assembled base plate flange, metal columnar shaft, luminaire tenon, mounting and lowering device and incidental hardware. For purposes of this specification, a structure shall be considered a high mast pole if the pole height, from base plate to the center of the luminaire, exceeds 55 feet.

The design, materials and fabrication of Light Standards shall meet the requirements of the current edition of AASHTO "LRFD Specifications for Structural Supports for Highway Signs, Luminaires, and Traffic Signals" and interims thereto, as noted below except as otherwise indicated within these specifications or on the plans.

Figure A.9 Maine DOT Light Standard Notes

Minnesota Data Source:

http://www.dot.state.mn.us/trafficeng/lighting/2010_Roadway%20Lighting_Design_Manual2.pdf

2.2.3 Light Bases/Foundations

In order to adequately support the lighting structure, the foundation must be designed to support the weight of the structure as well as resist wind loads and vibrations. The four standard light bases that Mn/DOT uses are P, E, H, and tower. Poles mount on the bases according to the pole height as follows:

- P Base (concrete or steel): ≤ 20 foot poles
- E Base (concrete or steel): ≤ 40 foot poles
- H Base (concrete): ≤ 49 foot poles (Steel H Base design not approved at this time)

These light bases and the anchorage for light standards mounted on a bridge or median barrier are detailed in the Mn/DOT Standard Plates Manual. Standard Plates 8127 and 8128 describe bases E and H respectively and are located in the Appendix. A detail sheet for the P type base is also included in the Appendix. A tower base detail sheet is included in the 35W sample plan located in Chapter 6. Pole anchorages in a median

Figure A.10 Minnesota DOT Standard Foundation Types

New Hampshire Data Source:

https://www.nh.gov/dot/org/projectdevelopment/highwaydesign/specifications/documents/2016NHDOTSpecBookWeb.pdf

SECTION 625 -- LIGHT POLE BASES

Description

1.1 This item shall consist of concrete light pole bases constructed at the locations and of the design shown on the plans or as ordered.

Materials

2.1 Concrete shall be Class B conforming to Section 520.

2.2 Granular backfill shall be gravel conforming to 209.2.1.2.

Construction Requirements

3.1 Light pole bases shall be either precast or cast in place.

3.1.1 When precast bases are used, the hole shall be dug wide enough to allow for proper placement and compaction of the required backfill. The bases shall be placed on a prepared surface which shall provide a firm foundation. Where rock or unstable soil is encountered, the material shall be excavated 6" below the bottom of the base, and granular backfill placed and compacted in place of the excavated material.

3.1.2 When bases are to be cast in place, the holes shall be dug wide enough to allow the placement of concrete of the required diameter. Except when solid rock is encountered, the excavation shall be made to the full depth required on the plans. When solid rock is encountered, the bottom of the hole shall be at least 3 ft. from the top of the base and the concrete shall be firmly bonded to the rock with approved anchor rods. Forms will be required for the top of the light pole base only to a minimum distance of 12" below the finished grade of the ground at the base. Sufficient excavation shall be made about that elevation to allow the proper placement of the forms and the proper placement and compaction of the required backfill.

3.2 After the precast bases have been set, or after the removal of the forms for cast-in-place bases, granular backfill shall be placed in the entire space outside the bases, to the level of the finished grade unless otherwise ordered. Backfill shall be made in layers not greater than 6", with each layer thoroughly compacted.

Method of Measurement

4.1 Light pole bases will be measured by the number of units installed.

4.1.1 When more than 3 ft. of conduit, measured horizontally, is required to be installed from the center of the base, the first 3 ft. will be subsidiary.

Figure A.11 New Hampshire DOT Light Pole Base Considerations

New Jersey Data Source:

https://www.state.nj.us/transportation/eng/documents/BSDM/pdf/2016DesignManualforBridgesandStructures20180604.pdf

36.4 Foundations

1. The *NJDOT Standard Electrical Details* should be referred to for foundation detailing. If existing soil appears to be unstable (soft, wet, compressible, muck, etc.), and may not support the foundation and handle construction equipments, NJDOT Geotechnical Engineering Unit should be contacted. If a unique design is required, the design shall be in accordance with applicable requirements in the *AASHTO Standard Specifications for Structural Supports* as well as in the 17th Edition of the *AASHTO Standard Specifications for Highway Bridges.*
2. At the time of work request, the following information for lighting support structures, on an individual contract basis, will be furnished by the Department's Traffic Signal and Safety Engineering Unit.
   a. Interchange layout showing location of towers by station and offset.
   b. Height of towers and number of luminaires.
   c. If other than 3 inches above existing (or finished) ground line, elevations of the top of concrete pedestals.
3. The Structural Design Engineer shall initially refer to previous construction contracts to review previous borings which may be useful in determining preliminary foundation design. Boring log identification numbers for previous construction contracts shall be shown on the contract plans.
4. The proposed subsurface exploration (see Section 34) at each tower lighting location shall be submitted to the Geotechnical Engineering Unit for approval. One deep boring and one or more shallow borings may be required by the Geotechnical Engineer. Continuous sampling, to a reasonable depth, may be necessary and if so will be ordered by the Geotechnical Engineer.

   Boring requests shall be directed to the Geotechnical Engineering Unit as soon as possible.
5. The foundations of tower lighting support structures that are located on undisturbed soils shall be designed for an allowable soil pressure that is estimated for a differential settlement that shall not exceed ½ inch.

   Careful consideration shall be given to ground water conditions when estimating allowable pressure and settlement of the soil.

   Rotation and displacement of a foundation must be restricted to alleviate the possibility of failure of the structure or its having an unsightly visual appearance. Deep foundations shall be used when soil conditions do not readily and reliably indicate the use of spread footings.

   The foundation design criteria for tower lighting located on embankment fill shall be established with respect to soil bearing capacity and settlement. Consideration must be given to the stability of the embankment with respect to any possible vertical and/or horizontal movements.

   The most important factor to be considered in the foundation design of a lighting support structure is the overturning factor. This will require an adequate provision for passive resistance and upward pull on spread footing and deep foundation design, respectively.
6. Adverse foundation conditions, property lines, subsurface utilities, temporary sheeting, traffic maintenance, and other special conditions which may require individual foundation designs shall be investigated by the Structural Design Engineer at each support structure location.

Figure A.12 New Jersey DOT Foundation General Notes

New York Data Source:

https://www.dot.ny.gov/divisions/engineering/technical-services/geotechnical-engineering-bureau/geotech-eng-repository/GDM_Ch-19_Culverts.pdf

19.2.3 Luminaires

Typical foundation types can be found in the Standard Sheets for Highway Lighting System, specifically Standard Sheet 670-01 *Lamppost Foundations*. The Regional Geotechnical Engineer or the Geotechnical Engineering Bureau should be consulted to determine the proper foundation treatment.

Figure A.13 New York DOT Luminaire Note

Oregon Data Source:

https://www.oregon.gov/ODOT/Engineering/BaselineReport/TM653.pdf

The signal support Standard drawing has been in existence since the Bridge drawing 31006 was released on October 31, 1975. This drawing shows up to four three section heads with an area of 9 ft^2 each that are separated by a minimum of 8 feet and up to four signs with an area of 5 ft^2 that are located 3 feet from each signal head. The foundation was 3 feet in diameter and was 5 feet, 6 feet, or 7 feet in depth. There were different depth and rebar configurations for the foundations over the years. TM653 was released in July 2005 that specified depths for a "Good", "Average", and "Poor" soil and was designed to resist the larger design loads shown on TM650.

The old Standard Drawing foundations were designed using the Rutledge method. The standard soil strength was a value of 1500 psf and this was considered a poor soil condition that could be used in most locations in the State. This design method is shown in Section 13.10 of the 4th Edition AASHTO Standard Specifications for Structural Supports for Highway Signs, Luminaires, and Traffic Signals. Section 13.10 is used for the design embedment of lightly loaded small poles and posts. The new signal poles, especially with the larger loading, are not considered lightly loaded and are not used for signal pole foundation designs.

The original classifications for the soils had a "Good" soil with at least a phi of 35 degrees and an "Average" soil with a phi of 25 degrees. In practice, the signal foundation locations would sometimes come close to the 35 degree phi, but almost never reached this good soil condition. The result was to almost always use the average soil depths with the low phi of 25 degrees. A report was released by the FHWA that stated the signal pole depths appeared excessive and this prompted ODOT to revise the signal pole foundation depths.

In many cases, a boring had to be performed to get the phi of the soil to determine if the soil was "Good, "Average" or "Poor". Having a soils report for the location results in the Geotechnical Engineer having all of the information needed to provide a report and design values for an Engineer to use Section 13.6.1.1 from the 4th Edition AASHTO Standard Specifications for Structural Supports for Highway Signs, Luminaires, and Traffic Signals to calculate embedment depths. This site specific foundation design significantly reduced the foundation depths and provided valuable Geotechnical reports that are used by Contractors during construction.

Figure A.14 Oregon DOT Design Parameters and Considerations

Rhode Island Data Sources:

http://www.dot.ri.gov/documents/about/research/Geotechnical.pdf

15.2 DESIGN

15.2.1 Fatigue Category

The Basic Wind Speed, V, used in the determination of the design wind pressure shall be 130 mph.

All sign and luminaire structures on interstate or limited access type facilities must comply with fatigue category 1 requirements, including galloping, vortex shedding (if applicable), natural wind gusts, and truck-induced gusts. The truck induced loading shall be based on a 65 mph velocity.

All sign, traffic signal, and luminaire structures on all other roadways must comply with fatigue category 2 requirements, including galloping, vortex shedding (if applicable), natural wind gusts, and truck-induced gusts. The truck induced loading shall be based on a 30 mph velocity.

Figure A.15 Rhode Island DOT design procedure values

Rhode Island Data Sources (continued):

http://www.dot.ri.gov/documents/doingbusiness/Compilation_of_Approved_Specifications_2016.pdf

M.15.06.2 Light Standard Foundation.

a. Concrete. Light standard foundations may be cast in place or precast units. Cast-in-place units shall be constructed of Class A(AE) cement concrete masonry. Precast units shall be constructed of Class XX(AE) cement concrete masonry.

Cement concrete masonry shall conform to the applicable provisions of **SECTION 601** of these Specifications.

b. Steel Reinforcement. Steel reinforcement shall conform to the requirements of **Subsection M.05.01.**

c. Anchor Bolts. Anchor bolts shall be high strength steel having a minimum yield of 55,000 psi. They shall be 1 inch in diameter by 66 inches long, with a 4-inch L bend on the unthreaded end. Each anchor bolt shall have cut or rolled thread 6 inches long. These threads shall be one inch-8 National Coarse Class 2 fit. A hexagon nut and leveling washers shall be furnished with each bolt. The anchor bolt, washers and the hexagon nut shall be hot dipped galvanized conforming to ASTM A153.

Anchor bolts for roadway lighting are to be provided and set according to templates furnished by the manufacturer.

Anchor bolts for bridge lighting are to be furnished as detailed on structural drawings.

d. Steel Conduit. Steel conduit, elbows, and fittings shall conform to the provisions of **Subsection M.15.04** of this Section.

e. Breakaway Support Couplings. The breakaway support couplings shall be the same as those manufactured by Manitoba Safe-T-Base of Winnipeg, Canada, or an approved equal.

Figure A.16 Rhode Island Light Standard Foundation Notes

Vermont Data Source:

https://outside.vermont.gov/agency/VTRANS/external/docs/construction/02ConstrServ/PreContract/2018SpecBook/2018%20Standard%20Specifications%20for%20Construction.pdf

Street Lights shall be designed to withstand an equivalent wind load of 100 mph velocity with an allowable angular deflection of 70 arc minutes or less.

All wiring shall meet the current *National Electrical Code*.

Street lighting design shall conform to the current edition of the *AASHTO Standard Specifications for the Structural Supports for Highway Signs, Luminaires and Traffic Signals* and its latest revisions.

Figure A.17 Vermont DOT Design Notes

Appendix B Characterization of Soil Parameters State DOT Review

The data provided in this appendix was compiled by Mr. Taylor Drahota in partial fulfillment of his appointment in the University of Nebraska-Lincoln Undergraduate Creative Activities and Research Experiences (UCARE) program, and is supplementary to Sections 2.5.1 and 2.5.3. Figure B-1 graphically summarizes the general ranges of friction angles versus SPT blow count values observed across state DOTs with boxes having different edge colors. Similarly, Figure B-2 graphically summarizes the general ranges of undrained shear strength versus SPT blow count values.

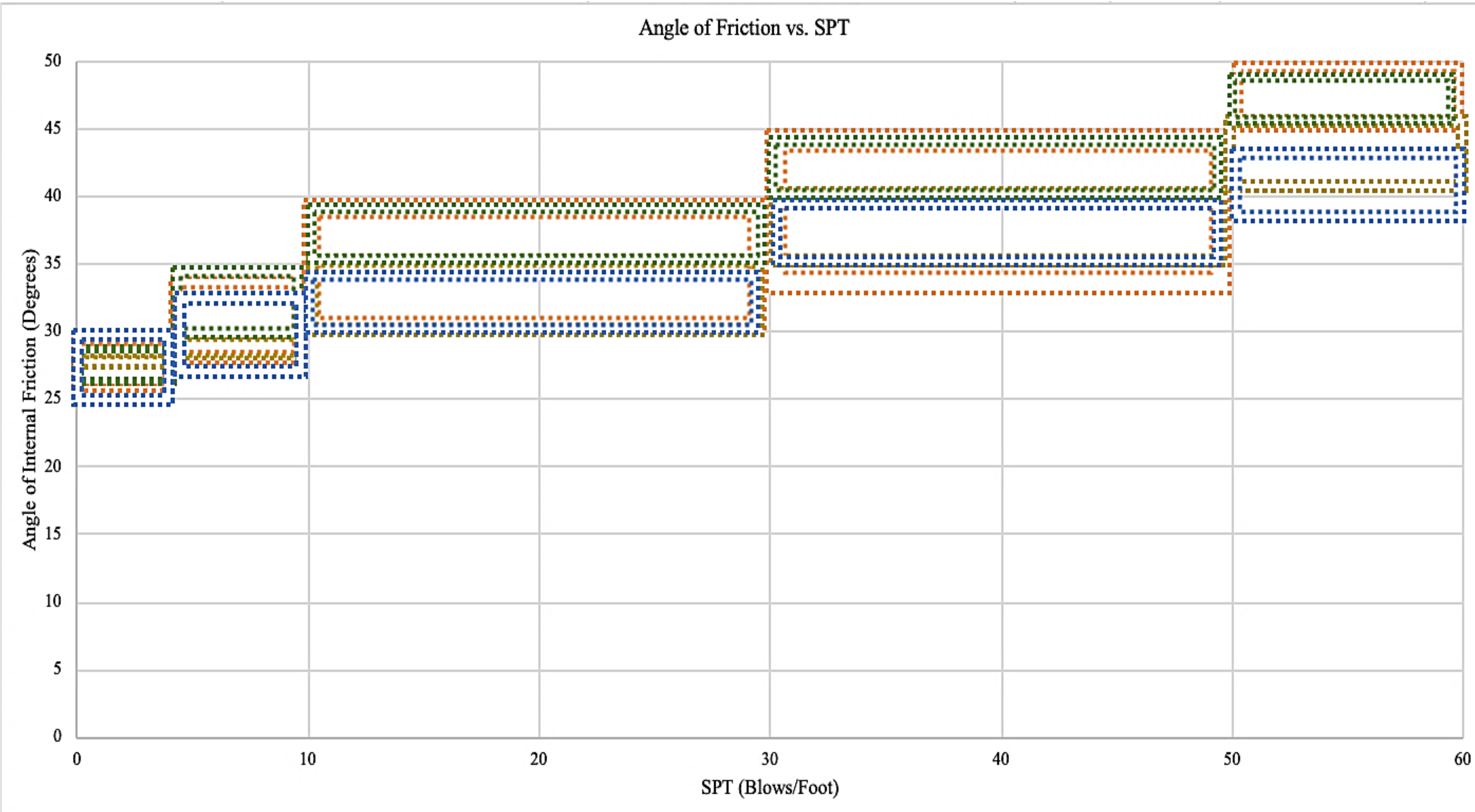

Figure B.1 DOT Recommended Friction Angle vs. SPT Ranges

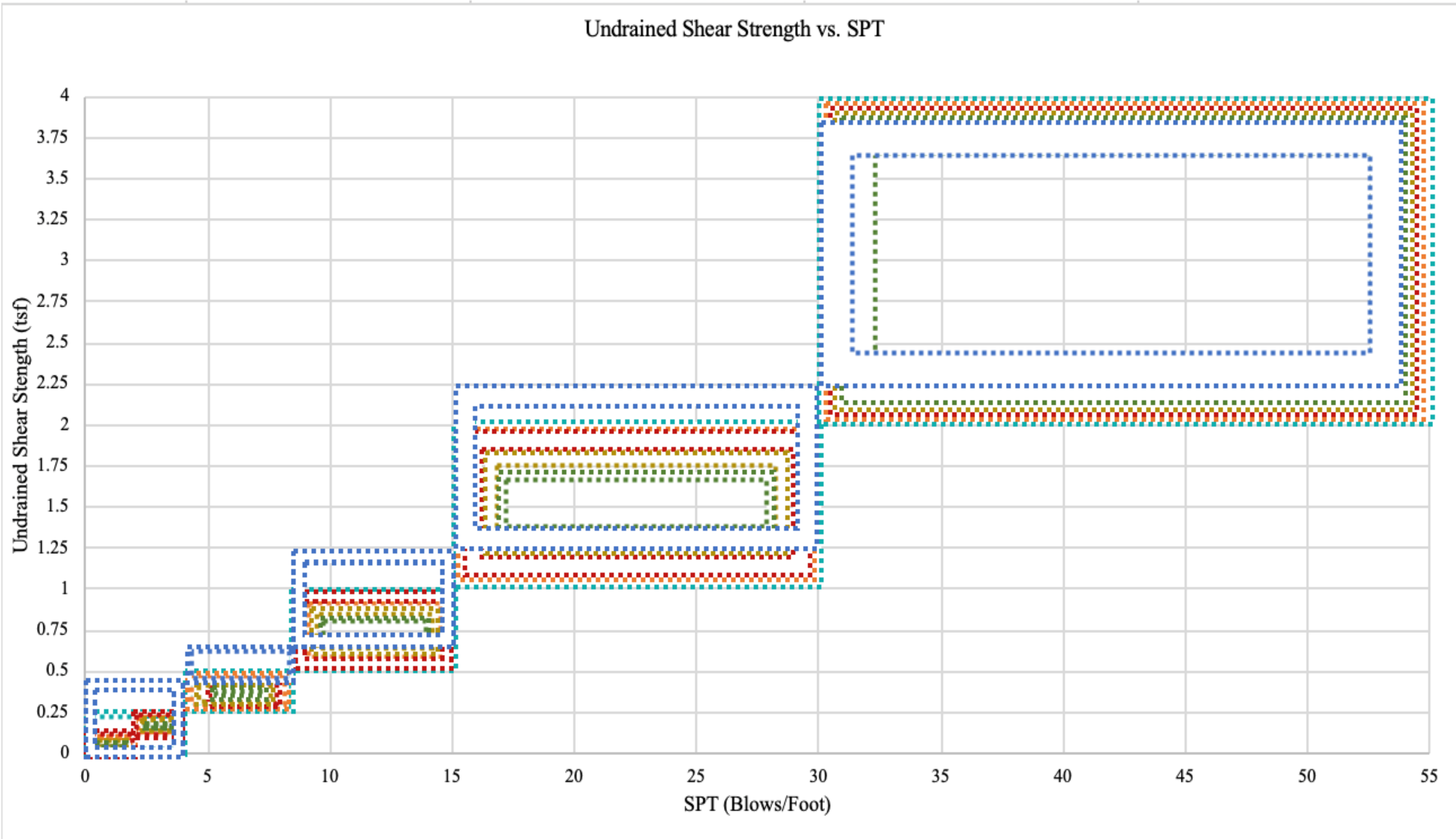

Figure B.2 DOT Recommended Undrained Shear Strength vs. SPT Ranges

Alaska Data Source:

http://stsp.alaska.gov/stwddes/desmaterials/assets/pdf/geo_man/geotechmanual_all_07.pdf

Table 3-1
Criteria for Describing Consistency
(ASTM D 2488 Table 5)

Description	Criteria
Very soft	Thumb will penetrate soil more than 1 inch.
Soft	Thumb will penetrate soil about 1 inch.
Firm	Thumb will indent soil about ¼ inch.
Hard	Thumb will not indent soil. Thumbnail readily indents soil.
Very hard	Thumbnail will not indent soil.

Table 3-2
Criteria for Describing Dry Strength
((ASTM D 2488 Table 8)

Description	Criteria
None	The dry specimen crumbles into powder with mere pressure of handling.
Low	The dry specimen crumbles into powder with some finger pressure.
Medium	The dry specimen breaks into pieces or crumbles with considerable finger pressure.
High	The dry specimen cannot be broken with finger pressure. Specimen will break into pieces between thumb and a hard surface.
Very high	The dry specimen cannot be broken between the thumb and a hard surface.

Figure B.3 Alaska DOT Soil Consistency Criteria

Table 5-4
Density Based on Blow Count for Non-Cohesive Soils
(Adapted from several sources)

Number of blows per foot	Density
0-4	Very loose
5-10	Loose
11-30	Medium dense
31-50	Dense
>50	Very dense

Table 5-5
Consistency Based on Blow Count for Cohesive Soils
(Adapted from several sources)

Number of blows per foot	Consistency
<2	Very soft
2-4	Soft
5-8	Firm
9-15	Stiff
16-30	Very stiff
>30	Hard

Figure B.4 Alaska DOT SPT Correlations

California Data Sources:

https://dot.ca.gov/-/media/dot-media/programs/engineering/documents/geotechnical-services/soil-correlations-mar2013-a11y.pdf

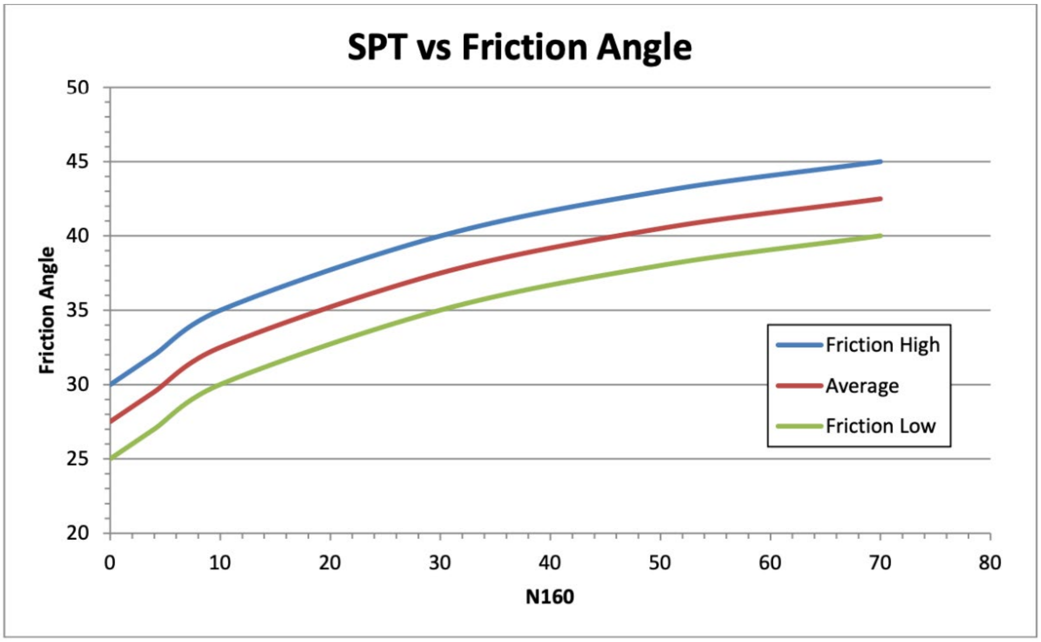

Figure B.5 California DOT SPT vs. Angle of Friction for Granular Soils

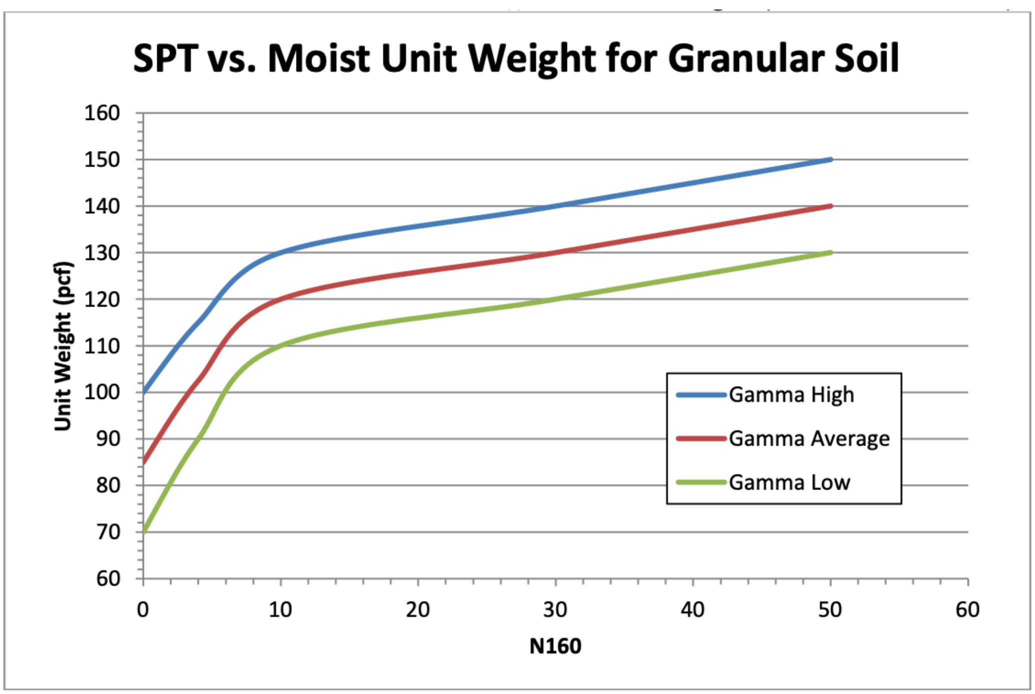

Figure B.6 California DOT SPT vs. Unit Weight Cohesionless Soil

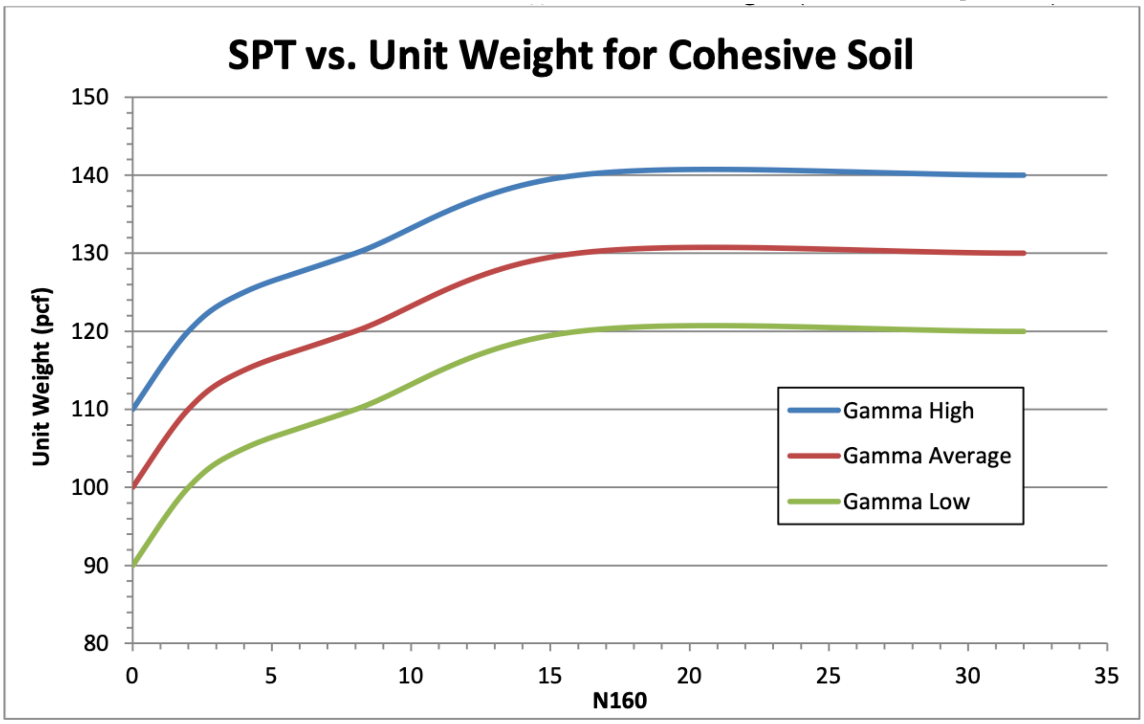

Figure B.7 California DOT SPT vs. Unit Weight Cohesive Soil

Connecticut Data Source:

https://portal.ct.gov/-/media/DAS/OEDM/2016-CD-HO/2016_sp_cd_soils_and_foundations_2_slide.pdf?la=en

CLASS OF MATERIALS	ALLOWABLE FOUNDATION PRESSURE (psf)[d]	LATERAL BEARING (psf/f below natural grade)[d]	LATERAL SLIDING	
			Coefficient of friction[a]	Resistance (psf)[b]
1. Crystalline bedrock	12,000	1,200	0.70	—
2. Sedimentary and foliated rock	4,000	400	0.35	—
3. Sandy gravel and/or gravel (GW and GP)	3,000	200	0.35	—
4. Sand, silty sand, clayey sand, silty gravel and clayey gravel (SW, SP, SM, SC, GM and GC)	2,000	150	0.25	—
5. Clay, sandy clay, silty clay, clayey silt, silt and sandy silt (CL, ML, MH and CH)	1,500[c]	100	—	130

Figure B.8 Connecticut DOT Lateral and Axial Soil Strength Conditions

Florida Data Source:

https://www.fdot.gov/docs/default-source/structures/manuals/SFH.pdf

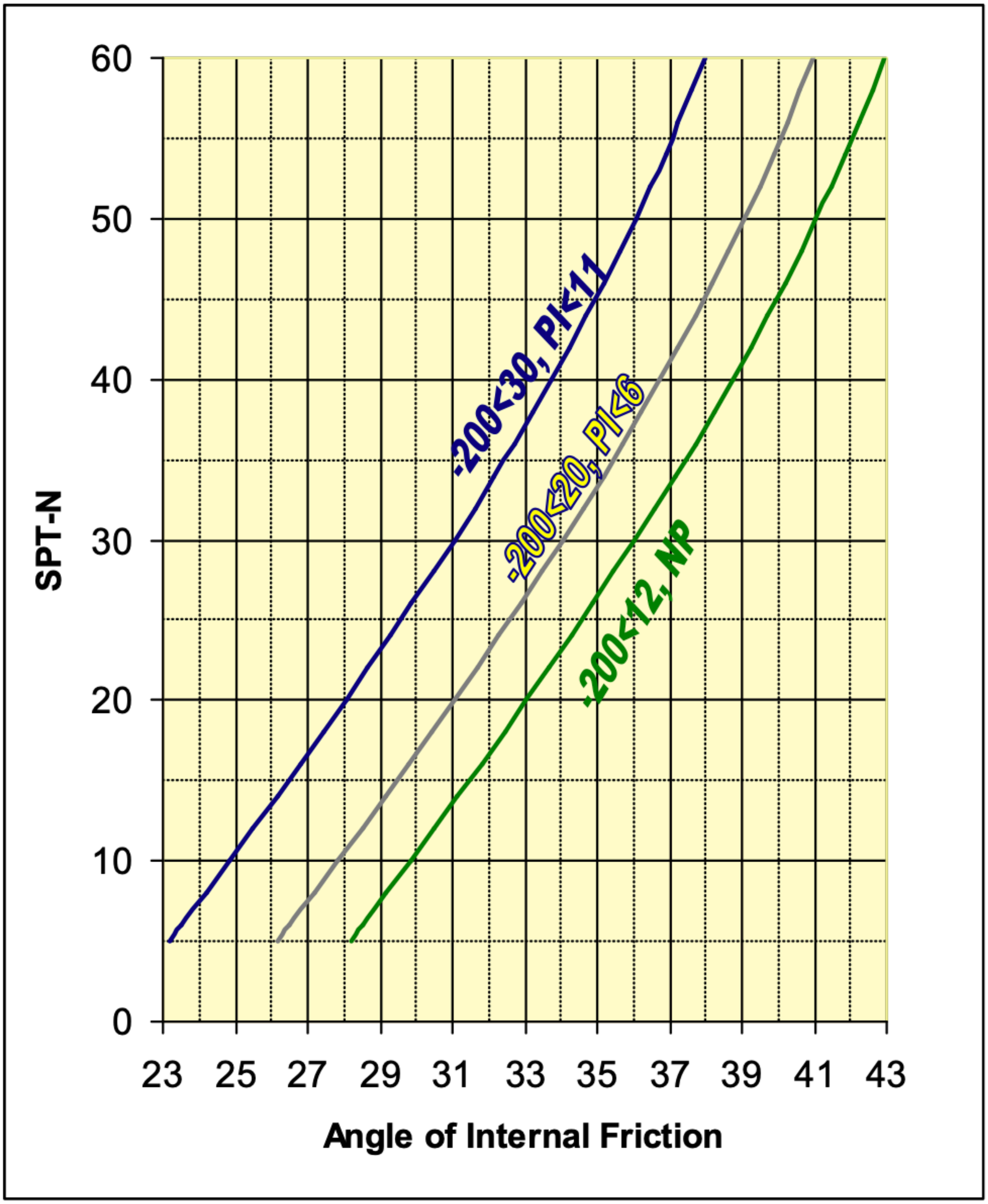

Figure B.9 Florida DOT SPT vs. Internal Angle of Friction

Hawaii Data Source:

https://hidot.hawaii.gov/?s=geotechnical+manual&type=usa

RELATIVE DENSITY / CONSISTENCY

Granular Soils			Cohesive Soils			
N-Value (Blows/Foot)		Relative Density	N-Value (Blows/Foot)		PP Readings (tsf)	Consistency
SPT	MCS		SPT	MCS		
0 - 4	0 - 7	Very Loose	0 - 2	0 - 4		Very Soft
4 - 10	7 - 18	Loose	2 - 4	4 - 7	< 0.5	Soft
10 - 30	18 - 55	Medium Dense	4 - 8	7 - 15	0.5 - 1.0	Medium Stiff
30 - 50	55 - 91	Dense	8 - 15	15 - 27	1.0 - 2.0	Stiff
> 50	> 91	Very Dense	15 - 30	27 - 55	2.0 - 4.0	Very Stiff
			> 30	> 55	> 4.0	Hard

Figure B.10 Hawaii DOT SPT and Soil Density/Consistency

Illinois Data Sources:

http://idot.illinois.gov/Assets/uploads/files/Doing-Business/Manuals-Guides-&-Handbooks/Highways/Materials/Geotechnical%20Manual.pdf

Relative Density and Friction Angle as a Function of the N-Value		
N Value	Relative Density	Friction Angle*, ϕ, Deg.
0 - 4	Very Loose	26 - 30
4 - 10	Loose	28 - 34
10 - 30	Medium Dense	30 - 40
30 - 50	Dense	33 - 45
Over 50	Very Dense	≤ 50
* Lower limits are for fine, clean sand; and should be reduced by up to 5º for silty sands. The upper limits are for coarse clean sands.		

Table 4.4.6.1.2-1 Relative Density and Friction Angle of Cohesionless Soils

Strength and Consistency as a Function of the N-Value		
N Value	Consistency	Strength*, Q_u, tsf
< 2	Very Soft	< 0.25
2 - 4	Soft	0.25 - 0.50
4 - 8	Medium Stiff	0.50 - 1.0
8 - 15	Stiff	1.0 - 2.0
15 - 30	Very Stiff	2.0 - 4.0
> 30	Hard	4.0 - 8.0
* Not an exact conversion.		

Table 4.4.6.1.2-2 Strength and Consistency of Cohesive Soils

Figure B.11 Illinois DOT SPT and Friction Angle/Compressive Strength Correlation

Illinois Data Sources (continued):

http://www.idot.illinois.gov/Assets/uploads/files/Doing-Business/Standards/Highway-Standards/216%20Highway%20Standards%20Complete%20Set.pdf

SHAFT LENGTH TABLE											
SOIL CONSISTENCY		AVERAGE STRENGTH	LIGHT TOWER HEIGHT								
		Qu in tsf (Qu in kPa)	80′ (24 m)	90′ (27 m)	100′ (30 m)	110′ (34 m)	120′ (37 m)	130′ (40 m)	140′ (43 m)	150′ (46 m)	160′ (49 m)
Cohesive	SOFT	< 0.5 (< 50)	20′-6″ (6.2 m)	21′-6″ (6.5 m)	22′-6″ (6.9 m)	24′-0″ (7.2 m)	25′-0″ (7.6 m)	26′-6″ (8.0 m)	27′-6″ (8.3 m)	28′-6″ (8.7 m)	30′-0″ (9.1 m)
	MEDIUM	0.5 to 1 (50 to 100)	17′-0″ (5.1 m)	17′-6″ (5.3 m)	18′-6″ (5.6 m)	19′-0″ (5.8 m)	20′-6″ (6.2 m)	21′-6″ (6.4 m)	22′-0″ (6.7 m)	23′-6″ (7.0 m)	24′-0″ (7.3 m)
	STIFF	1 to 2 (100 to 200)	14′-6″ (4.4 m)	15′-0″ (4.5 m)	15′-6″ (4.7 m)	16′-0″ (4.8 m)	17′-6″ (5.2 m)	18′-0″ (5.4 m)	18′-6″ (5.5 m)	19′-6″ (5.9 m)	20′-0″ (6.1 m)
	VERY STIFF	2 to 4 (200 to 400)	13′-0″ (3.8 m)	13′-0″ (3.9 m)	13′-6″ (4.1 m)	14′-0″ (4.2 m)	15′-0″ (4.5 m)	15′-6″ (4.6 m)	16′-0″ (4.7 m)	17′-0″ (5.1 m)	17′-6″ (5.2 m)
	HARD	> 4 (> 400)	11′-6″ (3.5 m)	12′-0″ (3.5 m)	12′-0″ 3.6 m)	12′-6″ (3.7 m)	13′-6″ (4.0 m)	13′-6″ (4.1 m)	14′-0″ (4.2 m)	15′-0″ (4.5 m)	15′-6″ (4.6 m)
		N in BLOWS/FT. (N in BLOWS/0.3m)									
Granular	VERY LOOSE	< 5 (< 5)	16′-6″ (5.0 m)	17′-6″ (5.2 m)	18′-0″ (5.4 m)	18′-6″ (5.6 m)	19′-0″ (5.8 m)	20′-0″ (6.0 m)	20′-6″ (6.2 m)	21′-0″ (6.3 m)	21′-6″ (6.5 m)
	LOOSE	5 to 10 (5 to 10)	15′-0″ (4.6 m)	16′-0″ (4.8 m)	16′-6″ (4.9 m)	17′-0″ (5.1 m)	17′-6″ (5.3 m)	18′-0″ (5.5 m)	18′-6″ (5.6 m)	19′-0″ (5.7 m)	19′-6″ (5.9 m)
	MEDIUM	10 to 25 (10 to 25)	14′-6″ (4.4 m)	15′-0″ (4.5 m)	15′-6″ (4.7 m)	16′-0″ (4.9 m)	16′-6″ (5.0 m)	17′-0″ (5.2 m)	17′-6″ (5.3 m)	18′-0″ (5.5 m)	18′-6″ (5.6 m)
	DENSE	25 to 50 (25 to 50)	14′-0″ (4.1 m)	14′-6″ (4.3 m)	15′-0″ (4.5 m)	15′-6″ (4.6 m)	15′-6″ (4.7 m)	16′-6″ (4.9 m)	16′-6″ (5.0 m)	17′-0″ (5.2 m)	17′-6″ (5.3 m)
	VERY DENSE	> 50 (> 50)	13′-0″ (3.9 m)	13′-6″ (4.1 m)	14′-0″ (4.2 m)	14′-6″ (4.4 m)	15′-0″ (4.5 m)	15′-6″ (4.7 m)	16′-0″ (4.8 m)	16′-6″ (4.9 m)	17′-0″ (5.1 m)

Figure B.12 Illinois DOT Average Soil Strength and Shaft Length

Iowa Data Source:

https://www.iowadot.gov/research/reports/Year/2004/fullreports/tr486vol2.pdf

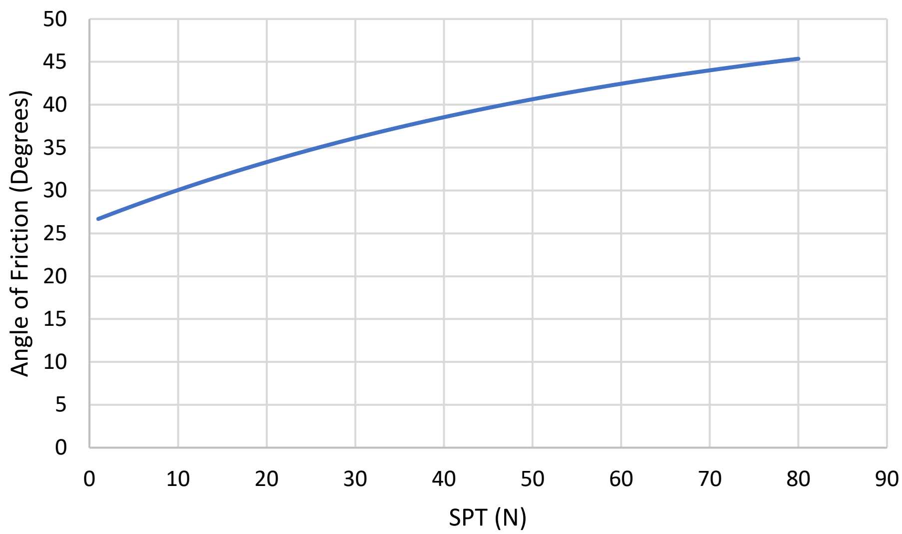

Figure B.13 Iowa DOT Angle of Friction and SPT Blow Count Graph

$$\phi = 53.881 - \left(27.6034 * e^{-0.0147\ N}\right)$$

where:

N = SPT blow count.

ϕ = Soil friction angle.

Figure B.14 Iowa DOT Angle of Friction and SPT Blow Count Equation

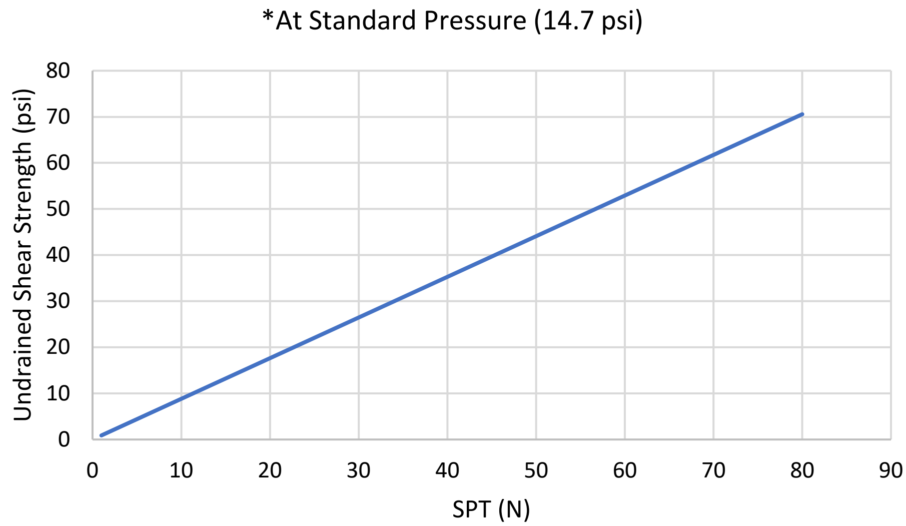

Figure B.15 Iowa DOT Undrained Shear Strength and SPT Blow Count Graph at STP

$$c_u = 0.06 * N * P_{ATM}$$

where:

c_u = Soil undrained shear strength.

N = SPT blow count.

P_{ATM} = Atmospheric pressure.

Figure B.16 Iowa DOT Undrained Shear Strength and SPT Blow Count Equation

Maine Data Sources:

https://www.maine.gov/mdot/contractors/projects/2015/016705.00-howland-enfield/gr016705.00.pdf

http://mainegov-images.informe.org/mdot/bdg/docs/Complete2003BDG.pdf

Table 3-3 Material Classification

Soil Type	Soil Description	Internal Angle of Friction of Soil, ϕ	Soil Total Unit Weight (pcf)	Coeff. of Friction, tan δ, Concrete to Soil	Interface Friction, Angle, Concrete to Soil δ
1	Very loose to loose silty sand and gravel Very loose to loose sand Very loose to medium density sandy silt Stiff to very stiff clay or clayey silt	29° *	100	0.35	19°
2	Medium density silty sand and gravel Medium density to dense sand Dense to very dense sandy silt	33°	120	0.40	22°
3	Dense to very dense silty sand and gravel Very dense sand	36°	130	0.45	24°
4	Granular underwater backfill Granular borrow	32°	125	0.45	24°
5	Gravel Borrow	36°	135	0.50	27°

Figure B.17 Maine DOT Soil Types and Parameters

UNIFIED SOIL CLASSIFICATION SYSTEM

MAJOR DIVISIONS			GROUP SYMBOLS	TYPICAL NAMES
COARSE-GRAINED SOILS (more than half of material is larger than No. 200 sieve size)	GRAVELS (more than half of coarse fraction is larger than No. 4 sieve size)	CLEAN GRAVELS (little or no fines)	GW	Well-graded gravels, gravel-sand mixtures, little or no fines
			GP	Poorly-graded gravels, gravel sand mixtures, little or no fines
		GRAVEL WITH FINES (Appreciable amount of fines)	GM	Silty gravels, gravel-sand-silt mixtures.
			GC	Clayey gravels, gravel-sand-clay mixtures.
	SANDS (more than half of coarse fraction is smaller than No. 4 sieve size)	CLEAN SANDS (little or no fines)	SW	Well-graded sands, gravelly sands, little or no fines
			SP	Poorly-graded sands, gravelly sand, little or no fines.
		SANDS WITH FINES (Appreciable amount of fines)	SM	Silty sands, sand-silt mixtures
			SC	Clayey sands, sand-clay mixtures.
FINE-GRAINED SOILS (more than half of material is smaller than No. 200 sieve size)	SILTS AND CLAYS (liquid limit less than 50)		ML	Inorganic silts and very fine sands, rock flour, silty or clayey fine sands, or clayey silts with slight plasticity.
			CL	Inorganic clays of low to medium plasticity, gravelly clays, sandy clays, silty clays, lean clays.
			OL	Organic silts and organic silty clays of low plasticity.
	SILTS AND CLAYS (liquid limit greater than 50)		MH	Inorganic silts, micaceous or diatomaceous fine sandy or silty soils, elastic silts.
			CH	Inorganic clays of high plasticity, fat clays.
			OH	Organic clays of medium to high plasticity, organic silts
	HIGHLY ORGANIC SOILS		Pt	Peat and other highly organic soils.

Desired Soil Observations: (in this order)
Color (Munsell color chart)
Moisture (dry, damp, moist, wet, saturated)
Density/Consistency (from above right hand side)
Name (sand, silty sand, clay, etc., including portions - trace, little, etc.)
Gradation (well-graded, poorly-graded, uniform, etc.)
Plasticity (non-plastic, slightly plastic, moderately plastic, highly plastic)
Structure (layering, fractures, cracks, etc.)
Bonding (well, moderately, loosely, etc., if applicable)
Cementation (weak, moderate, or strong, if applicable, ASTM D 2488)
Geologic Origin (till, marine clay, alluvium, etc.)
Unified Soil Classification Designation
Groundwater level

Maine Department of Transportation
Geotechnical Section
Key to Soil and Rock Descriptions and Terms
Field Identification Information

TERMS DESCRIBING DENSITY/CONSISTENCY

Coarse-grained soils (more than half of material is larger than No. 200 sieve): Includes (1) clean gravels; (2) silty or clayey gravels; and (3) silty, clayey or gravelly sands. Consistency is rated according to standard penetration resistance.

Modified Burmister System

Descriptive Term	Portion of Total
trace	0% - 10%
little	11% - 20%
some	21% - 35%
adjective (e.g. sandy, clayey)	36% - 50%

Density of Cohesionless Soils	Standard Penetration Resistance N-Value (blows per foot)
Very loose	0 - 4
Loose	5 - 10
Medium Dense	11 - 30
Dense	31 - 50
Very Dense	> 50

Fine-grained soils (more than half of material is smaller than No. 200 sieve): Includes (1) inorganic and organic silts and clays; (2) gravelly, sandy or silty clays; and (3) clayey silts. Consistency is rated according to shear strength as indicated.

Consistency of Cohesive soils	SPT N-Value blows per foot	Approximate Undrained Shear Strength (psf)	Field Guidelines
Very Soft	WOH, WOR, WOP, <2	0 - 250	Fist easily Penetrates
Soft	2 - 4	250 - 500	Thumb easily penetrates
Medium Stiff	5 - 8	500 - 1000	Thumb penetrates with moderate effort
Stiff	9 - 15	1000 - 2000	Indented by thumb with great effort
Very Stiff	16 - 30	2000 - 4000	Indented by thumbnail
Hard	>30	over 4000	Indented by thumbnail with difficulty

Rock Quality Designation (RQD):

$$RQD = \frac{\text{sum of the lengths of intact pieces of core* > 100 mm}}{\text{length of core advance}}$$

*Minimum NQ rock core (1.88 in. OD of core)

Correlation of RQD to Rock Mass Quality

Rock Mass Quality	RQD
Very Poor	<25%
Poor	26% - 50%
Fair	51% - 75%
Good	76% - 90%
Excellent	91% - 100%

Desired Rock Observations: (in this order)
Color (Munsell color chart)
Texture (aphanitic, fine-grained, etc.)
Lithology (igneous, sedimentary, metamorphic, etc.)
Hardness (very hard, hard, mod. hard, etc.)
Weathering (fresh, very slight, slight, moderate, mod. severe, severe, etc.)
Geologic discontinuities/jointing:
-dip (horiz - 0-5, low angle - 5-35, mod. dipping - 35-55, steep - 55-85, vertical - 85-90)
-spacing (very close - <5 cm, close - 5-30 cm, mod. close 30-100 cm, wide - 1-3 m, very wide >3 m)
-tightness (tight, open or healed)
-infilling (grain size, color, etc.)
Formation (Waterville, Ellsworth, Cape Elizabeth, etc.)
RQD and correlation to rock mass quality (very poor, poor, etc.)
ref: AASHTO Standard Specification for Highway Bridges 17th Ed. Table 4.4.8.1.2A
Recovery

Sample Container Labeling Requirements:

PIN	Blow Counts
Bridge Name / Town	Sample Recovery
Boring Number	Date
Sample Number	Personnel Initials
Sample Depth	

Figure B.18 Maine DOT Boring Log Sample for Soil Parameters

Coarse-grained soils (more than half of material is larger than No. 200 sieve): Includes (1) clean gravels; (2) silty or clayey gravels; and (3) silty, clayey or gravelly sands. Consistency is rated according to standard penetration resistance.

Modified Burmister System

Descriptive Term	Portion of Total
trace	0% - 10%
little	11% - 20%
some	21% - 35%
adjective (e.g. sandy, clayey)	36% - 50%

Density of Cohesionless Soils	Standard Penetration Resistance N-Value (blows per foot)
Very loose	0 - 4
Loose	5 - 10
Medium Dense	11 - 30
Dense	31 - 50
Very Dense	> 50

Figure B.19 Maine DOT Coarse Grained Soil Parameters

Fine-grained soils (more than half of material is smaller than No. 200 sieve): Includes (1) inorganic and organic silts and clays; (2) gravelly, sandy or silty clays; and (3) clayey silts. Consistency is rated according to shear strength as indicated.

Consistency of Cohesive soils	SPT N-Value blows per foot	Approximate Undrained Shear Strength (psf)	Field Guidelines
Very Soft	WOH, WOR, WOP, <2	0 - 250	Fist easily Penetrates
Soft	2 - 4	250 - 500	Thumb easily penetrates
Medium Stiff	5 - 8	500 - 1000	Thumb penetrates with moderate effort
Stiff	9 - 15	1000 - 2000	Indented by thumb with great effort
Very Stiff	16 - 30	2000 - 4000	Indented by thumbnail
Hard	>30	over 4000	Indented by thumbnail with difficulty

Figure B.20 Maine DOT Fine Grained Soil Parameters

Maryland Data Sources:

https://www.roads.maryland.gov/OPR_Research/MD-02-SP007B49-Updating-Bearing-Capacity-SPT-Graphs-Report.pdf

$$N_{60} = N_f \cdot \left(ER_f / 60\right)$$

where:

N_{60} = SPT N value corrected to 60% of the theoretical free fall hammer energy

N_f = SPT N value obtained in the field

ER_f = rod energy ratio for hammer used in the investigation (measured)

Figure B.21 Maryland DOT N60 Correction Equation

The angle of friction of granular soils, φ, has been correlated to the standard penetration number. Peck, Hanson, and Thornburn (1953) gave a correlation between N and φ in a graphical form, Fig 2.1, which can be approximated as (Wolff, 1989)

$$\varphi^\circ = 27.1 + 0.3N - 0.00054N^2 \tag{2.1}$$

In Japan the "Road Bridge Specifications" (Shioi and Fukui 1982) suggests for $N > 5$,

$$\varphi = \left(15N\right)^{1/2} + 15 \tag{2.2}$$

and the "Design Standards for Structures" (Shioi and Fukui, 1982):

$$\varphi = 0.3N + 27^\circ \tag{2.3}$$

Figure B.22 Maryland DOT SPT Correlations with Angle of Friction for Granular Soil

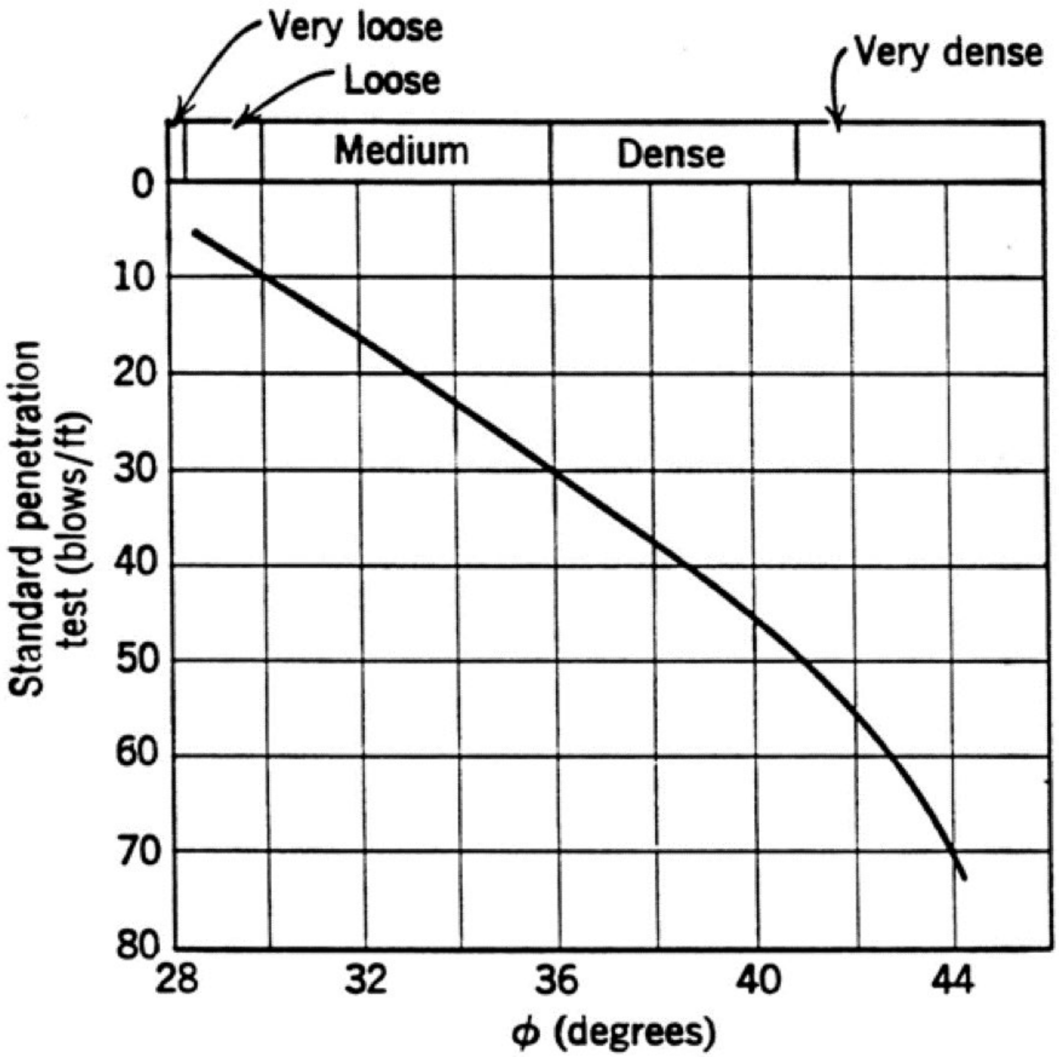

Figure B.23 Maryland DOT SPT vs Angle of Friction for Granular Soils

The Japanese "Road Bridge Specifications" (Shioi and Fukui, 1982) offer a correlation between the cohesion, c, and the SPT N-value for cohesive soils:

$$c = (0.061 \text{ to } 0.102)N \text{ tsf}$$

Sowers (1979) presented the relationship between the SPT N-value and the underained shear strength S_u that is shown in Fig. 2.2. The relationship can be represented by:

For clays with high plasticity:

$$S_u = (0.102 \text{ to } 0.179)N \text{ tsf}$$

For clays with medium plasticity:

$$S_u = (0.051 \text{ to } 0.102)N \text{ tsf}$$

For clays of low plasticity and clayey silts:

$$S_u = (0.026 \text{ to } 0.051)N \text{ tsf}$$

In Fig. 2.3 the NAVFAC, 1982 relationships between the SPT N-value and the unconfined compressive strength are presented. They can be summarized as:

An average relationship for all clays by Terzaghi and Peck: $c = 0.066N$ tsf

For clay of high plasticity, Sowers,

$$c = 0.13N \text{ tsf}$$

For clays of Medium plasticity, Sowers,

$$c = 0.076N \text{ tsf}$$

For clays of low plasticity and clayey silts, Sowers,

$$c = 0.038N \text{ tsf}$$

Figure B.24 Maryland DOT SPT Correlations for Cohesive Soils

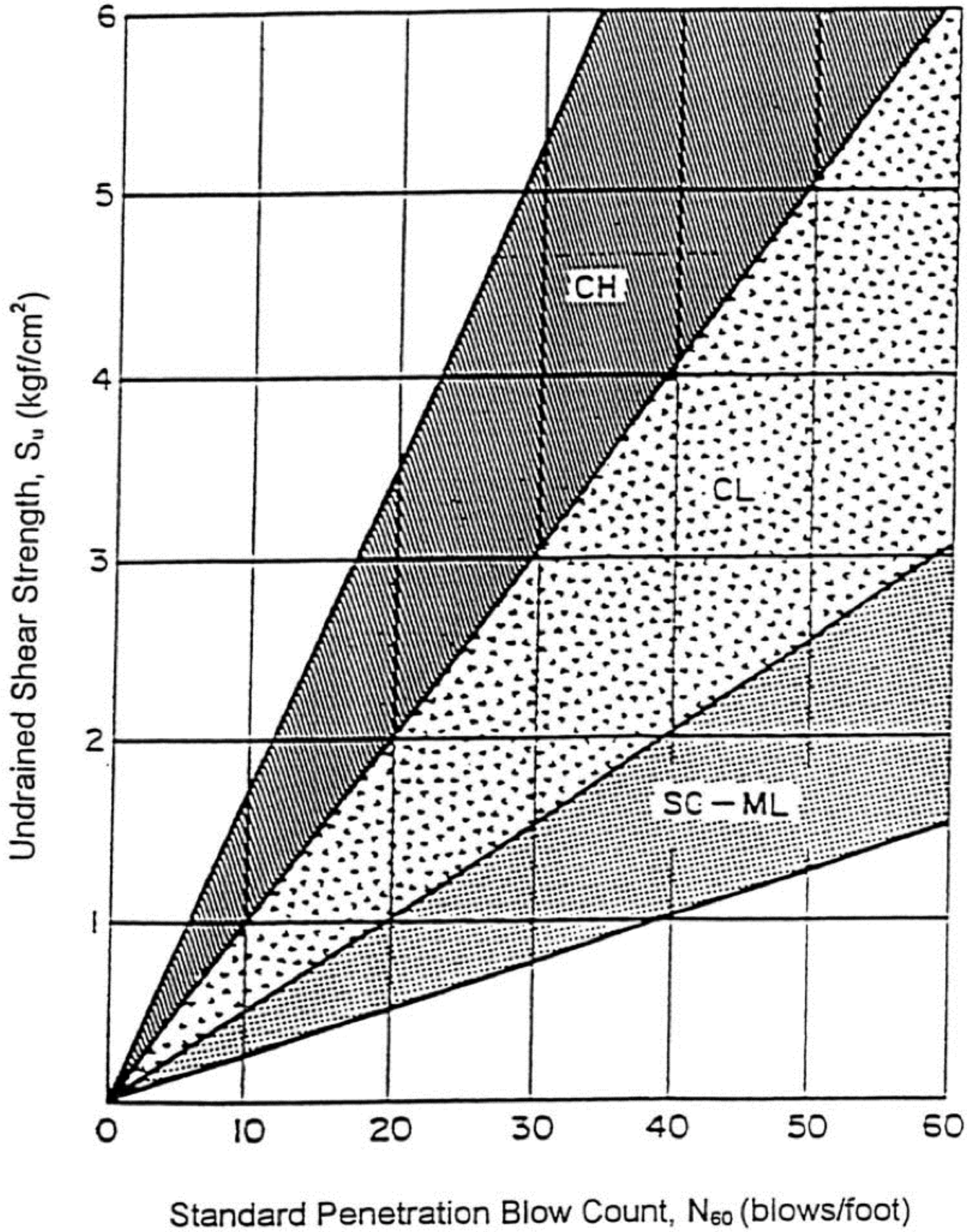

Figure B.25 Maryland DOT Undrained Shear Strength vs. SPT for Cohesive Soils

Michigan Data Source:

https://www.michigan.gov/documents/mdot/MDOT_Geotechnical_Manual_642589_7.pdf

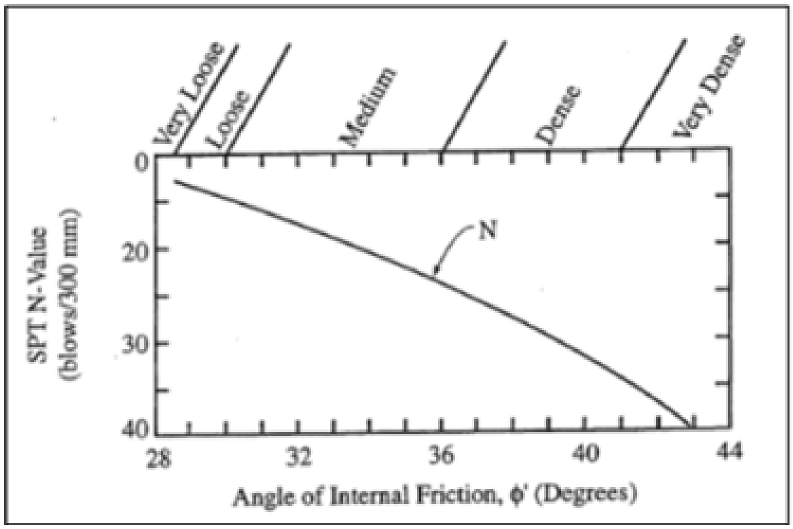

Figure B.26 Michigan DOT SPT vs. Angle of Friction

Descriptive Term	SPT – N_{60} (blows/ft) [1]	Relative Density %	Resistance to Spiral Auger
Very Loose	≤ 4	0 – 20	The auger can be forced several inches into the soil without turning under the bodyweight of the technician.
Loose	5 – 10	>20 – 40	The auger can be turned into the soil for its full length without difficulty. It can be chugged up and down after penetrating about 1 ft so that it can be pushed down 1 inch into the soil.
Medium Dense	11 – 30	>40 – 70	The auger cannot be advanced beyond ±2.5 ft without great difficulty. Considerable effort by chugging required to advance further.
Dense	31 – 50	>70 – 85	The auger turns until tight at ±1 ft and cannot be advanced further.
Very Dense	> 50	>85 -100	The auger can be turned into the soil only to about the length of its spiral section.

Figure B.27 Michigan DOT Relative Density for Cohesionless Soils

Descriptive Term	SPT – N_{60} (blows/ft)	Shear Strength – s_u (psf)	Manual Index for Consistency
Very Soft	≤ 2	0 - 250	Extrudes between fingers when squeezed
Soft	3 – 4	> 250 - 500	Molded by light to moderate finger pressure
Medium Stiff	5 – 8	>500 – 1000	Molded by moderate to firm finger pressure
Stiff	9 – 15	>1000 – 2000	Readily indented by thumb, difficult to penetrate
Very Stiff	16 - 30	>2000 – 4000	Readily indented by thumbnail
Hard	> 30	> 4000	Indented with difficulty by thumbnail

Figure B.28 Michigan DOT Consistency for Cohesive Soils

New Jersey Data Source:

https://www.state.nj.us/transportation/eng/documents/BSDM/pdf/2016DesignManualforBridgesandStructures20180604.pdf

16.2 Loads

1. Mass Density (Unit Weight) of Soil ……………………..…. 120 lbs./cu.ft
2. Mass Density (Unit Weight) of Concrete ……………..…..150 lbs./cu.ft
3. Surcharge loads shall be based on the criteria that is stated in Subsection 3.11.6 of the AASHTO LRFD Bridge Design Specifications.
4. To consider the vertical load per foot of approach slabs that react on the abutment backwall, 1/3 of the approach slab length shall be assumed to cause reactions onto the abutment. Also reference Subsection 17.2.7 of this manual
5. Compaction induced additional earth pressures, that are due to construction equipment, shall be considered. Subsection 3.11.2 of the *AASHTO LRFD Bridge Design Specifications* should be referred to for guidance in estimating such earth pressures.

16.3 Foundations

In order to prevent damage from frost heave, footings shall be founded at an elevation that is a minimum of 4 feet below the existing ground line or, other than when founded on sound rock, shall be embedded in a minimum 3-foot depth from the ground line to the top of the footing to provide adequate bearing, scour and frost heave protection, whichever is greater.

Also, refer to Section 39 of this Manual for guidance concerning scour considerations.

Figure B.29 New Jersey DOT Foundation Soil and Concrete Assumptions

Ohio Data Source:

http://www.dot.state.oh.us/Divisions/Engineering/Geotechnical/Geotechnical_Documents/ODOT_SGE_2020-07-17.pdf

404.3 Determination of N_{60} Value

Record the blow count (N) values for the Standard Penetration Testing. Correct the measured N value to an equivalent rod energy ratio of 60 percent, N_{60}, by the following equation:

$$N_{60} = N_m \times (ER/60)$$

Where:

N_m = measured N value = Y+Z
Y = number of blow counts in second 6-inch interval
Z = number of blow counts in third 6-inch interval
ER = drill rod energy ratio, expressed as a percent, for the system used

Record the N_{60} value to the nearest whole number. Utilize the hammer system measured ER value up to a maximum ER value of 90%. It is not necessary to correct refusal blow counts, defined as an SPT drive requiring more than 50 blows with less than 6 inches of penetration.

Figure B.30 Ohio DOT N60 Calibration

Oregon Data Source:

https://www.oregon.gov/ODOT/GeoEnvironmental/Docs_GeologyGeotech/GDM-16_2019.pdf

Description	SPT N'60* value (blows/ft.)	Approximate Angle of Internal Friction (Φ)**	Moist Unit Weight (pcf)	Field Approximation
Very Loose	0 – 4	< 30	70 – 100	Easily penetrated many inches (>12) with ½ inch rebar pushed by hand.
Loose	4 – 10	30 – 35	90 – 115	Easily penetrated several inches (>12) with ½ inch rebar pushed by hand.
Medium	10 – 30	35 – 40	110 – 130	Easily to moderately penetrate with ½ inch rebar driven by 5 lb. hammer.
Dense	30 – 50	40 – 45	120 – 140	Penetrated one foot with difficulty using ½ inch rebar driven by 5 lb. hammer.
Very Dense	> 50	> 45	130 – 150	Penetrated only a few inches with ½-inch rebar driven by 5 lb. hammer.

* N'_{60} is corrected for overburden pressure and energy

** Use the higher phi angles for granular material with 5% or less fine sand and silt.

Figure B.31 Oregon DOT Cohesionless Soil Parameters

Consistency	SPT N60 value (blows/ft.)	Approximate Undrained Shear Strength (psf)	Moist Unit Weight (pcf)	Field Approximation
Very Soft	< 2	< 250	100 – 120	Squeezes between fingers when fist is closed; easily penetrated several inches by fist.
Soft	2 – 4	250 – 500		Easily molded by fingers; easily penetrated several inches by thumb.
Medium Stiff	5 – 8	500 – 1000	110 – 130	Molded by strong pressure of fingers; can be penetrated several inches by thumb with moderate effort.
Stiff	9 – 15	1000 – 2000	120 – 140	Dented by strong pressure by fingers; readily indented by thumb but can be penetrated only with great effort.
Very Stiff	16 – 30	2000 – 4000	125 – 140	Readily indented by thumbnail.
Hard	31 – 60	4000 - 8000	130 – 140	Indented with difficulty by thumb nail
Very Hard	> 60	> 8000		

Figure B.32 Oregon DOT Cohesive Soil Parameters

Rhode Island Data Source:

http://www.dot.ri.gov/documents/about/research/Geotechnical.pdf

Soil Consistency	SPT N	S_u (psf)	S_u (kPa)
Very Soft	< 4	< 250	< 12
Soft	2 – 4	250 – 500	12 – 25
Medium	4 - 8	500 – 1000	25 – 50
Stiff	8 – 15	1000 – 2000	50 – 100
Very Stiff	15 – 30	2000 – 4000	100 – 200
Hard	> 30	> 4000	> 200

Figure B.33 Rhode Island DOT undrained shear strength based on SPT blow count

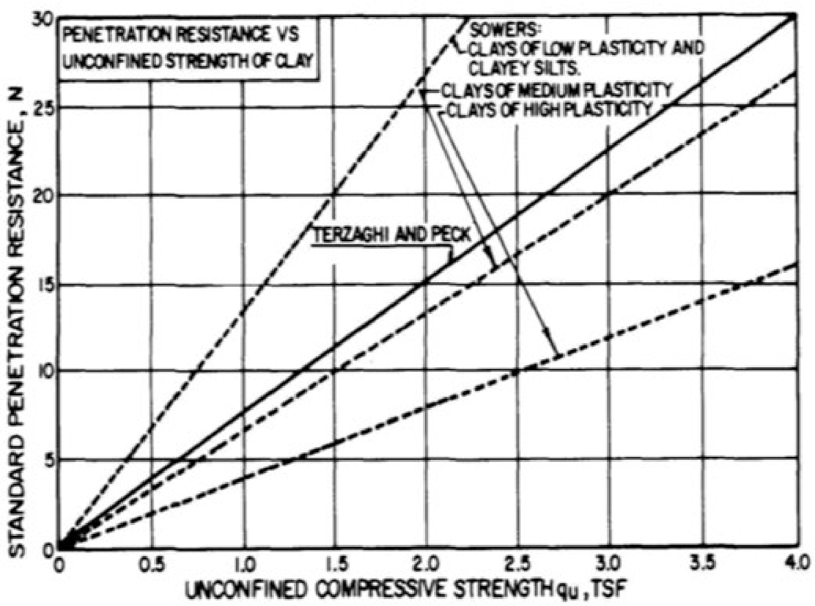

Figure B.34 Rhode Island DOT SPT blow count vs. Unconfined Compressive Strength

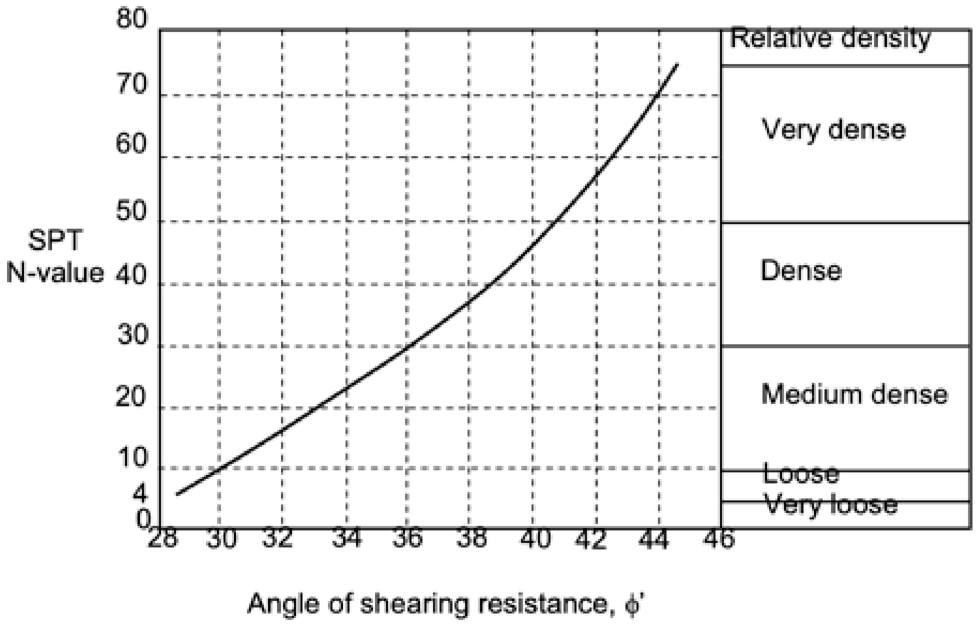

Figure B.35 Rhode Island DOT SPT vs. Angle of shearing resistance

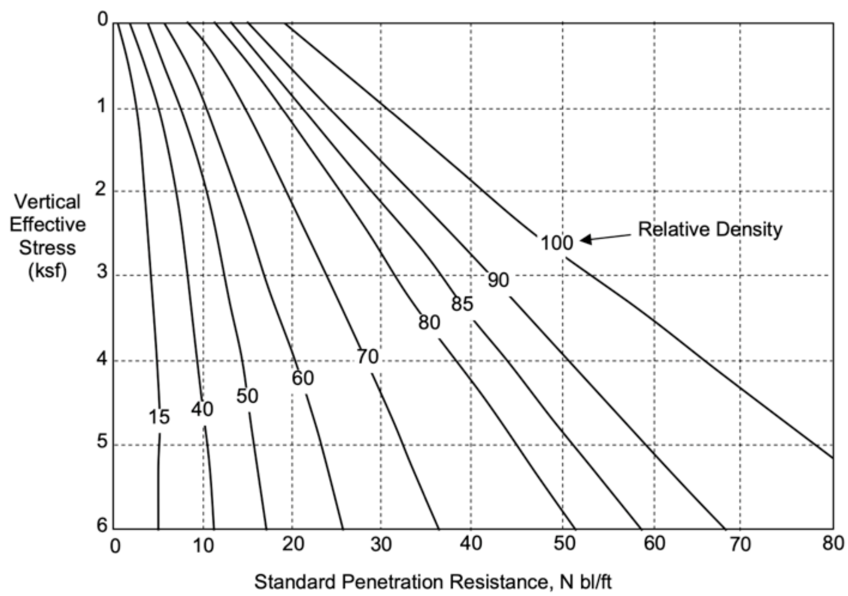

Figure B.36 Rhode Island DOT Vertical Effective Stress vs. SPT

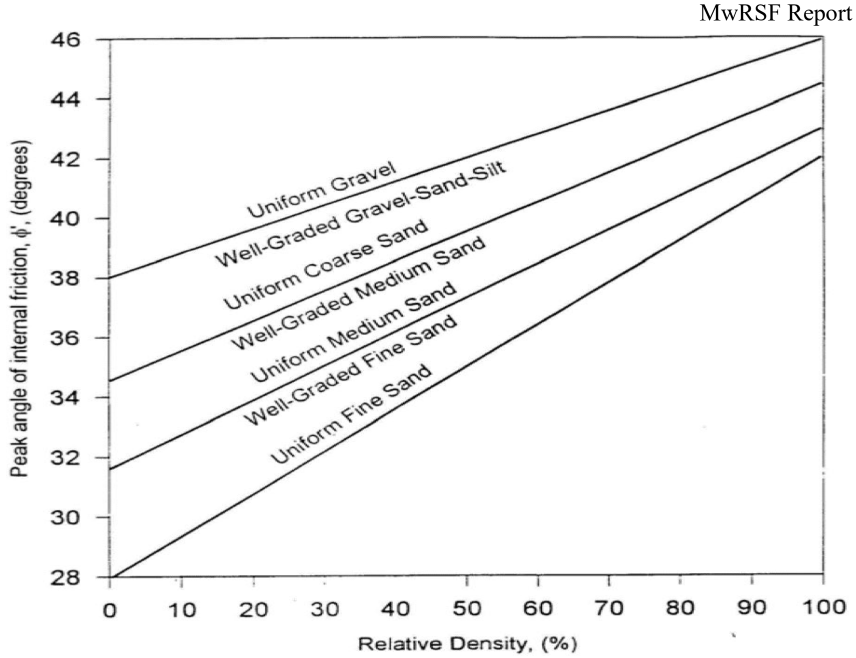

Figure B.37 Rhode Island Internal Friction and Relative Density for Sands and Gravels

Texas Data Source:

http://onlinemanuals.txdot.gov/txdotmanuals/geo/geo.pdf

Table 4-1: Soil Density or Consistency

Density (Cohesionless)	Consistency (Cohesive)	TCP Values	Field Identification
Very loose	Very soft	0 to 8	Core (height twice diameter) sags under own weight
Loose	Soft	8 to 20	Core can be pinched or imprinted easily with finger
Slightly compact	Stiff	20 to 40	Core can be imprinted with considerable pressure
Compact	Very stiff	40 to 80	Core can be imprinted only slightly with fingers
Dense	Hard	80 to 5 in./100	Core cannot be imprinted with fingers but can be penetrated with pencil

Density (Cohesionless)	Consistency (Cohesive)	TCP Values	Field Identification
Very dense	Very hard	0 in. to 5 in./100	Core cannot be penetrated with pencil

Figure B.38 Texas DOT Soil Consistency Based on TCP

Washington Data Source:

https://www.wsdot.wa.gov/publications/manuals/fulltext/M46-03/Geotech.pdf

Soil Consistency as Identified in Patterson (1962)	Standard Penetration Test Resistance, N (blows/ft)	Allowable Lateral Bearing Pressure (psf)
Very Soft Soil	2	750
	3	800
	4	900
	5	1000
	6	1100
	7	1200
Poor Soil	8	1300
	9	1400
	10	1500
	11	1700
	12	1900
Average Soil	13	2100
	14	2300
	15	2500
	16	2700
	17	2900
Good Soil	18	3100
	19	3300
	20	3500
Very Hard Soil	25	4200
	30	>4500
	35	>4500

Figure B.39 Washington DOT SPT and Lateral Soil Strength

SPT N (Blows/Foot)	Consistency
0 to 1	Very Soft
2 to 4	Soft
5 to 8	Medium Stiff
9 to 15	Stiff
16 to 30	Very Stiff
31 to 60	Hard
Over 60	Very Hard

Consistency of Cohesive Soils
Table 4-10

SPT N (Blows/Foot)	Relative Density
0 to 4	Very Loose
5 to 10	Loose
11 to 24	Medium Dense
25 to 50	Dense
Over 50	Very Dense

Relative Density of Cohesionless Soils
Table 4-11

Figure B.40 Washington DOT Soil Consistency

$N1_{60}$ from SPT (blows/ft)	φ (o)
<4	25-30
4	27-32
10	30-35
30	35-40
50	38-43

Figure B.41 Washington DOT Corrected SPT Value and Angle of Friction

Modulus Reduction Curve (Darendeli, 2001) – The modulus reduction curve for soil, as a function of shear strain, should be calculated as shown in Equations 6-1 and 6-2.

$$\frac{G}{G_{\max}} = \frac{1}{1+\left(\frac{\gamma}{\gamma_r}\right)^a} \tag{6-1}$$

where,

- G = shear modulus at shear strain γ, in the same units as G_{max}
- γ = shear strain (%), and
- a = 0.92

γ_r is defined in Equation 6-2 as:

$$\gamma_r = \left(\phi_1 + \phi_2 \times PI \times OCR^{\phi_3}\right) \times \sigma_0'^{\,\phi_4} \tag{6-2}$$

where,

- ϕ_1 = 0.0352; ϕ_2 = 0.0010; $^{\phi_3}$ = 0.3246; $^{\phi_4}$ = 0.3483 (from regression),
- OCR = overconsolidation ratio for soil
- σ'_0 = effective vertical stress, in atmospheres, and
- PI = plastic index, in %

Figure B.42 Washington DOT Shear Modulus Equation

Appendix C Pole Foundation Dimensions State DOT Review

The data provided in this appendix was compiled by Mr. Taylor Drahota in partial fulfillment of his appointment in the University of Nebraska-Lincoln Undergraduate Creative Activities and Research Experiences (UCARE) program, and is supplementary to Sections 2.5.1 and 2.5.4.

Typical foundation plans published by state DOTs showed varying ranges between the recommended minimum and maximum depths, as illustrated in Figure C.1. Variations were primarily attributed to specific design considerations and field conditions, such as pole heights and/or mast arm lengths, environmental loading, and on-site soil characteristics. Note that Mr. Drahota's review used past standards from Alaska, but the current standard includes depths up to 10 ft, exceeding the 8 ft value shown in the figure.

Most states demonstrated a moderate level of variation, with a standard deviation of 0.9 ft for the minimum depth and 1.5 ft for the maximum depth. Discrepancies in design procedures, analysis techniques, climate conditions, and personnel contributed to the variations in recommended depths across different states.

Approximately two-thirds of the reviewed states (20 out of 33) provided foundation dimension information through standard drawings. These drawings included dimensions for various depths and featured different diameter sizes for concrete luminaire foundations. Minimum and maximum foundation diameters for state DOTs are shown in Figure C.2. Among the state DOTs considered, there was a standard deviation of 4.3 in. for minimum diameters and 5.9 in. for maximum diameters.

The average values for the state DOT foundation diameters are shown in Table C.1. Notable variations were found in the minimum (4 ft) and maximum (11.5 ft) design depths obtained from Maryland DOT standard drawings. These differences were primarily attributed to variations in luminaire geometric conditions within standard foundation plans. Design parameters such as pole height and mast arm length had a significant impact on the design.

Most foundation depths fell within the range of 6 to 8 ft, with some states including poor soil conditions in their design considerations. Diameter size exhibited less variability as a number of states adopted a uniform diameter across all depths. The data set range supported the consistency of the minimum and maximum diameter values at 18 and 36 in., respectively. The average diameter obtained from this survey ranged between 2 to 2.5 ft, which was similar to the current Alaska DOT&PF average diameter of 2.5 ft from a corrugated metal form.

Table C.1 Average Values for DOT Foundation Sizes

Average Minimum Diameter (in)	25.5
Average Maximum Diameter (in)	29.8
Average Minimum Foundation Depth (ft)	5.9
Average Maximum Foundation Depth (ft)	7.6

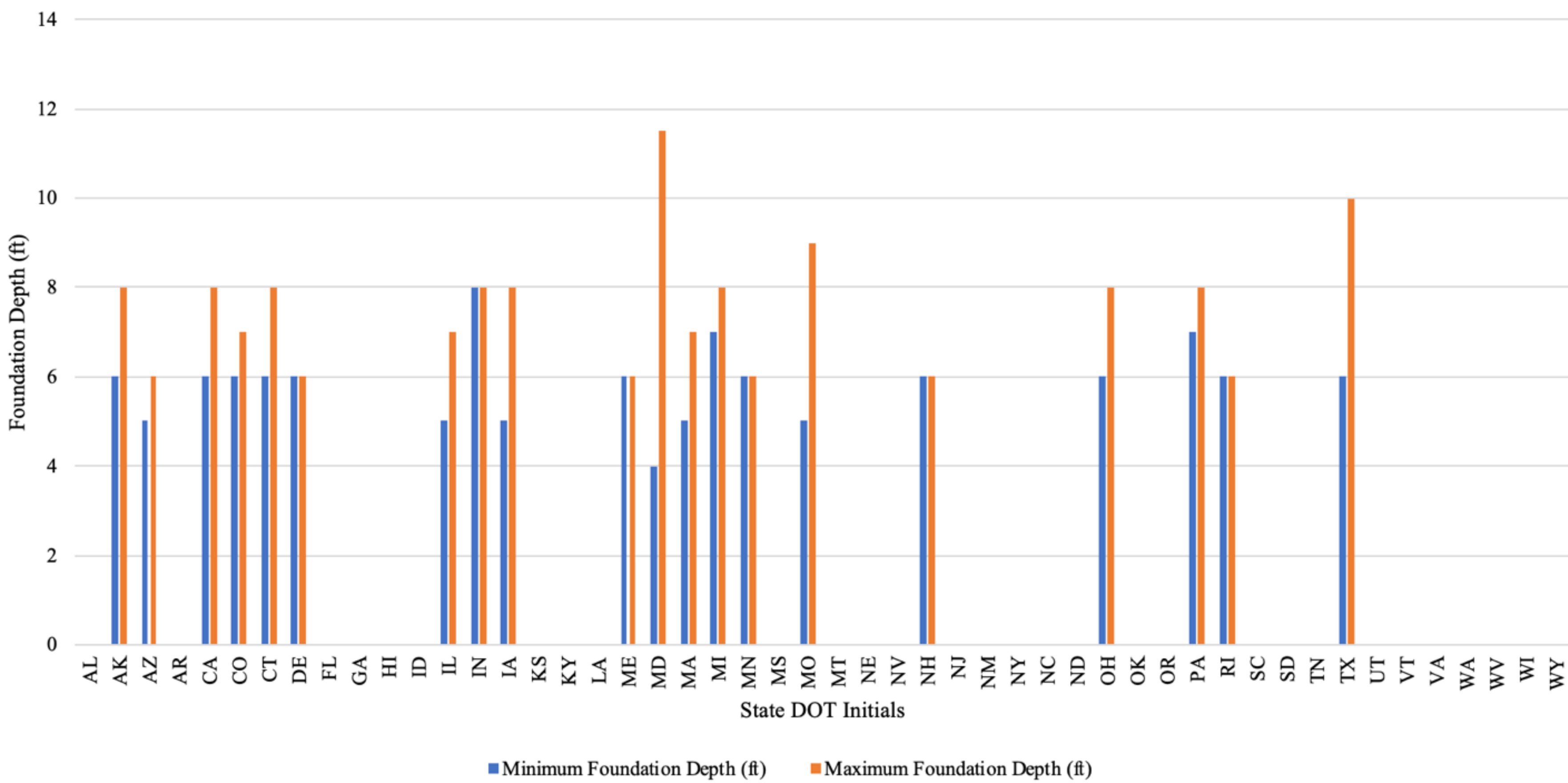

Figure C.1 Minimum and Maximum State DOT Foundation Depths

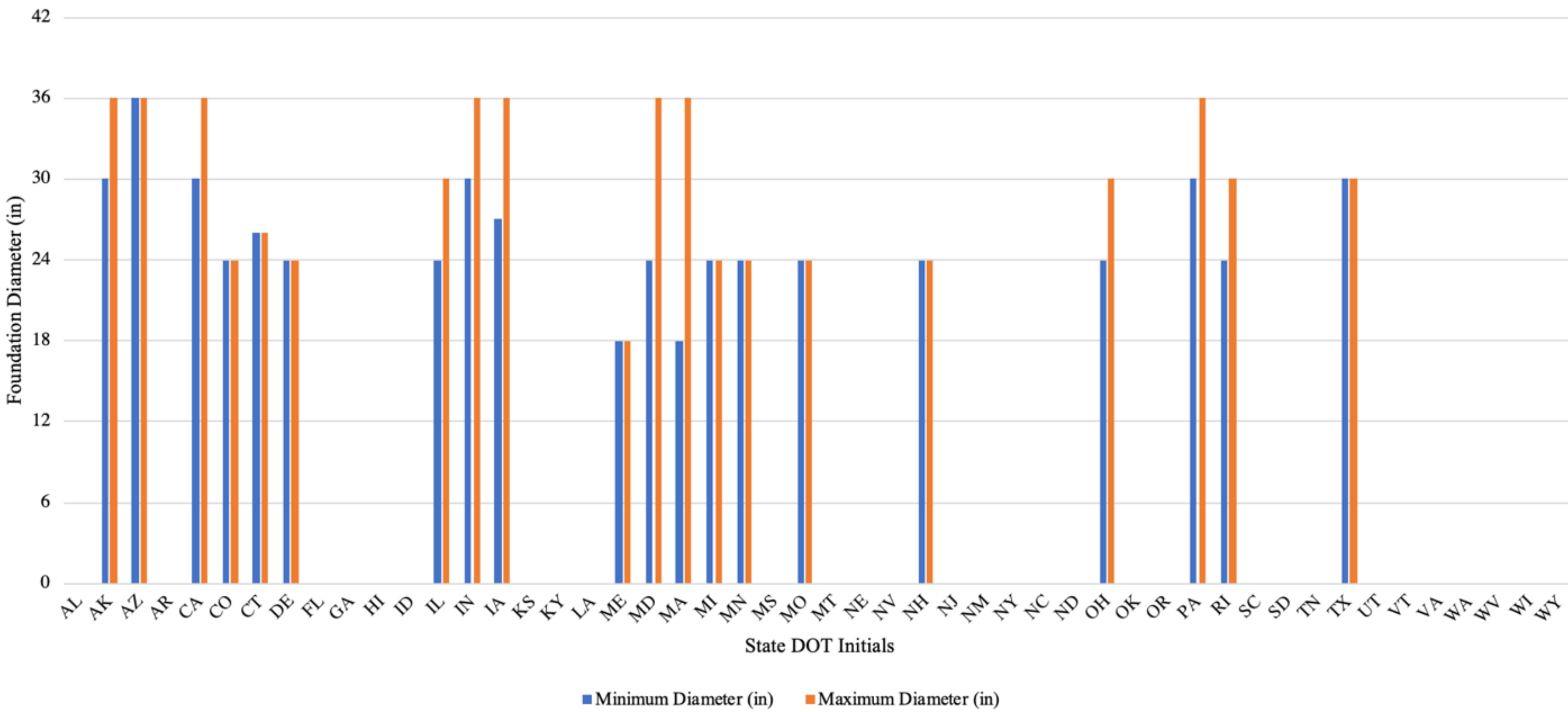

Figure C.2 Minimum and Maximum State DOT Foundation Diameters

The following sources were used to compile foundation size data.

Alaska:

L-30.11 Concrete Street Light Pole Foundation

http://www.dot.state.ak.us/stwddes/dcsprecon/assets/pdf/stddwgs/eng/l3011.pdf

Arizona:

T-SL 4.02 Type S Pole

https://apps.azdot.gov/files/Traffic/SignalLighting/current/etsl-4.02.pdf

T-SL 4.02 Type T Pole

https://apps.azdot.gov/files/Traffic/SignalLighting/current/etsl-4.03.pdf

California:

ES-6A Electrical Systems (Lighting Standard, Types 15 and 21)

https://dot.ca.gov/-/media/dot-media/programs/design/documents/2018-std-plns-for-web-a11y.pdf

Colorado:

Roadway Lighting Standard Plan No. M-613-1, Sheet No. 3 of 4

https://www.codot.gov/business/designsupport/standard-plans/copy_of_2012-m-standards-plans/2012-m-standards-pdfs/45-roadway-lighting/m-613-1-roadway-lighting

Connecticut:

Light Standard & Foundation for Vehicle Detection

https://portal.ct.gov/-/media/DOT/documents/dtrafficdesign/ctdot_traffic_gs-ls_and_found.pdf?la=en

Foundation Class Dimensions

https://portal.ct.gov/-/media/DAS/OEDM/2016-CD-HO/2016_sp_cd_soils_and_foundations_2_slide.pdf?la=en

Delaware:

Standard No. T-5(2017), Sheet 3 of 4, Pole Bases

https://deldot.gov/Publications/manuals/const_details/pdfs/2017/sd_t05-3.pdf?cache=1599175110493

Table IV-11 Pole Base Type Selection for Varying Soil Condition

https://deldot.gov/Publications/manuals/traffic_design/pdfs/2015/2015_complete_with_appendices.pdf?cache=1601920115874

Illinois:

Standard 836001-02, Light Pole Foundation

http://www.idot.illinois.gov/Assets/uploads/files/Doing-Business/Standards/Highway-Standards/216%20Highway%20Standards%20Complete%20Set.pdf

Indiana:

Standard Drawing No. E 807-LTFD-05, Light Foundation

https://www.in.gov/dot/div/contracts/standards/drawings/sep19/e/800e/e800%20combined%20pdfs/E807-LTFD.pdf

Iowa:

LI-201 Light Pole Foundation

https://www.iowadot.gov/design/SRP/IndividualStandards/eli201.pdf

Maine:

SKE-03 Light Pole Base Detail

https://www1.maine.gov/mdot/comprehensive-list-projects/ba011623.00a.pdf

Maryland:

Standard No. MD 801.02 Lighting Structure Foundation

http://apps.roads.maryland.gov/businesswithsha/bizstdsspecs/desmanualstdpub/publicationsonline/ohd/bookstd/pdf/category8.pdf

Massachusetts:

Overhead Signal Structure & Foundation Mast Arm Cored Pier Foundations

https://www.mass.gov/doc/overhead-signal-structure-foundation-standard-drawings/download

Michigan:

SIGN-230-A Foundation (Break-away)

https://mdotjboss.state.mi.us/TSSD/getCategoryDocuments.htm?categoryPrjNumbers=1403886,2028779,1403887,1403888,1403889,1403890,1797786&category=Traffic%20Signing

Minnesota:

Standard Plate No. 8127D Light Foundation – Design E, Precast, 40 ft Pole or less

https://standardplates.dot.state.mn.us

Missouri:

901.00AB Highway Lighting – Poles, Foundations and Appurtenances for 30' Mounting Height

https://www.modot.org/sites/default/files/documents/90100.pdf

901.01AJ Highway Lighting – Poles, Foundations and Appurtenances for 45' Mounting Height

https://www.modot.org/sites/default/files/documents/90101.pdf

New Hampshire:

Standard No. SL-2 Concrete Foundations & Light Pole Base, Type B

https://www.nh.gov/dot/org/projectdevelopment/highwaydesign/standardplans/documents/sl-2.pdf

CCTV Foundation Item, 677.41001 Drilled Shaft

https://www.nh.gov/dot/projects/derrylondonderry13065/documents/13065-cds-020620.pdf

Ohio:

HL-20.11 Misc. Light Pole Foundation & Trench Details

http://www.dot.state.oh.us/Divisions/Engineering/Roadway/DesignStandards/traffic/SCD/Documents/HL_02011_2020-07-17.pdf

Pennsylvania:

TC-8801 Traffic Signal Support Foundation Notes and Anchor Bolt Details

https://www.dot.state.pa.us/public/PubsForms/Publications/PUB%20148.pdf

Rhode Island:

Standard 18.1.0 Concrete Light Standard Base

http://www.dot.ri.gov/documents/doingbusiness/RIDOT_Std_Details.pdf

Texas:

RID(FND)-11 Roadway Illumination Details (Rdwy Illum Foundations)

ftp://ftp.dot.state.tx.us/pub/txdot-info/cmd/cserve/standard/traffic/ridfn11.pdf

Appendix D Weak Soil Considerations State DOT Review

The data provided in this appendix was compiled by Mr. Taylor Drahota in partial fulfillment of his appointment in the University of Nebraska-Lincoln Undergraduate Creative Activities and Research Experiences (UCARE) program, and is supplementary to Sections 2.5.1 and 2.5.5.

Geotechnical engineers can conduct analyses to identify groundwater table depths within specific regions of a state. This information should include seasonal fluctuations, precipitation events, and time-dependent variations. The Rhode Island Department of Transportation (RIDOT) recognizes that significant design challenges arise from the presence of groundwater. These challenges include variations in the effective strength of soil, consolidation of compressible organic soils, hydrostatic loads on structures, and long-term drainage issues.

In addition, several other factors highlighted by various DOTs deserve attention. These include liquefaction susceptibility, which refers to the soil's instability under seismic activity, the presence of soft clay or organic soil beneath the foundation location, slopes with gradients greater than 2:1, exposure to aggressive environments (including those extending through water), and potential problems encountered during drilled shaft casing installation. Further measures must be taken to ensure appropriate solutions are developed to address these specific cases.

Florida Data Source:

https://www.fdot.gov/docs/default-source/structures/manuals/SFH.pdf

Layer	Soil Description	Elev., ft	Thickness, ft	Ave N-value	Unit Side shear, ksf	Side Resistance, Kips/ft
1	sand	5.7 to -13	18.7	9	-*	-
2	Soft limestone	-13 to -23	10	16	-**	-
3	sand	-23 to -64	41	25	-*	-
4	limestone	-64 to -109	45	>50	23.4	294.4

Notes: *Neglected because of high ground water table and casing may be used.
**The soft limestone layer is very close to the top of the shaft. If casing is used, the rock-casing interface will shatter during the installation. In the second case, if casing is not used, the rock-shaft interface will slip and the deformation will pass the peak strength strain into the residual strength range due to high stress concentration at the top part of the shaft. Thus, in both cases, the upper limestone stratum will behave like granular material and should be designed as such.

Figure D.1 Florida DOT Shaft Design Soil Types

Hawaii Data Source:

https://hidot.hawaii.gov/?s=geotechnical+manual&type=usa

FACTORS	LIQUEFACTION SUSCEPTIBILITY
Grain Size Distribution	Fine and uniform sands and silts are more susceptible to liquefaction than coarse or well-graded sands.
Initial Relative Density	Loose sands and silts are most susceptible to liquefaction. Liquefaction potential is inversely proportional to relative density.
Magnitude and Duration of Vibration	Liquefaction potential is directly proportional to the magnitude and duration of the earthquake.

Figure D.2 Hawaii DOT Liquefaction Factors

Kansas Data Source:

https://www.wycokck.org/WycoKCK/media/Public-Works/Engineering/Documents/Technical-Provisions-2008-Edition.pdf

Unsuitable Foundation: If material encountered at the foundation or slab subgrade is frozen, saturated, or softer than indicated by the drawings, Engineer shall be called for identification and directions. Engineer's directions to remedy unsuitable foundations shall be followed. Remediation directed by Engineer may include resizing/redesigning of the foundation; rescheduling to avoid severe weather; or overexcavation and disposal of the soft foundation.

Figure D.3 Kansas DOT Unsuitable Foundation Recommendations

New Jersey Data Source:

https://www.state.nj.us/transportation/eng/documents/BSDM/pdf/2016DesignManualforBridgesandStructures20180604.pdf

When drilled shafts, that are constructed in moderately or extremely aggressive environments and that extend through water, are used in bents, they shall be detailed to eliminate construction joints within the Splash Zone. Additionally, it is preferred that such shafts extend to the bottom of the bent cap without a construction joint.

Figure D.4 New Jersey DOT Weak Soil Adjustments

New York Data Source:

https://www.dot.ny.gov/divisions/engineering/technical-services/geotechnical-engineering-bureau/geotech-eng-repository/GDM_Ch-19_Culverts.pdf

If the geotechnical information indicates any of the following, contact the Geotechnical Engineering Bureau for recommendations:

- Ground water is located within the foundation depth.
- Soft clay, organic soil or miscellaneous fill/debris is located within or below the foundation depth.
- The foundation is placed on a slope with a finished grade steeper than two horizontal to one vertical (Minimum cover and overall stability must be checked).

If any of these conditions exist, the Geotechnical Engineering Bureau may recommend increases to the standard foundation size and/or depth. In such a case, a special foundation design is required and it should be presented on a separate plan sheet in the contract documents.

Figure D.5 New York DOT Poor Soil Conditions

Oregon Data Source:

https://www.oregon.gov/ODOT/Engineering/Documents_TrafficStandards/Traffic-Structures-Design-Manual.pdf

Foundation design according to section 13.6 of the 4th Edition 2001 AASHTO code. This will address water, sand, and cohesive soils.

Figure D.6 Oregon DOT water considerations

Rhode Island Data Source:

http://www.dot.ri.gov/documents/about/research/Geotechnical.pdf

2.5 Groundwater Levels and Issues

Groundwater typically occurs at shallow depth in Rhode Island, often within 20 feet of the ground surface. Shallow groundwater would be expected in areas adjacent to wetlands, lowland areas adjacent to local ponds, rivers, and upper Narragansett Bay. In coastal areas and along local rivers and streams, groundwater levels can often be anticipated based upon surface water levels. However, in areas of the State characterized by uneven terrain, shallow tills and bedrock, or where subsurface soils may include significant thicknesses of impermeable soils, subsurface water levels may not exhibit uniform or "expected" levels.

The major design issues associated with groundwater occurrence and relative elevations will include the effective strengths of foundation soils, consolidation of compressible and organic soils, in-service hydrostatic loads on substructures, and long-term drainage along roadcuts or through embankments. Construction phase impacts are usually associated with drainage and dewatering of excavations, and the stability of wet or saturated subgrade soils when subjected to trafficking of construction equipment. Consequently it is important that the exploration program anticipate the issues associated with near-surface groundwater upon both design and construction.

Appropriately sited monitoring wells can be installed as the geotechnical borehole is completed, or in separate shallow borings. Such wells when included in the subsurface exploration program allow estimates of groundwater elevations which can be assumed to be representative of "stabilized" measurements. Significantly, the monitoring at specific locations can be repeated over time to estimate fluctuations seasonal fluctuations, or changes in groundwater level associated with specific precipitation events.

Figure D.7 Rhode Island DOT Saturated Soil Issues and Identification

Texas Data Source:

Refer to Appendix E (AASHTO ScoTE 2015 Survey)

When in the field, bad soils or rock may be observed. If so, Texas decides whether a pole should be placed at that location. The soil conditions are evaluated with penetrometer measurements. For extremely poor conditions, geotechnical engineers may have to design a special foundation for the location. If options have been exhausted, a different location will need to be selected.

Figure D.8 Texas DOT Paraphrased from 2015 AASHTO SCoTE Luminaire Foundation Survey Results

Appendix E AASHTO Subcommittee on Traffic Engineering Survey: Luminaire Foundations in Poor Soil Conditions

In the course of the literature search, the research team discovered a survey performed in 2015 by the AASHTO Subcommittee on Traffic Engineering (ScoTE), collecting information from states on their practices for installing luminaire foundations in poor soil conditions. These survey responses complement and supplement the review compiled by Mr. Taylor Drahota provided in other Appendices, and are supplementary to Sections 2.5.1 and 2.5.5.

State	1. Do you install luminaire foundations in poor soil conditions (loose granular and/or organic soils, and in soils with high water table)?	Respondent
Oregon	YES The Oregon Department of Transportation uses the Equations from Figure C13.10-2 in Section 13.10 titled “Embedment of Lightly Loaded Small Poles and Posts” to analyze the depth of the foundation with an assumed S1 poor soil pressure. The project Geotechnical Engineer is responsible to verify that the specific luminaire locations will satisfy the assumed S1 value. When the soil is worse than the assumed S1 condition or there is water, the Geotechnical Engineer will provide recommendations for a custom foundation design. The depth will be determined by a Geotechnical or Structural designer and this information is included in the plans and specifications.	Scott U. Jollo, P.E. Traffic Structures Engineer | (: (503) 986-3069 Oregon Department of Transportation | 4040 Fairview Industrial Dr SE, MS#5 Traffic-Roadway Section | Salem, Oregon 97302-1142 http://www.oregon.gov/ODOT/HWY/TS/Pages/structures.aspx
Oklahoma	In Oklahoma, we conduct a soil report for the areas that we will install luminaire and based on that we design the footings. The length or depth of the drill shaft vary accordingly.	Tarek Ahmad Maarouf, P.E. Engineering Manager Traffic Engineering Division Oklahoma Dept. of Transportation 200 NE 21st street, Rm 2A-7 Oklahoma City, OK, 73105-3204 office: 405-522-2584 Fax : 405-521-2865
New York	YES In poor soils, we design the foundation for the conditions. Sometimes, it is just a larger version of a standard foundation, but sometimes it is a totally different solution. We have even put traffic signal poles on driven pile foundations. We prefer a reliable foundation to having to do it over when the pole starts to tilt (which has also happened).	Bob Burnett Director, Geotechnical Engineering Bureau NYSDOT, 50 Wolf Road, MP42 518-457-4711 Albany, NY 12232

Figure E.1 AASHTO ScoTE Luminaire Foundation Installation in Poor Soils Survey

State	1. Do you install luminaire foundations in poor soil conditions (loose granular and/or organic soils, and in soils with high water table)?	Respondent
Iowa	NO In Iowa, the issue is the opposite of what you have. We encounter rock and shale and switch to a spread footing in these situations. We have not developed an alternative footing for the soil conditions you have described.	Timothy D. Crouch, PE, PTOE State Traffic Engineer Iowa Department of Transportation 515-239-1513 fax 515-239-1891
New Jersey	YES We have one lighting foundation that ... is the worst case scenario state wide. Therefore our junction box foundations, JBFs, are used throughout the state. Mostly contractors install pre cast foundations due to the faster installation with less labor. We have two standard pole heights for this foundation and all designs utilize either standard height. Our lighting was made uniform many years ago. The 100 foot high mast towers require consultants to take boring samples and then provide a design that must be approved by our Geotech engineers. Otherwise our lighting is installed on the jbfs throughout the state.	Dan Black (609) 530-5383 NJDOT Electrical Operations
South Dakota	YES ...most of our soils are competent enough and free of organic material that they do not cause an issue. We do regularly encounter granular soils, sometimes loose, but certainly with high water tables. I would also like to mention that we conduct soil borings for both luminaires and traffic signals. At most traffic signal locations and occasionally at some of the luminaire locations we utilize a lateral bearing testing apparatus, developed and fabricated in-house in the late 60's, to measure the in-situ soil strength. In addition soil samples are collected and ran for classification purposes.	John Weeldreyer, PE Foundation Engineer Geotechnical Engineering Activity 700 E. Broadway Ave. (605)773-8174 SDDOT Pierre, SD 57501

Figure E.2 AASHTO ScoTE Luminaire Foundation Installation in Poor Soils Survey, Cont.

State	1. Do you install luminaire foundations in poor soil conditions (loose granular and/or organic soils, and in soils with high water table)?	Respondent
Wyoming	YES	Joel A. Meena, P.E. State Traffic Engineer 5300 Bishop Blvd. Cheyenne, Wy 82009 Wydot (307) 777-4374
Massachusetts	YES Yes, MassDOT will install luminaire foundation supports in poor soil conditions.	Neil E. Boudreau | State Traffic Engineer | Massachusetts Department of Transportation - Highway Division 10 Park Plaza Suite 7210 Boston MA 02116 857.368.9655
Nevada	NO In Nevada we are fortunate to have good soil conditions state wide.	Thomas Moore, P.E. Asst. Chief Traffic Engineer Nevada Department of Transportation
Delaware	YES	Mark Luszcz, P.E., PTOE Delaware Department of Transportation 169 Brick Store Landing Road Chief Traffic Engineer Smyrna, DE 19977 P: (302) 659-4062
Nebraska	YES We do install foundations in poor soil conditions.	Carl R. Humphrey, P.E. Nebraska Department of Roads Phone - (402) 479-3842 carl.humphrey@nebraska.gov Urban & Lighting Engineer – Roadway Design

Figure E.3 AASHTO ScoTE Luminaire Foundation Installation in Poor Soils Survey, Cont.

State	1. Do you install luminaire foundations in poor soil conditions (loose granular and/or organic soils, and in soils with high water table)?	Respondent
Minnesota	YES We have, but not a common issue	Sue Zarling, P.E., PTOE MnDOT OTST 1500 West Cty Rd B2 651-234-7052 Traffic Electrical Systems Engineer Roseville, MN 55113
Texas	YES	Meg Moore, PE Director, Traffic Engineering Section TX DOT Austin, TX

Figure E.4 AASHTO ScoTE Luminaire Foundation Installation in Poor Soils Survey, Cont.

State	2. Do you have a standard drawing/plan that specifically addresses such conditions?	
		a. Can you send a copy or link to your standard drawing?
Oregon	NO	n/a
Oklahoma	NO	n/a
New York	NO	Our standard foundations assume soils with at least 100 pound per cubic foot density and a 30 degree friction angle. The standard drawings for those can be found here: https://www.dot.ny.gov/main/business-center/engineering/cadd-info/drawings/standard-sheets-us Section 645 is for signs, Section 680 is for traffic signals
Iowa	NO	You can look at our footing details at the following link - http://www.iowadot.gov/design/SRP/IndividualStandards/eli201.pdf
New Jersey	YES	Attached PDF
South Dakota	NO We do install footings in poor soil conditions but it is not a common occurrence. These would include both loose granular soils (occasionally) and soils with high water tables (often). We rarely encounter organic soils of significant thickness at footing locations.	No standard drawing that addresses such conditions. It is considered and addressed as needed in the recommendations provided by the Foundation Section.
Wyoming	NO	

Figure E.5 AASHTO ScoTE Luminaire Foundation Installation in Poor Soils Survey, Cont.

State	2. Do you have a standard drawing/plan that specifically addresses such conditions?	
		a. Can you send a copy or link to your standard drawing?
Massachusetts	YES	Our drawings, which date back to 1968, may be found here: http://www.massdot.state.ma.us/Portals/8/docs/manuals/TrafficDetails68.pdf
Nevada	YES	
Delaware	NO Expect an effort in the near future to apply process from new Traffic Design Manual on lighting pole foundation design, utilizing soil conditions and other data, similar to current practice for signal pole foundation design.	Type 6 is our standard for lighting poles. Although our process seems to lack engineering, I am unaware of there ever being a light pole foundation failure.
Nebraska	NO We do not have any standard plans to address this. This would all be handled from the field (on–site project manager / engineer) in the few cases that we run in to.	
Minnesota	NO Not specific to poor soil conditions.	The link to the standard plate (two pages) http://dotapp7.dot.state.mn.us/edms/download?docId=1457989 http://dotapp7.dot.state.mn.us/edms/download?docId=1457990
Texas		The standard drawing for roadway illumination foundations is RID(FND)-11 ftp://ftp.dot.state.tx.us/pub/txdot-info/cmd/cserve/standard/traffic/ridfn11.pdf

Figure E.6 AASHTO ScoTE Luminaire Foundation Installation in Poor Soils Survey, Cont.

State	3. Can you describe your approach to addressing such conditions? For example:			
	a. engineer the foundation using a set of poor soil assumptions – it is what it is	b. install our deepest foundation and call it good	c. don't install luminaire supports in such conditions	d. Other
Oregon	Custom foundation design based on poor soil information			
Oklahoma	custom design for conditions			
New York	Case-by-case design for conditions			
Iowa			Don't have such conditions. Design spread footings for opposite case - rocky soil	
New Jersey		Use worst case junction box foundation design statewide		
South Dakota	We typically engineer the foundation using actual soil parameters collected in the field (it is what it is). In these situations it generally results in deeper foundation.			
Wyoming	YES			
Massachusetts	Our luminaire foundations are designed for the worst case scenario. Therefore, we overbuild a significant majority of the foundations.			

Figure E.7 AASHTO ScoTE Luminaire Foundation Installation in Poor Soils Survey, Cont.

State	3. Can you describe your approach to addressing such conditions? For example:			
	a. engineer the foundation using a set of poor soil assumptions – it is what it is	b. install our deepest foundation and call it good	c. don't install luminaire supports in such conditions	d. Other
	We are in the process of revising our standard drawings to provide multiple sizes for foundations based upon varying soil conditions; once this step is completed, we will expect the Design Engineer to obtain the soil conditions prior to project advertisement so that there are no field changes to the design. This is similar to how we treat traffic signal mast arm designs.			
Nevada		Our foundation for luminaires is a standard 2.5 ft x 5 ft pile and is used state wide.		
Delaware				install our standard foundation and make field revisions (e.g., make deeper, revise to spread footing) if there are concerns during installation
Nebraska		We try to make something work. We have had to pour larger foundations in sandy soil or have had to do a poured foundation rather		

Figure E.8 AASHTO ScoTE Luminaire Foundation Installation in Poor Soils Survey, Cont.

State	3. Can you describe your approach to addressing such conditions? For example:			
	a. engineer the foundation using a set of poor soil assumptions – it is what it is	b. install our deepest foundation and call it good	c. don't install luminaire supports in such conditions	d. Other
		than a power foundation (screw-in) in some cases. (Generally the contractor can do either a concrete or a power foundation, unless specified.		
Minnesota				If it came back that the conditions did not fall within these categories or when in the field bad soils or rock was observed we would work with the foundations group to try to resolve the issue before we would decide that we could not place a pole at a location.
Texas				The evaluation of soil conditions is based on penetrometer measurements. From the table of recommended foundation depths on RID(FND)-11, the foundation can be from 6' to 10' in depth, depending on pole height and number of blows/ft from the penetrometer. For extremely poor soil conditions, we may have our

Figure E.9 AASHTO ScoTE Luminaire Foundation Installation in Poor Soils Survey, Cont.

State	3. Can you describe your approach to addressing such conditions? For example:			
	a. engineer the foundation using a set of poor soil assumptions – it is what it is	b. install our deepest foundation and call it good	c. don't install luminaire supports in such conditions	d. Other
				geotechnical engineers evaluate the location and design a special foundation. We also could try to avoid bad locations with a different pole layout, or not install light poles at all.

Figure E.10 AASHTO ScoTE Luminaire Foundation Installation in Poor Soils Survey, Cont.

Appendix F Material Specifications

Table F.1 Bill of Materials, AKLP-1 through AKPL-6

Item No.	Description	Material Specification	Reference
a1	30" Diameter Sonotube	-	N/A
a2	W6x16, 72" Long Steel Post	ASTM A992	H#58050412-03
b1	#5 Bar, 1036 3/8" Long	ASTM A615 Gr. 60	H#7019522
b2	#8 Bar, 67" Long	ASTM A615 Gr. 60	H#7019919
c1	Concrete	AKDOT & PF Class A or Equivalent, f'c=4000 psi	Ticket# 4251447
d1	Clean, Fine Sand	AASHTO Type A-3	N/A
-	Coupling	-	Transpo COC

GERDAU

US-ML-MIDLOTHIAN
300 WARD ROAD
MIDLOTHIAN, TX 76065
USA

CERTIFIED MATERIAL TEST REPORT

Page 1 / 1

CUSTOMER SHIP TO	CUSTOMER BILL TO	GRADE	SHAPE / SIZE	DOCUMENT ID:
STEEL AND PIPE SUPPLY CO INC 401 NEW CENTURY PKWY NEW CENTURY,KS 66031-1127 USA	STEEL AND PIPE SUPPLY CO INC MANHATTAN,KS 66505-1688 USA	A992/A572-50	Wide Flange Beam / 6 X 16# / 150 X 24.0	0000720884

LENGTH	PCS	WEIGHT	HEAT / BATCH
50'00"	12	9,600 LB	58050412/03

SALES ORDER	CUSTOMER MATERIAL Nº	SPECIFICATION / DATE or REVISION
11395046/000010	000000000376160050	ASTM A6-17 ASTM A709-18 ASTM A992-20, A572-21 CSA G40.21-13 345WM, 50W

CUSTOMER PURCHASE ORDER NUMBER	BILL OF LADING	DATE
4500522049	1327-0000456741	01/18/2022

CHEMICAL COMPOSITION

C (%)	Mn (%)	P (%)	S (%)	Si (%)	Cu (%)	Ni (%)	Cr (%)	Mo(%)	Sn (%)	V (%)	Nb (%)	Al (%)	CEqvA6 (%)
0.09	0.90	0.013	0.027	0.21	0.21	0.10	0.15	0.028	0.004	0.002	0.020	0.000	0.30

MECHANICAL PROPERTIES

YS 0.2% (PSI)	UTS (PSI)	YS (MPa)	UTS (MPa)	Y/T rati (%)	G/L (Inches)	G/L (mm)	Elong. (%)
57292	72043	395	497	0.800	8.000	200.0	24.80
57613	72245	397	498	0.800	8.000	200.0	24.80

COMMENTS / NOTES

The above figures are certified chemical and physical test records as contained in the permanent records of the company. We certify that these data are correct and in compliance with specified requirements. No weld repair was performed on this material. The material has not been in contact with mercury while in Gerdau possession. This material, including the billets, was produced (Electric Arc Furnace melted, Continuously cast, and/or Hot rolled) in the USA. CMTR complies with EN 10204 3.1.

Bhaskar
BHASKAR YALAMANCHILI
QUALITY DIRECTOR
Phone: (409) 267-1071 Email: Bhaskar.Yalamanchili@gerdau.com

Wade A. L.
WADE LUMPKINS
QUALITY ASSURANCE MGR.
Phone: 972-779-3118 Email: Wade.Lumpkins@gerdau.com

Figure F.1 72-in. Long Steel Post, Test Nos. AKLP-1, AKLP-2, AKLP-3, and AKLP-4 (Item No. a2)

CMC STEEL TENNESSEE
1919 Tennessee Avenue
Knoxville TN 37921-2686

CERTIFIED MILL TEST REPORT
For additional copies call
865-202-5972/888-870-0766

We hereby certify that the test results presented here are accurate and conform to the reported grade specification

Jim Hall
Quality Assurance Manager

HEAT NO.:7019522 SECTION: REBAR 16MM (#5) 40'0" 420/60 GRADE: ASTM A615-20 Gr 420/60 ROLL DATE: 07/31/2021 MELT DATE: 07/31/2021 Cert. No.: 83550743 / 019522L765	S O L D T O	Simcote Inc 1645 Red Rock Rd Saint Paul MN US 55119-6014 6517359660	S H I P T O	Simcote Inc 1645 Red Rock Rd Saint Paul MN US 55119-6014 6517359660		Delivery#: 83550743 BOL#: 2124083 CUST PO#: MN-3776 CUST P/N: DLVRY LBS / HEAT: 90120.000 LB DLVRY PCS / HEAT: 2160 EA

Characteristic	Value	Characteristic	Value	Characteristic	Value
C	0.33%	Rebar Deformation Avg. Spaci	0.384IN		
Mn	0.68%	Rebar Deformation Avg. Heigh	0.046IN		
P	0.018%	Rebar Deformation Max. Gap	0.122IN		
S	0.059%				
Si	0.25%				
Cu	0.41%				
Cr	0.21%				
Ni	0.13%				
Mo	0.023%				
V	0.003%				
Sn	0.012%				
Yield Strength test 1	84.2ksi				
Yield Strength test 1 (metri	580MPa				
Tensile Strength test 1	101.7ksi				
Tensile Strength 1 (metric)	701MPa				
Elongation test 1	13%				
Elongation Gage Lgth test 1	8IN				
Elongation Gage Lgth 1(metri	200mm				
Bend Test 1	Passed				

The Following is true of the material represented by this MTR:
Material is fully killed
100% melted and rolled in the USA
EN10204:2004 3.1 compliant
Contains no weld repair
Contains no Mercury contamination
Manufactured in accordance with the latest version of the plant quality manual
Meets the "Buy America" requirements of 23 CFR635.410, 49 CFR 661
Warning: This product can expose you to chemicals which are known to the State of California to cause cancer, birth defects or other reproductive harm. For more information go to www.P65Warnings.ca.gov

REMARKS : ALSO MEETS AASHTO M31

Page 1 OF 1 08/07/2021 22:31:34

Figure F.2 #5 Bar, Test Nos. AKLP-1, AKLP-2, AKLP-3, and AKLP-4 (Item No. b1)

CMC STEEL TENNESSEE
1919 Tennessee Avenue
Knoxville TN 37921-2686

CERTIFIED MILL TEST REPORT
For additional copies call
865-202-5972/888-870-0766

We hereby certify that the test results presented here are accurate and conform to the reported grade specification

Jim Hall
Quality Assurance Manager

HEAT NO.:7019919 SECTION: REBAR 25MM (#8) 60'0" 420/60 SIM GRADE: ASTM A615-20 Gr 420/60 SIM ROLL DATE: 08/15/2021 MELT DATE: 08/15/2021 Cert. No.: 83563022 / 019919L799	SOLD TO: Simcote Inc 1645 Red Rock Rd Saint Paul MN US 55119-6014 6517359660	SHIP TO: Simcote Inc 1645 Red Rock Rd Saint Paul MN US 55119-6014 6517359660	Delivery#: 83563022 BOL#: 2127756 CUST PO#: MN-3776 CUST P/N: DLVRY LBS / HEAT: 107492.000 LB DLVRY PCS / HEAT: 671 EA

Characteristic	Value	Characteristic	Value	Characteristic	Value
C	0.33%	Bend Test 1	Passed		
Mn	0.72%	Rebar Deformation Avg. Spaci	0.621IN		
P	0.009%	Rebar Deformation Avg. Heigh	0.065IN		
S	0.053%	Rebar Deformation Max. Gap	0.122IN		
Si	0.22%				
Cu	0.31%				
Cr	0.16%				
Ni	0.11%				
Mo	0.014%				
V	0.002%				
Sn	0.003%				
Yield Strength test 1	86.3ksi				
Yield Strength test 1 (metri	595MPa				
Tensile Strength test 1	104.6ksi				
Tensile Strength 1 (metric)	721MPa				
Elongation test 1	11%				
Elongation Gage Lgth test 1	8IN				
Tensile to Yield ratio test1	1.21				
Elongation Gage Lgth 1(metri	200mm				

The Following is true of the material represented by this MTR:
*Material is fully killed
*100% melted and rolled in the USA
*EN10204:2004 3.1 compliant
*Contains no weld repair
*Contains no Mercury contamination
*Manufactured in accordance with the latest version of the plant quality manual
*Meets the "Buy America" requirements of 23 CFR635.410, 49 CFR 661
*Warning: This product can expose you to chemicals which are known to the State of California to cause cancer, birth defects or other reproductive harm. For more information go to www.P65Warnings.ca.gov

REMARKS :

Page 1 OF 1 08/15/2021 20:29:42

Figure F.3 #8 Bar, Test Nos. AKLP-1, AKLP-2, AKLP-3, and AKLP-4 (Item No. b2)

Ready Mixed Concrete Company
6200 Cornhusker Hwy, Lincoln, NE 68529
Phone: (402) 434-1844 Fax: (402) 434-1877

Customer's Signature: ____________________

PLANT	TRUCK	DRIVER	CUSTOMER	PROJECT	TAX	PO NUMBER	DATE	TIME	TICKET
4	205	11071	62461		NTE	ALASKA	4/4/22	10:09 AM	4251447

Customer	Delivery Address	Special Instructions
UNL-MIDWEST ROADSIDE SAFETY	3630 NW 36TH ST	NW 36TH ST & W LUKE ST EAST TO TEST AREA NORTH OF THE GOODYEAR HANGAR

LOAD QUANTITY	CUMULATIVE QUANTITY	ORDERED QUANTITY	PRODUCT CODE	PRODUCT DESCRIPTION	UOM	UNIT PRICE	EXTENDED PRICE
3.00	3.00	3.00	QL3S4504	LNK47B1S384000H	yd	$148.50	$445.50
				MINIMUM HAUL			$40.00

Water Added On Job At Customer's Request: ____________

SLUMP
4.00 in

Notes:

TICKET SUBTOTAL	$485.50
SALES TAX	$0.00
TICKET TOTAL	**$485.50**
PREVIOUS TOTAL	
GRAND TOTAL	**$485.50**

CAUTION FRESH CONCRETE
KEEP CHILDREN AWAY

Contains Portland cement. Freshly mixed cement, mortar, concrete or grout may cause skin injury. Avoid prolonged contact with skin. Always wear appropriate Personal Protective Equipment (PPE). In case of contact with eyes or skin, flush thoroughly with water. If irritation persists, seek medical attention promptly.

Terms & Conditions

This concrete is produced with the ASTM standard specifications for ready mix concrete. Strengths are based on a 3" slump. Drivers are not permitted to add water to the mix to exceed this slump, except under the authorization of the customer and their acceptance of any decrease in compressive strength and any risk of loss as a result thereof. Cylinder tests must be handled according to ACI/ASTM specifications and drawn by a licensed testing lab and/or certified technician.
Ready Mixed Concrete Company will not deliver any product beyond any curb lines unless expressly told to do so by customer and customer assumes all liability for any personal or property damage that may occur as a result of any such directive.
The purchaser's exceptions and claims shall be deemed waived unless made in writing within 3 days from time of delivery. In such a case, seller shall be given full opportunity to investigate any such claim. Seller's liability shall in no event exceed the purchase price of the materials against which any claims are made.

Figure F.4 Concrete, Test Nos. AKLP-1, AKLP-2, AKLP-3, and AKLP-4 (Item No. c1)

TRANSPO INDUSTRIES, INC.

20 Jones Street
New Rochelle, NY 10801-6098
914-636-1000 | 800-321-7870
Fax: 914-636-1282 | info@transpo.com
WWW.TRANSPO.COM

Domestic Mill Certification (Safety Division)

Supplied to: **MIDWEST ROADSIDE SAFETY FACILITY**
Date: 05/23/2022
PO No.: E000982501
SO No.: 2001338
INV No.: 2001822

ITEM NO.:	ITEM DESC:	Qty. Shipped:
SPM5100	1" POLE SAFE SET OF 4 DOUBLE NECK MALE	5
SBABPK	1" TYPE B ANCHOR KIT	5

Donna M. Toone - Notary Public - State of New York
No. 01TO6165030 - Qualified in Westchester County
- Commission Expires - 20 23

Attached is documentation from our suppliers that the steel used in our products is both melted and manufactured in the U.S.A.

TRANSPO INDUSTRIES, INC.
Kenneth O'Conner
Materials Manager

Subscribed and sworn to before me on this 1 day of June 2022
Donna M. Toone
Notary Public

SAFER TRANSPORTATION THROUGH INNOVATION
An Equal Opportunity Employer

Figure F.5 Coupling COC, Test Nos. AKLP-5 and AKLP-6

Appendix G Bogie Test Results

The results of the recorded data from each accelerometer for every dynamic bogie test are provided in the summary sheets found in this appendix. Summary sheets include acceleration, velocity, and deflection vs. time plots as well as force vs. deflection and energy vs. deflection plots. Note that SLICE-2 data for test no. AKLP-4 was not recorded due to technical difficulties.

MIDWEST ROADSIDE SAFETY FACILITY

Bogie Test Summary

Test Information	
Test Description:	AK Evaluation of Light Pole Foundation Embedmer
Test Number:	AKLP-1
Test Date:	5/16/2022
Failure Type:	Post hinging at foundation
Post Properties	
Post Type:	
Post Size:	
Post Length:	
Embedment Depth:	
Orientation:	
Soil Properties	
Gradation:	Sand
Moisture Content:	3.00%
Compaction Method:	
Bogie Properties	
Impact Velocity:	18.9 mph (27.73 ft/s)
Impact Height:	25
Bogie Mass:	1860 lb
Data Acquired	
Accelerometer:	SLICE-1
Camera Data:	AOS-11, AOS-12

Test Results Summary		
Event Duration:	0.0647	sec
Max. Deflection:	8.1	in.
Peak Force:	42.8	k
Initial Linear Stiffness:	19.0	k/in.
Total Energy:	266.6	k-in.

	@ 5"	@ 10"	@ 15"	@20"
Average Force (k)	31.14	NA	NA	NA
Energy (k-in.)	155.7	NA	NA	NA

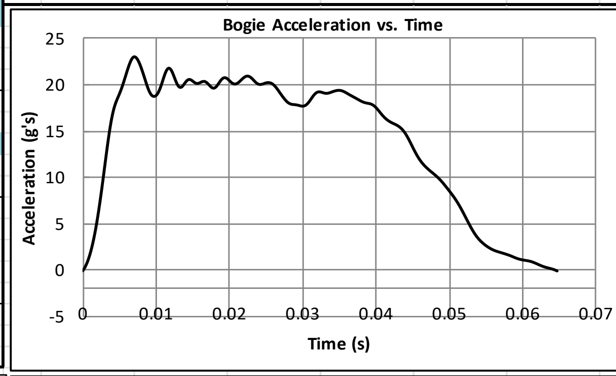

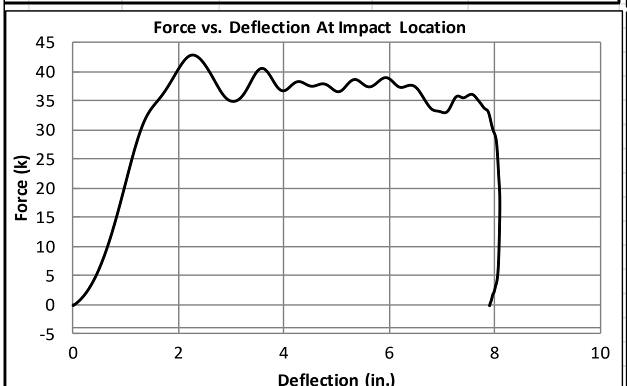

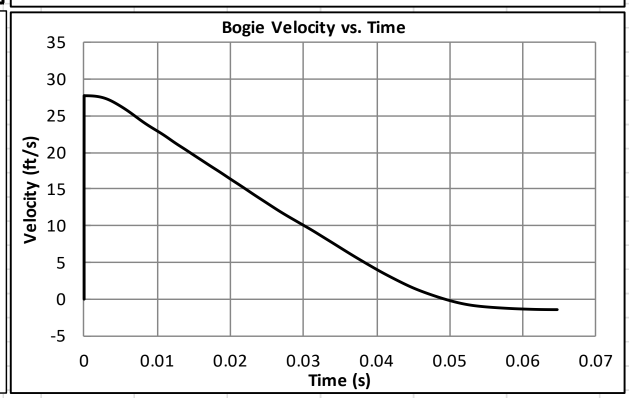

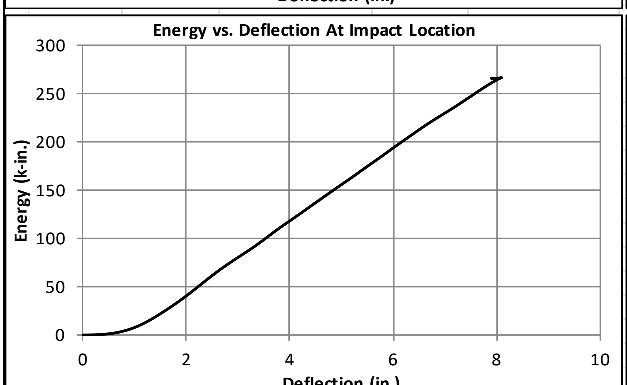

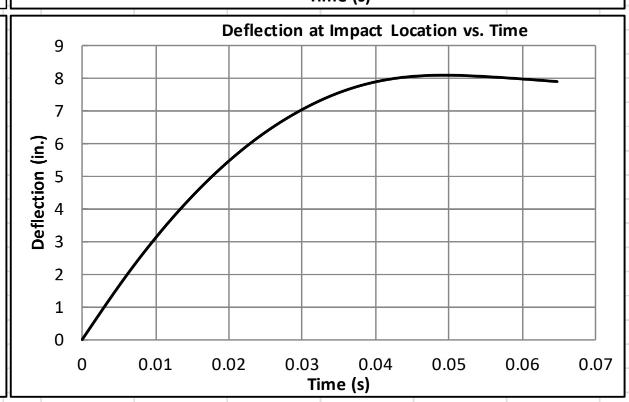

Figure G.1 Test No. AKLP-1 Results (SLICE-1)

MIDWEST ROADSIDE SAFETY FACILITY

Bogie Test Summary

Test Information

Test Description:	AK Evaluation of Light Pole Foundation Embedmer	
Test Number:	AKLP-1	
Test Date:	5/16/2022	
Failure Type:	Post hinging at foundation	

Post Properties

Post Type:	
Post Size:	
Post Length:	
Embedment Depth:	
Orientation:	

Soil Properties

Gradation:	Sand
Moisture Content:	3.00%
Compaction Method:	

Bogie Properties

Impact Velocity:	18.9 mph	(27.73 ft/s)
Impact Height:	25	
Bogie Mass:	1860 lb	

Data Acquired

Accelerometer:	SLICE-2
Camera Data:	AOS-11, AOS-12

Test Results Summary

Event Duration:	0.0647	sec
Max. Deflection:	8.3	in.
Peak Force:	38.5	k
Initial Linear Stiffness:	16.2	k/in.
Total Energy:	266.6	k-in.

	@ 5"	@ 10"	@ 15"	@20"
Average Force (k)	29.84	NA	NA	NA
Energy (k-in.)	149.2	NA	NA	NA

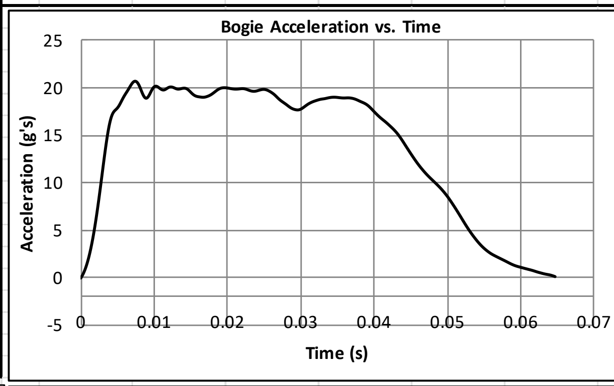

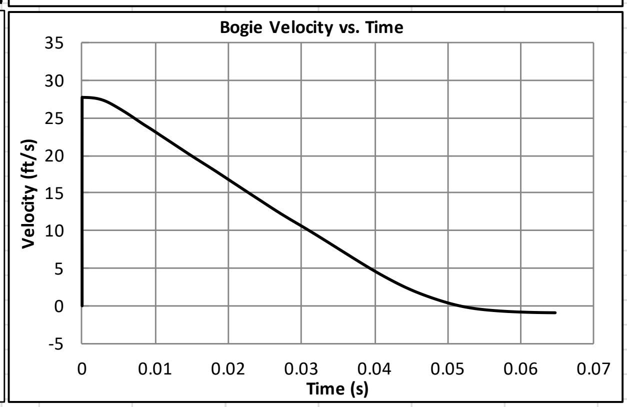

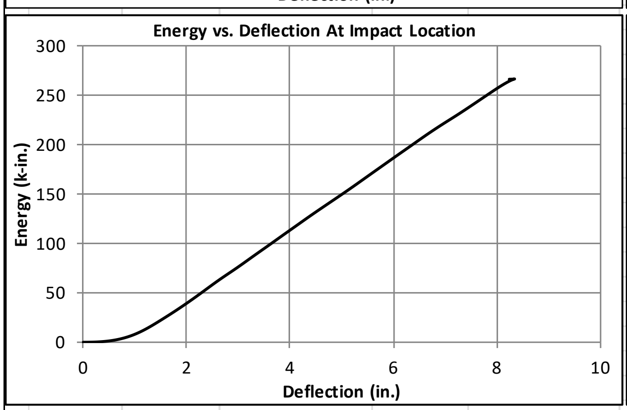

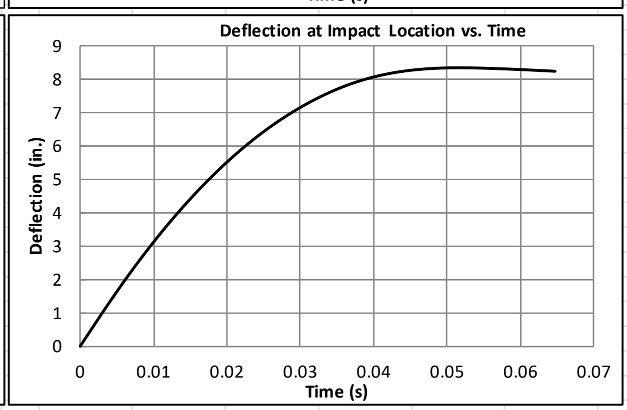

Figure G.2 Test No. AKLP-1 Results (SLICE-2)

MIDWEST ROADSIDE SAFETY FACILITY

Bogie Test Summary

Test Information	
Test Description:	AK Evaluation of Light Pole Foundation Embedmer
Test Number:	AKLP-2
Test Date:	5/19/2022
Failure Type:	Post hinging at foundation, foundation rotation
Post Properties	
Post Type:	Long Steel Post
Post Size:	W6X16
Post Length:	72
Embedment Depth:	36
Orientation:	Strong Axis
Soil Properties	
Gradation:	Dry Sand
Moisture Content:	3.00%
Compaction Method:	None
Bogie Properties	
Impact Velocity:	18.96 mph (27.8 ft/s)
Impact Height:	25
Bogie Mass:	1860 lb
Data Acquired	
Accelerometer:	SLICE-1
Camera Data:	AOS-11, AOS-12

Test Results Summary		
Event Duration:	0.2469	sec
Max. Deflection:	25.8	in.
Peak Force:	37.6	k
Initial Linear Stiffness:	17.1	k/in.
Total Energy:	268.1	k-in.

	@ 5"	@ 10"	@ 15"	@20"
Average Force (k)	27.41	18.58	14.25	11.86
Energy (k-in.)	137.0	185.8	213.8	237.2

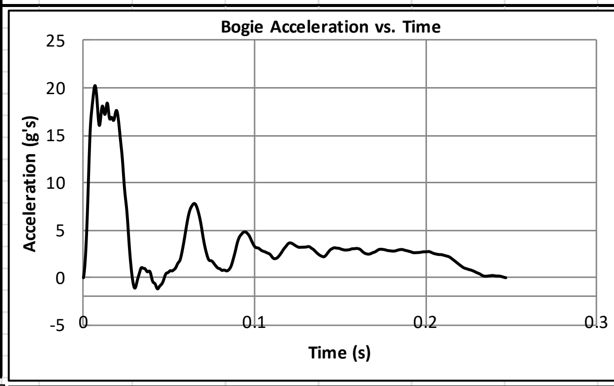

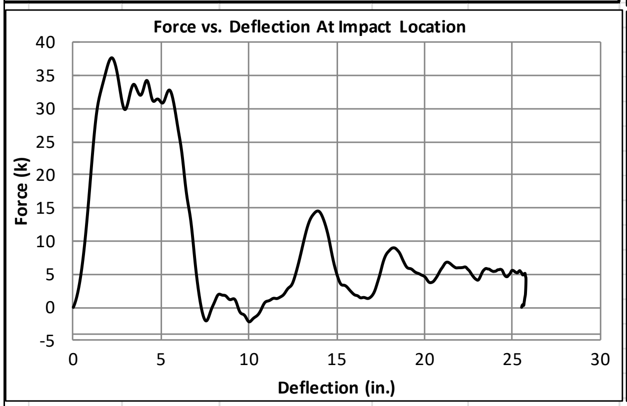

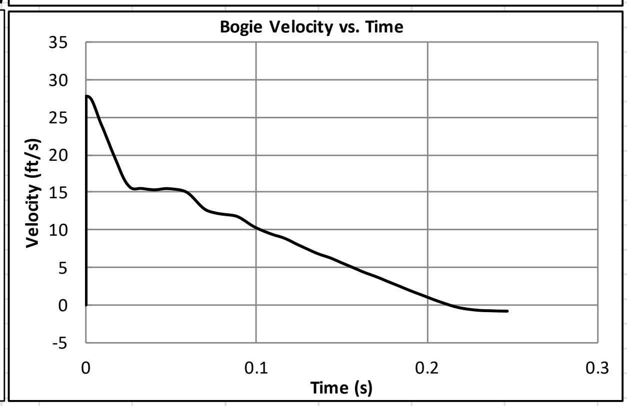

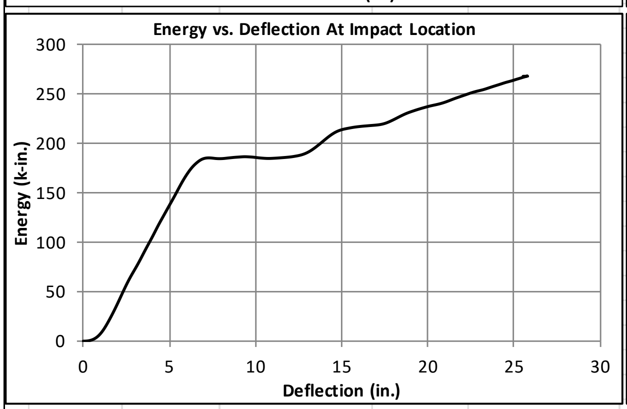

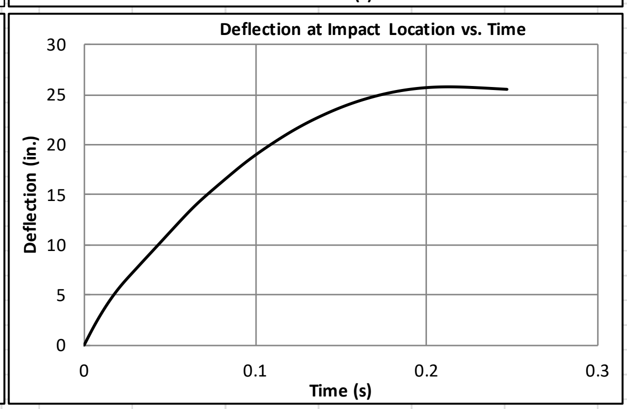

Figure G.3 Test No. AKLP-2 Results (SLICE-1)

MIDWEST ROADSIDE SAFETY FACILITY

Bogie Test Summary

Test Information

Test Description:	AK Evaluation of Light Pole Foundation Embedmer
Test Number:	AKLP-2
Test Date:	5/19/2022
Failure Type:	Post hinging at foundation, foundation rotation

Post Properties

Post Type:	Long Steel Post
Post Size:	W6X16
Post Length:	72
Embedment Depth:	36
Orientation:	Strong Axis

Soil Properties

Gradation:	Dry Sand
Moisture Content:	N/A
Compaction Method:	None

Bogie Properties

Impact Velocity:	18.96 mph	(27.8 ft/s)
Impact Height:	25	
Bogie Mass:	1860 lb	

Data Acquired

Accelerometer:	SLICE-2
Camera Data:	AOS-11, AOS-12

Test Results Summary

Event Duration:	0.2469	sec
Max. Deflection:	26.1	in.
Peak Force:	34.9	k
Initial Linear Stiffness:	15.2	k/in.
Total Energy:	268.1	k-in.

	@ 5"	@ 10"	@ 15"	@20"
Average Force (k)	26.56	18.34	14.02	11.73
Energy (k-in.)	132.8	183.4	210.3	234.6

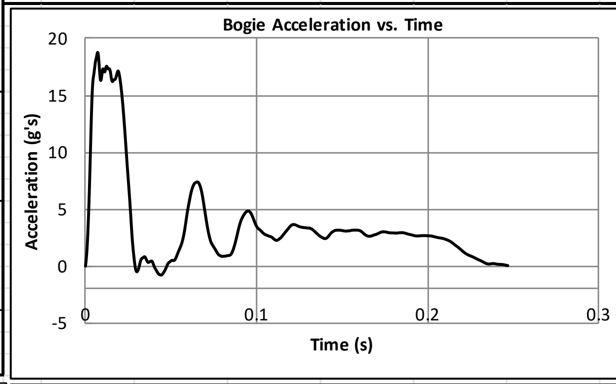

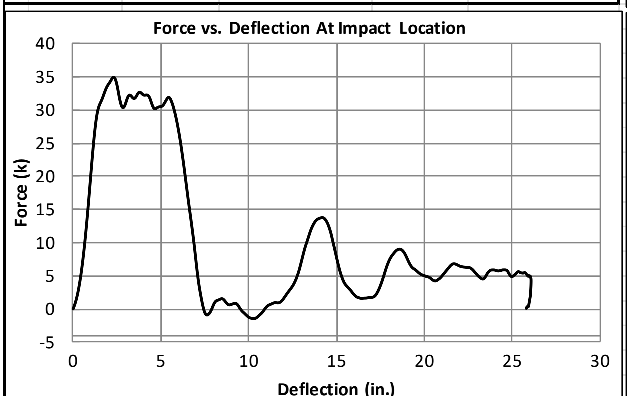

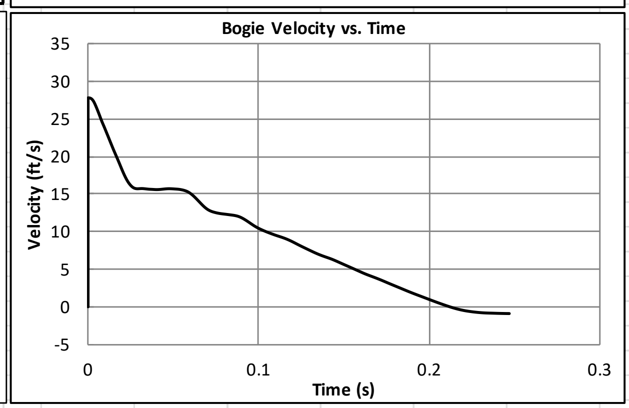

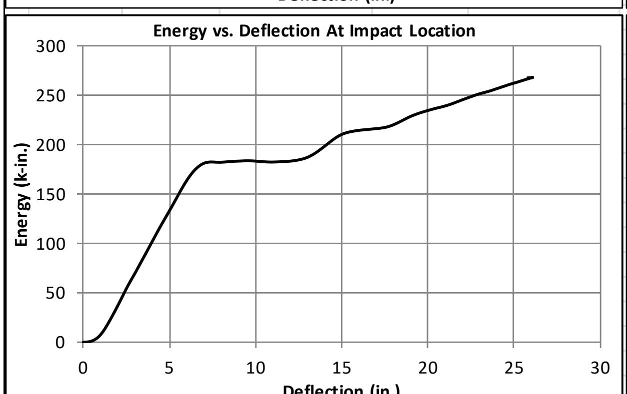

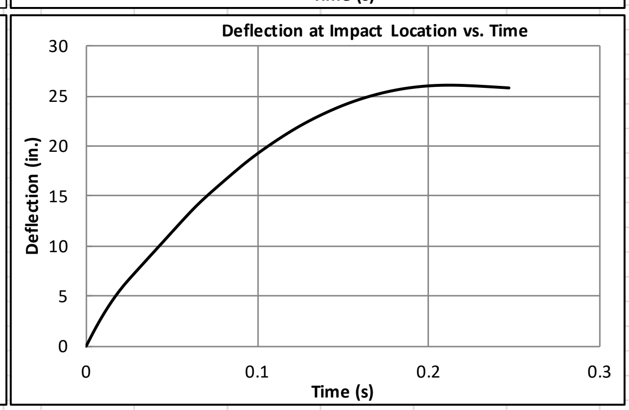

Figure G.4 Test No. AKLP-2 Results (SLICE-2)

MIDWEST ROADSIDE SAFETY FACILITY

Bogie Test Summary

Test Information

Test Description:	AK Evaluation of Light Pole Foundation Embedmer
Test Number:	AKLP-3
Test Date:	7/28/2022
Failure Type:	Post hinging at foundation

Post Properties

Post Type:	
Post Size:	
Post Length:	
Embedment Depth:	
Orientation:	

Soil Properties

Gradation:	Sand
Moisture Content:	Approximately 5% to 8%
Compaction Method:	

Bogie Properties

Impact Velocity:	18.9 mph	(27.73 ft/s)
Impact Height:	25	
Bogie Mass:	1871 lb	

Data Acquired

Accelerometer:	SLICE-1
Camera Data:	AOS-11, AOS-12

Test Results Summary

Event Duration:	0.0680	sec
Max. Deflection:	9.6	in.
Peak Force:	35.0	k
Initial Linear Stiffness:	16.1	k/in.
Total Energy:	268.0	k-in.

	@ 5"	@ 10"	@ 15"	@20"
Average Force (k)	25.75	NA	NA	NA
Energy (k-in.)	128.7	NA	NA	NA

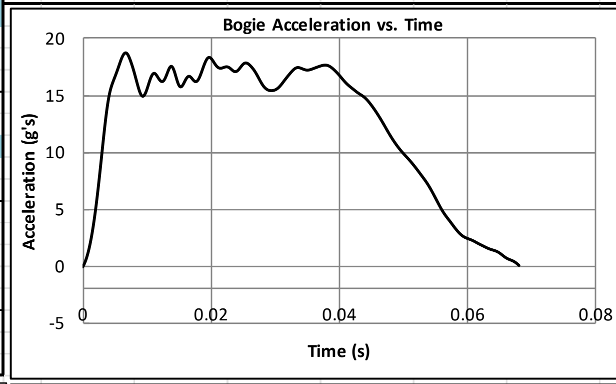

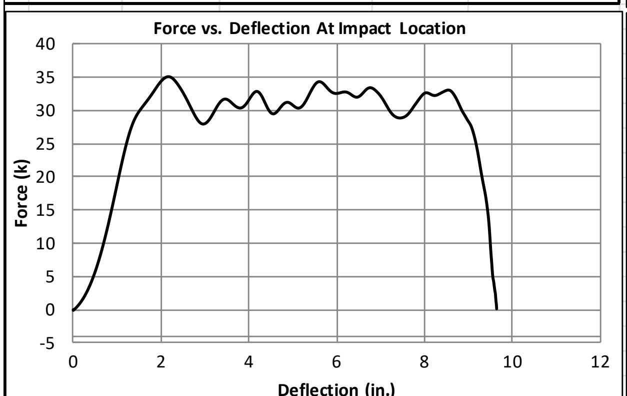

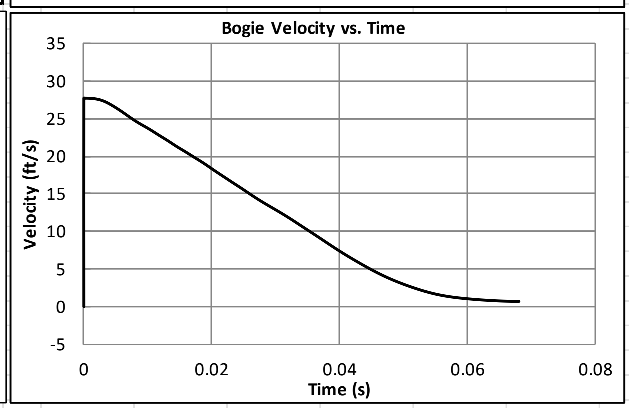

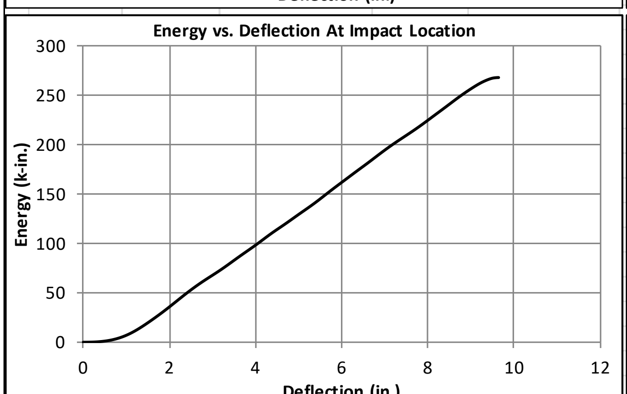

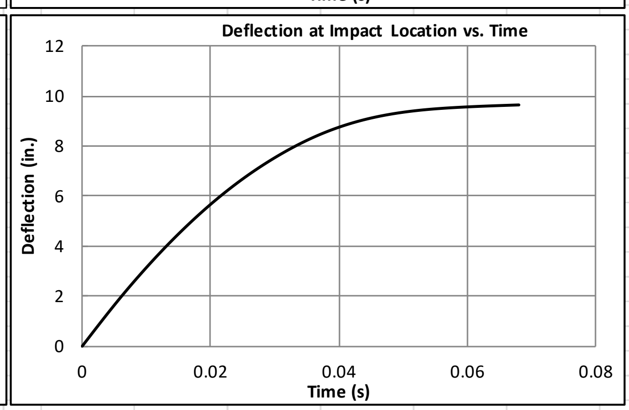

Figure G.5 Test No. AKLP-3 Results (SLICE-1)

MIDWEST ROADSIDE SAFETY FACILITY

Bogie Test Summary

Test Information

Test Description:	AK Evaluation of Light Pole Foundation Embedmer
Test Number:	AKLP-4
Test Date:	8/5/2022
Failure Type:	Post hinging at foundation

Post Properties

Post Type:	
Post Size:	
Post Length:	
Embedment Depth:	
Orientation:	

Soil Properties

Gradation:	Sand
Moisture Content:	Dry sand
Compaction Method:	

Bogie Properties

Impact Velocity:	19.78 mph	(29.01 ft/s)
Impact Height:	25	
Bogie Mass:	1860 lb	

Data Acquired

Accelerometer:	SLICE-1
Camera Data:	AOS-11, AOS-12

Test Results Summary

Event Duration:	0.0679	sec
Max. Deflection:	9.5	in.
Peak Force:	37.9	k
Initial Linear Stiffness:	6.5	k/in.
Total Energy:	291.9	k-in.

	@ 5"	@ 10"	@ 15"	@20"
Average Force (k)	26.90	NA	NA	NA
Energy (k-in.)	134.5	NA	NA	NA

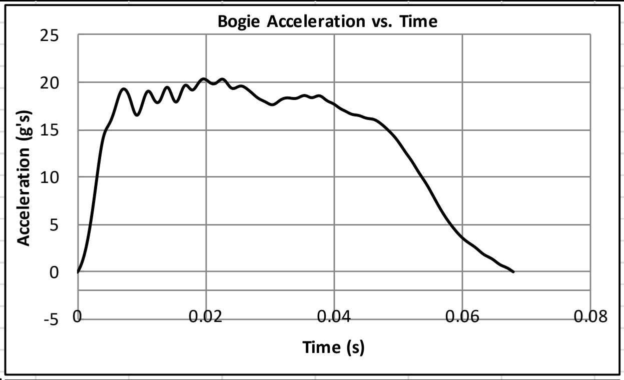

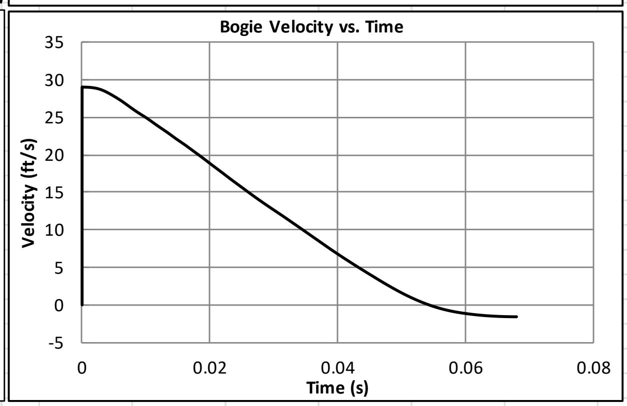

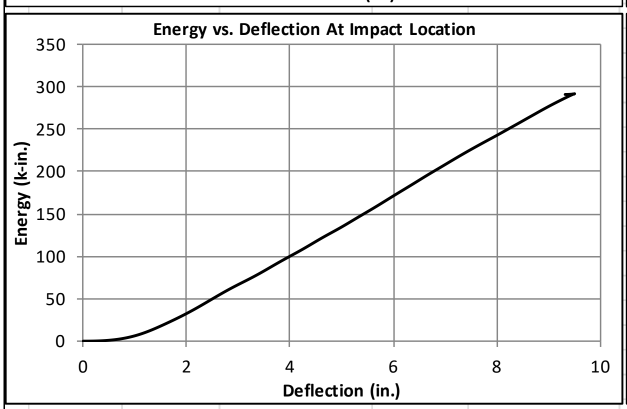

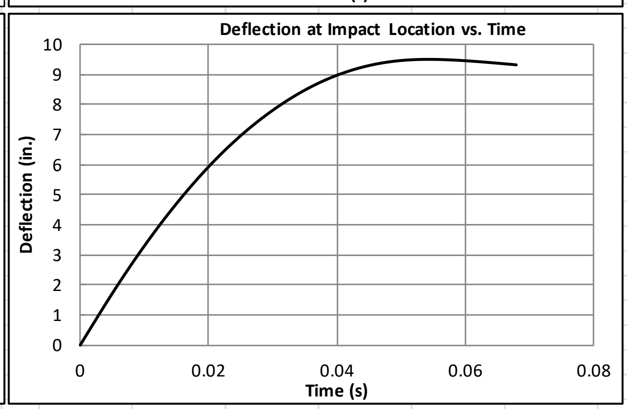

Figure G.6 Test No. AKLP-4 Results (SLICE-1)

MIDWEST ROADSIDE SAFETY FACILITY

Bogie Test Summary

Test Information

Test Description:	AK Evaluation of Light Pole in non-compounded d
Test Number:	AKLP-5
Test Date:	11/1/2022
Failure Type:	broke away at couplings

Post Properties

Post Type:	N/A
Post Size:	N/A
Post Length:	N/A
Embedment Depth:	N/A
Orientation:	N/A

Soil Properties

Gradation:	Sand
Moisture Content:	Dry sand
Compaction Method:	none

Bogie Properties

Impact Velocity:	20.35 mph	(29.85 ft/s)
Impact Height:	25	
Bogie Mass:	1858 lb	

Data Acquired

Accelerometer:	SLICE-1
Camera Data:	AOS-8, AOS-11, AOS-12

Test Results Summary

Event Duration:	0.2401	sec
Max. Deflection:	68.2	in.
Peak Force:	27.8	k
Initial Linear Stiffness:	6.1	k/in.
Total Energy:	126.5	k-in.

	@ 5"	@ 10"	@ 15"	@20"
Average Force (k)	16.59	12.40	8.40	6.22
Energy (k-in.)	83.0	124.0	126.0	124.3

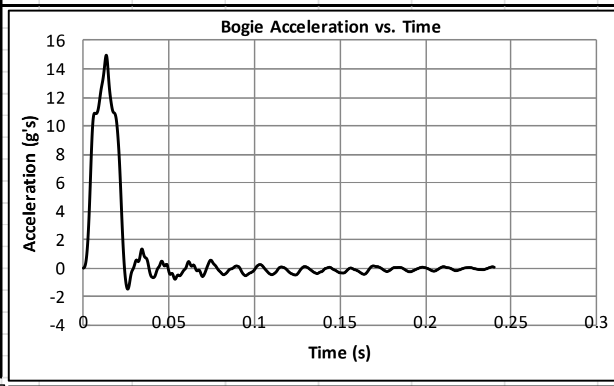

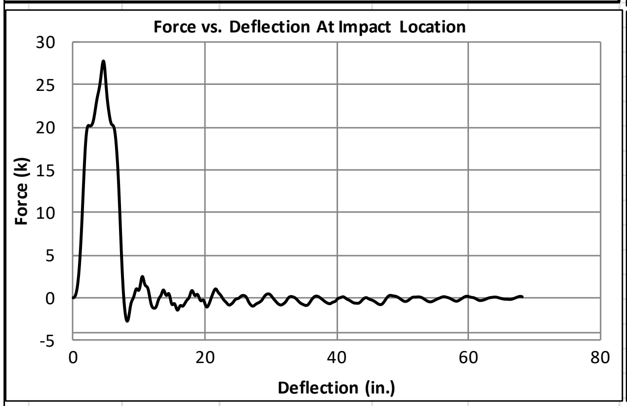

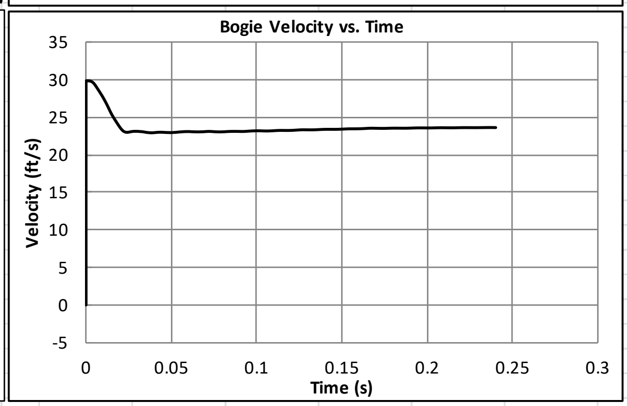

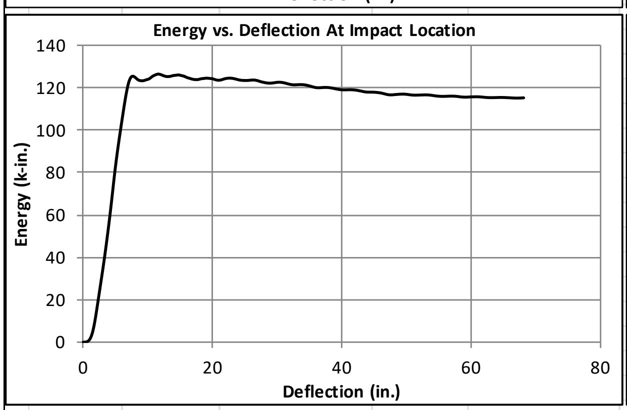

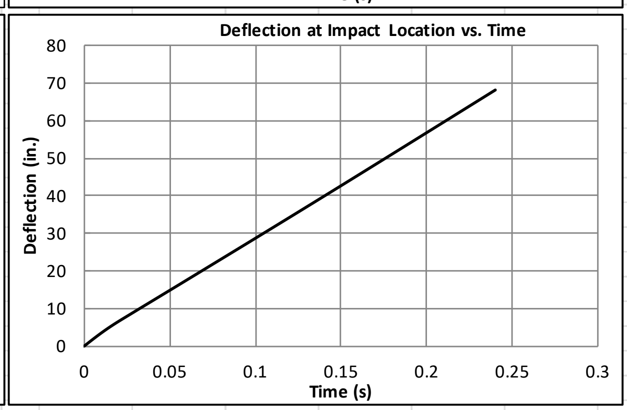

Figure G.7 Test No. AKLP-5 Results (SLICE-1)

MIDWEST ROADSIDE SAFETY FACILITY

Bogie Test Summary

Test Information

Test Description:	AK Evaluation of Light Pole in non-compacted dry
Test Number:	AKLP-5
Test Date:	11/1/2022
Failure Type:	broke away at couplings

Post Properties

Post Type:	N/A
Post Size:	N/A
Post Length:	N/A
Embedment Depth:	N/A
Orientation:	N/A

Soil Properties

Gradation:	Sand
Moisture Content:	Dry sand
Compaction Method:	none

Bogie Properties

Impact Velocity:	20.35 mph	(29.85 ft/s)
Impact Height:	25	
Bogie Mass:	1858 lb	

Data Acquired

Accelerometer:	SLICE-2
Camera Data:	AOS-8, AOS-11, AOS-12

Test Results Summary

Event Duration:	0.2401	sec
Max. Deflection:	68.3	in.
Peak Force:	26.8	k
Initial Linear Stiffness:	6.1	k/in.
Total Energy:	123.3	k-in.

	@ 5"	@ 10"	@ 15"	@20"
Average Force (k)	16.64	12.14	8.18	6.08
Energy (k-in.)	83.2	121.4	122.8	121.7

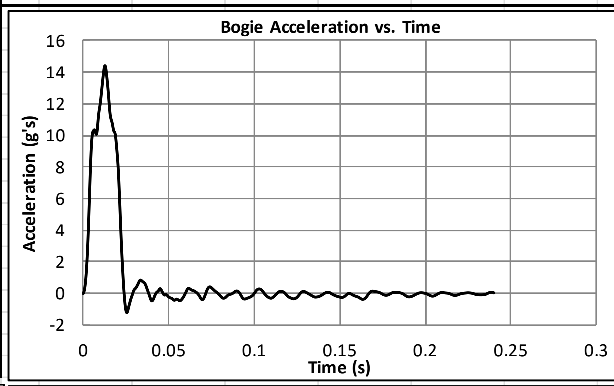

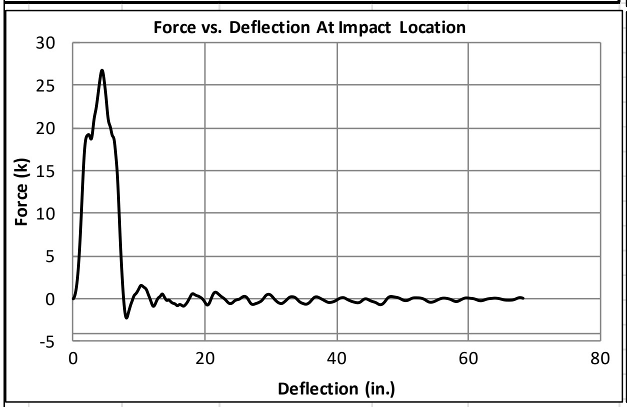

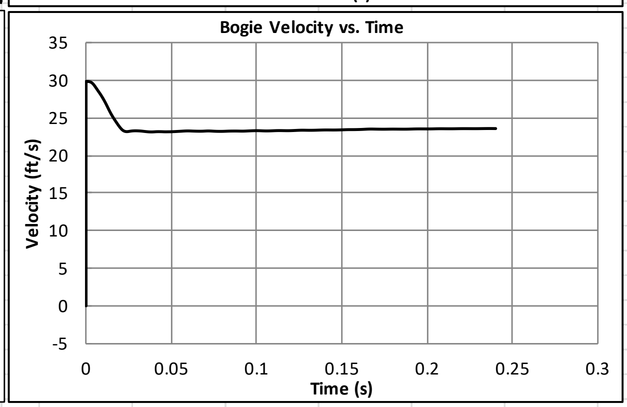

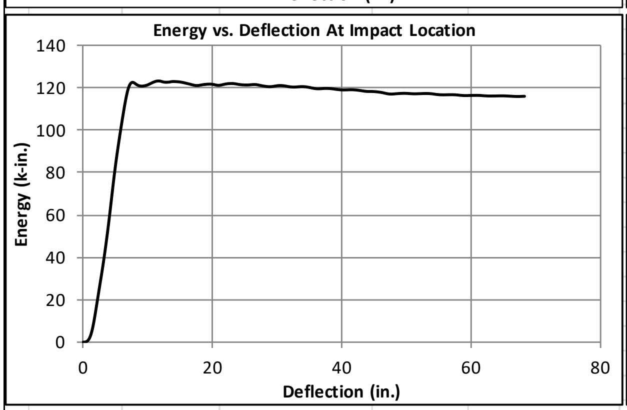

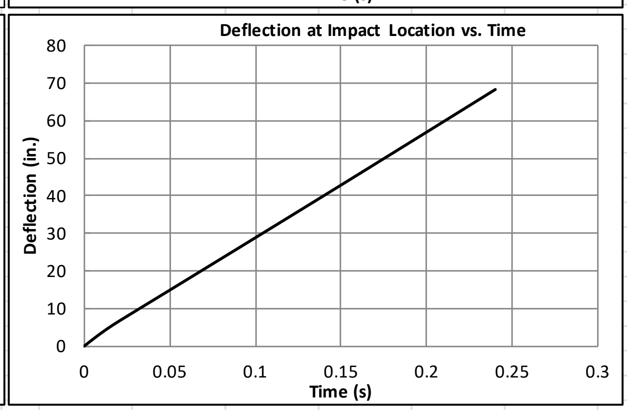

Figure G.8 Test No. AKLP-5 Results (SLICE-2)

MIDWEST ROADSIDE SAFETY FACILITY

Bogie Test Summary

Test Information

Test Description:	AK Evaluation of Light Pole in non-compounded s
Test Number:	AKLP-6
Test Date:	12/1/2022
Failure Type:	Broke away at couplings

Post Properties

Post Type:	N/A
Post Size:	N/A
Post Length:	N/A
Embedment Depth:	N/A
Orientation:	N/A

Soil Properties

Gradation:	Sand
Moisture Content:	Saturated
Compaction Method:	none

Bogie Properties

Impact Velocity:	19.98 mph	(29.3 ft/s)
Impact Height:	25	
Bogie Mass:	1782 lb	

Data Acquired

Accelerometer:	SLICE-1
Camera Data:	AOS-8, AOS-11, AOS-12

Test Results Summary

Event Duration:	0.5000	sec
Max. Deflection:	134.0	in.
Peak Force:	27.5	k
Initial Linear Stiffness:	10.8	k/in.
Total Energy:	188.3	k-in.

	@ 5"	@ 10"	@ 15"	@20"
Average Force (k)	17.57	9.52	6.39	4.85
Energy (k-in.)	87.9	95.2	95.8	97.0

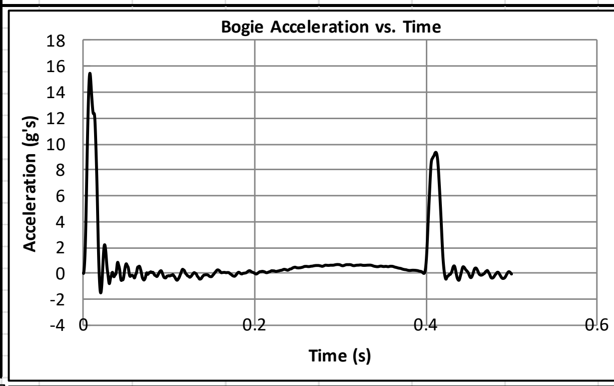

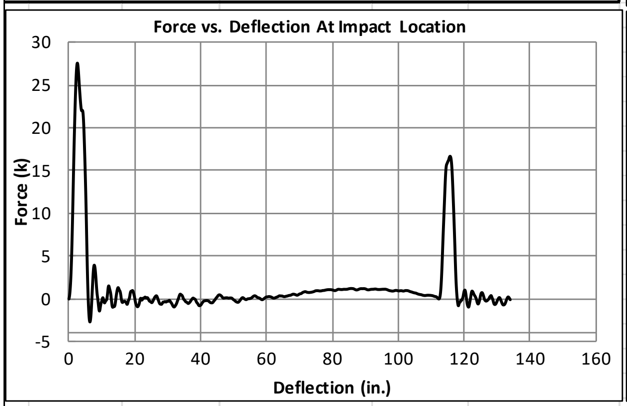

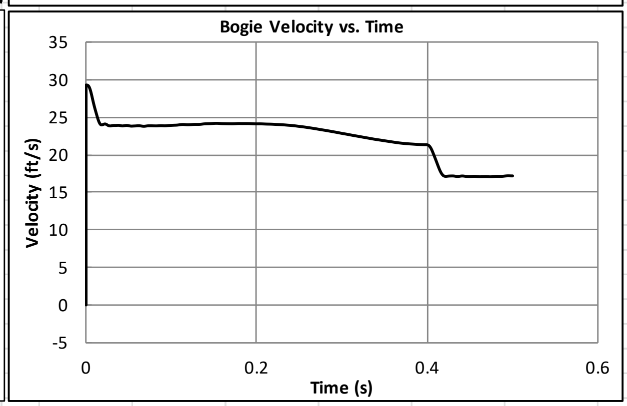

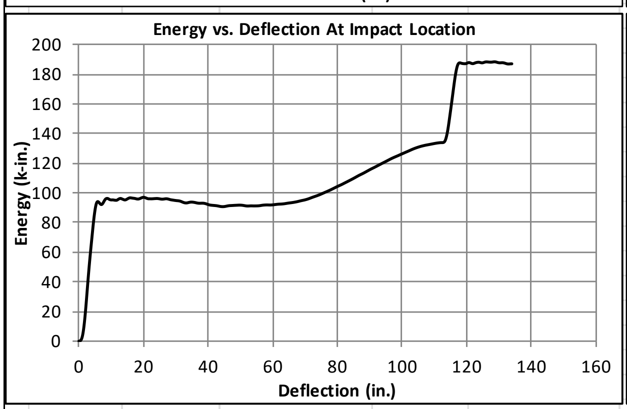

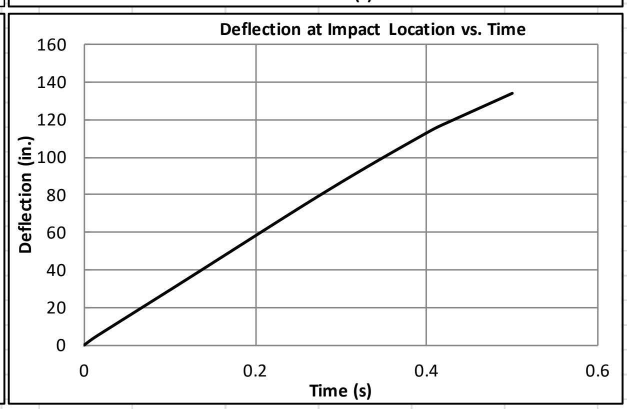

Figure G.9 Test No. AKLP-6 Results (SLICE-1)

MIDWEST ROADSIDE SAFETY FACILITY

Bogie Test Summary

Test Information	
Test Description:	AK Evaluation of Light Pole in non-compacted satu
Test Number:	AKLP-6
Test Date:	12/1/2022
Failure Type:	Broke away at couplings
Post Properties	
Post Type:	N/A
Post Size:	N/A
Post Length:	N/A
Embedment Depth:	N/A
Orientation:	N/A
Soil Properties	
Gradation:	Sand
Moisture Content:	Saturated
Compaction Method:	none
Bogie Properties	
Impact Velocity:	19.98 mph (29.3 ft/s)
Impact Height:	25
Bogie Mass:	1782 lb
Data Acquired	
Accelerometer:	SLICE-2
Camera Data:	AOS-8, AOS-11, AOS-12

Test Results Summary		
Event Duration:	0.5000	sec
Max. Deflection:	133.1	in.
Peak Force:	26.9	k
Initial Linear Stiffness:	10.8	k/in.
Total Energy:	189.3	k-in.

	@ 5"	@ 10"	@ 15"	@20"
Average Force (k)	17.62	9.53	6.38	4.82
Energy (k-in.)	88.1	95.3	95.6	96.4

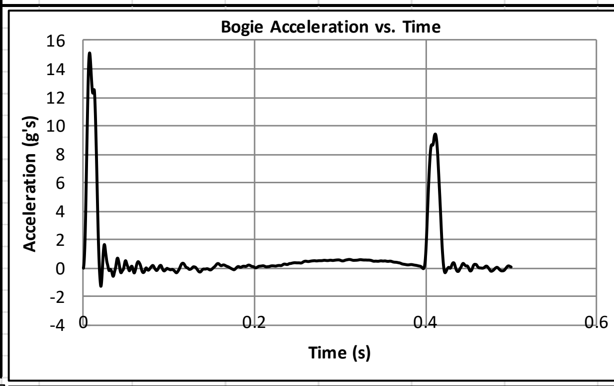

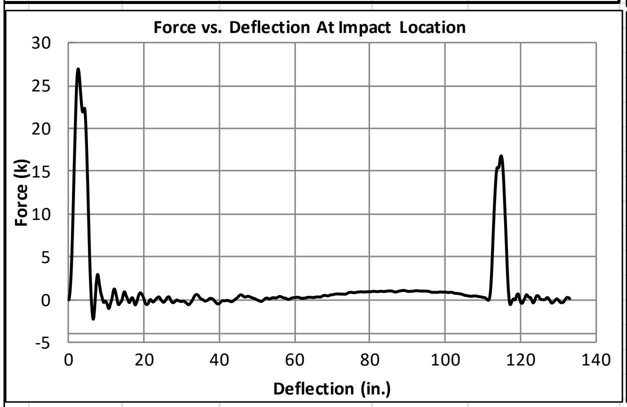

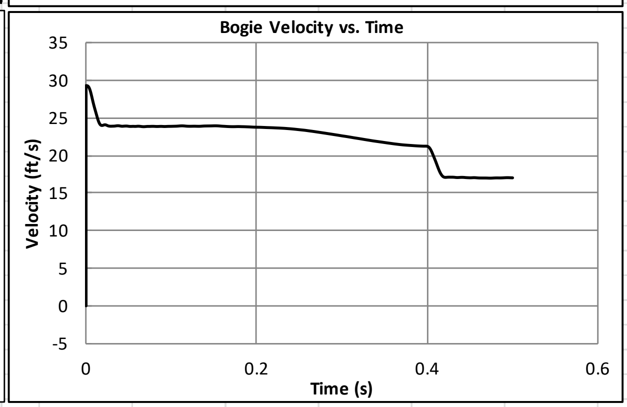

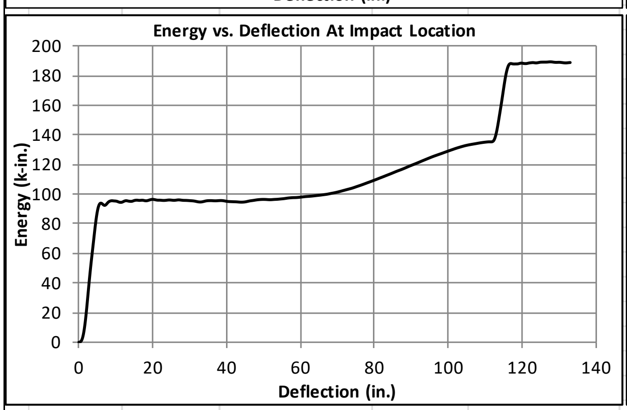

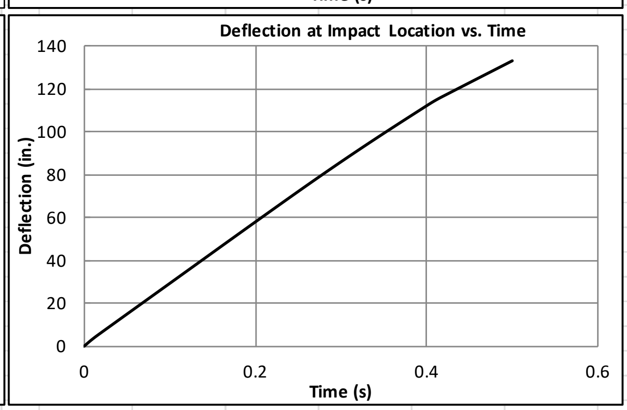

Figure G.10 Test No. AKLP-6 Results (SLICE-2)

Appendix H String Potentiometer Data

MIDWEST ROADSIDE SAFETY FACILITY

String Potentiometer Summary

Test Information:

Test No:	AKLP-1
Date:	5/16/2022
System / Test Article:	AK Evaluation of Light Pole Foundation Embedment
SP Location / Component:	0
Additional Notes:	

String Potentiometer Information:

String Pot No.:	25023706	
Calibration Factor:	12.40002	mV/V/in.
Input Voltage (excitation):	10.01	Volts
Gain:	1	
Full Scale Load:	1	
Sample Rate:	10000	Hz
Cutoff Frequency:	100	Hz

Results:

Max. Displacement:	1.55	in.
Time of Max. Displacement:	0.0502	sec
Event Duration:	0.1893	sec
Final Displacement:	0.91	in.

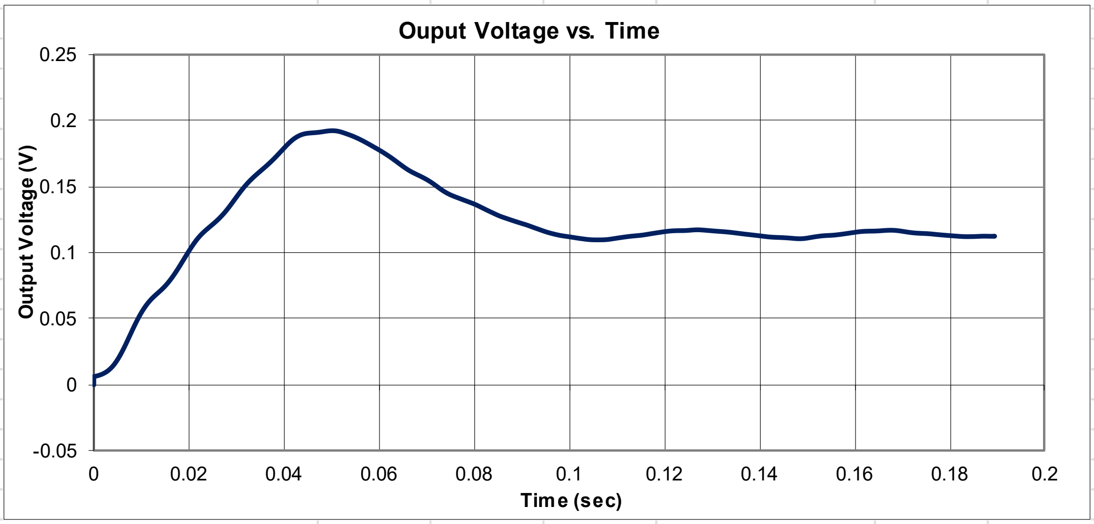

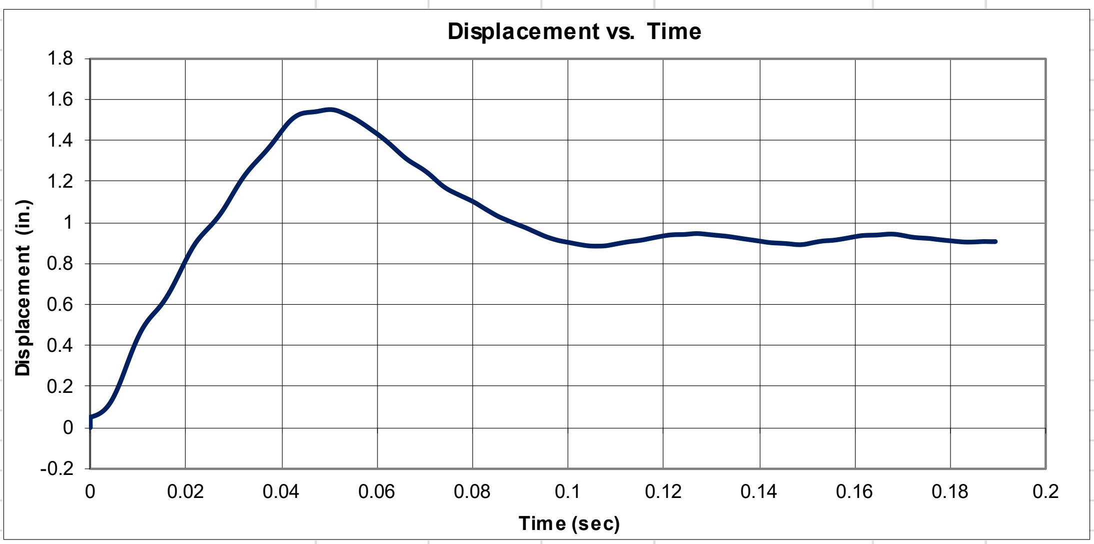

Figure H.1 String Potentiometer Data, Test No. AKLP-1

MIDWEST ROADSIDE SAFETY FACILITY

String Potentiometer Summary

Test Information:

Test No:	AKLP-2
Date:	5/19/2022
System / Test Article:	AK Evaluation of Light Pole Foundation Embedment
SP Location / Component:	0
Additional Notes:	

String Potentiometer Information:			Results:		
String Pot No.:	25023706		Max. Displacement:	12.86	in.
Calibration Factor:	12.40002	mV/V/in.	Time of Max. Displacement:	0.4392	sec
Input Voltage (excitation):	10	Volts	Event Duration:	0.5	sec
Gain:	1		Final Displacement:	12.85	in.
Full Scale Load:	1				
Sample Rate:	10000	Hz			
Cutoff Frequency:	100	Hz			

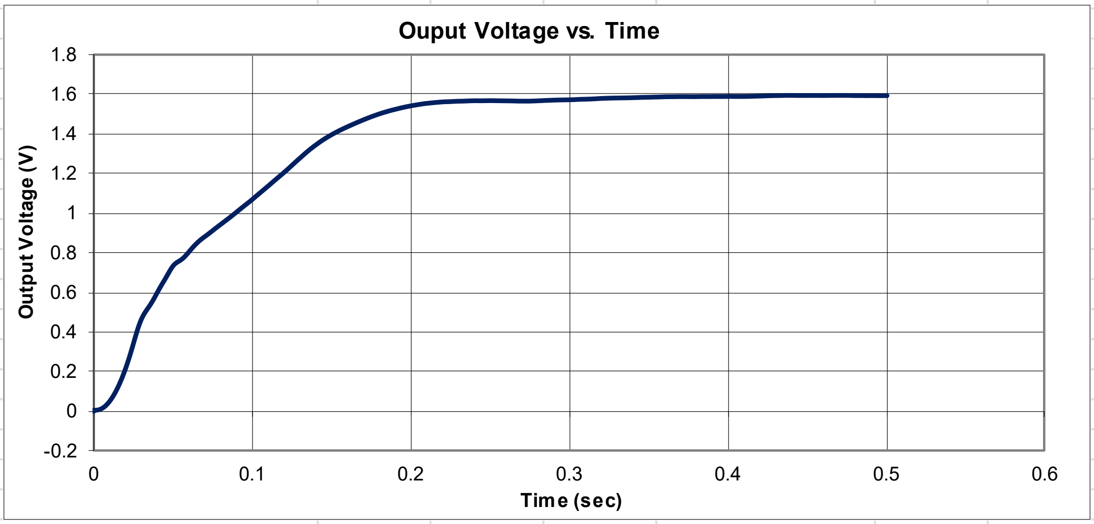

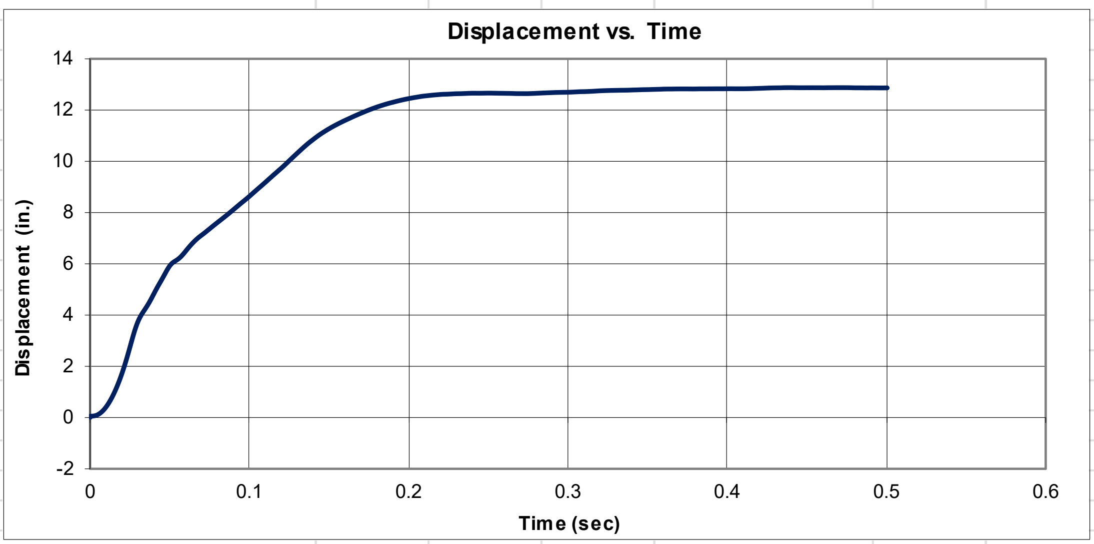

Figure H.2 String Potentiometer Data, Test No. AKLP-2

MIDWEST ROADSIDE SAFETY FACILITY

String Potentiometer Summary

Test Information:

Test No:	AKLP-3
Date:	7/28/2022
System / Test Article:	AK Evaluation of Light Pole Foundation Embedment
SP Location / Component:	0
Additional Notes:	

String Potentiometer Information:			**Results:**		
String Pot No.:	27039202		Max. Displacement:	1.77	in.
Calibration Factor:	18.82133	mV/V/in.	Time of Max. Displacement:	0.0465	sec
Input Voltage (excitation):	10	Volts	Event Duration:	0.184	sec
Gain:	1		Final Displacement:	1.21	in.
Full Scale Load:	1				
Sample Rate:	10000	Hz			
Cutoff Frequency:	100	Hz			

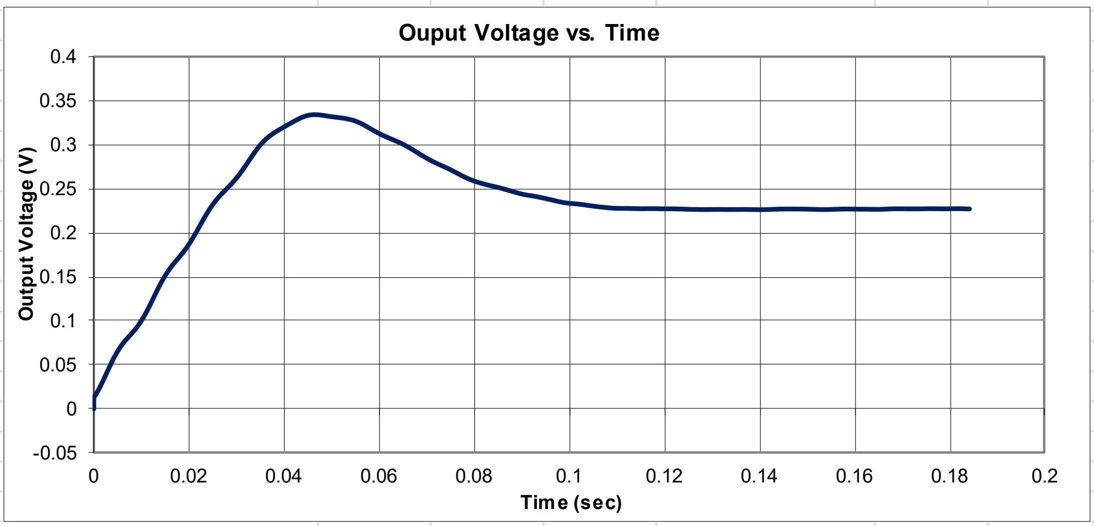

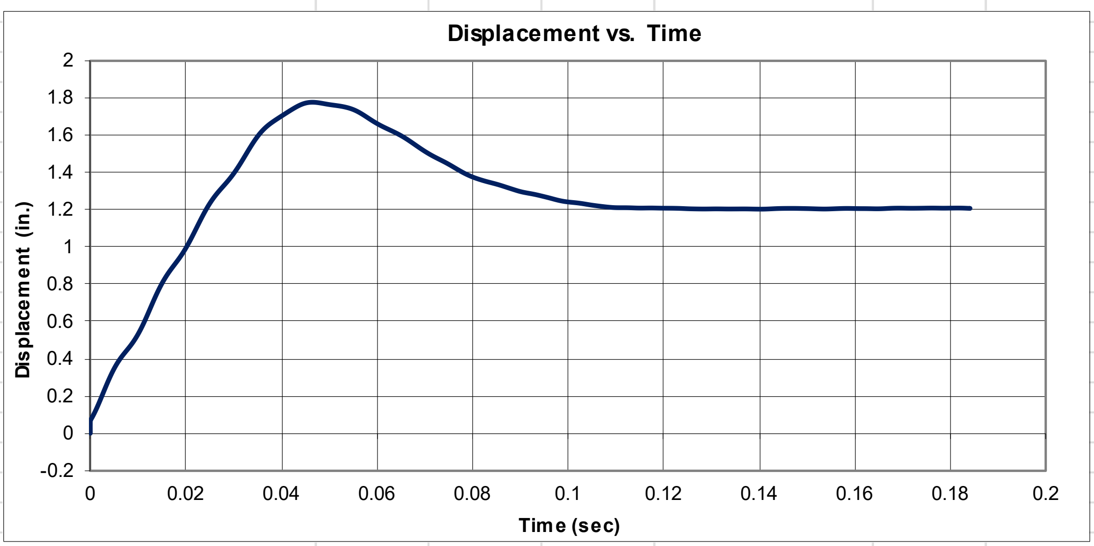

Figure H.3 String Potentiometer Data, Test No. AKLP-3

MIDWEST ROADSIDE SAFETY FACILITY

String Potentiometer Summary

Test Information:

Test No:	AKLP-4
Date:	8/5/2022
System / Test Article:	AK Evaluation of Light Pole Foundation Embedment
SP Location / Component:	0
Additional Notes:	

String Potentiometer Information:			**Results:**		
String Pot No.:	27039202		Max. Displacement:	1.56	in.
Calibration Factor:	18.82133	mV/V/in.	Time of Max. Displacement:	0.0522	sec
Input Voltage (excitation):	10.02	Volts	Event Duration:	0.1814	sec
Gain:	1		Final Displacement:	0.93	in.
Full Scale Load:	1				
Sample Rate:	10000	Hz			
Cutoff Frequency:	100	Hz			

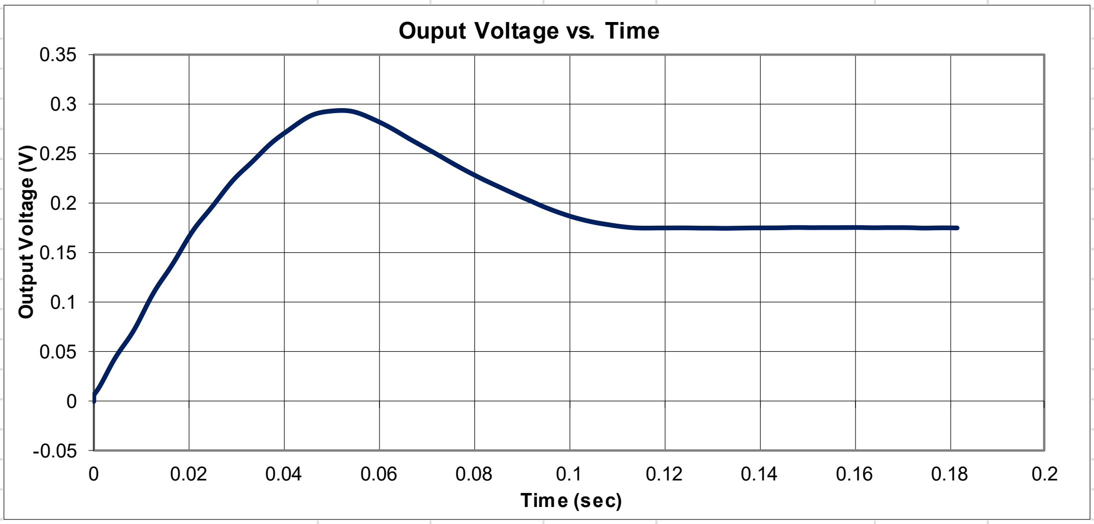

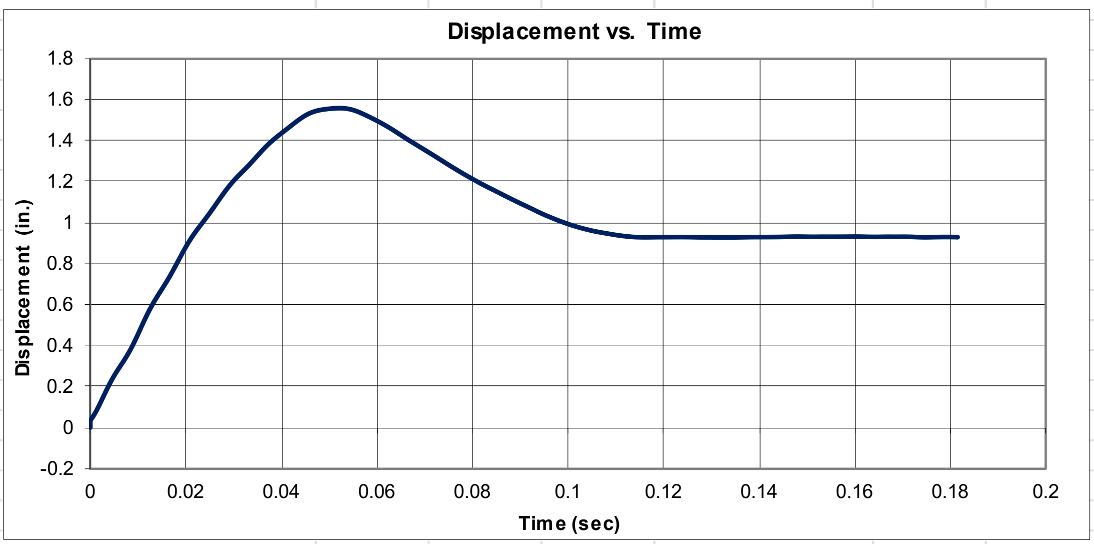

Figure H.4 String Potentiometer Data, Test No. AKLP-4

MIDWEST ROADSIDE SAFETY FACILITY

String Potentiometer Summary

Test Information:

Test No:	AKLP-5
Date:	11/1/2022
System / Test Article:	AK Evaluation of Light Pole in non-componded dry sand
SP Location / Component:	0
Additional Notes:	

String Potentiometer Information:

String Pot No.:	27039202	
Calibration Factor:	18.82133	mV/V/in.
Input Voltage (excitation):	10	Volts
Gain:	1	
Full Scale Load:	1	
Sample Rate:	10000	Hz
Cutoff Frequency:	100	Hz

Results:

Max. Displacement:	1.18	in.
Time of Max. Displacement:	0.0489	sec
Event Duration:	0.1814	sec
Final Displacement:	0.96	in.

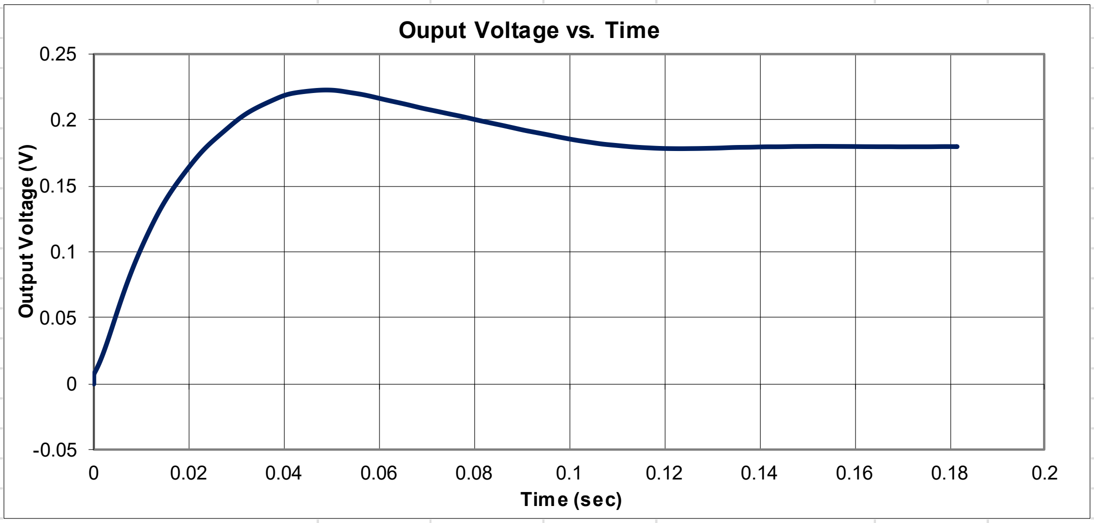

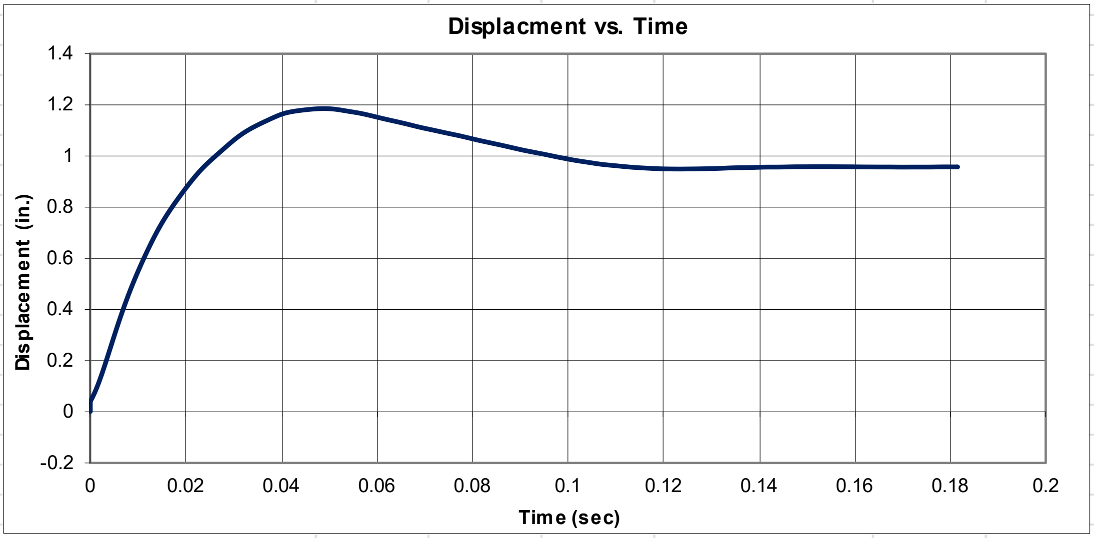

Figure H.5 String Potentiometer Data, Test No. AKLP-5

MIDWEST ROADSIDE SAFETY FACILITY

String Potentiometer Summary

Test Information:			
Test No:	AKLP-6		
Date:	12/1/2022		
System / Test Article:	AK Evaluation of Light Pole in non-componded saturated sand		
SP Location / Component:	0		
Additional Notes:			

String Potentiometer Information:			**Results:**		
String Pot No.:	27039202		Max. Displacement:	0.32	in.
Calibration Factor:	18.82133	mV/V/in.	Time of Max. Displacement:	0.0465	sec
Input Voltage (excitation):	10	Volts	Event Duration:	0.7022	sec
Gain:	1		Final Displacement:	0.12	in.
Full Scale Load:	1				
Sample Rate:	10000	Hz			
Cutoff Frequency:	100	Hz			

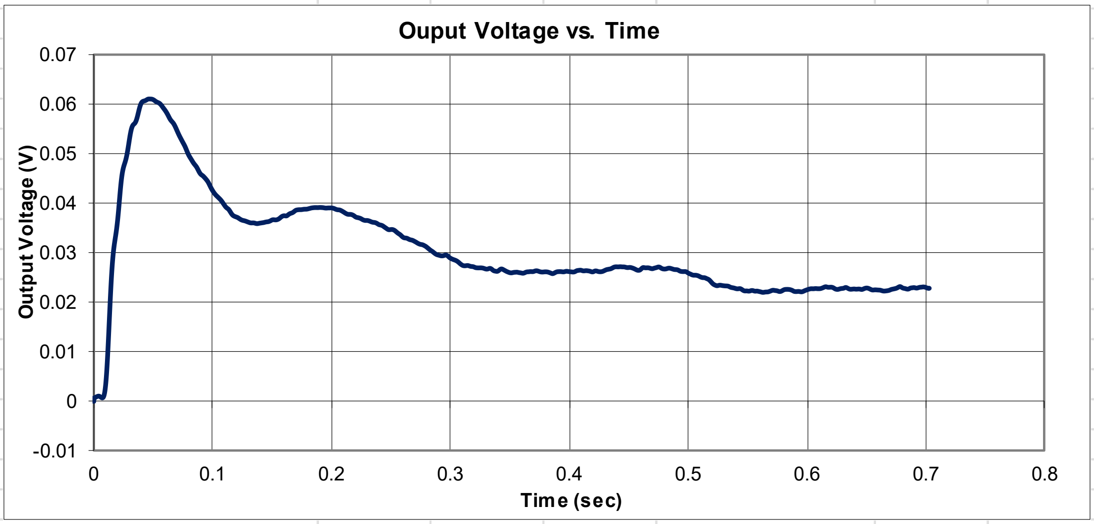

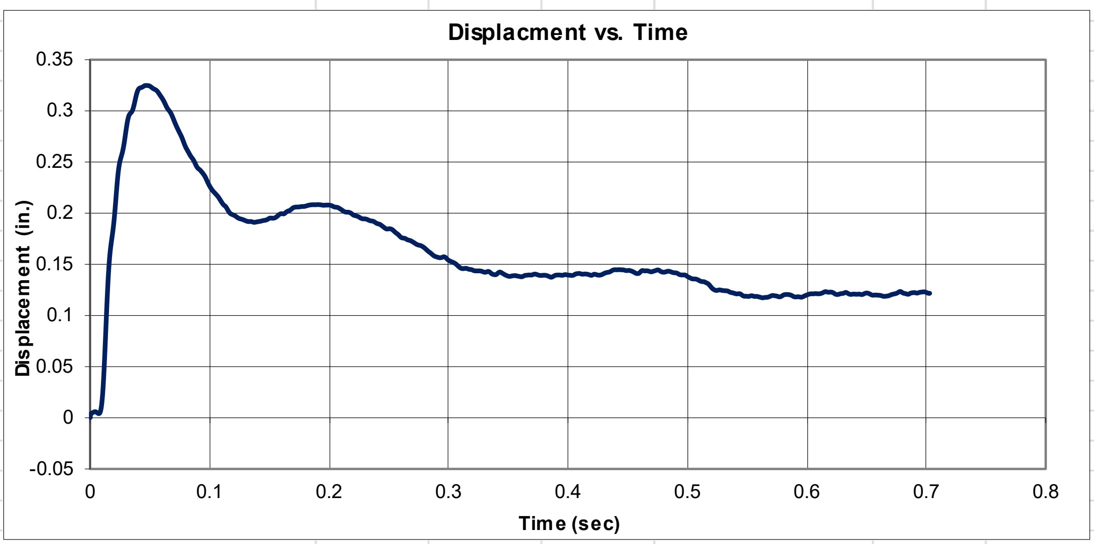

Figure H.6 String Potentiometer Data, Test No. AKLP-6